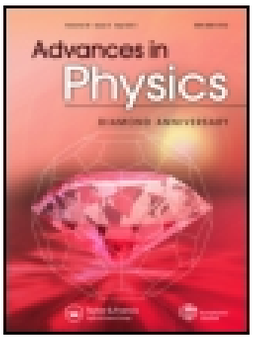

Advances in Physics

ISSN: 0001-8732 (Print) 1460-6976 (Online) Journal homepage: www.tandfonline.com/journals/tadp20

# Collective and single particle diffusion on surfaces

T. Ala-Nissila, R. Ferrando & S. C. Ying

**To cite this article:** T. Ala-Nissila, R. Ferrando & S. C. Ying (2002) Collective and single particle diffusion on surfaces, Advances in Physics, 51:3, 949-1078, DOI: 10.1080/00018730110107902

**To link to this article:** https://doi.org/10.1080/00018730110107902

ADVANCES IN PHYSICS, 2002, VOL. 51, NO. 3, 949–1078

# Collective and single particle diffusion on surfaces

T. ALA-NISSILA†‡*, R. FERRANDO§* and S. C. YING‡*

† Helsinki Institute of Physics and Laboratory of Physics, Helsinki University of Technology, Espoo, Finland

‡ Physics Department, Brown University, Providence, Rhode Island, USA

§ INFM and CFSBT/CNR, Dipartimento di Fisica dell'Università di Genova, Genova, Italy

[Received 30 April 2001; accepted 9 October 2001]

**Abstract**

We review in this article the current theoretical understanding of collective and single particle diffusion on surfaces and how it relates to the existing experimental data. We begin with a brief survey of the experimental techniques that have been employed for the measurement of the surface diffusion coefficients. This is followed by a section on the basic concepts involved in this field. In particular, we wish to clarify the relation between jump or exchange motion on microscopic length scales, and the diffusion coefficients which can be defined properly only in the long length and time scales. The central role in this is played by the memory effects. We also discuss the concept of diffusion under nonequilibrium conditions. In the third section, a variety of different theoretical approaches that have been employed in studying surface diffusion such as first principles calculations, transition state theory, the Langevin equation, Monte Carlo and molecular dynamics simulations, and path integral formalism are presented. These first three sections form an introduction to the field of surface diffusion. Section 4 contains subsections that discuss surface diffusion for various systems which have been investigated both experimentally and theoretically. The focus here is not so much on specific systems but rather on important issues concerning diffusion measurements or calculations. Examples include the influence of steps, diffusion in systems undergoing phase transitions, and the role of correlation and memory effects. Obviously, the choice of topics here reflects the interest and expertise of the authors and is by no means exhaustive. Nevertheless, these topics form a collection of issues that are under active investigation, with many important open questions remaining.

**Contents** PAGE



* e-mails: alanissi@csc.fi; ferrando@fisica.unige.it; ying@physics.brown.edu

*Advances in Physics* ISSN 0001–8732 print/ISSN 1460–6976 online © 2002 Taylor & Francis Ltd
http://www.tandf.co.uk/journals
DOI: 10.1080/00018730110107902

## Glossary of notation and acronyms

| | |
|---|---|
| $S[x]$ | action, |
| $E_A$ | activation energy, |
| $V_A(\mathbf{r})$ | adiabatic potential, |
| $D_\omega$ | angular diffusion coefficient, |
| $\mathbf{\Omega}$ | angular velocity, |
| $\langle \mathbf{v}_d \rangle$ | average drift velocity, |
| $\Delta$ | bare barrier parameter in the Transition Dynamics Algorithm, |
| $\Delta V_b(\mathbf{r})$ | bias potential, |
| $E_B$ | binding energy at the step edge, |
| $k_B$ | Boltzmann constant, |
| $D_{CM}$ | centre-of-mass diffusion coefficient, |
| $\mathbf{R}$ | centre-of-mass position, |
| $\bar{x}$ | centroid, |
| $\mu$ | chemical potential, |
| $S(\mathbf{q}, \omega)$ | coherent dynamic structure factor, |
| $f_c$ | collective correlation factor, |
| $D_c$ | collective or chemical diffusion coefficient, |
| $\eta_c, \tilde{\eta}$ | collision frequencies (rates), |
| $Z_0, Z_s$ | configuration integrals, |
| $\xi_c$ | correlation length, |
| $W(\mathbf{r}, \mathbf{q})$ | coupling function, |
| $\theta$ | coverage, |
| $\theta_e$ | coverage at step edges of stepped surfaces, |
| $\theta_t$ | coverage on the terraces of stepped surfaces, |
| $\theta_c$ | critical coverage, |
| $T_c$ | critical temperature, |
| $S(\mathbf{r}, t)$ | density correlation function, |
| $\rho_S(t)$ | density matrix, |
| $\nu_S, \nu_B, \nu_2$ | diffusion prefactors on stepped surfaces, |
| $d$ | dimensionality of the system, |
| $\gamma = \Gamma / n_s$ | directional jump rate, |
| $\Delta_d$ | dissipation, |
| $E_{\text{eff}}, E_A^D, E_s$ | effective diffusion barriers, |
| $D_{c,\alpha\alpha}^{(n)}$ | effective collective diffusion (mobility) coefficient within the $n$th time regime, |
| $D_{T,\alpha\alpha}^{(n)}$ | effective tracer diffusion (mobility) coefficient within the $n$th time regime, |
| $e$ | electron charge, |
| $n_s$ | electron density per unit volume, |
| $\eta_{el}$ | electronic friction, |
| $E_S$ | Ehrlich–Schwoebel additional barrier, |
| $E_2$ | energy barrier for jumps along lower step edges, |
| $E_0$ | energy barrier for jumps on terraces, |
| $\Delta S$ | entropy change, |
| $E_{ex}(T, t)$ | excess energy, |
| $\mathbf{F}$ | external force, |
| $\mathbf{f}(t)$ | fluctuating random force, |
| $\psi(t)$ | flux–flux (collective) autocorrelation function, |
| $\Omega_0(\mathbf{q})$ | frequency function, |
| $C_c(t)$ | generalized flux autocorrelation function, |

| | |
|---|---|
| $C_t(t)$ | generalized velocity autocorrelation function, |
| $\mathcal{H}$ | Hamiltonian, |
| $S_s(\mathbf{q},\omega)$ | incoherent dynamic structure factor, |
| $\chi_T$ | isothermal compressibility, |
| $\Gamma_0, \Gamma_1, \Gamma_1', \Gamma_u, \Gamma_d$ | jump rates on stepped surfaces, |
| $\mathbf{u}$ | lattice displacement vector, |
| $a$ | lattice spacing, |
| $L_B$ | linear system size (in simulation studies), |
| $\mathcal{L}$ | Liouville operator, |
| $\rho(\mathbf{r},t)$ | local density, |
| $\mathbf{J}(\mathbf{r},t)$ | local particle flux, |
| $\rho_0$ | mass density of the substrate, |
| $m$ | mass of the particle, |
| $\Delta\mathbf{r}^2(t) \equiv \langle\lvert\mathbf{r}(t)-\mathbf{r}(0)\rvert^2\rangle$ | mean square displacement of a single particle, |
| $\Delta\mathbf{R}^2(t) \equiv \langle\lvert\mathbf{R}(t)-\mathbf{R}(0)\rvert^2\rangle$ | mean square displacement of the centre of mass, |
| $\langle l^2\rangle$ | mean square jump length, |
| $\sum(t,t')$ | memory function in the generalized Langevin equation, |
| $M(\mathbf{q},i\omega)$ | memory function of $S(\mathbf{q},\omega)$, |
| $\eta$ | microscopic friction, |
| $\mathbf{r}_d(t), \mathbf{r}_a(t)$ | minimal paths, |
| $\omega(i)$ | normal mode frequency, |
| $F(T,t)$ | normalized excess energy, |
| $\eta^*$ | normalized microscopic friction, |
| $n_s$ | number of equivalent saddle points from a minimum position, |
| $\phi_c$ | order parameter, |
| $N$ | particle number, |
| $\langle(\Delta N)^2\rangle$ | particle number mean square fluctuation, |
| $n_{\mathbf{l}}$ | particle occupation variable, |
| $\mathbf{r}$ | particle position, |
| $\mathbf{v}$ | particle velocity, |
| $Z$ | partition function, |
| $P(\mathbf{r},\mathbf{v},t),\ P(\mathbf{n},t)$ | phase space distribution functions, |
| $\eta_{ph}$ | phononic friction, |
| $h;\ \hbar = h/2\pi$ | Planck's constant, |
| $V(\mathbf{r})$ | potential energy, |
| $\phi$ | potential of the external force, |
| $\Phi(\mathbf{l},t)$ | probability distribution of displacement $\mathbf{l}$ after time $t$, |
| $P[\mathbf{r}(t)],\ P(x)$ | probability functional (distribution), |
| $p_{\mathbf{l}}$ | probability of a jump from the origin to a site $\mathbf{l}$, |
| $\mathcal{P},\ \mathcal{Q}$ | projection operators, |
| $f_\mu$ | random number, |
| $\Delta\rho$ | resistivity change (in a thin film), |
| $\Psi(T,\theta,t)$ | response function, |
| $V_S(\mathbf{r})$ | rigid substrate potential, |
| $D_r$ | rotational diffusion coefficient, |
| $e(x)$ | scaled (position dependent) energy, |
| $C_\mu, C_\mu^\dagger$ | scattering operators, |
| $\delta p_\mu$ | scattering probability, |
| $D_t$ | single-particle or tracer diffusion coefficient, |
| $\bar{\eta}$ | sliding friction, |
| $\nu_{\mathrm{osc}} = \omega_{\mathrm{osc}}/2\pi$ | small-oscillation frequency, |
| $\tau_{\mathrm{osc}}$ | small-oscillation period, |
| $S(\mathbf{q},t)$ | spatial Fourier transform of the density correlation function, |
| $S(\mathbf{q}) = S(\mathbf{q},t=0)$ | structure factor, |
| $S_0 = S(\mathbf{q}=0)$ | structure factor at zero momentum, |
| $\mathbf{R}_\ell, \mathbf{P}_\ell$ | substrate coordinates and momenta, |
| $T;\ \beta = (k_B T)^{-1}$ | temperature, |

$L$ terrace width,
$k$ thermal transition rate,
$d_s$ thickness of the substrate,
$t$ time,
$S^{(n)}(\mathbf{r}, \mathbf{r}', t)$ time dependent (transient) density fluctuation correlation function,
$\Omega^{(n)}_{\alpha\alpha}(t)$ time-dependent (transient) mean square deviation,
$\tau_0, \delta t$ time intervals (steps),
$t_m$ time of onset of the hydrodynamic regime,
$\Gamma$ total jump rate,
$\mathbf{J}_T(t) = \sum_{i=1}^{N} \mathbf{v}_i(t)$ total particle (velocity) flux,
$f_t$ tracer correlation factor,
$p(\mathbf{n}, \mathbf{n}')$ transition probability,
$w(\mathbf{n} \rightleftarrows \mathbf{n}') = p(\mathbf{n}, \mathbf{n}')/\tau_0$ transition rate,
$x^*$ transition state coordinate,
$c_T$ transverse sound velocity,
$\ell$ tunnelling length,
$P_\ell$ tunnelling length distribution,
$\mathbf{u}(t)$ unit vector (e.g. parallel to a polymer molecule),
$\bar{\omega}_s$ unstable frequency (at the saddle point),
$t_f$ upper limit for (simulation) time,
$\phi(t)$ velocity–velocity (tracer) autocorrelation function,
$|\Psi(t)\rangle$ wave function,
$\Delta\omega$ width of the quasi-elastic peak of the dynamic structure factor,

BM Boltzmann–Matano,
CJ Concerted Jump,
CEM Corrected Effective Medium,
DFT Density Functional Theory,
DR Dissociation–Reassociation,
DMF Dynamical Mean Field,
EMT Effective Medium Theory,
EAAFW Embedded Atom in Adams–Foiles–Wolfer parametrization,
EAFDB Embedded Atom in Foiles–Daw–Baskes parametrization,
EAVC Embedded Atom in Voter–Chen parametrization,
EAM Embedded Atom Method,
EC Evaporation–Condensation,
FIM Field Ion Microscopy,
FEM Field Emission Microscopy,
FLL Flux Line Lattice,
FWHM Full Width at Half Maximum,
GGA Generalized Gradient Approximation,
GLE Generalized Langevin equation,
HAS Helium Atom Scattering,
HRLEED High Resolution Low Energy Electron Diffraction,
IVA Initial Value Approximation,
LITD Laser Induced Thermal Desorption,
LOD Linear Optical Diffraction,
LDA Local Density Approximation,
MCFM Matrix Continued Fraction Method,
MEM Memory Expansion Method,
MW Metastable Walk,
MPA Minimal Path Approximation,
MD Molecular Dynamics,
MC Monte Carlo,
MCWF Monte Carlo Wave Function,
ML Monolayer(s),
NN Nearest Neighbour,
PD Periphery Diffusion,

| | |
|---|---|
| PEEM | Photoemission Electron Microscopy, |
| PES | Potential Energy Surface, |
| PO | Projection Operator, |
| QTST | Quantum Transition State Theory, |
| QHAS | Quasi-elastic Helium Atom Scattering, |
| SCPM | Scanning Contact Potential Microscopy, |
| STM | Scanning Tunnelling Microscopy, |
| TAD | Temperature Accelerated Dynamics, |
| TD | Terrace Diffusion, |
| TBSMA | Tight-Binding Second Moment Approximation, |
| TDA | Transition Dynamics Algorithm, |
| TST | Transition State Theory, |
| TO | Truncated Octahedron, |
| TP | Truncated Pyramid, |
| WKB | Wentzel–Kramers–Brillouin. |

## 1. Introduction

### 1.1. *Theoretical overview of surface diffusion*

The field of surface diffusion has seen explosive growth in the past decade. It has of course long been recognized that the diffusion of adparticles is the key controlling rate in most dynamical processes occurring on surfaces such as chemical reactions and growth of islands and epitaxial layers [1, 2]. Indeed, the knowledge of the diffusive properties of single adatoms and of clusters on crystal surfaces is a fundamental step in surface nanostructuring [3], the latter being of increasing technological importance in recent years. However, until recently, there were relatively few direct measurements of surface diffusion rates. For example, the motion of single adatoms was observed in the 1960s on the tip of the field ion microscope [4], thus giving a direct demonstration of the atomic motion on crystal surfaces. However, the use of FIM was limited to refractory metal surfaces, such as tungsten, iridium, platinum and a few others [5, 6]. The advent of many new experimental techniques such as STM (which reaches full atomic resolution, see figure 1, taken from reference [7]), QHAS, and optical diffraction grating changed

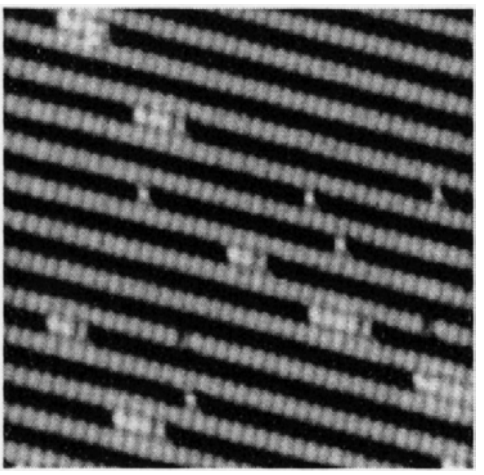

Figure 1. STM image of a terrace on the missing row surface of Pt(110) [7]. Adatoms and clusters (chains of three and four atoms) can be seen in the atomic channels. A detailed discussion of diffusion on this surface can be found in section 4.2.

the whole field. Now surface diffusion coefficients for more and more systems have been measured directly and with high accuracy. The new experimental data quite often challenge the simple accepted theoretical framework and further stimulate new theoretical investigations using different approaches in this area.

In this review, we will try to present an overview of the theoretical approaches to the study of surface diffusion and the progress made in the last few years in understanding the different issues in this field. There already exist several excellent reviews focussing mainly on the experimental side of surface diffusion (see the reviews of references [8, 9, 5, 10–14]; a very nice short introductory review article is found in reference [15]). For this reason, we have decided to omit a systematic discussion of the different experimental techniques and survey of the experimental data. However, many of the recent theoretical investigations are stimulated by experimental findings, and our understanding is often advanced by a detailed comparison of the theoretical and experimental results. Thus in this regard, many recent experimental investigations will be discussed throughout this review.

For most adsorbed atoms and molecules their masses are so heavy that for the entire temperature range of practical relevance, the motion can be treated as classical. The exception is for the adsorption of H atoms and the related isotopes where there is strong evidence that diffusion by the quantum tunnelling mechanism dominates at low temperatures [8]. We will discuss this interesting subject in a separate section. Otherwise in the review, we concentrate on the classical motion of the adsorbates. Also, in most of the studies, the internal degrees of freedom of the adsorbed atoms and molecules do not come into play; the adatoms can just be viewed as point particles and we will use indiscriminately the expression adatom or adparticle for this purpose. In cases where the internal degrees of freedom become important, the specific nature of the adsorbed molecule will be considered more explicitly.

The simplest type of surface diffusive motion occurs when the substrate is not active in the role of mass transport. In this case, the substrate atoms just perform small vibrations around their equilibrium positions. Let us place a single adatom above such a substrate. The influence of the substrate on the adatom dynamics can be separated into two categories. The first is the adiabatic potential $V_A(\mathbf{r})$ which is just the free energy of the entire adsorption system with the positions of the substrate atoms fixed. This is an effective potential that the adatom experiences with the electronic and vibrational excitation degrees of freedom averaged out. The difference between the value of $V_A(\mathbf{r})$ at the saddle point and at the minimum is the classical activation barrier $E_A$ for the diffusion process (see figure 2). At low temperatures, the motion of the adatom consists of localized oscillations around the minima of $V_A(\mathbf{r})$ with occasional jumps to the neighbouring minima, i.e., of jumps from one adsorption site to another. As with all thermally activated processes [16], an Arrhenius form separating the rate into a prefactor and an exponential of the form $\exp[-E_A/(k_BT)]$ is usually employed to analyze the temperature dependence.

However, the adiabatic barrier is an equilibrium quantity. Even though the magnitude of the diffusion coefficient is controlled mainly by the activation barrier, the real dynamical information is all contained in the prefactor. Microscopically, the dynamical information comes from the non-adiabatic coupling of the adatom to the substrate excitations. This gives rise to the fluctuation and damping of the adatom motion and changes its character from ballistic to Brownian. Without this coupling, there is no means for the adatom to acquire enough energy to jump over the barrier

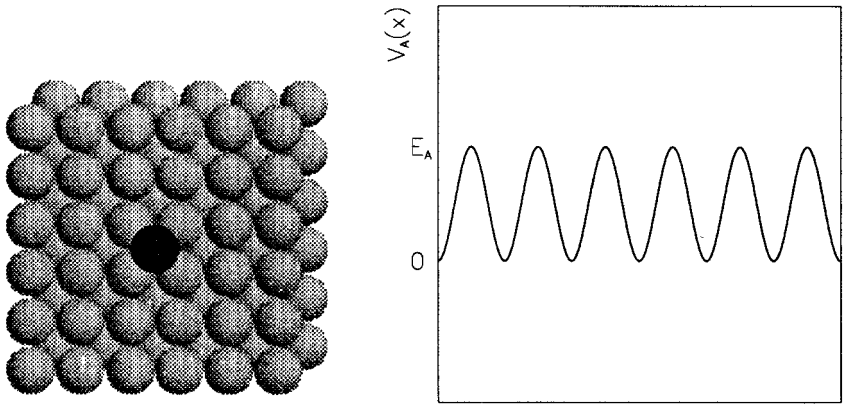


(*a*) (*b*)

Figure 2(*a*). An adatom sitting in a fourfold minimum on a substrate of square symmetry. (*b*): Schematic representation of the adiabatic potential $V_A(x)$ along a 1D path connecting subsequent minima along the $x$ direction. The activation barrier $E_A$ is the difference between the saddle points and minima. The former correspond to the maxima in the 1D case.

and equilibrate at a new adsorption site. In the simplest Markovian approximation, the stochastic forces acting on the adatom at different times can be treated as statistically independent. In this approximation, the non-adiabatic coupling can be characterized by a simple friction parameter $\eta$. For the more general case, the fluctuation and damping of the adatom at any moment depends on its past history, that is the 'memory' effects become important and the frictional coupling has to be in this case characterized by a memory function $M(t, t')$ which is essentially the correlation function of the random stochastic force at the times $t$ and $t'$.

The above scenario of an isolated adatom performing thermally activated hopping between adjacent adsorption sites is conceptually the simplest picture for surface diffusion. In recent years it has been recognized that, in particular for homoepitaxial metallic systems, exchange processes where an adatom exchanges with a substrate atom which continues the diffusive motion, could be comparable or even become the dominant mechanism over the simple hopping motion. Other more exotic mechanisms such as multiple exchanges or concerted movements involving a large complex of atoms have also been proposed to explain observed data and seen in numerical simulation studies. Moreover, experiments and simulations have revealed the occurrence of long jumps, where the adatom directly hops to distant sites.

So far, we have discussed the motion of the adatom at short time and length scales. The proper single particle (or tracer) diffusion coefficient $D_t$, however, is defined through the mean square displacement of the adatom at asymptotically long times. For isolated adatoms, subsequent jumps are statistically independent (uncorrelated jumps), and there exists a simple relation between the transport coefficient $D_t$ and the microscopic jump rate: $D_t$ is proportional to the product of the jump rate with the average square jump length. The relation becomes much more complicated when the jumps are correlated, as happens at finite coverages, this being another example of memory effects.

At finite coverages, as long as one can follow the trajectory of individual adatoms or more generally the center of mass of each individual moving complex, the concept of single particle or tracer diffusion is still useful. However, in this case we do not have a single well-defined adiabatic barrier. Because of the adatom–adatom interactions, the actual activation barrier depends on the configuration of all the other adatoms and the effective barrier that controls the diffusion results from a complicated average over all the fluctuating configurations. Obviously, a strict Arrhenius form for the temperature dependence is no longer correct. Also, successive configurations of the adsorbate are highly correlated which results in correlations between the jumps and additional memory effects. In addition to the single particle diffusion, there is also a new transport coefficient at finite coverages, namely the collective diffusion coefficient $D_c$ which measures the rate at which deviations from the equilibrium density spread out in the long time limit. The relation of $D_c$ to the microscopic individual adatom jump rates or to $D_t$ is more complicated and a qualitative understanding only begins to develop with the detailed study of memory effects as discussed in the following chapters.

Another interesting issue concerns the role of nonequilibrium effects in diffusion. The system has to be either in equilibrium or only slightly out of equilibrium for the transport coefficient $D_c$ to be able to describe the actual mass transport. Under many experimental situations, the system can be either in the nonlinear and/or non-equilibrium regime and the linear response diffusion coefficients cannot account for the mass transport rate. When the length scale of the density variations is sufficiently long, one can invoke the concept of local equilibrium and introduce a coverage dependent $D_c$ which is a function of the local coverage and analyze the data even when the density varies over a wide range of values. In particular, the Boltzmann–Matano analysis can be used when the geometry involves only a density variation along one spatial direction [8, 17]. Attempts have been made to generalize the definition of the diffusion coefficients to nonlinear and non-equilibrium situations, but this is on a much less firm theoretical basis and probably has to be carefully defined for different systems.

To study these challenging problems, a number of theoretical approaches have been adopted. With the advances in semi-empirical potential and first principles (*ab initio*) calculations for the interaction energy between atoms and molecules, the adiabatic diffusion barriers (at least at $T = 0$) have been evaluated for many systems. This itself of course does not yet determine the jump rates or the diffusion coefficients as one still needs to determine the prefactor and the entropic contributions. The transition state theory (TST), which was first developed for chemical reaction rate calculations [16], provides a simple and intuitive picture of the activated hopping, and yields naturally the Arrhenius form of the temperature dependence. However, TST only involves equilibrium properties of the adsorption system. It provides an approximate expression for the prefactor but does not provide any insights into the true dynamics of the diffusion process. In the Langevin equation and equivalently the Fokker–Planck equation approaches [18, 19], there is a natural separation of the adiabatic potential and non-adiabatic frictional coupling. They have been studied both at an empirical level with model friction parameters, and at a more detailed microscopic level involving explicitly the substrate degrees of freedom [20]. Molecular dynamics simulation studies [21] with either simple model or more accurate semi-empirical, or even *ab initio* interactions would provide the most complete picture. In MD studies, both the adiabatic potential and the nonadiabatic coupling

to the phonon degrees of freedom can be included exactly. The only missing ingredient is the frictional coupling to electronic excitations.

At low temperatures and with relatively weak adatom interactions, the adatoms are mostly localized around the adsorption sites. In this case, the lattice gas model characterized by a lattice gas Hamiltonian and a prescribed dynamical algorithm for transitions between different configurations becomes a very useful model for the study of surface diffusion. This can be accomplished by the analytical projection operator techniques [22], or more commonly through Monte Carlo (MC) simulations of the corresponding master equation [21]. However, as we will discuss in this review in some detail, the lattice-gas approach to calculating dynamical quantities must be executed with particular care due to the dependence of the results on the transition rates chosen for the simulations.

The outline of this review is as follows. We will first expand on the basic concepts discussed above in section 2 and then describe the different modern theoretical approaches to surface diffusion in section 3. In section 4 we discuss the application of these approaches to the study of surface diffusion for many adsorption systems. Rather than carrying out an exhaustive survey of the vast number of different systems that have been studied in the literature, the emphasis here is on some specific issues which we deem important in surface diffusion studies, and the physics behind such issues. Examples of topics that we have chosen and which play an important role include diffusion near a phase transition boundary of either the substrate or the adsorbate layer, influence of steps and impurities on observed diffusion rates, memory effects, nonequilibrium conditions, quantum effects, and diffusion of adatom complexes (islands). In selecting these topics we have been of course limited by our own knowledge and expertise in the field. Nevertheless, we have tried to choose the topics discussed in this review in such a way that they hopefully spur further research on the many remaining open issues in the field.

### 1.2. *Brief discussion of different experimental techniques for measuring surface diffusion*

Even though we have emphasized that this review mainly focusses on the theoretical aspects of surface diffusion, many of the theoretical results cannot be discussed without touching upon the relevant experimental data. Fortunately, in a very recent review article [12], the relative merits of the various experimental techniques for surface diffusion and the systems that have been studied, have been discussed in some detail. Rather than repeating the discussion here, we will summarize some of the salient features in table 1, and add some observations that perhaps have not been emphasized previously. We refer the reader to the article by Barth [12] for detailed references and results for various systems obtained with these techniques. There are also some promising new techniques such as measuring the temporal fluctuation in HRLEED [23]; they are not included here since it is too early to judge their potential. For the meaning of the various acronyms, we refer the reader to the list of notations and acronyms at the beginning of this review.

We want to make the following observations about the techniques listed in table 1. First these techniques can be classified into two main groups. The first group, including STM and FIM, can image and follow the motion of individual adatoms. As such, they can provide a true measure of the single particle tracer diffusion coefficient $D_t$. This includes the case where exchange processes take place and where the moving particle is not always the same one. The second group, including QHAS,

Table 1. Principal experimental techniques for surface diffusion studies; for a thorough description of the different techniques the reader can refer to references [9, 8, 5, 12] and references therein.

| Technique | Remarks | Sensitivity | Length scale | Range of $D$ ($cm^2s^{-1}$) |
|---|---|---|---|---|
| STM | Direct Imaging | $\theta \geq 0$ | few — | $10^{-19}$–$10^{-16}$ |
| FIM | Direct Imaging | $\theta \geq 0$ | few — | $10^{-19}$–$10^{-16}$ |
| QHAS | Density Fluctuations | $\theta \geq 0.010$ | 10 — | $\gtrsim 5 \times 10^{-6}$ |
| FEM | Density Fluctuations | $\theta \geq 0.10$ | 100–1000 — | $10^{-14}$–$10^{-9}$ |
| HAS | Density Decay | $\theta \geq 0.01$ | 1 μm | $10^{-12}$–$10^{-14}$ |
| LOD | Density Decay | ? | 1 μm | $10^{-15}$–$10^{-7}$ |
| PEEM | Density Decay | $\theta \geq 0$ | 0.1–1000 μm | $10^{-9}$–$10^{-5}$ |
| LITD | Density Decay | $\theta \geq 0.1$ | 10–1000 μm | $10^{-8}$–$10^{-5}$ |
| SCPM | Density Decay | $\theta \geq 0.01$ | $\gtrsim 1$ μm | $10^{-10}$–$10^{-4}$ |

FEM, HAS, LOD, PEEM, LITD, SCPM, and HRLEED, constitute the majority of the techniques. They are all based on the measurement of either equilibrium density fluctuations (QHAS, FEM, HRLEED) or the decay of (hopefully) small non-equilibrium density profiles (HAS, LOD, PEEM, LITD, SCPM). As such, they measure the collective diffusion coefficient $D_c$. However, for the techniques that have high sensitivity and can operate at very low coverages such as QHAS, the tracer diffusion coefficient $D_t$ can also be studied by taking the limit of the result for $D_c(\theta)$ at small coverages, based on the fact that in the limit $\theta \rightleftarrows 0$ the two diffusion coefficients $D_c$ and $D_t$ are identical. It should also be noted that the STM technique is constantly being refined. The latest advance is that the motion of all the adatoms can be followed in real time, so a time series of the entire configuration is generated. This can then be used to obtain the collective diffusion coefficient $D_c$ as well.

Second, the length scales listed in the table deserve some comments. Aside from the direct imaging methods such as STM and FIM which obviously probe atomic length scales, most of the other techniques with the exception of QHAS have rather long length scales amounting to many lattice constants. For example, LOD has a length scale of a few μm. This is basically the maximum wavelength of the decaying density that is being probed. The large wavelength is advantageous in the sense that the gradient corrections to Fick's law are negligible and one is truly observing the linear response transport coefficient $D_c$. However, it also means that for real systems steps and impurities cannot be avoided at this length scale, and their influence must be taken into account in the extraction of the diffusion coefficient(s) from the data. The resulting value could be dramatically different from the corresponding value on a perfect terrace. This effect may be the reason for many mutually inconsistent data of diffusion coefficients obtained for the same system [24]. The techniques which have intrinsically short length scales have the advantage that over a length scale of $\leq$10 lattice spacings or so, steps or impurities can be avoided. However, other complications such as nonlinearity or nondiffusive motion can complicate the analysis. For example, the length scale of QHAS is limited by the resolution to be $\leq$10 —. At this length scale, the anharmonic components of the adatom vibrational motion have been shown [25–27] to substantially contribute to the quasi-elastic scattering peak. Thus the proper extraction of the diffusion coefficient from the data is a non-trivial task as will be discussed in section 4.1 of this review. The other

comments on short length scales apply to the case of finite coverages where memory effects are strong and successive jumps are correlated. In this case, in a STM measurement for example, to deduce the intrinsically long length scale and time scale diffusion coefficient $D_t$ or $D_c$ from the short length scale measurements, one must measure the correlation between the jumps in addition to the jump rates.

Third, and finally, we note that in some of these techniques, the diffusion coefficients are not directly measured but deduced indirectly by fitting the data to a rather elaborate analysis involving the diffusion coefficient as a parameter. The most representative example of this is the use of STM in the static rather than the dynamic mode to measure the distribution of island sizes after adatom deposition in a growth experiment [11]. The diffusion coefficient can then be extracted from a scaling analysis that involves some assumptions about the nucleation process and the mobility of the adatoms on the terrace. Recent works have demonstrated that, in some cases (in particular, in systems characterized by low activation barriers, as in the case of metal-on-metal diffusion on fcc(111) surfaces), a small change in the other parameters can have significant impact on the value of the diffusion coefficient deduced in this manner [28–30].

## 2. Basic concepts

In this section, we introduce some basic concepts and formulae for surface diffusion. First, we focus on the short time and length scales and examine the microscopic nature of the diffusive motion of the adatoms. The most common elementary move at low temperatures is the so-called diffusion jump (or hop). In some systems, substitutional diffusion (exchange diffusion) also takes place. This latter mechanism is especially relevant in homoepitaxial metallic systems, where the diffusing particles are of the same species as the substrate particles. Then we define the tracer and collective diffusion coefficients $D_t$ and $D_c$. These transport coefficients are intrinsically defined only in the long time and long length scale 'hydrodynamic' limit. They are related to the short time jump rates in a simple way only when the jumps are treated as being uncorrelated or, in other words, when memory effects are neglected. After defining the diffusion coefficients and the relevant correlation functions, we introduce the memory expansion method (MEM). Through the memory expansion, we not only gain insight into the connection between the long time definitions of the diffusion coefficients to the short time jump rates, but also a better understanding of the relation between $D_t$ and $D_c$. The last section of this section is devoted to non-equilibrium diffusion.

### 2.1. *Microscopic mechanisms for adatom diffusion: jumps and exchanges*

#### 2.1.1. *Jump diffusion: single and long jumps*

Let us consider the diffusion of an isolated adatom on a crystal surface, and assume that the adatom does not enter the substrate, i.e., that exchange diffusion (see the following section for the definition) does not take place. If temperature is low enough, the adatom spends most of its time making small-amplitude oscillations in the minima localized at the adsorption sites. Occasionally, it receives enough energy from the substrate (heat bath) to make a successful jump, after which it thermalizes again in another adsorption site. If thermalization occurs in a nearest-neighbour cell from the original site of departure, we call it a *single jump*; if not, we speak of a *long jump* or of a *multiple jump*. Assuming that the site of departure is the origin (site **0**),

the important quantities with respect to jump diffusion are the total jump rate $\Gamma$ and the probability $p_{\mathbf{l}}$ of thermalizing in the adsorption site at $\mathbf{l} = (l_x, l_y)$.

The temperature dependence of the jump rate can be written in the so-called *Arrhenius form* [31] (see also an interesting historical survey by Van't Hoff [32]), where any rate constant is written in an activated form as

$$\Gamma = \Gamma_0 \exp\left(-\frac{E_A}{k_B T}\right). \tag{1}$$

This can be shown to arise from a microscopic theory of surface diffusion at low temperatures in the appropriate limits [33, 20, 34]. It can also be derived from the more phenomenological Transition State Theory (TST) in the harmonic approximation [16] (see discussions on TST and the solution of the Langevin equation in sections 3.2 and 3.3, respectively). Obviously, the diffusion of hydrogen at low temperatures (below about 100 K) needs to be ruled out, since then the role of quantum tunnelling effects is very important [35, 8, 36]. Quantum diffusion will be treated separately in section 4.8. In the simplest limit of high friction and rigid substrate, the activation barrier $E_A$ is precisely the difference in the potential between the lowest saddle point that the particle has to cross to move from one unit cell to another, and its value at the minimum [33, 20] (see figure 2). The prefactor $\Gamma_0$ then contains all the dynamical information.

Mostly due to its simplicity, the Arrhenius description is widely used to analyze and interpret experimental diffusion data [8, 5]. We wish to emphasize here that this approach can be dangerous, however, even for the single adparticle case. First, as mentioned above, proofs of the Arrhenius form exist only in some special limits [33, 20, 34]. In all these approaches, the Arrhenius form only emerges when the temperature is sufficiently low (see below). The reason is easy to see. The path of diffusion through the saddle point to the next well only dominates at low temperatures. At higher temperatures, many other paths become increasingly important and one has to average over a continuous distribution of barriers and a simple Arrhenius form is no longer valid. Moreover, anharmonicity and thermal expansion can also cause high-temperature deviations [37–41]. Also memory effects arising from the surface excitations can change the effective Arrhenius barrier, as will be discussed in section 4.6. Barring these complications, a rough estimate of $\Gamma_0$ is given by

$$\Gamma_0 = n_s \nu_{\mathrm{osc}}, \tag{2}$$

where $\nu_{\mathrm{osc}}$ is a typical vibrational frequency of the adatom in the adsorption site, and $n_s$ is the number of equivalent saddle points from a minimum position ($n_s = 4$ and 6 on square and triangular lattices, respectively). Typically, the jump diffusion description is valid provided that $\Gamma \ll \nu_{\mathrm{osc}}$; from equation (2) it follows that $E_A/k_B T \gtrsim 4$ is a sufficient criterion for the temperature to be low enough in the Arrhenius regime. From the random-walk theory [42–44], an expression for the diffusion coefficient $D_t$ for the isolated particle (see section 2.2 for the formal definition of $D_t$) follows easily:

$$D_t = \frac{1}{4}\Gamma \langle l^2 \rangle, \tag{3}$$

where $\langle l^2 \rangle$ is the mean square jump length.

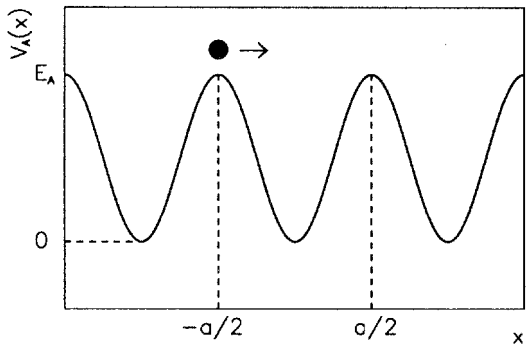


Figure 3. A periodic potential $V_A(x)$ where the particle starts at the saddle point at the left side of the cell, with potential energy $E_A$ and kinetic energy $k_BT$, and crosses the cell dissipating energy to the thermal bath due to the friction $\eta$.

The occurrence of long jumps can be discussed qualitatively in the framework of a one-dimensional model of diffusion in a periodic potential $V_A(x)$ (see figure 3), where the adatom dissipates energy to the substrate with a constant friction per unit mass $\eta$. Here we discuss the general condition for the occurrence of long jumps, and in section 3.3 we shall calculate explicitly the long-jump distribution within the Langevin model. Let us calculate how much energy the adatom dissipates in crossing a lattice cell [45]. We let the particle start at the saddle point at the left side of the cell (in $-a/2$, see figure 3) with an initial kinetic energy $k_BT$, corresponding to a total initial energy $E_0 = k_BT + E_A$. Then the particle crosses the cell dissipating an energy $\Delta$ which is given by:

$$\Delta = \int_{-a/2}^{a/2} m\eta v(x)\,\mathrm{d}x, \tag{4}$$

where $m$ and $v(x)$ are the mass and the velocity of the particle. Long jumps are likely to occur when $\Delta < k_BT$, so that the particle does not dissipate all of its kinetic energy by crossing a single cell. When this condition is fulfilled, $v(x)$ can be estimated as

$$v(x) \simeq \sqrt{\frac{2}{m}\,[E_0 - V_A(x)]}, \tag{5}$$

leading to

$$\Delta \simeq \eta \int_{-a/2}^{a/2} \sqrt{2m[E_0 - V_A(x)]}. \tag{6}$$

In the limit of low temperatures, the integral in equation (6) can be approximated by $E_A\tau_{\mathrm{osc}}$, where $\tau_{\mathrm{osc}}$ is the period of small oscillations at the bottom of the well. This leads to the following condition for long jumps:

$$\frac{\eta}{\nu_{\mathrm{osc}}} < \frac{k_BT}{E_A}. \tag{7}$$

Concerning the behaviour of the jump probabilities $p_l$ in one dimensional models, both analytical and numerical results [46–48, 25, 49–52] show that the decay is asymptotically exponential for large $l$, while at small $l$ the decay can be even faster.

In higher dimensions, there is strong indication that the precise topology of the adiabatic potential plays a role. In fact, it has been shown by the solution of two dimensional models, that the percentage of long jumps is considerably reduced when the minima and saddle points are not along the same straight line [53, 54], or even when the saddle points are on the same straight line of the minima, but they are narrower than the minima [55–57]. The latter result is evident also from MD simulations [58]. This happens because long jumps are favoured when the most probable diffusion paths are straight lines, along which inertial trajectories can easily propagate. Any geometrical restrictions leading to non-straight paths (which arise when the potential is not separable, i.e., when coupling terms among different co-ordinates are present) effectively increase the dissipation parameter $\Delta$ [59] thus causing an easier retrapping and reducing the probability of long jumps. On the other hand, the probability of long jumps can be enhanced by applying external fields, such as those obtainable by using an STM tip [61–63].

Long jumps have been observed in several molecular-dynamics simulations [64–66, 37, 67–69, 40, 70, 71, 58, 72], see an example in figure 4. The percentage of long jumps is typically about 10% for metal-on-metal systems at intermediate temperatures [58]. On the other hand, the experimental observation of long jumps is a challenging task. Indeed, long jumps are not directly observed in the experiments, because it is not possible at present to resolve the motion of the adatoms on such a fast time scale as to distinguish a true long jump from a sequence of single jumps. Thus the evidence of long jumps is indirect. In STM or FIM experiments [73, 6, 74, 7], one can deduce the occurrence of long jumps by measuring the probability distribution of the final displacements $\Phi(\mathbf{l}, t)$ (which is the probability for a given adatom of being at site $\mathbf{l}$ at time $t$ if it was at position $\mathbf{0}$ at time zero). The random-walk expression for $\Phi(\mathbf{l}, t)$ depends on the probabilities $p_{\mathbf{l}}$ as parameters

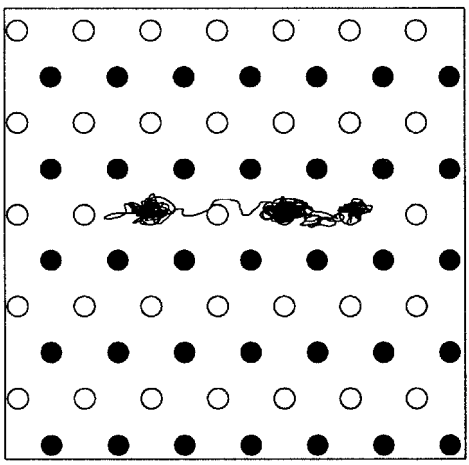

Figure 4. Molecular dynamics trajectory for an Ag adatom diffusing on Ag(110) at $T = 550$ K. The simulation method is described in references [70, 58]. Full and open circles correspond to the equilibrium positions of the first and second layer atoms, respectively. A long jump (of two lattice cells) is evident, followed by a sequence of single jumps (back and forth between two equilibrium sites). The adatom oscillates in the well for hundreds of ps; the 'time of flight' during a jump (either single or double) is of the order of 1 ps.

[74, 7]. Therefore, after assuming this expression, the $p_l$ can be extracted from a fit to the experimental final-displacement distribution. Such a method requires huge statistics of atomic displacements, not easily achieved in experiments (see the case of Pd/W(211) [74]). On the other hand, this method does not allow to separate the true long jumps from other mechanisms which cause 'effective' long jumps (see the case of Pt/Pt(110) $(1 \times 2)$ [7], which is discussed in more detail in section 4.2). Another piece of indirect evidence for long jumps comes from helium scattering experiments, for example on Na/Cu(001) [75, 25] and on premelting of Pb/Pb(110) [76, 77]. In these experiments, the width $\Delta\omega$ of the quasi-elastic peak of the dynamic structure factor is measured as a function of the parallel momentum exchange $\mathbf{q}$; the functional form of $\Delta\omega(\mathbf{q})$ depends on the long jump probabilities as parameters, which are thus fitted on the experimental data. The main shortcoming of helium scattering is that it cannot separate single-particle from collective effects. Moreover, the coupling between diffusive and vibrational motion complicates the fitting at large $\mathbf{q}$ (see section 4.1 for a detailed discussion).

Finally, we would like to remark that the occurrence of long jumps may induce an additional temperature dependence in $\langle l^2 \rangle$ and thus in the prefactor of the diffusion coefficient, causing deviations from the Arrhenius law. This is especially true at high temperatures, where long jumps become more and more likely. However, in some cases, competing effects may compensate each other. For example, MD simulations of diffusion of Cu on Cu(110) [58] have shown that $\Gamma$ deviates from the low $T$ Arrhenius behaviour at $T > 400\,\mathrm{K}$, in such a way that the real rate is smaller than the one predicted from the extrapolation of the low $T$ Arrhenius law. However, a significant number of long jumps appear at $T > 400\,\mathrm{K}$, causing an increase of $\langle l^2 \rangle$ which compensates the deviation of $\Gamma$, so that the diffusion coefficient, given by equation (3), is almost perfectly fitted by an Arrhenius law.

The fact that long jumps may cause deviations from the Arrhenius law in the diffusion coefficient can be understood also by noticing that different barriers (and different Arrhenius behaviour) can be associated to jumps of different lengths, because *on the average*, jumps of different lengths need different energies (remember the meaning of the energy dissipation $\Delta$ above) [45, 7]. In this case the diffusion barrier is given by some average over the different activation energies.

### 2.1.2. *Exchange diffusion*

Even on flat surfaces the diffusion of adatoms may take place by other mechanisms than the jumps. The most common of such alternative processes is the exchange mechanism. In exchange diffusion, the adatom enters the substrate pushing up and replacing a substrate atom. At the end of the process, a new adatom diffuses on the surface (see figures 5–8). As mentioned earlier, the definition of the diffusion coefficient requires a modified definition of the 'adatom' co-ordinates. They should be replaced by the centre of mass coordinates of the moving complex. When dealing with homoepitaxial diffusion of well isolated adatoms, one considers the diffusive motion as if it were the random walk of an 'equivalent' single particle which is moving on the surface, forgetting that after each move, the diffusing particle is not the same as before. Indeed, exchange diffusion is especially important in homoepitaxial systems: in heteroepitaxy, if the adatom tends to incorporate into the substrate, it usually stays at the site where incorporation takes place (an exception to this behaviour is found in systems where vacancies are moving very fast, so that the

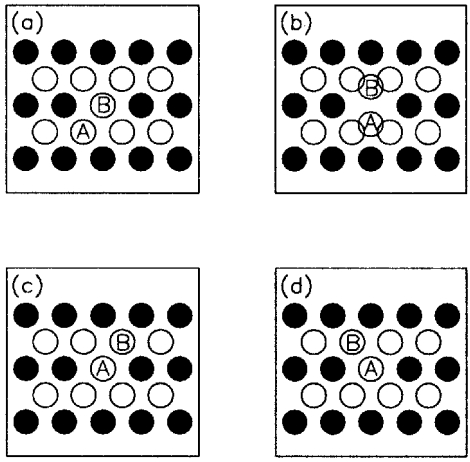


Figure 5. Simple exchange on an fcc(110) surface. The adatom (atom A) is initially on a hollow site in a channel along the [110] direction ($x$ direction in (a)); then atom A pushes one of the close-packed row atoms (atom B) into the symmetric dumb-bell configuration (shown in (b)). After staying for some time in this metastable configuration, the exchange can be completed either as in (c) (diagonal exchange) or in (d). Finally, B becomes the new adatom.

incorporated adatom moves by a vacancy-assisted mechanism. See for example the system In/Cu(001) [78]).

The exchange mechanism was first discovered in metal-on-metal diffusion, and in such systems exchange often plays a major role. Because of this, in the following examples we focus our attention on the diffusion of metal adatoms on metal surfaces. We treat both the simple exchange processes which have been observed both in experiments and in simulations, and the more complicated multiple-exchange and jump-exchange processes which have only been seen in simulations up to now, and are still waiting for an experimental verification.

*Simple exchange on rectangular symmetry: fcc(110) surfaces*—The role of exchange diffusion was first recognized in the case of the unreconstructed fcc(110) surfaces. These surfaces are highly anisotropic, with rows along the $[1\bar{1}0]$ direction (see figure 5). In 1978, Bassett and Webber [79] discovered by FIM that Pt/Pt(110) diffuses rapidly in the cross-channel direction already at very low temperatures. Since jump diffusion is unlikely in the [001] (cross-channel) direction, due to the very unfavourable position of the saddle point, this result was unlikely to be due to a simple thermally activated jump. A concerted exchange mechanism was proposed by Halicioglu and Pound [80]. In the concerted exchange (see figure 5), the adatom (atom A) pushes one atom of the row (atom B) out of it to an intermediate configuration (the dumb-bell configuration) where A and B occupy symmetric positions. This is often a slightly metastable configuration [81]. Simple bond-counting indicates that this configuration is more favourable than the saddle point for the cross-channel jump. After reaching the dumb-bell configuration, the two atoms may either come back to their original positions or complete the exchange move. In the latter case, atom B becomes the new adatom in the nearby channel. Atom B can end either in position (c) of figure 5 or in position (d). Ending up in (c) leads to a diagonal exchange. Ending up in (d) causes mass transport only along the

[001] direction. Experiments on Pt/Ni(110) and Ir/Ir(110) [82, 83] indicate that the diagonal exchange should be more likely; on the other hand, in MD simulations of Ag/Ag(110) [70] it has been found that both possibilities are equally likely. This different behaviour can be related to the depth of the metastable minimum in the dumbbell configuration. If the minimum is deep, the intermediate configuration is rather long-lived; atom B loses the memory of the initial direction of atom A, and the final position is chosen at random. The simulations show that a depth of about 0.02 eV is enough to randomize the final direction up to 600 K in the case of Ag. Many semiempirical total-energy calculations and MD simulations have been performed for exchange diffusion on the (110) surfaces of transition and noble metals [84–89, 58]. All these calculations agree in predicting that cross-channel mobility on such surfaces is possible essentially only by exchange. Unfortunately, both experiments and *ab initio* calculations are still lacking for exchange diffusion on noble metal surfaces. *Ab initio* calculations were performed for Al/Al(110) [90, 91], confirming that exchange is dominant. In this case, the calculations predict that also in-channel diffusion should occur through an exchange mechanism.

*Simple exchanges on square symmetry: fcc(001) surfaces* — Exchange was not believed to take place frequently on fcc and bcc(001) surfaces because they are less open than the fcc(110). However, this belief was contradicted first by the MD simulations [92] of bcc Lennard-Jones crystals, and by *ab initio* calculations for the Al/Al(001) system [93]. In particular, Feibelman [93] showed that a symmetrical position as in figure 6(b) is a favourable saddle-point configuration, because both the Al adatoms which are involved in the exchange can retain three covalent bonds in

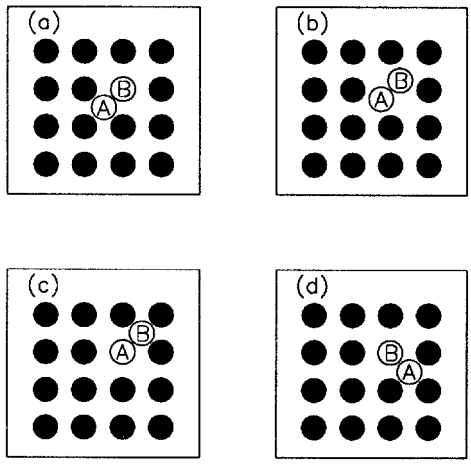


Figure 6. Simple exchange and single jump on an fcc(001) surface. The adatom (atom A) is initially at the fourfold hollow site (see (a)). In the exchange process, atom A pushes one of the neighbouring surface atoms (atom B) to the saddle point configuration as shown in (b). The exchange ends up as in (c), and causes mass transport in the diagonal direction. On the other hand, the jump process ends as in (d), and causes mass transport either in the $x$ or in the $y$ direction at each step. Therefore, the jump mechanism allows the exploration of the complete lattice of adsorption sites, while the exchange process allows the exploration of only one sublattice, i.e., of the one containing the sites that can be reached by making only diagonal moves from the starting point. This fact is the key point in the experimental demonstration of the occurrence of exchange diffusion on Pt/Pt(001) and Ir/Ir(001) [94, 95].

such a configuration. It has been demonstrated by FIM experiments that exchange diffusion is dominant for Pt/Pt(001) and Ir/Ir(001) [94, 95]. However, not in all fcc(001) metals is exchange diffusion more likely than jump diffusion. To a good approximation, the latter mechanism has barriers close to one sixth of the bulk metal cohesive energy [96]. Both semiempirical [87, 58] and *ab initio* [97] calculations predict that in Cu and Ag the activation barrier for jump is lower than the one for exchange, while on 5d metals (Ir, Pt, Au) the opposite is true. A first explanation of this finding was related to the surface tensile stress, which is higher in 5d metals [97]. This explanation has been criticized in [98], where it has been pointed out that the barrier for exchange is lower on those transition metal surfaces where the energy gain due to the substrate relaxation of the adatom is greater. On the other hand, tensile stress calculations along the exchange diffusion path show that lower exchange barriers do not correspond in general to larger tensile stress reductions [98].

*Multiple-exchange and jump-exchange processes*—The occurrence of multiple exchanges on metal surfaces was first observed in high-temperature simulations of Cu diffusion on flat Cu(001) [99]. Later, multiple exchanges were observed at terraces of stepped Cu(11$m$) surfaces ($m = 5, 7, 9, \ldots$) vicinal to Cu(001) [100, 101], and in other simulations [38, 69, 70, 58] on flat (001) and (110) surfaces. In a multiple exchange (see figure 7), the adatom enters the substrate and creates a strain along a close-packed row. Then an atom in the strained row is ejected above the substrate thus relieving the strain. The multiple exchanges may involve many atoms, and are usually characterized by large activation barriers [38]. However, at high temperatures, they become frequent (almost dominant) because the activation barrier is lowered when the substrate expands and its vibration amplitudes increase [38, 100, 101]. This is even more true at descending steps [39]. The multiple-exchange processes can be also described in the framework of the Frenkel–Kontorova model [102]; within this description, mass transport is caused by a solitonic mechanism. Jump-exchange and exchange-jump processes have been observed in simulations of

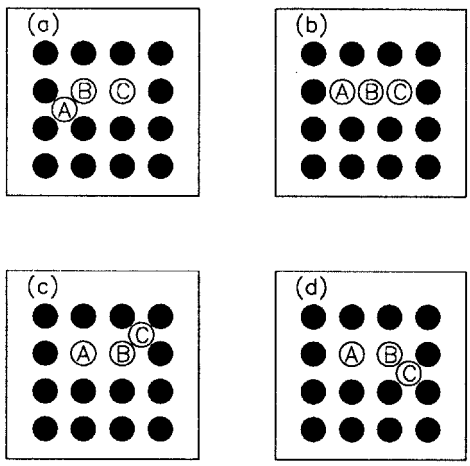


Figure 7. Schematic representation of a double exchange on an fcc(001) surface. Three atoms are involved in this process. Atom A enters the substrate, and a metastable configuration with the three atoms in the substrate is created as in (b). The successful completion of the process may end up either as in (c) or in (d).

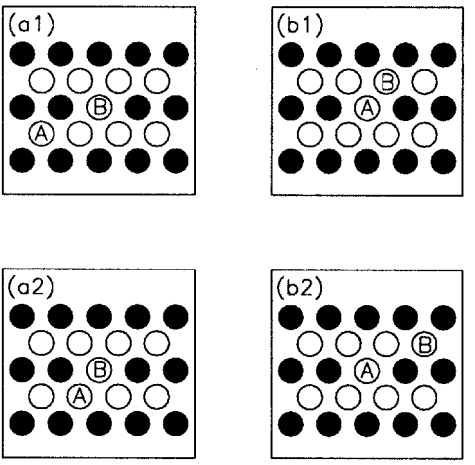


Figure 8. Schematic representation of the jump exchange ((a1)$\rightleftarrows$(b)) and exchange jump processes ((a2)$\rightleftarrows$(b2)) on an fcc(110) surface.

adatom diffusion on Ag, Cu and Au(110) (the latter in the unreconstructed geometry) [70, 58, 103, 104]. In a jump-exchange (see figure 8), the adatom diffuses first along the channel in the $[1\bar{1}0]$ direction without stopping in the nearest-neighbour cell. Then the adatom is pushed (or pulled) along the cross-channel direction while it is crossing the second saddle point, by one of the atoms of a nearby close-packed row. In this way, instead of performing a double in-channel jump, the adatom exchanges with the row atom and stops in the row. At high temperatures, these correlated events become a considerable fraction of the total exchanges, especially in Cu [58].

### 2.2. *Tracer and collective diffusion coefficients*

In this section, we consider the case of adparticles moving on an ideal substrate. The motion of the adparticles is diffusive rather than ballistic because of the frictional coupling to substrate excitations. The purpose of this section is to define precisely the two relevant transport coefficients for surface diffusion: the single-particle or tracer diffusion coefficient $D_t$ and the collective or chemical diffusion coefficient $D_c$. For any interacting many-particle system, it is important to make a distinction between these two. Moreover, we shall introduce two well-known approximations to the diffusion coefficients, namely the Dynamical Mean Field (DMF) theory and the Darken equation. These approximations are discussed in the framework of the Memory Expansion Method (MEM), which gives a systematic procedure to develop better and better approximations to the diffusion coefficients. The MEM is also a very useful practical tool in numerical simulations or even experimental measurements of diffusion.

#### 2.2.1. *Single-particle (tracer) diffusion*

We consider here a system of adparticles in equilibrium with the substrate. This is the only limit in which the diffusion coefficients of the adparticles can be defined precisely. In section 2.3 we will discuss approaches to generalize the concept of diffusion to nonequilibrium systems. The *tracer diffusion coefficient* $D_t$ is the relevant

transport coefficient for the simplest case where we can follow the diffusive motion of each individual adparticle [8]. In this case, $D_t$ is defined as

$$D_t = \lim_{t\to\infty} \frac{1}{2Ntd} \sum_{i=1}^{N} \langle |\mathbf{r}_i(t) - \mathbf{r}_i(0)|^2 \rangle = \lim_{t\to\infty} \frac{1}{2Nd} \frac{\mathrm{d}}{\mathrm{d}t} \sum_{i=1}^{N} \langle |\mathbf{r}_i(t) - \mathbf{r}_i(0)|^2 \rangle, \qquad (8)$$

where $N$ is the total number of adparticles in the system, $d$ is the spatial dimension (for surface diffusion $d = 2$), $\mathbf{r}_i(t)$ denotes the position of the $i$th particle at time $t$, and $\langle \cdot \rangle$ is the equilibrium ensemble average. The diffusion coefficient $D_t$ is well defined only when the asymptotic mean square displacement of each diffusing particle increases linearly with time [105, 106]. Equation (8) is valid for an isotropic system. The generalization to anisotropic systems is straightforward. In that case, one can define the corresponding diffusion coefficient along each principal axis with the coordinates $x_i(t)$ replacing $\mathbf{r}_i(t)$ in equation (8). There are several alternate forms of $D_t$ that are useful, and they follow readily from the definition in equation (8) [105]. The first is in terms of the velocity autocorrelation function:

$$D_t = \frac{1}{Nd} \sum_{i=1}^{N} \int_0^\infty \mathrm{d}t \langle \mathbf{v}_i(t) \cdot \mathbf{v}_i(0) \rangle. \qquad (9)$$

Equation (9) is known as the Green–Kubo formula [105]. From the Green–Kubo formula, a third expression for the tracer diffusion coefficient can be derived as

$$D_t = \pi \lim_{\omega\to 0} \omega^2 \lim_{q\to 0} \frac{1}{q^2} S_s(\mathbf{q}, \omega). \qquad (10)$$

This expression relates $D_t$ to the incoherent part of the dynamic structure factor $S_s(\mathbf{q}, \omega)$, a quantity of immediate experimental relevance, for example in incoherent neutron scattering [107], defined as

$$S_s(\mathbf{q}, \omega) = \frac{1}{2\pi} \int_{-\infty}^{+\infty} \mathrm{d}t \exp(-i\omega t) \frac{1}{N} \sum_{i=1}^{N} \langle \exp[-i\mathbf{q} \cdot (\mathbf{r}_i(t) - \mathbf{r}_i(0))] \rangle. \qquad (11)$$

Despite the apparent simplicity of the various definitions for $D_t$, there are many cases where the concept of tracer diffusion must be considered carefully. For many-particle diffusion, the concept of $D_t$ is useful only if individual particle trajectories can be identified—a task of considerable challenge for experiments. It is also possible that the substrate participates actively in the diffusion process. For example, in the exchange mechanism (discussed in section 2.1), an adatom can exchange position with the substrate particles, meaning that the particle diffusing along the surface is not the original one. Thus the strict definition of $D_t$ becomes meaningless. In more complicated mechanisms involving the concerted motion of a group of particles, the failure of the concept of tracer diffusion is even more obvious. However, we can extend the definition of $D_t$ to include such cases by interpreting the coordinate $\mathbf{r}_i(t)$ that appears in the formulae above as the centre of mass coordinate of the complex of atoms that is moving at time $t$.

The tracer diffusion coefficient $D_t$ can be expressed in terms of the total jump rate $\Gamma$ and the jump length distribution $p_\mathbf{l}$ (see section 2.1.1) in the ideal case where the

jumps are uncorrelated. In this case, we simply have

$$D_t = \frac{1}{2d}\,\Gamma \sum_{\mathbf{l}} l^2 p_{\mathbf{l}} = \frac{1}{2d}\,\Gamma \langle l^2 \rangle, \tag{12}$$

where $l^2 = \mathbf{l} \cdot \mathbf{l}$. If only nearest neighbour jumps are allowed then $l^2 = a^2$, where $a$ is the lattice constant. In general, there will be correlations between the jumps and there are corrections to the simple formula in equation (12). The generalization to include the correlation or memory effects is discussed in the following section 2.2.3.

Finally, we would like to mention that there are some cases where the adparticles can have rotational degrees of freedom characterized by a finite angular velocity $\mathbf{\Omega}_i$. This is the case for, e.g., polymers of rigid rodlike molecules on surfaces [108]. For such cases, the *rotational (tracer) diffusion coefficient* $D_r$ can be defined by [109]

$$D_r = \lim_{t \to \infty} \frac{1}{2Ntd} \sum_{i=1}^{N} \langle |\mathbf{u}_i(t) - \mathbf{u}_i(0)|^2 \rangle, \tag{13}$$

where $\mathbf{u}_i(t)$ is a unit vector parallel to the polymer. This definition is only valid for short times $D_r t \ll 1$; for a more general definition the corresponding Smoluchowski equation for rotational Brownian motion must be examined [109]. Another useful quantity is the *angular (tracer) diffusion coefficient* $D_\omega$ defined by [108]

$$D_\omega = \frac{1}{Nd} \sum_{i=1}^{N} \int_0^\infty \mathrm{d}t \langle \mathbf{\Omega}_i(t) \cdot \mathbf{\Omega}_i(0) \rangle. \tag{14}$$

This quantity can be used to study orientational correlations for rodlike molecules.

### 2.2.2. *Collective diffusion*

The *collective diffusion coefficient* $D_c$ measures the rate at which long-wavelength density fluctuations of particle (mass) density decay in the system [8, 110, 111, 22]. To this end, consider a system of $N$ interacting particles in $d$ dimensions. We denote by $\rho(\mathbf{r}, t)$ the coarse grained density at point $\mathbf{r}$ and at time $t$. Coarse graining means that it is averaged over a time scale around $t$ much larger than the microscopic time scale. Now we denote the deviation of the density from its equilibrium value as

$$\delta\rho = \rho(\mathbf{r}, t) - \langle \rho \rangle. \tag{15}$$

This deviation of the local density from the average can be either due to an external perturbation or just a thermal fluctuation.

In the presence of a density deviation, there is a corresponding flux $\mathbf{J}(\mathbf{r}, t)$ trying to restore the system to equilibrium. Expanding $\mathbf{J}(\mathbf{r}, t)$ to lowest order in the gradient of density (Fick's first law), we can write:

$$\mathbf{J}(\mathbf{r}, t) = -D_c \nabla \rho(\mathbf{r}, t). \tag{16}$$

The proportionality constant $D_c$ in equation (16) is by definition the collective diffusion coefficient. Combining the first Fick's law with the local continuity equation yields the diffusion equation (Fick's second law),

$$\frac{\partial \delta\rho}{\partial t} = \nabla \cdot (D_c \nabla \delta\rho). \tag{17}$$

Because we have kept only the lowest order gradient term in the expansion of $\mathbf{J}(\mathbf{r}, t)$ in the above derivation, Fick's law is only valid for small long wavelength density

fluctuations. Furthermore, Fick's law is also restricted to fluctuations at time scales much longer than the time scale required for the coarse graining procedure to obtain $\delta\rho$. This means that the collective diffusion coefficient $D_c$ is a measure of the decay of density fluctuations only at very large length and time scales.

It follows directly from Fick's law [8, 22] that the collective diffusion coefficient is related to the dynamical structure factor as

$$D_c = \frac{\pi}{S_0} \lim_{\omega \to 0} \omega^2 \lim_{q \to 0} \frac{1}{q^2} S(\mathbf{q}, \omega). \tag{18}$$

Here the coherent dynamic structure factor $S(\mathbf{q}, \omega)$ is the Fourier transform of the time-dependent dynamic structure factor $S(\mathbf{q}, t)$ defined as

$$S(\mathbf{q}, t) = \int \mathrm{d}\mathbf{r} \int \mathrm{d}\mathbf{r}' \exp\left[-i\mathbf{q} \cdot (\mathbf{r} - \mathbf{r}')\right] S(\mathbf{r} - \mathbf{r}', t), \tag{19}$$

where the density correlation function $S(\mathbf{r} - \mathbf{r}', t)$ is given by

$$S(\mathbf{r} - \mathbf{r}', t) = \frac{1}{N} \langle \delta\rho(\mathbf{r}', 0) \delta\rho(\mathbf{r}, t) \rangle = \frac{1}{N} \langle \delta\rho(\mathbf{0}, 0) \delta\rho(\mathbf{r} - \mathbf{r}', t) \rangle. \tag{20}$$

Equation (18) can be derived easily since an equation identical to equation (17) holds also for $S(\mathbf{q}, \omega)$ [22]. The quantity $S_0$ is defined by $S_0 \equiv S(\mathbf{q} = \mathbf{0}, t = 0)$. We note that the $q \rightleftarrows 0$ and $\omega \rightleftarrows 0$ limit in equation (18) is a reflection of the long wavelength and slow time variation restrictions for the validity of Fick's law.

In analogy to the case of tracer diffusion, one can also derive an Kubo–Green expression for the collective diffusion coefficient in terms of flux correlations [110]:

$$D_c = \frac{1}{N S_0 d} \int_0^\infty \mathrm{d}t \langle \mathbf{J}_T(t) \mathbf{J}_T(0) \rangle, \tag{21}$$

where $\mathbf{J}_T(t)$ is the total (velocity) flux given by

$$\mathbf{J}_T(t) = \sum_{i=1}^{N} \mathbf{v}_i(t). \tag{22}$$

The term $1/S_0$ is the so-called thermodynamic factor related to the isothermal compressibility $\chi_T$ of the system as follows [105]:

$$\chi_T = \frac{S_0}{\langle \rho \rangle k_B T}. \tag{23}$$

In the grand canonical ensemble, the thermodynamic factor can be expressed also in terms of the derivative of the chemical potential $\mu$, or the particle number fluctuation $\langle (\Delta N)^2 \rangle$:

$$\frac{1}{S_0} = \frac{1}{k_B T} \frac{\partial \mu}{\partial \log \theta} = \frac{\langle N \rangle}{\langle (\Delta N)^2 \rangle}, \tag{24}$$

where $\theta$ is the surface coverage defined as the ratio of the number of adatoms to the number of adsorption sites. These expressions are quite useful in numerical calculations, cf. section 3.5. The flux correlation function can be related to the mean square displacement of the collective co-ordinate $\mathbf{R} = \sum_i \mathbf{r}_i$ (which is $N$ times the co-ordinate of the centre of mass), in analogy to the case of tracer diffusion. It is

convenient to introduce the centre of mass (CM) diffusion coefficient $D_{CM}$ defined as

$$D_{CM} = \lim_{t\to\infty} \frac{1}{2Ntd} \langle |\mathbf{R}(t) - \mathbf{R}(0)|^2 \rangle. \tag{25}$$

Comparing this with (8), we recognize that $D_{CM}$ is just $N$ times the tracer diffusion coefficient for a fictitious single particle located at the CM position $\mathbf{R}/N$. $D_c$ can now be expressed as the product of two factors:

$$D_c = \frac{1}{S_0} D_{CM}. \tag{26}$$

Equation (26) is a useful starting point for calculation and interpretation of $D_c$ because it separates $D_c$ into the product of a true dynamical quantity $D_{CM}$ and a thermodynamic factor $1/S_0$ which is an equilibrium quantity related to the isothermal compressibility. Thus, all the dynamical correlations are contained in $D_{CM}$. However, $D_{CM}$ itself is also a meaningful physical quantity that can be directly compared with experimental measurements. An example where the concept of $D_{CM}$ is useful is the diffusion of an island or a cluster of atoms on a surface. This topic has received much attention recently [112–119], and will be discussed in section 4.9. Here, the traditional definitions of the collective diffusion coefficient $D_c$ and tracer diffusion coefficient $D_t$ are not appropriate, and the quantity relevant to the experimental measurement is closely related to $D_{CM}$.

We have already discussed above the close relationship between the two diffusion coefficients $D_{CM}$ and $D_c$. However, in general, no simple relation exists between either $D_{CM}$ and $D_t$, or $D_c$ and $D_t$. A simple relation between $D_{CM}$ and $D_t$ would indeed be very useful in practice, because (as we will discuss in the section on MC simulations) $D_{CM}$ is often much more difficult to calculate numerically than $D_t$. A rather popular *approximate* expression connecting $D_{CM}$ and $D_t$ is the so-called Darken equation [8], which reads

$$D_c = \frac{1}{S_0} D_t. \tag{27}$$

By comparing equation (26) and equation (27), it can be easily seen that the Darken equation simply amounts to approximating $D_{CM}$ by $D_t$. However, it can be shown rigorously [110] that the two coefficients $D_t$ an $D_{CM}$ are equal only for non-interacting systems. For any realistic interacting system (including even the simple Langmuir gas model, a lattice-gas model where the only interaction is site exclusion, see figure 9), the validity of this heuristic approximation of setting them equal is not apparent, and will be discussed later on. Because of that, a more systematic method for deriving approximations for the diffusion coefficients is needed, and this is the subject of the next section.

### 2.2.3. *The memory expansion method*

In the last two sections, we have introduced several expressions for the tracer and collective diffusion coefficients. Some of them, equations (8), (10) and equations (18), (25) explicitly involve correlations in the long-time or small-frequency limit. In the numerical evaluation of diffusion coefficients, for example through Monte Carlo or Molecular Dynamics simulations, these expressions present difficulties because of the decreasing statistics at longer and longer times. Consider for example the co-ordinate $\mathbf{r}(t)$ of a particle, to calculate $\Delta\mathbf{r}^2(t) = \langle [\mathbf{r}(t) - \mathbf{r}(0)]^2 \rangle$. The tracer diffusion coefficient

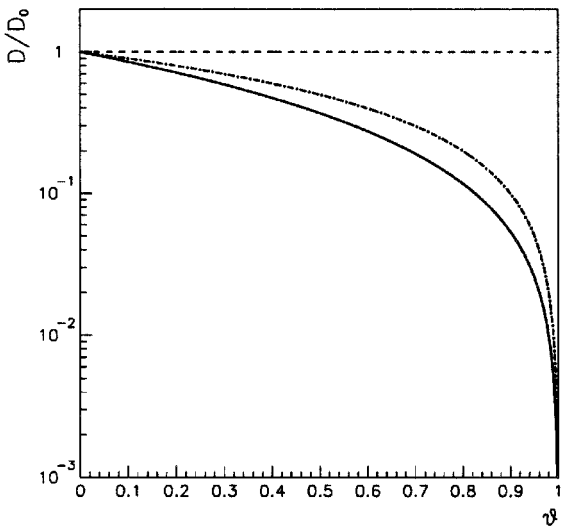


Figure 9. Behaviour of $D_t$ (full line), $D_c$ (dashed line) and $D_{CM}$ (dash-dotted line) as functions of the coverage $\theta$ for the Langmuir gas on a square lattice. $D_0$ is the common value of the diffusion coefficients in the limit $\theta \rightleftarrows 0$. The Langmuir gas is a lattice gas model where the only interaction among the particles is site exclusion. In this case $D_{CM}/D_0 = 1 - \theta$ (the DMF is exact for $D_{CM}$ in the Langmuir gas) and $S_0 = 1 - \theta$, so that $D_c = D_0$ independent of $\theta$ [8]. $D_t$ is very well approximated by the expression $D_t/D_0 = (1 - \theta)[1 - 2\theta/(6 - \theta - 2\xi + \xi\theta)]$, where $\xi = 10440/9443$ [148]. Even in this simple case memory effects on $D_t$ are different than those on $D_{CM}$, and the Darken equation (27) is not exact.

$D_t$ is related to the asymptotic slope of $\Delta\mathbf{r}^2(t)$ at long times. In interacting systems at low temperatures, for example when ordered phases are present, the asymptotic regime will be reached at very late times only (see figure 10). The time $t_m$ when this happens signals the onset of the hydrodynamic regime. After having reached this regime, one has to go further for rather long times in order to get a good estimate of the slope. In many cases, this is cumbersome, essentially because the statistical

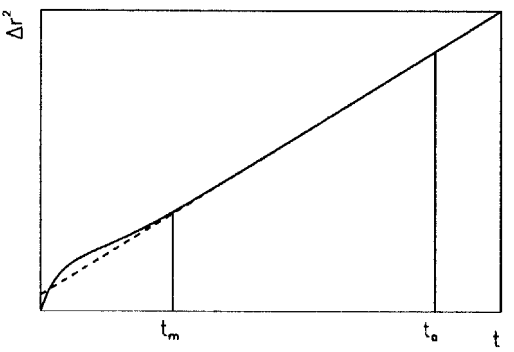


Figure 10. Typical behaviour of the mean square displacement $\Delta\mathbf{r}^2(t)$. The onset of the hydrodynamic regime is at $t = t_m$; at $t_m$ the memory expansion also converges. On the other hand, for a direct evaluation of the diffusion coefficient via equations (8), (25), $\Delta\mathbf{r}^2(t)$ must be followed for some $t_a \gg t_m$.

accuracy of $\Delta\mathbf{r}^2(t)$ decreases with increasing time for a fixed number of simulation runs and particles in the system. Therefore, an accurate calculation of the asymptotic slope becomes time consuming. The other expressions involving the velocity correlations, equation (9) (or equation (21)), have contributions mainly from the short time regime. However, the evaluation of the velocity variable is more challenging than the position variable, and in the case of Monte Carlo simulations (see section 3.5.), the velocity is not even well-defined. The familiar expression in equation (12) gives the diffusion coefficient in terms of the product of jump rate and the mean square jump length and is widely used. This involves only the short time physical quantities and is easy to compute. However, as mentioned earlier, it neglects the correlations (memory effects) between successive jumps.

In this section, we present alternate expressions for the diffusion coefficients under the name of 'Memory Expansion Method' (MEM) [120, 121]. They provide a better insight into the connection between the collective and tracer diffusion coefficients, the role of interactions, and most importantly, a much better practical expressions for numerical evaluation of the diffusion coefficients. The MEM essentially converges at $t_m$ (see figure 10), and therefore the calculation of $D_t$ necessitates much shorter simulations (or gives better statistics from the same simulation) than the use of the straightforward definition through $\Delta\mathbf{r}^2(t)$. The same happens for the CM diffusion coefficient $D_{CM}$, and this is even more important since, as we shall see in the following, $D_{CM}$ is not a self-averaging quantity (each simulation gives a single sample), and therefore is much more difficult to calculate than $D_t$.

In the following we first derive the MEM for $D_{CM}$, and then consider the MEM for $D_t$. From equation (25), it turns out that if we define $\mathbf{R}(t)$ as

$$\mathbf{R}(t) = \sum_{i=1}^{N} [\mathbf{r}_i(t) - \mathbf{r}_i(0)], \tag{28}$$

in an isotropic 2D system, then $D_{CM}$ is given by

$$D_{CM} = \lim_{t\to\infty} \frac{1}{4Nt} \langle \mathbf{R}^2(t) \rangle. \tag{29}$$

Now divide the time $t$ into $P$ equal intervals of length $\tau_0$, so that $t_p = p\tau_0$ and $p = 0, 1, \ldots, P$. From these definitions it follows that $\mathbf{R}(t) = \mathbf{R}(P\tau_0) = \sum_{p=1}^{P} \delta\mathbf{R}(t_p)$, where $\delta\mathbf{R}(t_p) \equiv \mathbf{R}(t_p) - \mathbf{R}(t_{p-1})$. We remark that, in principle, the observation interval $\tau_0$ can be chosen arbitrarily, but it should be considerably less than $t_m$ so that no information is lost [120, 122]. Having then defined the coefficients

$$C_c(p\tau_0) = \langle \delta\mathbf{R}(\tau_0) \cdot \delta\mathbf{R}((p+1)\tau_0) \rangle, \tag{30}$$

the following expansion can be obtained:

$$D_{CM} = \frac{1}{4N\tau_0} \left[ C_c(0) + 2 \sum_{p=1}^{\infty} C_c(p\tau_0) \right]. \tag{31}$$

In the case of $D_t$, the MEM leads to the analogous expression:

$$D_t = \frac{1}{4N\tau_0} \left[ C_t(0) + 2 \sum_{p=1}^{\infty} C_t(p\tau_0) \right], \tag{32}$$

where

$$C_t(p\tau_0) = \sum_{i=1}^{N} \langle \delta \mathbf{r}_i((p+1)\tau_0) \cdot \delta \mathbf{r}_i(\tau_0) \rangle, \tag{33}$$

and $\delta \mathbf{r}_i((p+1)\tau_0)$ is the displacement of particle $i$ between times $(p+1)\tau_0$ and $p\tau_0$.

There are several remarks to be made regarding the MEM. First, it should be noted that it is *not* a trivial discretization of the integral in equation (9) (or equation (21)). Rather, for discrete time steps it is a formally exact decomposition of equations (8) and (25). As such, it offers a better way of controlling the approach to $t_m$ than the traditional methods. We note that the MEM is valid for an arbitrary choice of $\tau_0$. Second, MEM allows one to define *generalized velocity autocorrelation functions* for cases, where true velocities are not available (e.g., MC simulations). This facilitates the quantitative study of memory effects, as will be demonstrated in section 4.6.

At low temperatures, the adparticles are localized most of the time about the adsorption sites with occasional jumps to neighbouring sites. This is the so-called lattice gas limit. The MEM yields a particularly simple insight into the memory effects and the relation between $D_{CM}$ and $D_t$ in this limit. Consider the first term in the memory expansion. Each of the $N$ particles in the system is jumping between the lattice sites at a frequency $\Gamma = \tau^{-1}$, where $\tau$ is the average time interval between subsequent jumps. This means that, on the average, each of the $N$ particles jumps once during $\tau$, so that $N$ jumps are expected in the interval $\tau$. Now we choose $\tau_0 = \tau/N$ so that on the average, only one particle jumps in the time interval $\tau_0$. In this case, this jump alone (say of a particle $i_1$) contributes to the sums in $C_c(0)$ and $C_t(0)$ such that

$$C_c(0) = \left\langle \sum_{i=1}^{N} [\mathbf{r}_i(\tau_0) - \mathbf{r}_i(0)] \cdot \sum_{j=1}^{N} [\mathbf{r}_j(\tau_0) - \mathbf{r}_j(0)] \right\rangle = [\mathbf{r}_{i_1}(\tau_0) - \mathbf{r}_{i_1}(0)]^2 = a^2, \tag{34}$$

where $a$ is the lattice spacing and we have assumed jumps to the nearest neighbours only. The same result can be obtained also for $C_t(0)$. If the successive jumps of the adparticles are uncorrelated, then all the other terms in the MEM vanish. Thus, the approximation of keeping the first term only in the MEM amounts to neglect memory effects or correlations between jumps and has been dubbed the 'Dynamical Mean Field' (DMF) theory [123, 111, 124, 125]. Thus the DMF expressions for the diffusion coefficients in the lattice-gas limit are:

$$D_{CM}^{\mathrm{DMF}} = D_t^{\mathrm{DMF}} = \frac{a^2\Gamma}{4}. \tag{35}$$

In interacting systems $\Gamma$ depends both on the coverage $\theta$ and on the temperature $T$. On the other hand, the exact expressions for $D_t$ and $D_c$ can be decomposed as follows:

$$\begin{aligned} D_{CM} &= \frac{a^2\Gamma}{4} f_t; \\ D_c &= \frac{a^2\Gamma}{4S_0} f_c, \end{aligned} \tag{36}$$

where $f_t(\theta, T)$ and $f_c(\theta, T)$ are the *tracer and collective correlation factors*, respectively, which take into account all the memory effects. The DMF is recovered at $f_t = f_c = 1$.

Alternatively, the DMF for the lattice gas model can also be derived through the Mori Projection operator (PO) formalism [126, 127], or using the Greens Function method [128–130]. The PO technique leads to the following expression [131, 124, 22]:

$$S(\mathbf{q}, \omega) = \frac{1}{\pi} \mathcal{R}\left\{ \frac{S(\mathbf{q})}{i\omega + \Omega_0(\mathbf{q}) + M(\mathbf{q}, i\omega)} \right\}, \tag{37}$$

where $\mathcal{R}\{\cdot\}$ indicates the real part, $\Omega_0(\mathbf{q})$ is the frequency function, and $M(\mathbf{q}, i\omega)$ is the memory function. $\Omega_0(\mathbf{q})$ has a simple expression

$$\Omega_0(\mathbf{q}) = \frac{a^2 \Gamma}{n_s S(\mathbf{q})} \sum_{\mathbf{a}} [1 - \exp(i\mathbf{q} \cdot \mathbf{a})], \tag{38}$$

where the sum is extended to all NN site vectors $\mathbf{a}$. When the memory function $M$ is set to zero, applying equation (18) to $S(\mathbf{q}, \omega)$ in equation (37) leads to precisely the DMF expression for $D_c$ as given in equation (35). A similar expression can be derived for $D_t$.

Although equation (37) is more compact than the MEM expansion, the memory function $M(\mathbf{q}, i\omega)$ involves complicated expressions and is not tractable in practice. It incorporates all the terms in the MEM beyond the leading term. Neglecting the memory function, the advantage of equation (37) is that a complete expression for the dynamic structure factor is given, and not only an expression for the diffusion coefficient.

Examples of the behaviour of $S_0$, $\Gamma$ and $D_c$ for some lattice-gas models are given in figures 9, 12, 13 and 14, just to show that complex behaviours arise already in quite simple models. For details, the reader is referred to the original literature (see the captions of the above figures). Other examples, related to a model of O/W(110) are found in section 4.5.

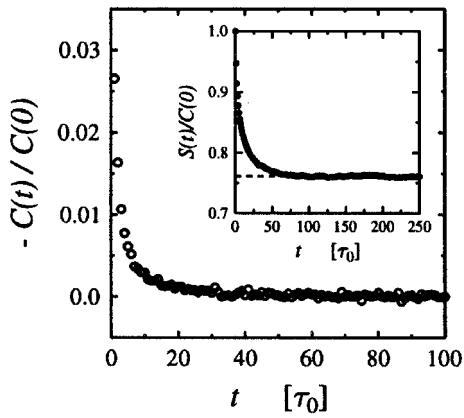


Figure 11. Example of the convergence of the memory expansion for the model of O/W(110) described in section 4.5, at $\theta = 0.45$ and $T = 0.833 T_c$, in the case of $D_{CM}$ [121]; the inset shows the partial sums $S(t = p\tau_0) = C(0) + 2\sum_{k=1}^{p} C(k\tau_0)$ (see equation (31)).

We wish to make some final comments about the relationship between the exact values of the diffusion coefficients, the DMF approximation and the Darken equation. From the above expressions, it turns out that the DMF amounts to treating subsequent transitions in the system as if they were independent (this corresponds to the Markovian limit, i.e. neglecting the memory effects). On the other hand, the Darken equation approximates $D_{CM}$ with $D_t$ and therefore this amounts to assuming that memory contributions to $D_{CM}$ and to $D_t$ are the same. But from equations (31) and (32) it follows that memory corrections cannot be the same for both diffusion coefficients, so that $D_{CM}$ and $D_t$ must be different for any system with interparticle interactions. In section 4.6, we shall show through a practical example how both approximations (DMF and Darken) compare to the 'exact' numerical results. Here we remark only that the DMF (equation (35)), or its equivalent formulations, have been used rather extensively in connection with lattice-gas models [125, 122, 132–145] giving always a very good qualitative estimate of the behaviour of $D_c$. Very often, also the quantitative agreement can be quite good [125, 146], especially in the disordered regions of the phase diagram. However, when ordered phases are present, memory effects must be included for a precise evaluation of $D_c$ and they even influence the effective activation barriers [147, 122]. Concerning $D_t$, equation (35) is a much poorer approximation, which can be somewhat improved by multiplying it by the tracer correlation factor of the Langmuir gas [125, 148]. Usually, memory effects slow down diffusion which is evident in the fact that the correlation factors are smaller than unity. In fact, the leading memory effect is the backward correlation of the second jump with respect to the first, since the first jump leaves a vacancy behind. On the other hand, memory effects are stronger on single-particle motion than on centre-of-mass motion, where most of the above backward correlations cancel out. This is the reason why the DMF approximation usually overestimates the diffusion coefficients, while the Darken equation gives a lower bound to $D_c$.

## 2.3. *Nonlinear and nonequilibrium diffusion*

### 2.3.1. *Modified diffusion equations*

In the previous sections, we have introduced the collective diffusion coefficient $D_c$ which is actually a transport coefficient introduced through the Fick's law in the current response of a system to a density gradient, as given in equation (16). For simplicity of discussion, we have assumed an isotropic system so that $D_c$ is just a scalar. It is important to note that for the Fick's law to be valid, one has to be in the linear regime of vanishingly small density gradient [149]. In general, the total flux $\mathbf{J}_{\text{tot}}$ can be expressed as a complicated functional $\mathbf{f}$ of the density function $\rho(\mathbf{r})$ in the form

$$\mathbf{J}_{\text{tot}} = \mathbf{f}[\rho(\mathbf{r})] = -D_c \nabla \rho + \mathcal{O}((\nabla \rho)^2)). \tag{39}$$

In the limit of a vanishingly small density gradient, one can discard the higher order terms and recover equation (16), defined earlier in the linear regime which then leads to Fick's law. We are not aware of any works on the corresponding macroscopic nonlinear diffusion equation in surface diffusion problems. There exists a general mesoscopic theory of diffusion for the case where there is a large gradient present and the microscopic dynamics follows Arrhenius behaviour [150]; however this has not been applied to surface diffusion, either.

The special case of a constant gradient in density has been analyzed recently by Chvoj [151] in the context of a lattice gas model and quasi-chemical approximation. The basic assumption is that the relaxation of the gradient is a slow process and only the fluctuations around this mean density are taken into account. In this case, the tracer diffusion coefficient $D_t$ is always reduced in magnitude proportional to $(\nabla\rho)^2$ as compared to its equilibrium value. On the other hand, the effective $D_c$ is proportional to the difference between the mean jump rates in the direction of $\nabla\rho$ and to the opposite direction. It remains positive for repulsive and weakly attractive interactions in the model, but may become negative in general indicating the need to include additional nonlinear terms. The analysis indicates that deviations of the effective diffusion coefficients from their equilibrium values are more pronounced near the phase boundaries of order-disorder transitions, in accordance with Boltzmann–Matano analysis [152, 153] (see the following section 2.3.2). The same case of a constant gradient in density has also been analyzed [154] by the projection operator techniques developed by Kawasaki [155]. This leads to a general (but complicated) equation of motion for the dynamic structure function, from which $D_c$ can be extracted in principle.

Far-from-equilibrium order-disorder dynamics has been studied for lattice-gas models (see section 3.5) in the mean-field approximation [156, 157]. In this approximation, the occupation variables in the master equation (see equation (98) in section 3.5) are replaced by their averages. The diffusion in a square lattice-gas with repulsive interactions has been studied within this approach [157], extracting $D_c$ via the Boltzmann–Matano analysis, and obtaining, below $T_c$, a sharp increase of $D_c$ at $\theta > 0.5$, in analogy with the equilibrium results shown in figure 12.

Another version of the diffusion equation with an additional term of the form $\rho|\nabla\rho|$ has been analyzed extensively in the context of hydrodynamics [158]. However, perhaps a more relevant equation from the surface diffusion point of view is the case where there are additional (non-equilibrium) relaxational processes present with a flux term $\tau_r(\partial\mathbf{J}/\partial t)$, leading to the Telegrapher's equation [159]

$$\frac{\partial\rho}{\partial t} + \tau_r \frac{\partial^2\rho}{\partial t^2} = D\nabla^2\rho, \tag{40}$$

where $\tau_r$ is a relaxation time of the flux. Physically, this equation corresponds to correlated random walk [159]. We are not aware of any analysis of surface diffusion problems with equation (40), either.

### 2.3.2. *Diffusion and spreading of density profiles*

A classical and widely used method to determine the collective diffusion coefficient $D_c(\rho)$ is based on the so-called Boltzmann–Matano (BM) method [8, 160, 161]. In the BM method, an inhomogeneous density profile $\rho(x, t)$ is created at the beginning, and then allowed to spread diffusively. Assuming that the diffusion equation is valid, an expression for $D_c(\rho)$ can be obtained from scaled density profiles as

$$D_c(\rho) = -\frac{1}{2t}\left(\frac{dx}{d\rho'}\right)\Bigg|_{\rho} \int_0^{\rho} x(\rho')\,\mathrm{d}\rho'. \tag{41}$$

The BM method is based on the assumption that, in the long-time limit, the density profiles $\rho(x, t)$ collapse to a single scaling function when expressed as $\rho(x/\sqrt{t})$. If this condition is truly satisfied, $D_c(\rho)$ obtained from equation (41) corresponds to the

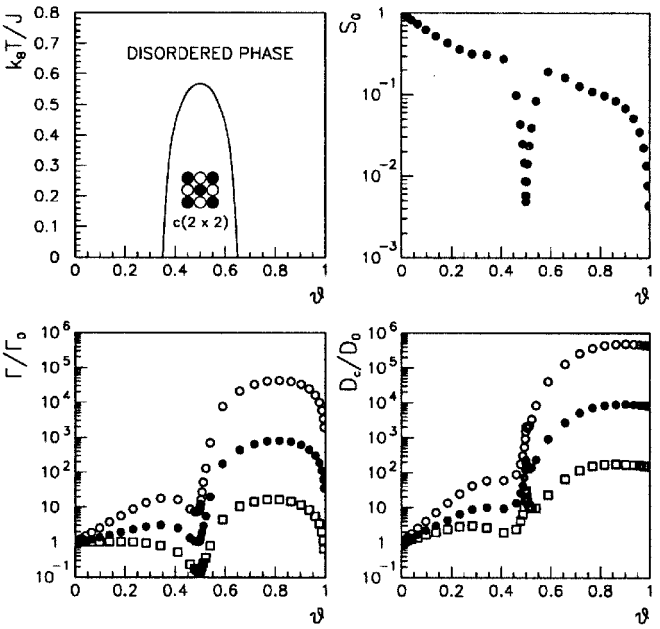


Figure 12. Numerical results for $S_0$, $\Gamma$ and $D_c$ (the latter in the DMF approximation) in a square lattice gas model with repulsive NN interactions and Initial Value kinetics with saddle point interactions (see section 3.5). Details about the model are found in references [22, 135]. In the top left panel, a schematic picture of the phase diagram is given. The results are calculated well below the critical temperature, at $k_BT/J = 1/3$ ($J$ is the strength of the NN repulsion). The full dots correspond to no saddle-point interactions, the open squares and circles correspond to positive and negative saddle point interactions $J'$ respectively ($J' = \pm k_BT$). The general trend is that positive (repulsive) values of $J$ enhance the average jump rate $\Gamma$ and lower $S_0$, i.e., the compressibility. Positive values of $J'$ raise the saddle-point energy, thus depressing $\Gamma$; negative values of $J'$ have the opposite effect. Both $S_0$ and $\Gamma$ show deep minima at $\theta = 0.5$, corresponding to the perfect ordered phase. The complicated behaviour of $D_c$ at low temperatures arises from the competition between these effects ($D_c = \Gamma/S_0$ in the DMF approximation).

actual diffusion coefficient in equilibrium. However, the BM method can be taken as an operational tool and applied to *any* density profile measured from an experiment or computer simulation, as long as the profiles change slowly enough that they exhibit scaling behaviour within some time regime. The corresponding $D_c(\rho)$ as determined from equation (41) then corresponds to an *effective, non-equilibrium* quantity, which may show significant deviations from its equilibrium limit [152, 153]. This is particularly the case for multilayer droplet spreading [162], or cases where there are density-dependent ordered phases present in the overlayer [163, 164, 152, 153]. Nevertheless, the BM method constitutes a useful tool to measure the effects of nonequilibrium conditions to surface diffusion.

2.3.3. *Diffusion during domain growth*

A particularly interesting special case on nonequilibrium mass transport occurs under growth conditions where large density gradients may exist on the surface. In fact, in practice such conditions occur more often than the small gradient

environment required for the linear equilibrium diffusion analysis. The diffusive motion of the adatoms clearly plays an important role in these nonequilibrium processes which include epitaxial growth, catalysis and ordering. The BM method presented above gives an operational way to compute an effective $D_c(\rho)$ from a set of density profiles. The question now is that is it possible under suitable conditions to define generalized non-equilibrium 'diffusion coefficients' in the same manner that we define the equilibrium diffusion coefficients, in terms of measurable correlation functions? This question has been addressed in the work of Vattulainen *et al.* [165], where the concept of equivalent time scales is introduced. To this end, let us assume that the system is in a state of nonequilibrium with excess free energy, and relaxing toward equilibrium in time such as in the case of domain ordering. First we define the normalized excess energy of the system as

$$F(T,t) = \frac{E_{ex}(T,t)}{E_{ex}(T,0)}, \tag{42}$$

with $E_{ex}(T,t)$ defined as the excess energy of the system over the equilibrium value,

$$E_{ex}(T,t) = E(T,t) - E(T,\infty). \tag{43}$$

The equivalent time regimes at different temperatures are chosen as intervals between times $t_n(T)$ with integer $n > 0$, which satisfy

$$F(T, t_n(T)) = \exp(-n). \tag{44}$$

Using these ideas, the tracer and collective diffusion coefficients within each time interval $[t_n, t_{n+1}]$ can be defined as follows. For tracer diffusion, we consider the quantity

$$\Omega_{\alpha\alpha}^{(n)}(\delta t) = \frac{1}{4N} \sum_{k=1}^{N} \langle |r_{\alpha,k}(t_n + \delta t) - r_{\alpha,k}(t_n)|^2 \rangle \tag{45}$$

with the time difference $\delta t$ restricted to $0 \le \delta t < t_{n+1}(T) - t_n(T)$. The effective tracer diffusion (or mobility) coefficient within the $n$th time regime $D_{T,\alpha\alpha}^{(n)}$ can be defined as the effective slope of $\Omega_{\alpha\alpha}^{(n)}$ within the $n$th time interval.

Similarly, an effective collective diffusion (mobility) coefficient $D_{c,\alpha\alpha}^{(n)}$ can be extracted from the spatially and temporally dependent density fluctuation correlation function

$$S^{(n)}(\mathbf{r}, \mathbf{r}', \delta t) = \langle \delta\rho(\mathbf{r}, \mathbf{t}_n + \delta\mathbf{t}) \delta\rho(\mathbf{r}', \mathbf{t}_n) \rangle. \tag{46}$$

In section 4.7, we will demonstrate and discuss the application of this formalism to non-equilibrium diffusion for a lattice-gas model of O/W(110).

### 2.3.4. *Sliding friction and diffusion*

In recent years, the dynamical response of a system to an external driving force has been the focus of many studies in connection with the problem of boundary lubrication [166] as well as electrical conductance in type II superconductors [167]. For these systems, the dynamical response is commonly analyzed in term of the sliding friction $\bar{\eta}$. This is defined through the relation

$$\langle \mathbf{v}_d \rangle = \frac{1}{m\bar{\eta}} \mathbf{F}. \tag{47}$$

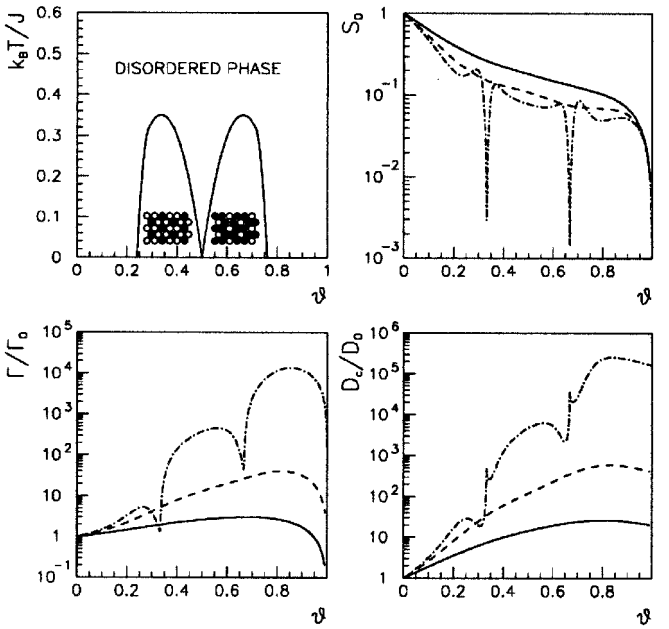


Figure 13. Numerical results for $S_0$, $\Gamma$ and $D_c$ (the latter in the DMF approximation) in a hexagonal lattice gas model with repulsive NN interactions, and Initial Value kinetics with saddle point interactions (see section 3.5). Details about the model are found in references [22, 135]. In the top left panel, a schematic picture of the phase diagram is given. The results are calculated at $k_BT/J = 1$, 0.5 (above the critical temperature $T_c$) and 0.25 (below $T_c$; full, dashed and dash-dotted lines, respectively). $J$ is the strength of the NN repulsion. At low temperatures, two perfect ordered phases are found at $\theta = 1/3$ and $2/3$. Around these coverages, the behaviour of $D_c$ results from the competition between a small $S_0$ (low compressibility) and a small jump rate $\Gamma$.

Thus $1/(m\bar{\eta})$ is the ratio of the induced drift velocity $\mathbf{v}_d$ to a driving force $\mathbf{F}$. It is important to note that the sliding friction is a macroscopic transport coefficient and is in general different from the microscopic friction that enters the Langevin description of the stochastic dynamics of the system as discussed in section 3.3.

There is an interesting relation between the sliding friction $\bar{\eta}$ and the collective diffusion constant $D_c$ in the linear regime. Consider a closed system with the driving force $\mathbf{F}$ as arising from an external potential $\phi$. At equilibrium, the current resulting from this external driving force is exactly balanced by the current generated by the density gradient in the opposite direction. Thus from equations (16) and (47) the following relation results:

$$D_c = -\frac{\rho}{m\bar{\eta}} \frac{\partial \phi}{\partial \rho}. \tag{48}$$

The quantity $\partial\phi/\partial\rho$ can be related to the isothermal compressibility $\chi_T$ through the well-know relation

$$\frac{\partial \phi}{\partial \rho} = -\frac{1}{\rho^2 \chi_T}. \tag{49}$$

The relation between $D_c$ and $\bar{\eta}$ as shown in equation (48) has also been derived by Persson [166] in a slightly different form. It follows from the general theory of linear response [106] that the sliding friction defined in equation (47) can be expressed in terms of the equilibrium time dependent flux–flux correlation function as

$$\frac{1}{m\bar{\eta}} = \frac{1}{dNk_BT}\int_0^\infty dt\langle \mathbf{J}_T(t)\cdot\mathbf{J}_T(0)\rangle. \tag{50}$$

Combining the results of equations (48) and (50) then leads to the well know Green–Kubo relation for $D_c$ in equation (21). Thus, the sliding friction is related to the centre of mass or mobility factor $D_{CM}$ without the thermodynamic factor which depends only on equilibrium properties of the system.

As discussed previously, in the nonlinear response regime where there exist large density gradients and the system is strongly inhomogeneous, the diffusion coefficient introduced through Fick's law is not of much use and at best one can only hope to describe a local region by a density dependent $D_c$. However, in the context of a system subject to a large external driving force $\mathbf{F}$, the sliding friction defined through equation (47) remains a perfectly useful concept. For an open system or a system with a source or a sink, the driven system under a large external force can be in a steady state with a constant drift velocity and uniform density. The corresponding sliding friction $\bar{\eta}$ would of course depend on the magnitude of the force $F$ itself in this nonlinear regime. Beyond a critical force $F_c$, the nature of the diffusion changes from an activated form with a finite diffusion barrier to nonactivated behaviour with the drift velocity $v_d$ rising rapidly in proportion to the driving force.

The whole subject of the dynamical response of an adsorbate layer under a driving force has received much attention recently. It is relevant for such diverse areas as boundary lubrication and vortex lattice dynamics in type II superconductors. The critical force basically determines the static friction between two macroscopic blocks with a boundary layer of lubricant in the microscopic contact areas in the case of boundary lubrication, and the magnitude of the critical current for the type II superconductors [167]. In the steady drifting state, the nonlinear nature of the problem gives rise to a rich variety of dynamical phases and the transitions between them lead to macroscopic observable behaviour such as stick-slip motion. For a detailed discussion of physics in this rich nonlinear regime, we refer the reader to the literature [166].

## 3. Theoretical approaches

This section treats the modern theoretical approaches relevant to the study of classical surface diffusion. First, we focus on the diffusion of isolated adatoms. In section 3.1 we introduce the concept of an adiabatic potential. The adiabatic potential is an equilibrium temperature-dependent quantity; the adiabatic potential difference between the saddle point along the diffusion path, and the nearby minimum defines the adiabatic barrier $E_A$, which enters the Arrhenius law (equation (1)). In the limit $T \rightleftarrows 0$, $E_A$ coincides with the potential energy barrier. This is the most commonly calculated quantity by different approaches, either *ab initio* or semi-empirical. However, the dynamical coupling between the adatom and the substrate is not contained in the adiabatic potential: in terms of the Arrhenius law, the dynamics enters the prefactor and not the activation barrier. The exact study of this dynamical coupling being well outside present possibilities, one has to resort to approximate

dynamical descriptions. The simplest, and very widely used, is the Transition State Theory (TST), which is the subject of section 3.2. Even in its most complete form, TST is not suited for the study of systems where the dynamical coupling is weak. This drawback can be overcome within the Langevin (Fokker–Planck) approach, which indeed includes TST as a special limit. The Langevin approach is treated in section 3.3. A powerful tool for solving the Langevin dynamics is the path integral approach (section 3.4).

The theoretical study of surface diffusion is often accomplished also by simulation methods, such as Monte Carlo (MC) and Molecular Dynamics (MD). These are the subjects of sections 3.5 and 3.6, respectively. MC simulations are more commonly used when treating dense overlayers within the lattice gas model. This is a very useful approximation when dealing with diffusion in strongly interacting systems of many particles, and especially when studying long-wavelength and slowly decaying density fluctuations. The MD technique, on the other hand, solves explicitly the equations of motion for a given interaction potential. MD simulations are much more accurate than MC modelling from the microscopic point of view, but they are limited to much shorter time scales and to much smaller systems, even if the situation has improved recently due to the development of accelerated MD methods.

All the theoretical methods described in the following have both merits and drawbacks, and preference to one or to another is given depending on the issues on hand and the system under study. Generally, analytic approaches such as Langevin or Fokker Planck equation yield more insights to the underlying physics at the expense of some simplifications, such as using a model friction to describe the non-essential degrees of freedom. The simulation methods yield more realistic results for actual physical systems but give relatively little insight into the basic physics. Whatever the approach chosen, the theoretical study of surface diffusion is not simply the accurate determination of static energy barriers as often overemphasized in the literature. The determination of the diffusion barrier is an important step, and it is the main factor that controls the magnitude of the diffusion constant at low temperatures. However, the diffusion coefficient is intrinsically a dynamic quantity. While the barrier plays an important role, it is only an equilibrium property. It is the prefactor which contains the true dynamical information, and the theoretical challenge is to understand this quantity properly within a dynamical theory. Quite often, the prefactor is arbitrarily assigned some typical values or evaluated in the framework of TST. This works reasonably for several systems but misses out some important physics. In many systems, the frictional coupling with the substrate must be taken explicitly into account, and memory effects cannot be left out. Finally, at high temperatures, the separation itself of the diffusion coefficient into prefactor and exponential factor becomes arbitrary, and the Arrhenius law does not hold.

## 3.1. *Adiabatic surface potentials*

### 3.1.1. *Adiabatic surface potential in diffusion*

The problem of adparticles moving on a surface is inherently of many-body type even in the case of a single adparticle due to the coupling of the particle to the substrate degrees of freedom. The fundamental quantity in surface diffusion is the so-called *adiabatic potential* $V_A(\mathbf{r})$ experienced by the diffusing adparticle. To properly define this quantity, one has to look into microscopic theories of surface

diffusion. A convenient way of defining $V_A(\mathbf{r})$ is to consider an interaction Hamiltonian of the form [20]:

$$\mathcal{H}_a = \mathcal{H}_s + \mathcal{H}_0 + \mathcal{H}_{\text{int}}. \tag{51}$$

Here $\mathcal{H}_s$ is the Hamiltonian for the substrate excitations (phonons and possible electronic excitations). The adparticle Hamiltonian $\mathcal{H}_0$ is given by

$$\mathcal{H}_0 = \frac{1}{2m_A} p^2 + V_S(\mathbf{r}), \tag{52}$$

where $m_A$, $\mathbf{r}$, and $\mathbf{p}$ denote the mass, position, and momentum of the adparticle, and $V_S(\mathbf{r})$ defines the *rigid* substrate potential. This is defined to be the periodic potential seen by the adparticle when the substrate atoms are in their ideal positions corresponding to an unperturbed surface. The last term $\mathcal{H}_{\text{int}}$ consists of two parts. It has an average adiabatic component which is due to the (local) relaxation caused by the presence of an adparticle. Its second component is called the nonadiabatic part and it is due to the rapid thermal fluctuations of the substrate. The adiabatic potential can then be defined as the sum of $V_S(\mathbf{r})$ and the adiabatic part of $\mathcal{H}_{\text{int}}$. Formally, we can write $\mathcal{H}_{\text{int}} = V(\mathbf{r}, \mathbf{R}_\ell)$ where $V(\mathbf{r}, \mathbf{R}_\ell)$ is a general interaction potential which contains the substrate co-ordinates $\mathbf{R}_\ell$ as well. Then the adiabatic potential can be defined by [20]

$$\exp\{-\beta[V_A(\mathbf{r}) - V_S(\mathbf{r})]\} \equiv \frac{1}{Z_s} \int \Pi_\ell \, \mathrm{d}\mathbf{P}_\ell \, \mathrm{d}\mathbf{R}_\ell \exp\{-\beta[\mathcal{H}_s + V(\mathbf{r}, \mathbf{R}_\ell)]\}, \tag{53}$$

where $Z_s$ is a configuration integral over the substrate degrees of freedom $\{\mathbf{P}_\ell, \mathbf{R}_\ell\}$:

$$Z_s = \int \Pi_\ell \, \mathrm{d}\mathbf{P}_\ell \, \mathrm{d}\mathbf{R}_\ell \exp(-\beta \mathcal{H}_s). \tag{54}$$

As can be seen from the definitions above, the adiabatic potential contains all the static information associated with the inclusion of an adparticle on the substrate. The absolute minima of $V_A(\mathbf{r})$ define the stable equilibrium adsorption sites of the adparticle, while the saddle points associated with $V_A(\mathbf{r})$ control the diffusion rates in the appropriate limits. More precisely, the adiabatic barrier appearing in the simple Arrhenius form of diffusion is given by the difference between the lowest energy saddle point and the minimum of $V_A(\mathbf{r})$ along a diffusion path connecting any two neighboring unit cells of the surface.

### 3.1.2. *Calculating the adiabatic potential*

The formal equations presented in the previous section for $V_A(\mathbf{r})$ are useful for understanding the physical nature of the adiabatic potential, but are perhaps of less practical importance. For any system with realistic interactions, the many-body nature of the various interactions significantly complicates the analytic calculation of $V_A(\mathbf{r})$. However, given the interaction potentials between the adparticle and the substrate, and the substrate atoms themselves, it is relatively straightforward to calculate $V_A(\mathbf{r})$ numerically. This can be done by simply fixing the co-ordinates $(x, y)$ of the adparticle on the plane along the surface, and bringing it in the vicinity of the substrate allowing the substrate to fully relax. The stable minimum of the potential corresponding to a particular point $(x, y)$ on the surface of the adiabatic potential is given by the value of the vertical co-ordinate $z$ where the force component along the $z$ axis is zero. Repeating this procedure over a fine mesh of points within the periodic

unit cell maps out the entire potential $V_A(x, y)$. In practice this is done by moving the adparticle systematically along the $x$ and the $y$ directions in the vicinity of the surface and allowing its $z$ co-ordinate to relax.

More recently, a number of extremely powerful saddle-point extrapolation methods have been developed to efficiently calculate reaction paths for many-body systems [168–173]. These methods can be readily applied to find saddle points and the corresponding adiabatic minimum energy paths for diffusion events [170, 174]. In particular, the so-called Nudged Elastic Band method [169] has proven to be an effective tool to find the path, when initial and final states of the transition are known.

There are two things that should be noted here regarding the adiabatic potential. First, the description above applies to the horizontal degrees of freedom only. Strictly speaking $V_A(\mathbf{r})$ is a function of the vertical co-ordinate $z$ as well. For example, if the vibrational states of the adparticle were to be studied, the adiabatic potential should be known for all its three variables. If it can be assumed that while diffusing, the motion of the adparticle along the $z$ direction on the surface of $V_A(\mathbf{r})$ consists of small oscillations only, the inclusion of this degree of freedom only renormalizes the value of the diffusion coefficient and the effective barrier at intermediate temperatures, but does not affect the adiabatic barrier in the low temperature limit [20]. The second point is that according to its definition, $V_A(\mathbf{r})$ is a function of temperature and should be averaged over all substrate excitations at different temperatures. However, unless the surface undergoes structural transitions, roughens or is close to its melting point, the dominant factor in determining $V_A(\mathbf{r})$ comes from the direct surface relaxation caused by the adparticle, and the contribution from the vibrational degrees of freedom can be neglected to a first degree of approximation.

*First Principles Methods*—The two main approaches that are commonly used in the practical calculation of $V_A(\mathbf{r})$ are first-principles (or *ab initio*) methods, and effective interaction potential methods. In the first-principles methods, the force fields between all the atoms in the system are calculated quantum-mechanically within some approximations (such as the density functional theory). The great advantage of these methods is that there are in principle no fitting parameters, and almost all cases except for strongly ionic systems and Van der Waals forces can be dealt with within the same framework. Indeed, there are many examples of first-principles calculations of adiabatic barriers in the recent literature, both for metallic systems (see the bibliography related to sections 2.1, 4.2 and 4.3) and for semiconductors (see for example references [175–178]). In actual electronic structure calculations [179–181], several approximations have to be made however. The local density approximation (LDA) is commonly used in bulk calculations, but does not always work well for surface problems. In the case of metal-on-metal diffusion, recent comparison between LDA calculations and additional gradient correction terms included show that the surface energetics is rather sensitive to these corrections terms, with significant changes in the adiabatic barriers even for simple diffusion events [182, 183]. The first-principles calculations are also highly demanding in terms of their numerical complexity, scaling at best proportional to $N_e \log(N_e)$ where $N_e$ is the number of electrons that must be included in the computations. At present, the practical limitation for most surface-adparticle systems is a system consisting of about $10^2$ atoms. Also, finite-temperature dynamical calculations using, e.g., the Car–Parrinello [184] method are very costly for the study of diffusion events, the

typical time scale extending to $\sim 10^2\,ps$ [185, 186]. At present, the first-principles calculations are thus limited to rather small systems and simple diffusion events such as jump and exchange.

*Effective Interaction Potential Methods*—In effective interaction potential methods, all the relevant interaction potentials are given explicitly as a function of the relative positions of the atoms, and the forces are classical, the dynamics following Newton's equations of motion. There are many classes of such potentials, varying in their degree of complexity and relation to first-principles calculations. For metallic systems, these include the effective medium theory [187], the embedded atom method [188, 189], second-moment tight-binding [190–194] and Finnis–Sinclair methods [195], and the glue model [196, 197]. For semiconductors, accurate tight-binding potentials have been developed for example for Si [200]. In these phenomenological methods, the total energy of the system has been parametrized in terms of a nonlinear expression, usually related to the local electronic density around each atom in the system, and a pair interaction potential. Of all these methods, the effective medium theory is least based on experimental data, with parameters fitted to LDA calculations. The main advantage of using classical many-body potentials is that the MD method is immediately feasible (see section 3.6), allowing the direct observation of diffusion events at high temperatures [201, 202]. The main drawback of all the phenomenological potentials is the fitting procedure which has to be done and tested for each case separately, and the accuracy of the results is sometimes questionable. Nevertheless, these methods allow the study of larger systems such as stepped surfaces or adatom islands, and the observation of direct diffusion events even up to the $\mu s$ time scale by standard MD, and up to the *ms* time scale using modern MD acceleration methods [189, 199] (see section 3.6).

The most straightforward way of calculating the adiabatic potential is through the canonical MD algorithm, where the whole system is coupled to a heat bath at a constant temperature. The temperature can be reduced in small steps, allowing the system to relax towards stable equilibrium where $V_A(\mathbf{r})$ can be computed as explained above. A commonly used technique to improve convergence for all the degrees of freedom is the so-called MD cooling algorithm. In this algorithm, the initial velocities of the particles in the system are obtained from the Boltzmann distribution corresponding to a finite temperature. In each step, the velocity of each particle is reduced in magnitude proportional to a component it has in the direction opposite to the local forces, and eventually the system ends up to a relaxed configuration at a very low temperature.

### 3.2. *Transition State Theory and approximate dynamics*

In the last section, we have described how the adiabatic diffusion barrier for a single adatom can be calculated either with first principles methods or through the use of semi-empirical potentials. However, while the adiabatic barrier is an important ingredient in determining the magnitude of the diffusion coefficient, it is only part of the story. After all, the adiabatic barrier is only an equilibrium quantity, while the diffusion coefficient is a transport coefficient and an explicit dynamic quantity. The dynamical information is contained in the prefactor, which is determined by how the adsorbed particle gets enough energy to climb over the barrier and then re-equilibrate in another well. The exact dynamical description of these activation and deactivation processes is difficult and various theoretical approaches are described in the following sections. Here we will discuss the simplest approach,

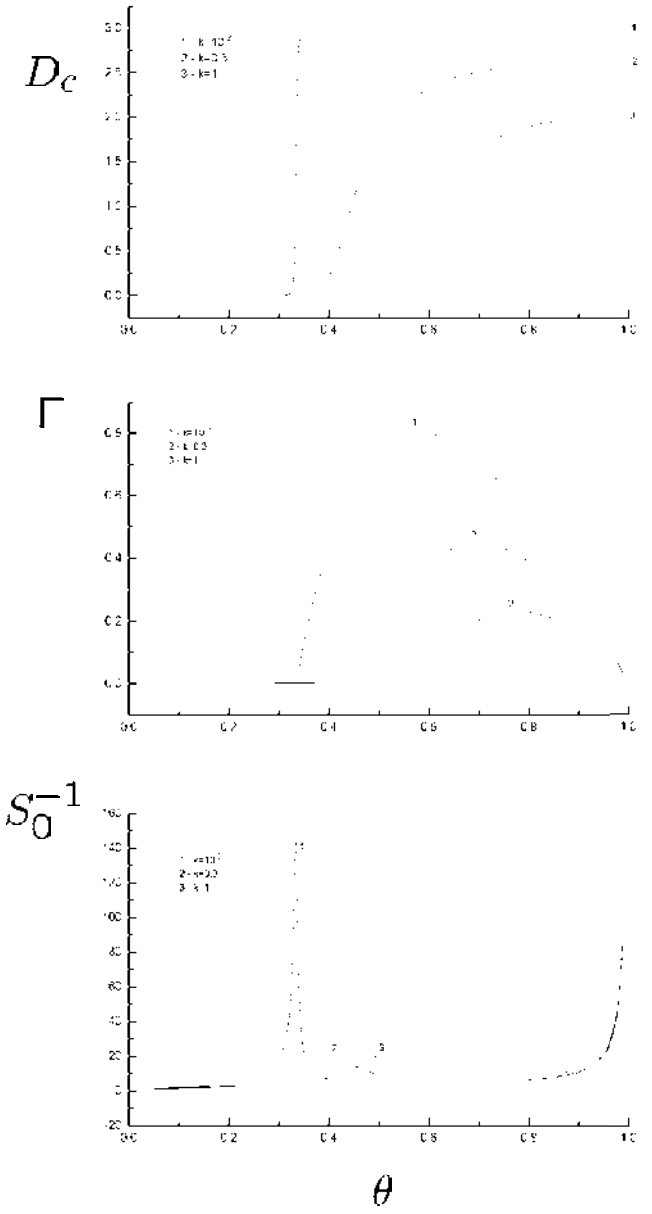


Figure 14. Collective diffusion in a model of a square lattice with two non-equivalent sublattices, and repulsive interactions of magnitude $J$. Sites on different sublattices differ in adsorption energy by the quantity $\Delta E$. Here the results are reported at fixed $\exp[2J/(k_BT)] = 100$ and for different values of $k = \exp[-\Delta E/(k_BT)]$: $k = 10^{-3}$, 0.3, and 1 (corresponding to curves 1, 2 and 3, respectively). The figure is reprinted from [138], with permission from Elsevier Science. From top to bottom: $D_c$, average jump rate $\Gamma$ and the inverse thermodynamic factor $S_0^{-1}$ as functions of the coverage $\theta$. The diffusion coefficient shows a steplike increase at a critical coverage $\theta_c$, whose value changes from $\theta_c = 1/3$ at $J = 0$ to $\theta_c = 1/2$ at large $J$. At $J = 0$ and small $k$, the steplike increase takes place when the low-energy sublattice (which contains 1/3 of the total sites) is completely filled, so that the remaining adatoms jump fast on the high-energy sublattice.

namely the application of the Transition State Theory (TST) to the calculation of the tracer diffusion coefficient $D_t$. It is like the 'mean-field theory' in other branches of many-body physics. It is relatively easy to apply, and has been shown to be fairly accurate at least for metal on metal systems, and could be expected to be semi-quantitative for other systems as well.

We first make the Markovian assumption that the adatom can jump only to its nearest neighbor site and that successive jumps are uncorrelated. This is strictly correct only in the zero coverage limit when we consider independent adatom motion, and neglect long jumps and memory effects arising from the substrate excitations (see section 4.6). In this case, as we have seen from equation (12), the tracer diffusion coefficient $D_t$ can be easily expressed in terms of the total jump rate $\Gamma$ as

$$D_t = \frac{1}{4}\,\Gamma\, a^2. \tag{55}$$

Thus the task of calculating $D_t$ is reduced to that of calculating the total jump rate $\Gamma$, which is connected to the directional jump rate $\gamma$ by $\Gamma = n_s\gamma$, where $n_s$ is the number of equivalent saddle points from a given minimum. The jump rate is just a special case of a general rate of chemical reaction for which TST was developed [203, 16].

In order to apply TST one has to define a reaction co-ordinate $x$ and a dividing surface (see figure 15). The reaction co-ordinate can be defined following the minimum energy path from one adsorption site to another through the saddle point. The conventional choice for the TST dividing surface is the hypersurface perpendicular to the unstable mode at the saddle point. Let us choose $x = 0$ as the dividing surface containing the saddle point separating the two neighbouring wells. In the simplest form of TST, the rate $\gamma$ can be expressed as the ratio of two partition functions

$$\gamma = \frac{k_B T}{h}\,\frac{Z_s}{Z_0}. \tag{56}$$

Here $Z_0$ is the partition function for the well region and $Z_s$ is a partition function for the saddle point region restricted to the hypersurface $x = 0$ separating the two wells, such that the reaction co-ordinate $x$ with negative curvature at the saddle point is

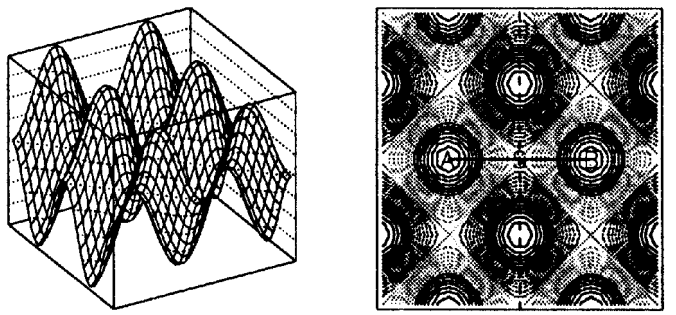


Figure 15. Left panel: periodic adiabatic potential $V_A(x, y)$. Right panel: contour plot of $V_A(x, y)$. The minima in A and B are connected by the reaction path (solid line) through the saddle point S. The dividing surface is perpendicular to the reaction path in S (dashed line).

excluded from the integration. Equation (56) is often explicitly written in terms of the energy change $E_A$ and the entropy change $\Delta S$ between the minimum and the saddle point, i.e. in the form

$$\gamma = \frac{k_B T}{h} \exp\left(\frac{\Delta S}{k_B}\right) \exp\left(-\frac{E_A}{k_B T}\right). \tag{57}$$

It is also possible to formulate a more general form for the TST in terms of the flux at the saddle point [204, 16]. At low temperatures, the harmonic approximation is often used to further simplify the TST. In this case, equation (56) simplifies to the following expression

$$\gamma = \frac{1}{2\pi} \frac{\Pi_i \omega_0(i)}{\Pi_i \omega_s(i)} \exp\left(-\frac{E_A}{k_B T}\right). \tag{58}$$

Here, $\omega_s(i)$ and $\omega_0(i)$ are the stable normal mode frequencies around the saddle point and the well, respectively, in the presence of the adatom. Equation (58) results in an explicit Arrhenius form for the jump rate $\gamma$ which is often assumed in phenomenological analysis. The prefactor can be interpreted as an attempt frequency, although it cannot be equated simply to the vibrational frequency of the adatom in the potential well. Calculations of prefactors in the TST framework are found for example in references [87, 210, 41].

The TST relies essentially on two assumptions:

(i) each particle crossing the dividing surface is assumed not to return back to the well of departure (i.e., recrossings are neglected);
(ii) the coupling with the thermal bath is strong enough to ensure that the energy distribution of the escaping particles at the dividing surface is a Boltzmann distribution.

As will be detailed in the sections below, the real dynamics is controlled by the rate of exchange of energy of the adatom reaction co-ordinate degree of freedom with the excitations of the rest of the system, such as phonons and electronic excitations. This results in both fluctuations in energy and frictional damping of the motion of the adatom. In the limit of high friction, recrossing of the dividing surface would lead to a reduction in the real rate from the TST expression. From this point of view, an improved TST rate may sometimes be obtained by choosing a non-conventional dividing surface in such a way to minimize recrossings. In the other limit of low friction, the assumption of an equilibrium distribution for the escaping particles at the dividing surface is no longer satisfied [205], and this again leads to a reduction of the rate. In addition, long jumps can occur in this low friction limit, and long jumps are not accounted for in the simplest version of TST theory.

It is important to note that in practice, the accuracy of the TST rate depends also on the level of coarse graining, i.e., on which part of the system phase space is explicitly taken into account in evaluating the partition functions $Z_s$ and $Z_0$, and which part is treated as a heat bath represented by a frictional coupling to the rest of the system. Consider first the simplest case where only the reaction co-ordinate degree of freedom is explicitly included in the phase space and the rest of the system is represented by a frictional coupling $\eta$ to the adatom. It was demonstrated in the pioneering work of Kramers [206] treating the one dimensional problem of escape of a particle from a well that the TST gives an upper limit to the true rate, and it only works reasonably well in the region of intermediate friction. When only a subset of

the co-ordinates of the full system is taken into account, then the validity of the TST depends again on the value of the frictional coupling coming from the heat bath variables that are not explicitly included, with best results in the intermediate friction regime.

When the full phase space of all the co-ordinates and momenta of the diffusing particle and of the substrate are included explicitly, it is commonly stated [16] that assumption (i) is practically satisfied, because recrossings tend to become negligible. This has been demonstrated explicitly [207] for a model of one reaction co-ordinate coupled to a system of harmonic phonons. In this case, the TST is shown to give the same results as the exact Kramers theory when the coupling of the reaction co-ordinate to the phonons is sufficiently strong. For a more realistic multidimensional TST, the absence of recrossing corrections probably requires the further condition that the curvatures at the saddle point in all directions other than the reaction path be steep enough for the harmonic approximation to be a good one. This can be qualitatively understood in the sense that if the bottleneck at the saddle point is narrow, there is little chance for a trajectory to recross.

As far as assumption (ii) is concerned, the situation cannot be helped by the inclusion of all degrees of freedom in TST. When the effective coupling of the reaction co-ordinate to the excitations of the rest of the system is weak, the distribution of the energy of the diffusing particle at the TST surface will deviate from the Boltzmann distribution, being larger on lower energies [205], and there will still be corrections to the TST result. In section 3.3 we shall compare the TST rate to the exact rate in models which can be exactly solved.

Some of the corrections to TST such as recrossings of the dividing surface and long jumps can be numerically implemented to obtain a jump rate that goes beyond the TST [208, 64, 209]. For example, dynamical corrections to the TST have been calculated for adatom diffusion on fcc (100) and (111) metal surfaces [208, 209]. In this framework, the conventional TST rate is calculated; after that, the adatom is started from the dividing surface with a (positive) velocity extracted from the Maxwell distribution. The trajectory of the adatom is propagated by Molecular Dynamics techniques, and recrossings and long jumps are counted. The recrossing percentage is then subtracted from the TST rate, and the distribution of the long jumps is employed for correcting the diffusion coefficient. While this procedure corrects for the recrossing of the adatom over the dividing surface, it still cannot account for the fact that in low-friction systems, the assumption of an underlying Boltzmann distribution for the energy of the escaping particles is incorrect, and the escape rate is lower than the TST estimate also because of the breaking down of the assumption (ii).

### 3.3. *Langevin and Fokker–Planck equation approaches*

A treatment of surface diffusion including all the adsorbate and substrate degrees of freedom is at the moment limited to systems being described by model or semi-empirical interparticle interactions. An entirely *ab initio* calculation is still out of reach at this point. Even with the approximation of using a model interaction potential between adatoms, full MD calculations include only the vibrational and translational degrees of freedom. The nonadiabatic coupling terms to the electronic excitations are still missing. Moreover, microscopically detailed MD simulations are perhaps not very illuminating with regard to the fundamental main issues in surface diffusion. A simpler approach is to first integrate out *all* the substrate degrees of

freedom in the equations of motion, leaving only an effective stochastic equation for the adatoms. This is precisely the content of the Langevin equation approach for the study of surface diffusion. In this equation for the adatoms, the effects of the substrate appear in two places. First, there is the adiabatic potential, which is just the free energy of the entire system with the position of the adatoms treated as fixed parameters, see section 3.1. In addition, a fluctuating frictional force arises from the non-adiabatic coupling of the adatom to the electronic and vibrational excitations of the substrate. This coupling leads to fluctuations in the energy and momentum of the adatom as well as to damping of its motion. Being a stochastic equation, the Langevin equation has an infinite number of solutions given a fixed boundary condition. This is too much information for most applications. It can be useful to focus instead on a distribution function $P(\mathbf{r}, \mathbf{v}, t)$ that describes these solutions. The distribution function $P(\mathbf{r}, \mathbf{v}, t)$ satisfies a Fokker–Planck equation that is equivalent to the Langevin equation for the evaluation of physical averages.

The Langevin equation (and equivalently the Fokker–Planck equation) is often used in a phenomenological approach, with the choice of a model adiabatic potential and a friction parameter $\eta$. However, it could be derived rigorously from a microscopic Hamiltonian that incorporates the full degrees of freedom of the adsorbate and the substrate. Here we outline an approach using the Mori PO formalism [126, 127, 211–214, 20]. The basic idea is to separate the variables into two Hilbert spaces, one for the 'slow degrees' of freedom denoted by $\mathbf{r}$ to be treated explicitly, and one for the 'fast' degrees of freedom to be integrated out. For the surface diffusion problem, an obvious choice is to identify all adatom variables as slow variables and the substrate variables as the fast degrees of freedom. However, this need not be the only choice. For example, the first few layers of the substrate or alternatively an active cluster of substrate atoms surrounding the adatoms can be included in the slow variables to be treated explicitly. For the purpose of simplicity in our discussion, we will identify the two Hilbert spaces as adatom space and the substrate space. We can define a projection operator $\mathcal{P}$ into the adatom space and the orthogonal projection operator $\mathcal{Q}$ such that $\mathcal{P} + \mathcal{Q} = 1$. By projecting out substrate degrees of freedom, we end up with a generalized Langevin equation (GLE) of motion for the adatoms of the form

$$m\ddot{\mathbf{r}}(t) = -\int_{-\infty}^{t} \Sigma(t, t')\mathbf{r}(t')\,\mathrm{d}t' - \nabla V(\mathbf{r}(t)) + \mathbf{f}(t). \tag{59}$$

Here $\mathbf{r}(t)$ stands for a multicomponent vector with dimension $Nd$, where $N$ is the number of adparticles and $d$ is the physical dimension of the system. $V(\mathbf{r})$ is a general potential including both the adiabatic potential exerted by the substrate on the adsorbate as well as the interactions between the adatoms. From the PO formalism, it can be shown rigorously [214] that $V(\mathbf{r})$ is exactly the free energy of the adsorption system including averages over all the substrate electronic and vibrational excitations while the adatom co-ordinates $\mathbf{r}$ are treated as fixed parameters.

Equation (59) serves to illustrate a number of important points concerning the motion of the adatom. First, the damping of the adatom motion is characterized by a memory function $\Sigma(t, t')$ that depends in a complicated manner on the past history of the motion of the adsorbate and the substrate. Second, it is not surprising to see that the damping in the form of the memory function $\Sigma$ and the fluctuating force $\mathbf{f}$ are not independent since they both arise from the coupling to the substrate

excitations. These quantities are related by the second fluctuation–dissipation theorem [215]:

$$\Sigma(t,t') = \frac{1}{k_B T}\langle \mathbf{f}(t)\cdot\mathbf{f}(t')\rangle. \tag{60}$$

This expression is deceptively simple. In fact, the fluctuating force is the component of the total force projected out of the adatom space and has a complicated time dependence given by

$$\mathbf{f}(t) = -\exp(-i\mathcal{Q}\mathcal{L}\mathcal{Q}t)\nabla V(\mathbf{r}), \tag{61}$$

where $\mathcal{L}$ is the Liouville operator. In the literature, the memory function is often approximated in the form of a simple exponential decay [16, 216, 217]. This is often an oversimplification in surface diffusion, since in the important short and intermediate time regimes, the memory function can deviate strongly from the asymptotic exponential form [218, 251], as will be shown in section 4.6. The only simple form of the memory function occurs in the Markovian limit when the time scale for the substrate motion is much faster than the adatom time scale. In this case, the memory function can be approximated by a delta function

$$\Sigma(t,t') \sim 2\eta\delta(t-t'). \tag{62}$$

This is equivalent to assuming that the fluctuating forces $\mathbf{f}(t)$ at different times are uncorrelated. This is also commonly referred to as the 'white noise' because of the independence on the frequency of the Fourier transform of $\Sigma(t,t')$. In this limit, the damping reduces to the familiar Langevin form $\eta\mathbf{v}_i$ that depends only on the instantaneous velocity of the adatom.

3.3.1. *The Markovian (white noise) case*

While the GLE illustrates the important concepts and provides a separation of the adiabatic and non-adiabatic effects, the memory function $\Sigma$ and the fluctuating force $f$ are complicated objects and not practical for actual computation. Thus, the GLE amounts to a reformulation of the many-particle problem in different terms. In practice, the damping is often approximated by the Markovian form characterized by a phenomenological friction constant. In this case, the Langevin equation becomes a powerful tool to study surface diffusion beyond the simple TST theory. To simplify the discussion, we consider now the diffusion of an isolated particle on a periodic substrate. The Langevin equation then takes the form

$$m\frac{d\mathbf{v}}{dt} = -m\eta\mathbf{v} + \mathbf{F}(\mathbf{r}) + \mathbf{f}(t), \tag{63}$$

where $\mathbf{f}(t)$ is white noise, related to the friction by the fluctuation–dissipation theorem. The probability density in phase space $P(\mathbf{r},\mathbf{v},t)$ obeys the corresponding Fokker–Planck (or Klein–Kramers) equation [18], which can be written as:

$$\frac{\partial P}{\partial t} = -\mathbf{v}\cdot\frac{\partial P}{\partial \mathbf{r}} - \frac{\mathbf{F}(\mathbf{r})}{m}\cdot\frac{\partial P}{\partial \mathbf{v}} + \eta\frac{\partial}{\partial \mathbf{v}}\cdot\left(\mathbf{v}P + \frac{k_B T}{m}\frac{\partial P}{\partial \mathbf{v}}\right), \tag{64}$$

where $\mathbf{F}(\mathbf{r})$ is the adiabatic force, derived from the adiabatic potential $V_A(\mathbf{r})$ [211–213, 20], and $\eta$ is the friction per unit mass. The adiabatic potential is periodic along the surface plane. The above model can be solved in different ways: the matrix continued fraction method (MCFM) [18], the path-integral method [173], and

through a direct simulation [21]. In the MCFM, one starts from the Fokker–Planck equation or the Langevin equation and develops a solution for the dynamic structure factor [219] on an orthonormal basis: plane waves for the spatial part and Hermite functions for the velocity part. The coefficients of the expansion are then related by a tridiagonal recurrence relation which is solved in terms of matrix continued fractions. From the dynamic structure factor, in addition to the usual correlation functions (mean-square displacement, velocity correlation function), also the jump rate and the probability distribution of the jump lengths can be extracted [48]. The MCFM is extremely precise and fast when dealing with one-dimensional problems for barriers $\leq 20\,k_BT$, and for any practical friction of interest in surface diffusion. On the other hand, the MCFM becomes cumbersome for higher barriers and much more difficult [55] for 2D problems even at medium-low barriers. In 3D, the MCFM is of no practical use.

The qualitative features of the Langevin description of diffusion can be easily understood in the case of one-dimensional diffusion in a periodic potential of lattice spacing $a$. Four different regimes can be singled out [45, 219]:

(i) at low $T$, when $\exp[-E_A/(k_BT)] \ll 1$ and $\eta/\nu_{\text{osc}} < k_BT/E_A$, we have long-jump diffusion;
(ii) at low $T$, when $\exp[-E_A/(k_BT)] \ll 1$ and $\eta/\nu_{\text{osc}} > k_BT/E_A$, we have single-jump diffusion;
(iii) at high $T$, when $\exp[-E_A/(k_BT)] \approx 1$ and $\eta < \sqrt{k_BT/(ma^2)}$, we have liquid-like low-friction diffusion;
(iv) at high $T$, when $\exp[-E_A/(k_BT)] \approx 1$ and $\eta > \sqrt{k_BT/(ma^2)}$ we have liquid-like high-friction diffusion.

These diffusion regimes can be easily identified by inspecting the behaviour of the mean square displacement $\Delta x^2(t) = \langle [x(t) - x(0)]^2 \rangle$ as a function of time [219]. In regime (i), $\Delta x^2(t)$ displays several oscillations, before accommodating on the asymptotic straight line; in regime (ii) no oscillations are evident, but a pronounced slope change in between the short and long-time behaviour is present; in regime (iii) $\Delta x^2(t)$ starts off parabolic, retains the parabolic behaviour on time scales of the order of $1/\eta$, and then accommodates on a straight line; in regime (iv) the initial parabolic behaviour is restricted to very short times and $\Delta x^2(t)$ becomes readily rectilinear.

In figure 16 we compare the total jump rate $\Gamma$ as a function of $\eta$ as calculated by the exact solution of the Fokker–Planck equation to the constant result from TST, $r_{TST} = 2\nu_{\text{osc}} \exp[-E_A/(k_BT)]$. TST gives an overestimate of the rate which is acceptable when $\eta$ is in the so-called turnover regime, where $\Gamma$ reaches a maximum.

Concerning the behaviour of long-jump probabilities [48], a logarithmic plot of $p_n$ as a function of $n$ (see figure 17) reveals an exponential decay at large $n$, whereas the decay at small $n$ is even faster. This can be explained by the fact that, at low friction, the energy distribution of the particles which are escaping from the well of departure is not the Maxwell distribution, but it contains more low-energy particles. The latter are more likely retrapped in the first wells; after crossing the first wells, the energy distribution of the jumping particles becomes Maxwell-like, and the probability of retrapping scales exponentially.

The Langevin equation has also been applied to the study of surface diffusion in higher dimensions. For the 2D case, the $xy$ coupling of the potential causes a reduction of the long-jump probabilities [53, 55, 56, 59, 220]. This does not mean

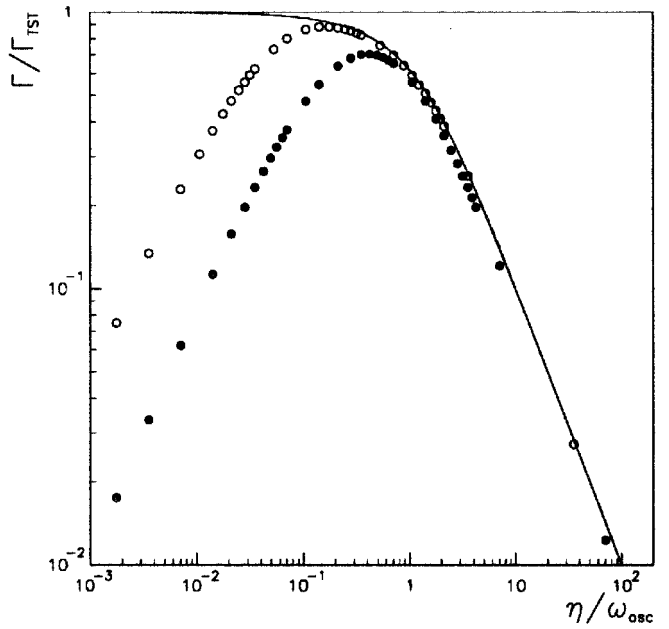


Figure 16. Ratio $\Gamma/\Gamma_{TST}$ for diffusion in a 1D cosine potential as a function of $\eta/\omega_{\mathrm{osc}}$. The circles correspond to exact numerical results obtained by the MCFM; the full and dashed lines) which practically coincide in the figure) are results from the Kramers approximation of equation (67). The full and open circles correspond to barriers $E_A = 4k_BT$ and $16k_BT$, respectively.

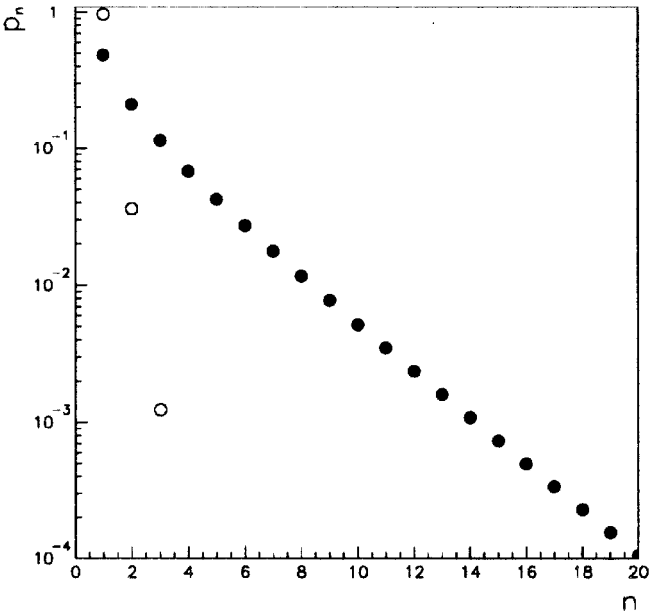


Figure 17. Probability $p_l$ of a long jump of length $l$ for diffusion in a 1D cosine potential at a barrier $E_A = 4k_BT$ and $\eta/\omega_{\mathrm{osc}} = 0.05$ (full circles) and $\eta/\omega_{\mathrm{osc}} = 0.5$ (open circles). The results are obtained by the MCFM.

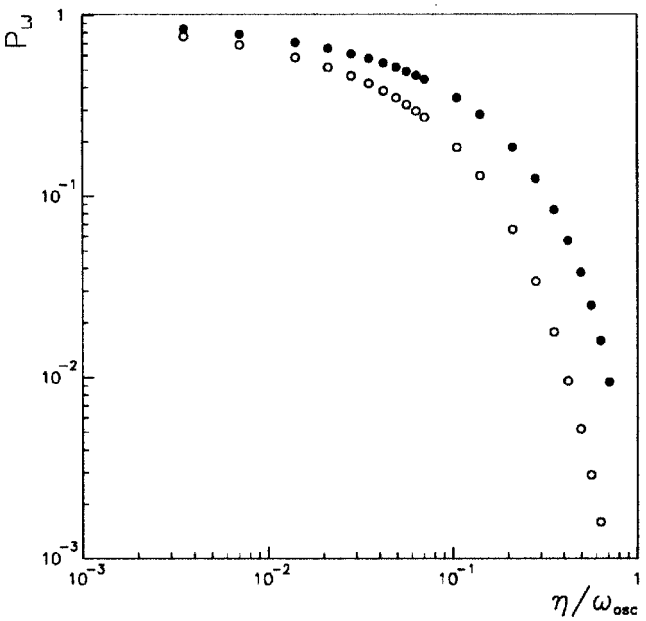


Figure 18. Probability of long jumps $P_{LJ} = 1 - p_1$ for diffusion in a 1D cosine potential at barriers $E_A = 4k_BT$ (full circles) and $E_A = 16k_BT$ (open circles) as a function of $\eta/\omega_{osc}$. The results are obtained by the MCFM.

that long jumps are forbidden, but simply that their probability is reduced relative to the 1D situation, due to an enhancement of retrapping. This reduction takes place both in geometries where minima and saddle points are not on the same straight line (see reference [53] for a Langevin simulation of a bcc(110) crystal surface) and in geometries where minima and saddle points are on the same line, but the saddles are narrower than the minima (see reference [56], where diffusion in a 2D egg-carton potential is studied). Indeed, the coupling may induce localization in conservative systems at energies above the saddle-point energy [221]. This enhancement of retrapping has also important consequences on the behaviour of the diffusion coefficient as a function of the friction $\eta$ in the low friction limit. For 1D (or decoupled) potentials, $D_t \propto \eta^{-1}$ [18, 47] at low friction. This arises from the fact that while the rate of escape from a well is proportional to $\eta$, the mean square jump distance varies as $\eta^{-2}$. For the 2D coupled potentials with enhanced retrapping, $D_t \propto \eta^{-\alpha}$, with $\alpha < 1$ [53, 56]. The exponent $\alpha$ is not universal but depends on the precise topology of the potential.

At high and intermediate friction there are some useful analytical formulae for the diffusion coefficient and the jump rate. Here we recall them and discuss their limits of validity; for their derivation the reader can refer to the original literature [18, 222, 55]. In the limit of high friction $\eta \rightleftarrows \infty$ (physically, when $\eta^{-1}$ is by far the shortest time scale in the system), an accurate multidimensional approximation to the diffusion coefficient is available [33, 55]. Here we write it for diffusion along the $x$ direction in the case of a 2D rectangular lattice with spacings $a$ and $b$ along the $x$ and $y$ directions, respectively (the generalization to 3D and to position-dependent friction is straightforward):

$$D_t^{xx} = \frac{a^2 k_B T}{m\eta} \frac{\int_0^b \mathrm{d}y \left\{ \int_0^a \mathrm{d}x \exp\left[\beta V_A(\mathbf{r})\right] \right\}^{-1}}{\int_0^b \mathrm{d}y \int_0^a \mathrm{d}x \exp\left[-\beta V_A(\mathbf{r})\right]}. \tag{65}$$

In 2D and 3D, this expression is very precise when the diffusion trajectories are dominated by rectilinear paths; in 1D it reduces to the following expression, which is exact in the high-friction limit [222]:

$$D_t = \frac{a^2 k_B T}{m\eta} \left\{ \int_0^a \mathrm{d}x \exp\left[-\beta V_A(x)\right] \int_0^a \mathrm{d}x \exp\left[\beta V_A(x)\right] \right\}^{-1}. \tag{66}$$

These formulae nicely extrapolate between the high-temperature Brownian limit and the low-temperature Arrhenius behaviour [20]. On the other hand, at intermediate friction ($\eta \gtrsim \nu_{\mathrm{osc}}$) and high barriers, the following expression for the directional jump rate $\gamma$ holds [223]:

$$\gamma = \frac{1}{2\pi} \frac{\Pi_i \omega_0(i)}{\Pi_i \omega_s(i)} \left[ \sqrt{1 + \frac{\eta^2}{4\overline{\omega}_s^2}} - \frac{\eta}{2\overline{\omega}_s} \right] \exp\left(-\beta E_A\right). \tag{67}$$

Here, $\omega_s(i)$ and $\omega_0(i)$ are the stable normal mode frequencies around the saddle point and the well respectively in the presence of the adatom, and $\overline{\omega}_s$ is the unstable frequency at the saddle point. In 1D, the total jump rate $\Gamma = 2\gamma$ from equation (67) is compared to exact numerical results in figure 16. From equation (67), an estimate for the diffusion coefficient $D_t$ is given by $D_t = \gamma n_s a^2$, where $n_s$ is the number of equivalent saddle points from a minimum position. Equation (67) takes into account recrossings and reduces formally to the TST expression in equation (58) at $\eta \rightleftarrows 0$; however in this limit TST is not valid due to the breaking down of the thermal equilibrium assumption (see the discussion in section 3.2). Analytical approximations at low friction do exist; they are however much more complicated (because one has to evaluate both the jump rate and the mean-square jump length to obtain $D_t$) and restricted to the 1D case, but valid in the whole range $\nu_{\mathrm{osc}} \gtrsim \eta$. These formulae can be found in references [46, 48, 49, 173]. A simple formula for $D_t$ has been given by Risken [18]:

$$D_t \simeq \frac{\pi k_B T}{2m\eta} \exp\left(-\frac{E_A}{k_B T}\right), \tag{68}$$

but its validity is restricted to extremely low friction [47], which is probably not common in surface diffusion. For a derivation of this formula, see also section 3.4. Finally, a quite accurate interpolation formula between high and low friction in 1D is given in reference [224].

The Langevin equation has also been applied to study diffusion of adatoms at finite coverages, i.e., in dense overlayers; in this case, the equation is usually solved by direct simulation [225, 226, 108, 227]; the interaction between each adsorbed particle and the substrate is treated within the Langevin scheme, while the interactions among diffusing particles are treated in full Hamiltonian description.

Finally, we remark that the Langevin model with white noise is quite often inadequate to describe quantitatively surface diffusion in real systems. It has been shown that for homoepitaxial diffusion of a Lennard–Jones particle on a Lennard–Jones crystal [211–213], the above simple description is quantitatively adequate (provided that a position-dependent friction is adopted) essentially because the adsorbed particles vibrates on a somewhat slower scale than the substrate, due to

its weaker bonding. On the other hand, when the mass of the particle is lighter, or the adparticle-substrate interaction is stiffer, the simple white-noise Langevin description is inadequate, and memory effects (see section 4.6) must be taken into account [218].

In the case of light adsorbates, when the typical time scale of the adatom is faster than the substrate vibrations, also a treatment based on different kinetic equations, like the Boltzmann equation with Bhatnagar–Gross–Krook (BGK) [228, 229] collision kernel [230, 51, 231, 232] may be considered an useful approximation. In the BGK scheme, the diffusing particle suffers well-separated collisions with the thermal bath phonons. These collisions happen at a frequency $\eta_c$, and after each collision the particle thermalizes suddenly its velocity. In the limit $\eta_c \rightleftarrows \infty$, both the Langevin approach and BGK reduce to the same Smoluchowski equation [18]. At low $\eta_c$, the two models give quantitatively different results, but no qualitatively different behaviour arises [231, 232]. The main difference between the Langevin and the BGK model is thus in the physical interpretation of $\eta$ (and $\eta_c$): in the Langevin model $\eta$ is a friction, which ensures a gradual energy transfer from the adparticle to the substrate; in the BGK model, $\eta_c$ is a collision frequency, and all collisions are strong, so that each of them thermalizes the kinetic energy. At large $\eta$ and $\eta_c$, both physical interpretations coincide.

### 3.3.2. *Evaluation of the friction*

The friction $\eta$ in the Langevin model is often taken as a phenomenological parameter which is fitted to experimental or simulation data. However, it is possible to give an estimate of the friction from the energy exchange between the adatom and the substrate. A very nice discussion of this subject is given in Chapter 8 of the recent book by Persson [166]; here we report only the main points.

The energy exchange between the adatom and the substrate occurs via phononic and electronic excitations. Thus $\eta$ can be written as a sum of an electronic and a phononic contribution:

$$\eta = \eta_{el} + \eta_{ph}. \tag{69}$$

We remark that the use of a static phononic friction is valid when the substrate vibrates much faster than the adatom; otherwise a memory (function) friction is needed. On the other hand, the typical time scale of electronic excitations is so fast that memory effects are always negligible in electronic friction.

The electronic contribution $\eta_{el}$ can be measured via the resistivity change $\Delta\rho$ in a thin film (substrate) induced by the adsorbed layer; at low coverages the following relation holds [233]:

$$\eta_{el} = \frac{n_e^2 e^2 d_s}{m\theta}\,\Delta\rho, \tag{70}$$

where $n_e$ is the electron density per unit volume in the substrate, and $d_s$ is the thickness of the substrate. On the other hand, a theoretical evaluation of $\eta_{el}$ has been done for covalent and van der Waals bonding. The formulae are reported in references [166, 233]. Here we remark that, for example, in the case of Ag/Ag, both the experimental (via equation (70)) and theoretical (via the formula for covalent bonding) evaluations of $\eta_{el}$ give an estimate of $\eta_{el} \simeq 10^{10}\,\mathrm{s}^{-1}$. For other adsorption systems, $\eta_{el}$ can be in the range of $10^8$–$10^{12}\,\mathrm{s}^{-1}$ [166, 233] (for example, ranging from $\eta_{el} = 2.8 \times 10^8\,\mathrm{s}^{-1}$ for $C_2H_6$/Ag to $\eta_{el} = 1.0 \times 10^{12}\,\mathrm{s}^{-1}$ for H/Ni).

The phononic contribution $\eta_{ph}$ can be evaluated in the framework of the elastic continuum model [234]

$$\eta_{ph} = \frac{3m}{8\pi\rho_0}\left(\frac{\omega_{\mathrm{osc}}}{c_T}\right)^3 \omega_{\mathrm{osc}}, \tag{71}$$

where $\rho_0$ is the mass density of the substrate and $c_T$ is the transverse sound velocity. Equation (71) gives $\eta_{ph} \simeq 10^{12}\,\mathrm{s}^{-1}$; this estimate is supported also by MD results of Ag/Ag(110) diffusion [58] at temperatures up to 600 K, and MD simulations of Cu/Cu(111) and Cu/Cu(100) systems [237]. Therefore, at least for Ag/Ag diffusion, $\eta_{ph}$ is larger than $\eta_{el}$ by two orders of magnitude. Other analytical and MD estimates of $\eta_{ph} \simeq 10^{12}\,\mathrm{s}^{-1}$ have been given also for homoepitaxial diffusion on Cu and Au surfaces [58, 235, 236].

In MD simulations (see section 3.6), the friction can be estimated by different methods. A very simple one [58, 72, 237] works in the limit of low temperatures. In that limit, the adatom is localized at the well bottom in such a way that it is exploring essentially the harmonic part of the well. The method is based on the calculation of the velocity-velocity correlation function $Z(t)$, and to its fitting with the expression deriving from the solution of the Fokker–Planck equation in a harmonic well:

$$Z(t) = \frac{k_B T}{2m}\exp\left(-\eta t/2\right)\cos\left(\omega t\right). \tag{72}$$

More generally, one can calculate the force–force fluctuation correlation function, whose time integral is proportional to the static friction [235, 237]. However, this method includes all dissipation in the system and gives results slightly different from those obtained from the correlation function. In the low temperature (and high friction) limit, the the diffusion is controlled by the saddle point value of the friction [20] which could be estimated numerically from a MD simulation.

### 3.4. *Path integral approach to stochastic processes and application to surface diffusion*

#### 3.4.1. *Path integral formalism for stochastic events*

We discussed the Langevin equation in the previous section and showed that it can be derived from a microscopic Hamiltonian by integrating out the substrate degrees of freedom, resulting in the explicit separation of adiabatic and non-adiabatic effects. Given a set of boundary conditions, the Langevin equation does not have a unique solution like the ordinary equations of motion. Instead, at thermal equilibrium, each trajectory compatible with the boundary condition occurs with a given probability, and physical quantities are obtained through the average of all these stochastic trajectories distributed according to a fixed probability distribution function. It has been shown [238, 173] that this stochastic averaging over the different trajectories can also be cast in the path integral formalism more familiar in the context of quantum mechanical averaging. According to this path integral formulation, the probability for an arbitrary path connecting the initial and the final configurations is determined by a positive-definite 'action' functional. Again, we limit the discussion here to the simple case of Markovian limit where the friction per unit mass can be characterized by a simple constant $\eta$. The extension to the more general case is straightforward.

Following the notation of the last section, we denote by $\mathbf{r}(t)$ the multicomponent vector representing the co-ordinate of all the atoms that are explicitly treated. The

remaining degrees of freedom are integrated out and represented by a friction parameter $\eta$. In the path integral formalism for stochastic motion, the probability functional $P[\mathbf{r}(t)]$ for the system to take a particular path $\mathbf{r}(t)$ starting at $(\mathbf{r}_1, \mathbf{v}_1, t_1)$ and ending at $(\mathbf{r}_2, \mathbf{v}_2, t_2)$ is given by the following expression [239]:

$$P[\mathbf{r}(t)] = \frac{1}{\mathcal{N}} \exp\left\{ -\int_{t_1}^{t_2} \frac{\mathrm{d}t}{4m\eta k_B T} \left[ m\ddot{\mathbf{r}} + m\eta\dot{\mathbf{r}} + \nabla V(\mathbf{r}) \right]^2 \right\} \Bigg|_{\{\mathbf{r}(t_1)=\mathbf{r}_1, \dot{\mathbf{r}}(t_1)=\mathbf{v}_1\}.}^{\{\mathbf{r}(t_2)=\mathbf{r}_2, \dot{\mathbf{r}}(t_2)=\mathbf{v}_2\}} \tag{73}$$

The total joint probability for the particle to be in $(\mathbf{r}_1, \mathbf{v}_1)$ at $t = t_1$ and in $(\mathbf{r}_2, \mathbf{v}_2)$ at $t = t_2$ is then given by the path (functional) integral [238, 240]

$$P(\mathbf{r}_1, \mathbf{v}_1, t_1 | \mathbf{r}_2, \mathbf{v}_2, t_2) = \int [\mathcal{D}\mathbf{r}] P[\mathbf{r}(t)]. \tag{74}$$

The functional integral is over all the possible paths $\mathbf{r}(t)$ subject to the boundary conditions $(\mathbf{r}, \dot{\mathbf{r}}) = (\mathbf{r}_1, \mathbf{v}_1)$ at $t = t_1$ and $(\mathbf{r}_2, \mathbf{v}_2)$ at $t = t_2$. The integrand in equation (74) though complicated, is positive-definite and thus the numerical implementation of the path integral in equation (74) is well-defined. When compared with the Langevin equation as described in equation (63), it can be seen that the combination $[m\ddot{\mathbf{r}} + m\eta\dot{\mathbf{r}} + \nabla V(\mathbf{r})]$ is exactly the random force $\mathbf{f}(t)$ acting on the system due to coupling to the background. Thus, the path integral can be understood simply from the fact that $\mathbf{f}(t)$ obeys a Gaussian distribution with a self-correlation function related to the friction $\eta$ through the fluctuation-dissipation theorem.

The path integral formalism provides an alternative method to a direct solution of the Langevin or Fokker–Planck equation. All physical quantities can be calculated as path integrals with the distribution function $P[\mathbf{r}(t)]$ in equation (74) as the weighting factor. In the study of quantum systems, many powerful methods have been developed for the evaluation of path integrals. Moreover, as demonstrated below, the extremal path contribution to the path integral completely dominates at low temperatures and provides a powerful practical way of approaching stochastic events and the evaluation of diffusion coefficients. Recently, Dellago *et al.* [241] have applied a similar idea of path sampling to evaluate the rate of simple activated events. Instead of having an explicit functional with an analytic action as in equation (73), they employed a numerical approach using 'shooting' and 'wiggling' algorithms to generate paths that are distributed according to the proper governing equation. They demonstrated that this path sampling method provides a practical way of evaluating the rates of activated processes without the approximations and limitations of the transition state theory. It is particularly powerful when the knowledge of the transition state is not known *a priori*.

### 3.4.2. *Minimal path approximation*

For a direct numerical or analytic simulation study or solution of the Langevin equation for activated events, the most challenging regime is at low temperatures such that the thermal energy $k_B T$ is much less than the activation barrier. In this case, the adatoms spend most of the time performing localized motion around an adsorption site and the jump events to neighbouring sites are of rare occurrence. A direct simulation study becomes increasingly impractical while analytic solutions of the Langevin equation are limited to one or two dimensional problems only. Unfortunately, this is also the regime of most experimental interest. In this section, we will show that this is precisely the regime in which the evaluation of the path

integral discussed in the previous section can be simplified, owing to the dominance of the path that minimizes the action in equation (74) at low temperatures and/or low friction.

To illustrate this more clearly, we introduce a length scale $r_0$, an energy scale $V_0$ and a time scale $\tau_0 \equiv \sqrt{mr_0^2/V_0} \equiv 1/\omega_0$ for the system under consideration. Equation (74) can then be expressed in terms of dimensionless, scaled variables in the form

$$P(\mathbf{r}_1, \mathbf{v}_1, t_1 | \mathbf{r}_2, \mathbf{v}_2, t_2) = \int [\mathcal{D}\mathbf{r}] \exp\left\{-\frac{1}{\lambda} I\right\}, \tag{75}$$

with the boundary conditions $\{\mathbf{r}(t_1) = \mathbf{r}_1, \dot{\mathbf{r}}(t_1) = \mathbf{v}_1\}$ and $\{\mathbf{r}(t_2) = \mathbf{r}_2, \dot{\mathbf{r}}(t_2) = \mathbf{v}_2\}$, and an effective action

$$I = \int_{t_1}^{t_2} \mathrm{d}t [\ddot{\mathbf{r}}(t) + \eta^* \dot{\mathbf{r}}(t) + \nabla V(\mathbf{r}(t))]^2, \tag{76}$$

where $\mathbf{r}, t, V$ are all in their dimensionless form. The dimensionless friction parameter $\eta^*$ is defined as $\eta^* \equiv \eta/\omega_0$, and the dimensionless parameter $\lambda$ appearing in the exponential of the functional integrand is $\lambda = 4\eta^* k_B T/V_0$.

Clearly, in the low temperature ($k_B T \ll V_0$) and/or underdamped regime ($\eta^* \ll 1$), $\lambda \ll 1$, the minimal path of the functional $I[\mathbf{r}(t)]$ carries the dominant weight in the path integration of equation (75). Since the action functional $I$ is positive-definite, deviations from the minimal path carry negligible contribution to the path integral in equation (75). The minimal path is determined from the condition that the functional derivative $\delta I/\delta \mathbf{r}(t)$ vanishes. This leads to the standard Euler equations for the minimal path

$$\ddot{\boldsymbol{\zeta}}(t) - \eta^* \dot{\boldsymbol{\zeta}}(t) + \boldsymbol{\zeta} \cdot \nabla \nabla V(\mathbf{r}(t)) = 0, \tag{77}$$

$$\boldsymbol{\zeta}(t) = \ddot{\mathbf{r}}(t) + \eta^* \dot{\mathbf{r}}(t) + \nabla V(\mathbf{r}(t)). \tag{78}$$

Here, all the quantities are in dimensionless form.

An obvious solution to equation (77) is $\boldsymbol{\zeta} = 0$, i.e.

$$\ddot{\mathbf{r}}_d(t) + \eta^* \dot{\mathbf{r}}_d(t) + \nabla V(\mathbf{r}_d(t)) = 0. \tag{79}$$

Solving equation (79) with boundary conditions $\mathbf{r}_d(t_M) = \mathbf{r}_M, \dot{\mathbf{r}}_d(t_M) = \mathbf{v}_M$ and $\mathbf{r}_d(t_f) = \mathbf{r}_f, \dot{\mathbf{r}}_d(t_f) = \mathbf{v}_f$, for $t_M < t_f$, a minimal path $\mathbf{r}_d(t)$ is obtained that characterizes deactivation from state $(\mathbf{r}_M, \mathbf{v}_M)$ at $t_M$ to state $(\mathbf{r}_f, \mathbf{v}_f)$ at $t_f$. Along this path $\mathbf{r}_d(t)$ the energy of the system decreases monotonously and the action $I = \int_{t_M}^{t_f} \mathrm{d}t \zeta(t)^2$ assumes its minimal value $I_d = 0$.

A less obvious solution to the minimal path equation (77) is that $\boldsymbol{\zeta} = 2\eta^* \dot{\mathbf{r}}_a$, i.e.

$$\ddot{\mathbf{r}}_a(t) - \eta^* \dot{\mathbf{r}}_a(t) + \nabla V(\mathbf{r}_a(t)) = 0. \tag{80}$$

Solving equation (80) with boundary conditions $\mathbf{r}_a(t_i) = \mathbf{r}_i, \dot{\mathbf{r}}_a(t_i) = \mathbf{v}_i$ and $\mathbf{r}_a(t_M) = \mathbf{r}_M, \dot{\mathbf{r}}_a(t_M) = \mathbf{v}_M$, for $t_i < t_M$, a minimal path $\mathbf{r}_a(t)$ is obtained that characterizes activation from $(\mathbf{r}_i, \mathbf{v}_i)$ at $t_i$ to $(\mathbf{r}_M, \mathbf{v}_M)$ at $t_M$. Along this path $\mathbf{r}_a(t)$ the energy of the system increases monotonously and the action $I = \int_{t_i}^{t_M} \mathrm{d}t \zeta(t)^2$ assumes its minimal value $I_a = 4\eta^*(E_M - E_i)$, where $E_M = \mathbf{v}_M^2/2 + V(\mathbf{r}_M)$ and $E_i = \mathbf{v}_i^2/2 + V(\mathbf{r}_i)$ are the energies in dimensionless form at times $t_M$ and $t_i$, respectively.

Sewing the activation path $\mathbf{r}_a(t)$ and deactivation path $\mathbf{r}_d(t)$ together, we obtain the following joint probability, within the minimal path approximation,

$$P(\mathbf{r}_i, \mathbf{v}_i, t_i | \mathbf{r}_M, \mathbf{v}_M, t_M | \mathbf{r}_f, \mathbf{v}_f, t_f) = \delta(\mathbf{r}_i - \mathbf{r}_a(t_i|M))\delta(\mathbf{v}_i - \dot{\mathbf{r}}_a(t_i|M)) \exp[-(I_a + I_d)/\lambda] \times \delta(\mathbf{r}_f - \mathbf{r}_d(t_f|M))\delta(\mathbf{v}_f - \dot{\mathbf{r}}_d(t_f|M)). \quad (81)$$

Here $(\cdot|M)$ indicates that the activation path $\mathbf{r}_a(t)$ and the deactivation path $\mathbf{r}_d(t)$ are joined at $t_M$, i.e., $\mathbf{r}_a(t_M) = \mathbf{r}_d(t_M) = \mathbf{r}_M$ and $\dot{\mathbf{r}}_a(t_M) = \dot{\mathbf{r}}_d(t_M) = \mathbf{v}_M$. This three-configuration joint probability can be used, together with the initial (equilibrium or non-equilibrium) distribution $P(\mathbf{r}_i, \mathbf{v}_i)$, to conveniently evaluate the expectation values of physical observables. This minimal path approach is accurate at low temperatures and thus complements the existing methods that work better at higher temperatures. For a temperature not low enough, fluctuations around the minimal paths can be sampled numerically to improve the computation. As an example, this approach has been applied to study the activation of a cluster of three Lennard–Jones particles over a narrow passage from one stable state to another in a two dimensional external potential [242]. With moderate numerical efforts, this formalism holds the promise of being able to identify the relevant activation mechanisms and to locate new stable/metastable states.

3.4.3. *Application to surface diffusion*

In the previous section, we have demonstrated that the path integral at low temperatures and/or low friction is dominated by the minimal path, and can be well approximated by the minimal path contributions only. In this section, we want to demonstrate the application of the minimal path approximation (MPA) to the study of surface diffusion and show that for simple low dimensional systems, the known analytical results discussed in the previous section through the solution of the Langevin equation are recovered in the MPA. We have seen in the last section that the minimal path can be decomposed into an activation part and a deactivation part. The activation part of the minimal path is useful for escaping the well in the absence of any knowledge about the saddle point. However, for many systems the saddle point location is known. They can also be determined by a number of powerful methods such as the Nudged Elastic Band and Eigenvector Following methods [169, 168, 172, 171]. For this reason, we will only consider the deactivation part of the minimal path in our discussion here.

To illustrate the application of the MPA, we consider a simple model system of a single particle moving in a 1D adiabatic potential $V(x) = 1 - \cos(2\pi x)$ (in dimensionless form with energy scale $V_0$ and length scale $r_0$), while the coupling with the substrate vibrational (and electronic) degrees of freedom is characterized by a friction $\eta$. The deactivation part of the minimal path equation (79) becomes a simple Newtonian equation with friction,

$$\ddot{x}(t) + \eta^* \dot{x}(t) + V'(x(t)) = 0. \quad (82)$$

Integration of this mimimal path equation produces a final configuration $(x_f, v_f)$ from a given initial configuration $(x_i, v_i)$. From equation (82), it follows easily that the scaled energy $e(x) = (1/2)\dot{x}^2 + V(x)$ decreases monotonously along the minimal path as

$$\frac{\mathrm{d}e(x)}{\mathrm{d}t} = -\eta^* \dot{x}^2 = -2\eta^*[e(x) - V(x)]. \quad (83)$$

Thus, starting from the initial location at $x_i$ with initial energy $e_i = (1/2)v_i^2 + V(x_i)$, the energy $e(x)$ at a new location $x$ following the minimal path is

$$e(x) - e_i = -\eta^* \int_{x_i}^{x} \mathrm{d}x(\pm)\sqrt{2(e(x) - V(x))}, \tag{84}$$

for $e, e_i \geq 2$ (i.e. when the actual energy $E$ is larger than or equal to the diffusion barrier $V_b = 2V_0$). Here the $\pm$ sign corresponds to $\dot{x} > 0$ or $\dot{x} < 0$. Once $e(x)$ drops below the value of 2, i.e., when the energy falls below the barrier, the minimal path in equation (82) starts to oscillate between two potential maxima with decreasing energy and eventually settles down to the well bottom, corresponding to the deactivation of the particle. Therefore, following the minimal path ($v_i > 0$) from $-1/2 < x_i < 1/2$ to the point $x$ where $e(x) = 2$, we conclude that the final position $x_f = l = [x + 0.5]$ [i.e., $(l - 1/2) < x < (l + 1/2)$] with the final velocity $v_f = 0$ (noting that we are interested in $t_f = \infty$). Thus, we have

$$x_f = l, v_f = 0 \quad \text{for} \quad e_l(x_i) < e_i < e_{l+1}(x_i), \tag{85}$$

where the energy boundary

$$e_l = 2 + \eta^* \int_{x_i}^{l-1/2+0} \mathrm{d}x\sqrt{2[e(x) - V(x)]}, \tag{86}$$

is determined by solving equation (84) for an $e(x)$ that satisfies the boundary conditions $e(x = x_i) = e_l$ and $e(x = l - 1/2 + 0) = 2$.

The solution of these different minimal paths corresponds nicely to the physical picture that at low temperatures, the actual motion of the adatom can be characterized by series of uncorrelated jumps of variable lengths. To evaluate the diffusion coefficient for this system, we can use the formula

$$D_t = \int_0^\infty \mathrm{d}t\langle v(0)v(t)\rangle \,\mathrm{d}t. \tag{87}$$

Applying the conclusion about the final configuration $x_f$ for a given $e_i$ in equation (85), we can decompose the expression for $D_t$ in equation (87) into contributions from different minimal paths of various jump lengths $l$ as

$$D_t = \frac{4d^2}{Z\tau_0}\int_{-1/2}^{1/2} \mathrm{d}x_i \sum_{l=1}^{\infty} \int_{e_l}^{e_{l+1}} \mathrm{d}e_i \exp\left(-\frac{V_0 e_i}{k_B T}\right) l. \tag{88}$$

Here the initial position $x_i$, velocity $v_i$ and energy $e_i = (1/2)v_i^2 + V(x_i)$ are all in dimensionless form. In the underdamped and overdamped limits corresponding to $\eta^* \ll 1$ or $\eta^* \gg 1$, analytical results can be obtained. First, we examine the underdamped limit. In this case, the energy of the particle in transit differs only slightly from the threshold value of $e = 2$ (i.e. $E = 2V_0$). Thus, to lowest order in $\eta^*$, we can replace the energy function $e(x)$ in the integrand of equation (86) by the constant value of 2, leading to the expression

$$e_l = 2 + \eta^* \int_{x_i}^{l-1/2} \mathrm{d}x\sqrt{2[1 + \cos(2\pi x)]} \ . \tag{89}$$

For $l \geq 1$,

$$e_l = 2 + (l - 1)\frac{4}{\pi}\eta^* + \eta^*\frac{2}{\pi}(1 - \sin \pi x_i). \tag{90}$$

Substitution of the result for $e_l$ in equation (90) into the expression for $D_t$ in equation (88) yields the following result valid for $\eta^* \ll 1$:

$$D_t = \frac{4d^2 k_B T}{Z\tau_0 V_0} \int_{-1/2}^{1/2} \mathrm{d}x_i \sum_{l=1}^{\infty} \left[ \exp\left(-\frac{V_0 e_l}{k_B T}\right) - \exp\left(-\frac{V_0 e_{l+1}}{k_B T}\right) \right] l$$
$$= \frac{4d^2 k_B T}{Z\tau_0 V_0} \exp\left(-\frac{2V_0}{k_B T}\right) \left[1 - \exp\left(-\frac{4V_0 \eta^*}{\pi k_B T}\right)\right]^{-1} g(\eta^*, V_0, T), \tag{91}$$

with

$$g(\eta^*, V_0, T) = \int_{-1/2}^{1/2} \mathrm{d}x_i \exp\left[-\frac{V_0 \eta^*}{k_B T} \frac{2}{\pi}(1 - \sin \pi x_i)\right]. \tag{92}$$

This expression for $D_t$ can be simplified even further in the 'low friction' limit when we have $\eta^* \ll k_B T/V_0$. In this case, equation (91) simplifies to

$$D_t = \frac{\pi k_B T}{2m\eta^* \omega_0} \exp\left(-\frac{2V_0}{k_B T}\right), \tag{93}$$

which coincides with the result of equation (68) derived by other means as discussed section 3.3. Note that in the low temperature regime s.t. $V_0 \gg k_B T$, the condition for the low friction limit required for the validity of equation (93) is much more stringent than the mere requirement of underdamping, i.e. $\eta^* \ll 1$.

In the high friction regime, when $\eta^* \gg 1$, the minimal path approximation again recovers the known analytical results. For $\eta^* \gg 1$, energy dissipates rapidly along the minimal path at a rate $\propto \eta^*$ (see equation (83)). It is clear that $e_l \geq e_1 + O(\eta^*)$ for $l = 2, 3, \ldots$ and therefore activated jumps are dominantly over one single barrier. Furthermore, considering a minimal path starting from $-1/2 < x_i < 1/2$ with $v_i > 0$, $e_1(x_i)$ strongly depends on the initial position $x_i$ and, in fact, the minimal path can reach the next well region $x > 1/2$ only when $x_i$ is very close to the barrier $x = 1/2$. Approximating the potential around $x = 1/2$ as $V(x) = 2 + 2\pi^2(x - 1/2)^2$, the minimal path solution of equation (82) gives

$$e_1 = 2 + \tfrac{1}{2}(\eta^*)^2 (x_i - 1/2)^2, \tag{94}$$

where the energy $e(x)$ (in the minimal path solution) satisfies the boundary conditions $e(x = x_i) = e_1$ and $e(x = 1/2 + 0) = 2$. In this, integrating equation (88), the diffusion coefficient is found to be

$$D_t = \frac{\omega_0^2}{2\pi\eta^*} \exp\left(-\frac{2V_0}{k_B T}\right), \tag{95}$$

which is in exact agreement with the low-$T$ limit of equation (66).

These results demonstrate the power of the MPA in the path integral approach. The MPA is valid over a wide range of values of temperature and friction of experimental interest. Moreover, it can be generalized in a straightforward manner to the multidimensional case. In this case, the sampling over the initial states $(\mathbf{x}_i, \mathbf{v}_i)$ can be achieved through Monte Carlo methods, while the integration of the deactivation path starting from $(\mathbf{x}_i, \mathbf{v}_i)$ is straightforward. Thus, the MPA is complementary to the direct simulation approach. It works precisely in the regime where a direct simulation study is no longer feasible. The rare activation problem at low temperatures is avoided by starting at or above the threshold energy at the

saddle point and sampling the neighborhood of these starting points. The MPA approach is a direct generalization of the transition state theory (TST) including all the dynamical corrections [243]. The effect of recrossings or long jumps are automatically included in the minimal paths. Unlike TST which breaks down at low friction, the sampling over the initial states in equation (79) is over all the states whether they start from the given well or on transit from another well. Thus the use of the Boltzmann distribution is correct even in the low friction limit. These minimal paths also are similar to the 'transition paths' discussed by Jacobsen *et al.* [71] in a different approach.

### 3.5. *Monte Carlo simulations*

Diffusion in dense adsorbed layers is often treated by means of lattice gas models. Apart from some analytical results obtained in the framework of the Frenkel–Kontorova model [244, 245], when dealing with 2D interacting systems, one has to resort to simulations [225, 226, 246], or to treat simplified models, such as the lattice gas. The lattice-gas description of diffusion is reasonable when the temperature is sufficiently low so that the diffusing particles are well localized about adsorption sites which form an ordered array, and move among these sites with a rate which is much smaller than the typical vibrational frequencies (see section 2.1). Lattice-gas models are most commonly studied by Monte Carlo (MC) simulations. Here we treat the lattice-gas models addressing the following issues: How does one choose the microscopic rates to mimic surface diffusion within the lattice gas description? Given the knowledge of the rates of the different microscopic processes, how can one extract information about the collective and the tracer diffusion coefficients in a MC simulation?

#### 3.5.1. *Lattice gas model and transition algorithms*

Let us consider a 2D lattice of $M$ sites, labelled by vectors $\mathbf{l}$. The lattice is filled by $N$ particles (for simplicity we assume that they are identical), with coverage $\theta = N/M$. To each site, an occupation variable $n_{\mathbf{l}}$ is associated; if site exclusion is assumed, each $n_{\mathbf{l}}$ can be either 0 or 1 and $\sum n_{\mathbf{l}} = N$. The particles interact with each other with a Hamiltonian $\mathcal{H}$ which depends on the full configuration of the lattice gas $\mathbf{n} = \{n_{\mathbf{l}}\}$:

$$\mathcal{H}(\mathbf{n}) = \frac{1}{2}\sum_{\mathbf{l}_1,\mathbf{l}_2} V_{\mathbf{l}_1,\mathbf{l}_2} n_{\mathbf{l}_1} n_{\mathbf{l}_2} + \frac{1}{6}\sum_{\mathbf{l}_1,\mathbf{l}_2,\mathbf{l}_3} V_{\mathbf{l}_1,\mathbf{l}_2,\mathbf{l}_3} n_{\mathbf{l}_1} n_{\mathbf{l}_2} n_{\mathbf{l}_3} + \cdots, \tag{96}$$

where two-body and many-body interaction terms can be included. If translational invariance is assumed on the lattice, $V_{\mathbf{l}_1,\mathbf{l}_2}$ depends only on $\mathbf{l}_1 - \mathbf{l}_2$.

The lattice gas Hamiltonian has been widely used in the literature to study both static and dynamic properties. For static properties such as critical exponents and phase transition boundaries, the lattice Hamiltonian as defined in equation (96) completely determines the problem. All one needs to do is to perform averages over a canonical or grand canonical distribution of configurations as defined by the Hamiltonian. This can be achieved either analytically (usually through some approximate schemes) or numerically through MC simulations which generate a set of configurations that satisfies the correct distribution. In particular, the rules for generating a new configuration from an existing one, i.e. the dynamical algorithms, can be rather arbitrary as long as the correct distribution is obtained. For the evaluation of dynamical properties such as diffusion coefficients or any other time

dependent correlation functions, the situation is entirely different, since the lattice gas Hamiltonian itself does not provide the dynamics for the transition from one state to another. We thus need to consider the specific form for the transition probabilities. Provided that detailed balance is satisfied, all choices give the same equilibrium properties, but they do *not* give the same dynamical properties. This point will be further discussed in section 4.5, with a specific example.

The evolution of the lattice gas can be described by a master equation. The master equation generally applies to the evolution of the probability $P(\mathbf{n}, t)$ of being in a given configuration $\mathbf{n}$ at time $t$, and it reads:

$$\frac{\mathrm{d}P(\mathbf{n}, t)}{\mathrm{d}t} = \sum_{\mathbf{n}'} [w(\mathbf{n}' \rightleftarrows \mathbf{n})P(\mathbf{n}', t) - w(\mathbf{n} \rightleftarrows \mathbf{n}')P(\mathbf{n}, t)], \tag{97}$$

where the $w$ are the transition rates among different configurations. The master equation can be also written in terms of the time evolution of the occupation variables (see reference [22] for a detailed derivation) as

$$\frac{\mathrm{d}n_{\mathbf{l}}}{\mathrm{d}t} = \sum_{\mathbf{a}} (n_{\mathbf{l}+\mathbf{a}} - n_{\mathbf{l}})w_{\mathbf{l},\mathbf{l}+\mathbf{a}}(\mathbf{n}), \tag{98}$$

where $w_{\mathbf{l},\mathbf{l}+\mathbf{a}}(\mathbf{n})$ is the transition rate between configuration $\mathbf{n}$ and the configuration $\mathbf{n}'$ in which the occupations of the two sites $\mathbf{l}$ and $\mathbf{l}+\mathbf{a}$ have been exchanged with each other (i.e. when the particle in $\mathbf{l}$ moves to $\mathbf{l}+\mathbf{a}$ or vice versa). A sufficient condition for the attainment of equilibrium in the lattice gas is the detailed balance condition

$$w_{\mathbf{l},\mathbf{l}+\mathbf{a}}(\mathbf{n}) \exp[-\beta\mathcal{H}(\mathbf{n})] = w_{\mathbf{l}+\mathbf{a},\mathbf{l}}(\mathbf{n}') \exp[-\beta\mathcal{H}(\mathbf{n}')]. \tag{99}$$

We remark again that the detailed balance condition does not uniquely determine the transition rates. Different choices are still possible; and the best choice would follow from a detailed knowledge of the microscopic dynamics of the system. This is in most cases not known in detail, because it is extremely difficult to calculate (or measure) barriers and prefactors for all processes in a dense overlayer with complicated interactions; therefore transition rates based on simple model assumptions are very often employed. This point must be always kept in mind when comparing lattice-gas calculations or simulations with experimental data. The transition rates $w(\mathbf{n} \rightleftarrows \mathbf{n}')$ are usually written in terms of the transition probabilities $p(\mathbf{n}, \mathbf{n}')$; the latter are related to the transition rates by

$$w(\mathbf{n} \rightleftarrows \mathbf{n}') = \frac{p(\mathbf{n}, \mathbf{n}')}{\tau_0}, \tag{100}$$

where $\tau_0$ is the elementary time unit in the system, chosen usually as the inverse of the frequency of the fastest possible transition in the system. Possible choices for $p$ are:

- The Metropolis algorithm [247, 21]:

$$p(\mathbf{n}, \mathbf{n}') = \begin{cases} 1, & \text{if } \delta E \leq 0; \\ \exp(-\beta\delta E), & \text{otherwise,} \end{cases} \tag{101}$$

  where $\delta E = E(\mathbf{n}') - E(\mathbf{n})$.
- The Kawasaki algorithm [248, 21]:

$$p(\mathbf{n}, \mathbf{n}') = \frac{1}{1 + \exp(\beta\delta E)}. \tag{102}$$

- The initial value algorithm [249, 17, 250]: This is the perhaps the simplest form such that $p(\mathbf{n}, \mathbf{n}')$ only depends on the initial configuration of the system before the transition (i.e. before the jump of the particle in our case). This algorithm assumes that lateral interactions among particles act only at the minima and not at saddle points [22]. The transition probability is written as

$$p(\mathbf{n}, \mathbf{n}') = p_0 \exp(\beta E_i), \tag{103}$$

  where $E_i$ is the energy shift of the jumping particle in its initial position due to lateral interactions, and $p_0 = \exp(-\beta E_{\max})$, where $E_{\max}$ is the maximum of such energy shifts. A microscopic justification of this algorithm can be given when the lateral interactions are among nearest-neighbour sites only [22]. In other cases, the use of this algorithm can be questionable, and it may be necessary to explicitly introduce the effect of the interactions at the saddle point [146, 135].
- The transition dynamics algorithm (TDA) [20]: an intermediate state $I$ is introduced and the transition probability of each jump is written as a product of two probabilities as

$$p(\mathbf{n}, \mathbf{n}') = p(\mathbf{n}, I)\, p(I, \mathbf{n}'). \tag{104}$$

  In this algorithm, the transition actually proceeds by two successive steps via the intermediate state with energy $E(I)$. Here $E(I)$ has to be chosen to describe a jump attempt of a particle in the presence of interactions as realistically as possible without violating the detailed balance condition. One possible choice is [20]

$$E(I) = \frac{[E(\mathbf{n}) + E(\mathbf{n}')]}{2} + \Delta, \tag{105}$$

  where the quantity $\Delta$ characterizes the activation barrier in the zero coverage limit due to the substrate–adatom interaction (i.e. from the adiabatic potential). For the rates $p(\mathbf{n}, I)$ and $p(I, \mathbf{n}')$ any suitable form such as the Metropolis form satisfying the condition of detailed balance is applicable. The *instantaneous activation barrier* $E_A$ for a jump attempt from a filled to a vacant site is then given by

$$E_A = \max(E(I) - E(\mathbf{n}), E(\mathbf{n}') - E(\mathbf{n}), 0). \tag{106}$$

  This illustrates the main advantage of the TDA method. Namely, for $\Delta > 0$ the rates can be of activated form also for jumps with $E(\mathbf{n}) \geq E(\mathbf{n}')$. Satisfying the detailed balance [20], the TDA method therefore complements the description of the Hamiltonian given by equation (96).

In section 4.5, we will discuss in the framework of the MC simulation study of specific systems how the results for the diffusion coefficient explicitly depend on the choice of the transition algorithm. This is especially important for systems near a phase transition where the different choice of dynamic algorithms lead to vastly different critical temperature dependence for the diffusion coefficients [251, 252]. In this case, proper conclusions can only be drawn when the transition algorithm chosen bears a close relation to the real dynamics as for example determined by a comparison with, e.g. MD simulations.

3.5.2. *Implementation of Monte Carlo simulations for surface diffusion studies*

A very convenient way of calculating diffusion coefficients and correlation functions in lattice-gas models relies on MC simulations. As underlined in section 3.5.1, analytical or semi-analytical methods become untractable in many cases. On the other hand, the MC method is a general tool for solving the master equation, and to calculate both static equilibrium properties and time-dependent correlation functions.

In the following we outline two methods based on MC simulations. The standard method originates from equilibrium statistical mechanics, and has its starting point in the development of the Metropolis algorithm [247, 21], followed later by several variants. They have been successfully adapted to the study of kinetic problems. The second method [112] is known as time-dependent Monte Carlo [253], and even though it was developed at first for the study of equilibrium properties [254], it is now often used for simulations of crystal growth and related problems [253, 300].

All MC methods are based on the general theory of Markov chains [21]. With numerical applications in mind, we assume that the state space of the lattice gas $S$ is discrete and of finite size $|S|$. The transitions from any state $\mathbf{n}$ to any other state $\mathbf{n}'$ are determined by the individual transition probabilities $p(\mathbf{n}, \mathbf{n}')$. A Markov chain is then specified by the following two ingredients:

(i) The initial distribution $\Omega$. Thus, the process will be defined in such a way that the probability density of state $\mathbf{n}$ at time $t = 0$ is $\Omega(\mathbf{n})$.
(ii) The transition probabilities $p(\mathbf{n}, \mathbf{n}')$. They give the conditional probability of being in configuration $\mathbf{n}'$ at a given step in the chain, knowing that the system was in $\mathbf{n}$ at the step immediately before.

These two conditions imply that the state of the system at the next step depends *only* on the state of the system at present, and not on the previous steps. This method of generating the configurations then yields a distribution function $P(\mathbf{n}, t)$ as obtained from the solution of the master equation in equation (97). A sufficient condition to attain equilibrium in the Markov chain is the detailed balance condition (see equation (99)), which can be easily written for the transition probabilities. Static equilibrium properties and time-correlation functions can be measured by sampling the different configurations in the chain, once the chain itself has reached the stationary state.

In the standard implementation of the MC simulation method for dynamical studies, at each step in the simulation a particle is randomly chosen. Then a jump direction is chosen, again randomly, towards a possible arrival site (which characterizes a possible final configuration $\mathbf{n}'$). If the arrival site is full, the move is rejected. If it is empty, the probability $p(\mathbf{n}, \mathbf{n}')$ is computed and a random number $0 < r \leq 1$ is generated. If $r \leq p(\mathbf{n}, \mathbf{n}')$, the move is accepted, otherwise it is rejected. Each MC step corresponds to one unit of time whose precise microscopic interpretation is difficult. For simple systems, this can be compared with, say, MD calculations to map out the dynamics back to real time. The main shortcoming of this implementation of MC simulations becomes evident at low temperatures, where the transition probabilities can become very small. Thus, a large part of the computing time is spent in attempting moves which are rejected, so that the generation of statistically independent configurations is very time-consuming. This drawback may be overcome by a MC scheme in which moves are chosen on the basis

of their *a priori* probability, so that no moves are rejected [254, 112]. This is the basis of the so-called time-dependent MC method.

In the time-dependent MC method, consider the system in a configuration $\mathbf{n}$ and label all the possible transitions $\mathbf{n} \rightleftarrows \mathbf{n}'$ to all the possible final states which can be reached from $\mathbf{n}$, with an index $k = 1, \ldots, K$. Then, a rate $w(\mathbf{n} \rightleftarrows \mathbf{n}')$ is associated to each of these transitions. The total transition rate $W(\mathbf{n})$ and the partial sums $W(\mathbf{n}; k)$ are built up as

$$W(\mathbf{n}) = \sum_{\mathbf{n}'} w(\mathbf{n} \rightleftarrows \mathbf{n}') = \sum_{k=1}^{K} w(\mathbf{n}; k);$$

$$W(\mathbf{n}; k) = \sum_{l=1}^{k} w(\mathbf{n}; l), \tag{107}$$

with $W(\mathbf{n}; 0) = 0$ by definition. A random number $r$ is generated such that $0 < r \leq W(\mathbf{n})$; if $W(\mathbf{n}, k-1) < r \leq W(\mathbf{n}, k)$, then event $k$ is chosen and executed. In this procedure, detailed balance is satisfied provided that time is incremented proportionally to the lifetime $\tau(\mathbf{n})$ of the configuration; the latter is inversely proportional to its total rate: $\tau(\mathbf{n}) = \tau_0 / W(\mathbf{n})$. The actual time increment of the transition is chosen randomly from the distribution of intervals with decay time $\tau(\mathbf{n})$ [254]. By choosing a variable time step scaled according to the inverse of the transition probability, the time-dependent MC overcomes the problem of rare transitions encountered in the standard Monte Carlo method. However, in this implementation, a large part of the computer time is spent in calculating the total and partial rates at each simulation step, and in choosing the process to execute. A very important point is thus to organize the simulation in such a way that these rates are calculated efficiently [253], and that the choice of the process is easy. Either processes are organized in classes ([254], an implementation of this kind for surface diffusion studies is found in reference [255]), or rates are associated to particles and grouped by a binary-tree scheme [256, 119]. Thus, when one considers complex systems, where many different jump processes are possible depending on the environment of each particle, the advantage of the time-dependent Monte Carlo over the standard method may be lost. It should also be noted that the method is useful only at temperatures low as compared to the energy barriers between the different states.

After the generation of the ensemble of time dependent configurations in a Monte Carlo simulation, one still has a different choice of evaluating the diffusion coefficient via the different formulae discussed in section 2.2. Here we outline the most efficient strategies to calculate the quantities of interest for surface diffusion in interacting lattice gases; we focus first on $D_t$, then on the thermodynamic factor and finally on $D_{CM}$, which is the most difficult quantity to calculate. The collective diffusion coefficient $D_c$ given by the product of the thermodynamic factor and of $D_{CM}$ (see equation (26)); however it can be directly calculated by different methods, which are briefly outlined in the final part of this section.

*Tracer diffusion coefficient* $D_t$—The calculation of $D_t$ by MC simulations is not usually very difficult, since $D_t$ is a self-averaging quantity: each particle in the lattice gas is sampled, so that a simulation with $N$ particles gives $N$ samples, and it is easy to accumulate a good statistics. The simple-minded way to calculate $D_t$ is to monitor the mean-square displacement $\Delta r^2(t)$ until the asymptotic linear behaviour is

reached, say at $t = t_m$ (see figure 10), and then to numerically calculate the slope of the linear part of the curve. This implies an accurate sampling of $\Delta r^2(t)$ for $t \gg t_m$, and because of that, some problems may arise within this approach. In fact, it must be kept in mind that given a fixed number of simulations in a system of a given fixed size, the statistical accuracy of $\Delta r^2(t)$ decreases with $t$, so that the numerical estimate of the asymptotic slope may become difficult. In the case of $D_t$ this is not usually a very serious drawback, since a huge statistics can be accumulated rather easily. However, when strong memory effects come into play, $t_m$ may be large, and the sampling at $t \gg t_m$ may be difficult. In this case, there is a noticeable advantage in using the MEM which converges at $t \sim t_m$ [120]. As shown in the following, this is much more important when calculating $D_{CM}$.

*Thermodynamic factor*—The thermodynamic factor is efficiently calculated by means of grand-canonical simulations; there the chemical potential $\mu$ is fixed, and the number of particles (and the coverage $\theta$) fluctuates. By simulating at different $\mu$, the curve $\mu(\theta)$ can be constructed, and the thermodynamic factor is then obtained by numerical derivation. This method works fairly well in almost all cases. However, when approaching phase boundaries, $\mu(\theta)$ may become a rapidly varying function; moreover, the statistical accuracy of each single point in $\mu(\theta)$ decreases due to the onset of long time correlations in the system. In this case, it may be very difficult to have a reliable estimate of the numerical derivative, and it may be convenient to monitor directly, again in grand-canonical simulations, the mean square fluctuation $\langle(\Delta N)^2\rangle$ of the particle number, which is directly related to the thermodynamic factor by equation (24). Also canonical simulations (i.e. at fixed particle number) can be used to calculate the thermodynamic factor. One possibility [250] is to single out a part of the simulation box (usually a square, say of size $\ell$ at the centre of the box of size $L_B$), and to monitor particle-number fluctuations in this part. At given $\ell$, this method however converges very slowly with $L_B$ [121]. This means a waste of computer time to reach a good numerical accuracy (see figure 19). Reasonable

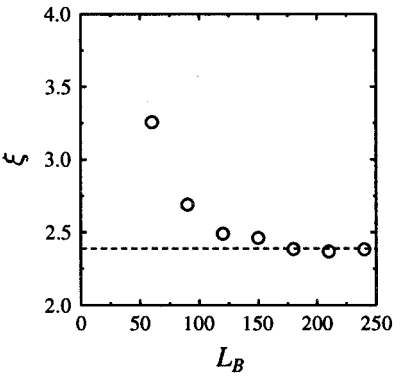


Figure 19. Thermodynamic factor $\xi = 1/S_0$ versus the simulation box size $L_B$ using the canonical simulation method where a probe system of size $l \times l$ ($l = 30$ here) is embedded in a larger system of size $L_B \times L_B$. This example [121] is for the model of O/W(110) described in section 3.5., at $\theta = 0.45$ and $T = 2.14T_c$. The convergence of the results is seen at $L_B \simeq 200$. Grand canonical simulations on the other hand converge already at $L_B = 30$ to the value represented by the dashed line.

numerical accuracy in this canonical method can only be reached for $L_B \gg \ell$, while grand-canonical simulations already give comparable results for a system of total size $\ell$. However, there exists a very efficient method in the canonical ensemble which can be easily used. It is based on the direct evaluation of $S_0$ as $S_0 = \lim_{\mathbf{q}\to 0} S(\mathbf{q})$ using simple and efficient Fast Fourier transform (see section 2.2.2).

*Centre-of-mass diffusion coefficient* $D_{CM}$—The centre-of-mass diffusion coefficient $D_{CM}$ is not a self-averaging quantity: even if all atomic displacements contribute to $D_{CM}$ (so that memory effects partially cancel out and become weaker than in the case of $D_t$) each simulation for a system of $N$ particles gives a single sample, and therefore several simulations are necessary to achieve a reasonable statistical accuracy. On the contrary, for $D_t$ a single simulation on a sufficiently large sample is usually sufficient. This explains why the numerical calculation of $D_{CM}$ is very often cumbersome, and the direct estimation of the asymptotic slope of $\Delta r^2(t)$ is difficult, even if memory effects in $D_{CM}$ are usually weaker that in $D_t$. Because of that, the use of the MEM is highly recommended.

*Other methods: direct evaluation of* $D_c$—Alternative methods allow a direct evaluation of $D_c$ without calculating the thermodynamic factor and $D_{CM}$ separately. The advantage of these methods is that $D_c$ can be calculated directly from standard canonical simulations. The disadvantage is that (as explained in the following) it is much more difficult to reach the same numerical accuracy as in the 'indirect' methods with the memory expansion, because the direct methods need the evaluation of asymptotic slopes, and the numerical evaluation of limits. However, these direct methods are well suited to explore the behaviour beyond the hydrodynamic limit, up to wavelengths close to the size of the lattice itself, and to mimic rather closely the real experimental situations. The direct methods can be divided into two classes: equilibrium and non-equilibrium methods. The equilibrium methods are based on the numerical computation of the characteristic function $S(\mathbf{q}, t)$ (equation (19)) and on the fitting of its asymptotic exponential decay with time in the hydrodynamic limit [257]. Here, two limits must be performed: a small $q$ limit, in order to reach the hydrodynamic regime of long distances, and a long-time limit in order to single out the asymptotic decay. The non-equilibrium methods are based on the monitoring of the decay of an initial profile, which can be either sinusoidal [258] or step-like [405, 259, 260, 152, 153]. In order to estimate the equilibrium $D_c$ by non-equilibrium methods, the initial perturbation should be sufficiently smooth to be treated within the linear-response regime. The sinusoidal profile is to be preferred with this respect since it is smoother than the step-like profile. The latter however mimics some typical experimental configurations, and can be treated also within the Boltzmann–Matano analysis [8]. The analysis of the decay of any kind of profile involves again both small $q$ and long-time limits, and moreover a limit to small periodic perturbations for linear response theory must be applied.

In conclusion, we would like to emphasize that as far as the calculation of $D_c$ is concerned, the most efficient method relies on the use of equation (26), with $D_{CM}$ calculated by the memory expansion, and the thermodynamic factor from the small $q$ limit of $S(\mathbf{q})$. For example, the extraction of $D_c$ from the decay of $S_c(\mathbf{q},t)$ requires larger simulation sizes than the memory expansion for a given accuracy, because quite small values of $q$ are needed. Moreover, the asymptotic decay in time is reached on a somewhat longer time scale [257], and this implies longer simulations (and a larger number of them, since statistical accuracy decreases at long times).

### 3.6. *Molecular Dynamics methods*

In Molecular Dynamics (MD) simulations, the equations of motion for a system of $N$ atoms are numerically solved [21]. In most of the studies concerning surface diffusion, classical MD has been employed. In this framework, a potential energy function $V(\mathbf{r}_1, \mathbf{r}_2, \ldots, \mathbf{r}_N)$ for the atomic cores is built up. The functional form of $V$ is derived by some approximation within the theory of electronic structure, and it contains parameters which are fitted on known properties of the element under study (semiempirical approach, see section 3.1., and references therein). In this way, electrons do not appear in the numerical calculations, and the motion of the cores in the potential $V$ is followed. Because of that, the coupling of the adatom to phononic excitations is automatically included in MD calculations, while the non-adiabatic electronic coupling (which is the cause of the electronic contribution to friction, see section 3.3) is missing. The Newton's equations of motion read

$$m_i \mathbf{a}_i = -\frac{\partial V}{\partial \mathbf{r}_i}, \tag{108}$$

where $m_i$ and $\mathbf{a}_i$ are the masses and the accelerations of the particles. In the simplest scheme, which is actually recommended for the study of surface diffusion, the total energy is conserved (microcanonical MD), and temperature is calculated as the average kinetic temperature [21]. In some cases, it is necessary to employ canonical MD, where the system is coupled to a thermostat. For example, when simulating growth, the adsorption energy of incoming adatoms must be taken away to avoid the heating of the system [261]. The thermostat usually alters the diffusive properties of the adatoms and thus it must be used with considerable care. In fact, the thermostat must be tuned in such a way that its effects on time-dependent correlation functions are negligible [261, 237]. This is rather easy to achieve in the case of Langevin or Andersen thermostats [21], where the energy exchange between the system and the thermostat is controlled by a parameter which has a simple physical meaning (an additional friction for the Langevin thermostat, a collision frequency for the Andersen thermostat), and the tuning of the parameter is relatively simple.

Compared to Monte Carlo modelling, MD is much more detailed from the microscopic point of view and has a natural dynamics arising from the Hamiltonian description, while in MC the dynamics is superimposed to the Hamiltonian description (see the discussion in section 3.5). On the other hand, standard MD can at present be performed on rather short time scales. In fact, the numerical solution of (108) is achieved by discretizing time in steps $\delta t$. The steps $\delta t$ must be much shorter than the typical vibrational periods which are of the order of $10^{-12}$–$10^{-13}$ s. Therefore $\delta t$ is usually chosen in the range of say $10^{-15}$ s. For system sizes of a few hundreds of atoms, the maximum number of time steps which can be reasonably simulated is less than $10^9$ by the present computational means. This sets an upper limit on the simulation time scale $t_f$: $t_f < 1\,\mu s$, provided that the system under study is not too large. This indeed allows the study of the basic processes in surface diffusion at high temperatures (see for example references [37, 100, 68, 69, 40, 70, 58, 72, 104]; a sequence of snapshots from a MD simulation of a rather complicated event is reported in figure 20). When $E_A/(k_B T) \leq 10$, a good statistics of events can be rather easily accumulated [58]. Compared to the typical experimental conditions the MD scale is however much faster, and usually MD simulations are performed at higher temperatures in order to speed up the diffusion processes. This gives very useful information in simple cases, for example when following the

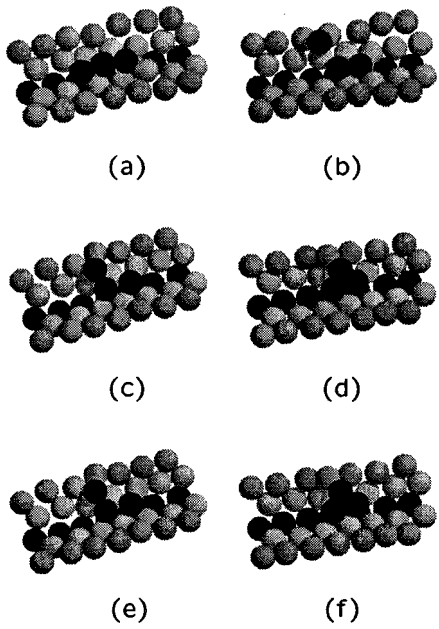


Figure 20. Example of a rather complicated diffusion event followed by standard classical MD. The snapshots are taken from a MD simulation of an Au trimer on the missing-row Au(110) surface at $T = 450\,\mathrm{K}$ [118]. The leapfrog process is taking place (see section 4.2.): a side atom of the trimer is promoted above the trimer itself (b), then it remains trapped in a deep metastable minimum (d) and finally jumps down at the opposite side of the trimer ((e) and (f)). The configuration in (d) may persist of the order of $10^2 - 10^3$ ps around this temperature, while configurations (b) and (e) have a shorter lifetime because they correspond to shallow metastable minima (see also figure 30).

motion of a single adatom or of a small cluster. On the other hand, when studying the diffusion of many adsorbed particles (for example, dense adsorbed layers, or large islands) standard MD, even if it can be still useful [262, 263], is of less help for the direct interpretation of experiments. In the case of adsorbed layers on (approximately) inert substrates, a possibility is to simulate the adsorbed layer by full MD, and the coupling with the rigid substrate within a Langevin description [53, 226, 225]. This can extend both the size and the time scale reachable by the simulations. However, even within this approach, in many cases there is still a considerable gap in the time scales between the MD simulations and experiments. In order to try to fill this gap, retaining at the same time the detailed microscopic description, accelerated MD methods have been recently developed.

3.6.1. *Accelerated Molecular Dynamics methods*

The fundamental reason for the slowness of straightforward MD calculations of surface diffusion at low temperatures is the fact that the adatom spends most of its time oscillating around the potential minimum. The rate of transitions is proportional to $\exp(-E_A/k_BT)$ which becomes very small for $E_A/k_BT \gg 1$. Recently, A. F. Voter [198, 264] has proposed two variants of the MD method, the hyper-MD

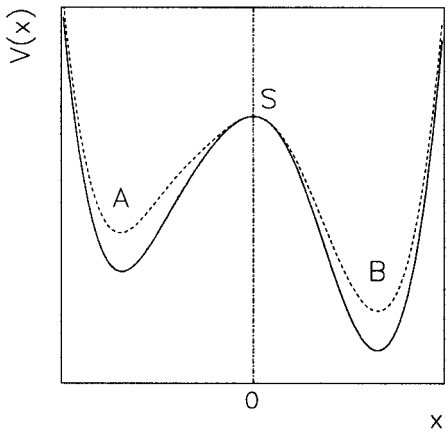


Figure 21. Potential energy of a two-state system (solid line). The vertical line located at the saddle point S denotes the TST dividing surface. A bias potential (dashed line) is added to raise the positions of the two minima A and B relative to S outside of the dividing surface.

method and the Temperature Accelerated Dynamics (TAD), in order to overcome this difficulty, thus extending the time scale of MD simulations.

*Hyper-MD*—The hyper Molecular Dynamics method is based on the idea of modifying the potential energy $V(\mathbf{r})$ by adding a *bias potential* $\Delta V_b(\mathbf{r})$ to it as shown schematically in figure 21. The application of the bias potential is based on the TST approximation, according to which the transition rates are determined by the flux through the dividing surface which in simple systems is located at the relevant saddle point. The bias potential is constructed in such a way as to keep the total potential at the saddle point unchanged. This leads to an enhanced escape rate from the minimum given by

$$\tau_e = \frac{1}{n_e} \sum_{i=1}^{n_{\text{tot}}} \delta t \, \exp\{\beta \Delta V_b[\mathbf{r}(t_i)]\}, \tag{109}$$

where $\delta t$ is the regular MD time step, $n_{\text{tot}}$ is the total number of MD steps, $t_i = i\delta t$, and $n_e$ is the number of escape attempts from the minimum. This equation shows that the application of a bias potential leads to a *boost* in the $i$th MD step given by

$$\delta t_i^b = \delta t \, \exp\{\beta \Delta V_b[\mathbf{r}(t_i)]\}. \tag{110}$$

This means that at low temperatures, there is in principle an exponential boost of the simulation time available through hyper-MD as compared to ordinary MD.

The main difficulty in the actual implementation of the hyper-MD method is the design of an appropriate bias potential $\Delta V_b(\mathbf{r})$. First of all, it must be exactly zero at the dividing surface not to affect the relative transition rates within the TST. Second, it must not introduce any correlations between the transitions which would violate the TST assumption. Third, it must not block any transition paths or hamper ergodic sampling of the system. In the case of complicated many-body systems, there is an additional difficulty in that the position of the TST dividing surface is not necessarily known. However, Voter has demonstrated that a bias potential can be

constructed from the local properties of $\Delta V_A(\mathbf{r})$ using its gradient and the Hessian matrix [264].

Concerning surface diffusion, in hyper-MD the local vibrational properties of the adatoms are lost, but the asymptotic behaviour of the temporal correlation functions remains unchanged within the TST. Voter [264] has tested the hyper-MD method against dynamically corrected TST for Ni/Ni(001) diffusion using the EAM potential, with good agreement between the two methods. More recently, hyper-MD has been extensively tested for Cu adatom diffusion on the Cu(111) surface against regular MD, using two different bias potentials [237]. In the low temperature limit, a very good agreement was obtained between MD and hyper-MD data for $D_t$, both for the Arrhenius behaviour *and* the prefactor for diffusion. In practice, boost factors of the order of $10^2$–$10^3$ are readily obtained for diffusion studies [264, 237], and much larger boost is in principle possible.

*Temperature Accelerated Dynamics (TAD)*—This method has been developed very recently [199] and as hyper-MD, relies on the assumption of the validity of TST. The TAD makes an even more restrictive assumption, namely that the *harmonic* TST is valid. From this point of view, the applicability of TAD is more restricted. However, the TAD method avoids all the difficulties connected with the construction of the bias potential, so that its applicability is more easily extended to different systems. Given a temperature of interest $T_{\mathrm{low}}$, the essence of the TAD method is to run MD simulations at a higher temperature ($T_{\mathrm{high}}$) and correct for the temperature-induced bias by filtering out some of the transitions and allowing only those transitions that should occur at the original temperature $T_{\mathrm{low}}$. Harmonic TST is assumed to be valid at both temperatures, and this implies that $k_B T_{\mathrm{high}} < \min_k[E_A^k]$, where the expression on the right means the lowest barrier between the minima in the system. At $T_{\mathrm{high}}$, *basin-constrained MD simulations* are performed. In such simulations, the system trajectory is confined to a particular potential energy basin. When the system tries to escape from that basin through a dividing surface, it is reflected back to the original state. During a basin-constrained simulation, the transition times $t_{\mathrm{high}}^i$ $(i = 1, \ldots, n_{\mathrm{path}})$ related to the $n_{\mathrm{path}}$ escape pathways are recorded. Then the sequence of escape times is extrapolated at $T_{\mathrm{low}}$ by the following relation [199]:

$$t_{\mathrm{low}}^i = t_{\mathrm{high}}^i \exp\left[E_A^i\left(\frac{1}{k_B T_{\mathrm{low}}} - \frac{1}{k_B T_{\mathrm{high}}}\right)\right], \tag{111}$$

where $E_A^i$ is the activation barrier of the $i$th pathway. Then the simulation is advanced by letting the process corresponding to the smallest $t_{\mathrm{low}}^i$ take place. In this way, a boost which increases exponentially $1/T_{\mathrm{low}}$ is obtained, and this allows even the simulation of crystal growth on realistic time scales at low temperatures [265] (see an example in figure 22).

The TAD method has been tested in several surface systems [199], such as adatom and trimer diffusion on Ag(001), and film ripening on Cu(111), obtaining boosts of several orders of magnitude. In the case of Ag(100), also the validity of the harmonic approximation has been tested, showing that anharmonic corrections are important only at very high temperatures. Therefore, the TAD method seems to be very promising for simulation studies of surface diffusion and growth.

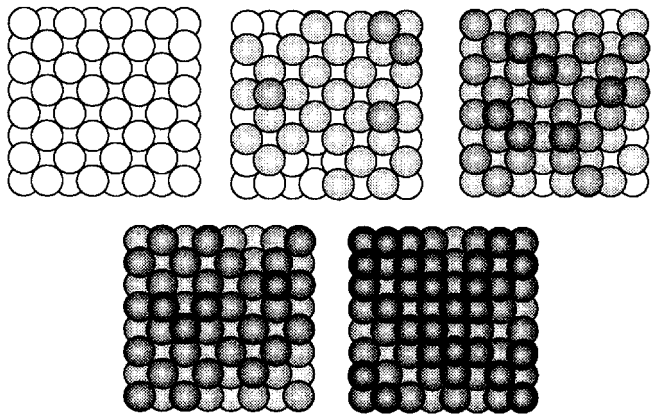

Figure 22. Temperature Accelerated Dynamics (TAD) simulation of the growth of Ag/Ag(001) at $T = 70$ K. Four layers are deposited at a flux of 0.075 ML/s, which is a typical experimental flux. The snapshots are taken at each monolayer completion, and the whole simulation covers a time scale of about 50 s. Top layer atoms are represented in dark grey, substrate atoms are represented in white, and intermediate layers are represented in light grey. This figure has been supplied by Dr Francesco Montalenti.

## 4. Specific issues illustrated by results from model systems

In this section, we have selected some issues which we think to be important in the field of surface diffusion, and discuss them in close relation to specific systems. Of course, our choice of topics here reflects both the personal bias and expertise of the authors; therefore, we do not pretend to treat here the most interesting or important issues in surface diffusion, but simply problems that have been interest to us. However, we would like to note that each of the issues discussed in this section has been and continue to be under considerable experimental and theoretical activity. We hope that the discussion here will encourage further experimental and theoretical works in the many problems that still remain unsolved.

### 4.1. *The potential energy surface and coupling of diffusive and vibrational motion*

The diffusive motion of adsorbed atoms and their vibrational motion near the minima of the adsorption potential are usually studied as separate topics because they involve different length and time scales [8, 266–268, 42, 269, 234, 75]. At low temperatures, the adatom spends most of its time vibrating rapidly around an adsorption potential minimum and diffusion proceeds by thermally activated rare events of jumping from one adsorption site to another in its neighborhood. Indeed, in a real space experimental probe such as STM, the local vibrational motion is automatically averaged out and only the jump events to neighboring sites are observed. In a $\mathbf{q}$ space experiment such as HAS, however, the separation between the diffusive and vibrational motion is not as easy. In principle, information about the diffusive motion can be extracted from the quasi-elastic spectrum of the dynamic structure factor at small wave vectors and small frequencies [270], whereas the adatom vibrational motion can be studied at finite frequencies. Qualitatively, the dynamic structure factor $S(\mathbf{q}, \omega)$ has a quasi-elastic peak at $\omega = 0$ due to the diffusive motion of adatom and a peak near $\omega = \omega_0$ due to the localized vibrational motion.

As the wave vector increases, the strength of the vibrational peak increases at the expense of the diffusive peak. The full width of the quasi-elastic peak can be written in the following form:

$$S(\mathbf{q},\omega) = \frac{A(\mathbf{q})}{\omega^2 + [\Delta E_D(\mathbf{q})/(2\hbar)]^2} + \tilde{S}(\mathbf{q},\omega), \tag{112}$$

where $\tilde{S}(\mathbf{q},\omega)$ is slowly varying near $\omega = 0$ but peaks at $\omega \approx \omega_0$. In equation (112), the pure Lorentzian part represents the contribution of the adatom jumping randomly from one site to another, whereas $\tilde{S}(\mathbf{q},\omega)$ contains the dynamics of motion in a continuous potential including vibrational motion which is neglected in a lattice gas model. To better understand the nature of these two terms, let us consider the zero coverage limit where only single adatom motion needs to be considered. In a square lattice, according to the Chudley–Elliott model [42], the contributions to $\Delta E_D(\mathbf{q})$ can be written as

$$\Delta E_D(\mathbf{q}) = \hbar\Gamma \sum_n P_n[2 - \cos(naq_x) - \cos(naq_y)]. \tag{113}$$

Here $\Gamma$ is the total jump rate and it is assumed that the particle jumps either along the $x$ or the $y$ direction; $P_n$ is the total probability (four directions together) for the event of jumping $n$ sites. Note that, in the limit of $q \rightleftarrows 0$, this reduces to the familiar expression $\Delta E_D(\mathbf{q}) = 2\hbar D_t q^2$. Thus, if the second term in equation (112) were absent, an analysis of $\Delta E_D(\mathbf{q})$ would not only yield the diffusion coefficient, but also microscopic information such as the jump path and long jump probabilities.

To illustrate the discussion above, we show in figure 23 the data on the width of the quasi-elastic peak from a He scattering study for the Na/Cu(001) system [27]. Experimentally, an effective $\Delta E(\mathbf{q})$ containing contributions from both the diffusive and vibrational motion was extracted after deconvoluting from the intrinsic instrumental resolution. The interaction effects are weak at the lowest experimental Na coverage ($\theta \approx 0.03$) and the adatom motion can be considered to be in the zero coverage limit. It has also been explicitly verified that the data remain unchanged between the coverage values of 0.03 and 0.1. Thus, the single adatom limit is appropriate for the analysis. For this system, the adsorption sites are the four-fold hollow sites. The jump paths crossing the saddle points are along the $x$ and $y$ directions correspond to [1,1,0] and [−1,1,0], and $a = 2.56$ Å. The dynamical structure factor was measured for wavevector $\mathbf{q}$ along both the [1,0,0] and the [1,1,0] directions. Beyond the first Brillouin zone, $\Delta E(\mathbf{q})$ increases rather than decreasing to zero toward the center of the second Brillouin zone as predicted by the Chudley–Elliott theory in equation (113). This indicates clearly the contribution of the vibrational mode to the quasi-elastic spectrum. The same conclusion about the importance of the contribution of the vibrational motion to the quasi-elastic peak has also been reached via MD simulation studies [75]. Along the $x$ ([1,1,0]) or equivalently the $y$ ([−1,1,0]) direction, the behaviour of $\Delta E(\mathbf{q})$ is closer to the simple predictions of the multi-jump theory whereas the deviation from the simple jump model is much more prominent along the [1,0,0] direction. As will be demonstrated below, this is due to the fact that the potential energy surface (PES) for Na on Cu(100) is much more anharmonic along the [1,0,0] direction than the [1,1,0] direction, leading to a larger contribution of the vibrational mode to the quasielastic peak along the [1,0,0] direction.

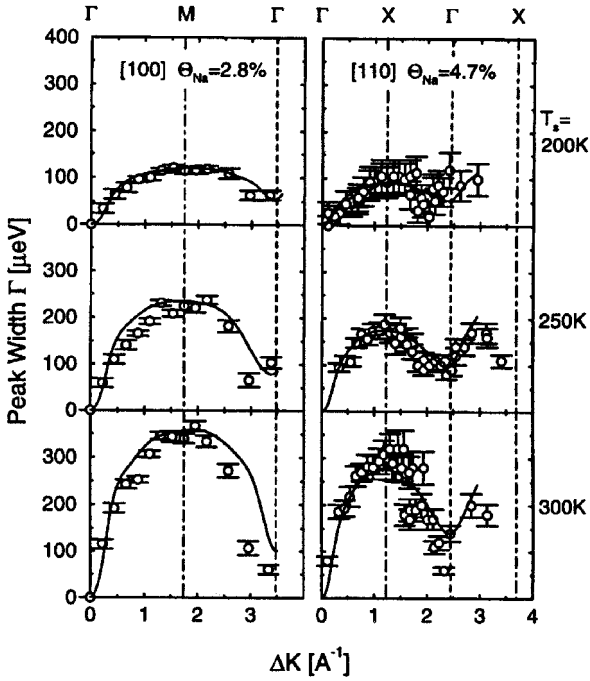


Figure 23. Parallel wave vector transfer dependence of the quasielastic peak width (FWHM) $\Delta E$ (**K**) for $T_s = 200\,\mathrm{K}$, 250 K, and 300 K along the Cu(001) [100] and [110] azimuths. The incident beam energy was 11.2 meV and the sodium coverage was $\theta = 0.028$ for the [100] azimuth and $\theta = 0.047$ for the [110] azimuth. The solid lines are the theoretical results from a numerical solution of the Langevin equation as discussed in the text.

In principle, one can go to the $q \rightleftarrows 0$ limit to eliminate the vibrational contribution to the quasielastic peak. In practice, the finite resolution of the He scattering method means that the quasi-elastic peak can only be studied at larger wavevectors corresponding to the motion of the adatom at small length scales. While the coupling of the diffusive and vibrational motion makes it difficult to extract the diffusion coefficient from the quasielastic peak directly, the wealth of information provided by the scattering data at the full range of wavevector values contain detailed information of the adiabatic PES as well as on the nonadiabatic frictional coupling of the Na adatom to the Cu substrate. Thus, a full theoretical analysis of the scattering data should yield information not just about the macroscopic diffusion coefficient $D_t$, but also microscopic information about the PES and the friction $\eta$. This kind of analysis has indeed been performed for Na/Cu(100) [225] and we describe the results below.

To analyse the data fully from the quasi-elastic He scattering experiment for Na/Cu(100), the Langevin equation as described in section 3.3 was solved numerically:

$$m\frac{\mathrm{d}\mathbf{v}}{\mathrm{d}t} = -m\eta\mathbf{v} - \nabla V_A(\mathbf{r}) + \mathbf{f}(t), \tag{114}$$

with

$$\frac{1}{k_B T}\langle \mathbf{f}(t)\cdot\mathbf{f}(t')\rangle = 2\eta\delta(t-t'). \tag{115}$$

The input to the equation is the (adiabatic) PES $V_A(\mathbf{r})$ and the friction $\eta$. Several comments need to be made about this model. First, the motion of the adatom is restricted to be 2D in the surface plane. This is justified since the motion of the Na adatom normal to the surface involves a vibrational mode with a much higher frequency than the in-plane mode. Also, recent calculations for a similar system Na/Al(111) show that the height of the Na atom above the surface is nearly independent of the adsorption site [271]. Thus the potential $V_A(x, y)$ is taken to be dependent only on the in-plane coordinates $(x, y)$. Second, the Markovian approximation has been adopted so the damping is instantaneous and characterized by a friction parameter $\eta$ rather than a frequency dependent memory function. This is justified because the in-plane vibrational mode (T-mode) has a frequency of $\approx 1.5$ THz which is considerably less than the Debye frequency of the substrate at about 5.7 THz. As discussed in section 3.3, the difference in time scales allows one to approximate the random fluctuating force at different times to be uncorrelated.

Within these assumptions, equation (114) was solved numerically and the dynamic structure factor calculated to extract the width of the quasi-elastic peak at different wavevectors. The adiabatic potential $V_A(x, y)$ and the friction $\eta$ were adjusted until a best fit of the data shown in figure 23 was achieved. In the earlier theoretical treatments of this system [25, 34], a simple cosine potential was chosen for the PES as

$$V_0(x, y) = V_0\left[2 - \cos\left(\frac{2\pi}{a}x\right) - \cos\left(\frac{2\pi}{a}y\right)\right]. \tag{116}$$

For this simple PES, the potential rises to a maximum of $2V_0$ at the bridge sites along the $x$ and $y$ ([110] and [1$\bar{1}$0]) directions. For trajectories along the [100] and [010] directions, the barrier is two times higher at $4V_0$ so that jumps along these directions are negligible at low temperatures. This would then lead to a prediction that the ratio of the maxima of the quasielastic peak width $\Delta E_D(\mathbf{q})$ along [100] and [110] should be 1 to 2. The actual observed value in the experiment is 1 to 1.2. This indicates that the actual motion of the adatom also involves paths other than those directly over the saddle point. Moreover, the sizable width beyond the first Brillouin zone boundary along [100] also indicates a highly anharmonic potential along this direction. All these lead to the conclusion that the potential at the on-top sites needs to be lowered relative to the simple cosine PES. This was achieved by adding a term of the form

$$V_1(x, y) = -\sum_{n,m} A \exp\{-B[(x/a - n - 1/2)^2 + (y/a - m - 1/2)^2]\}, \tag{117}$$

localized at the on-top sites. The parameter $A$ was chosen to be large enough to lower the barrier for diffusion paths along the [100] direction while $B$ was chosen such that $V_1(x, y)$ decays sufficiently fast that it does significantly alter $V_0(x, y)$ at the minima or the saddle points. Finally, another correction term $V_2(x, y)$ which is centred at the equilibrium four-fold hollow sites was added:

$$V_2(x, y) = CV_0\pi^2 \sum_{n,m} [(x/a - n)^2 + (y/a - m)^2] \exp[-(x/a - n)^2 - (y/a - n)^2]. \tag{118}$$

This term serves to slightly alter the curvatures and the anharmonicity near the minima. Following extensive optimization, the parameters that yield the best fit between the experimental and theoretical values were found to be: $A = 2V_0$,

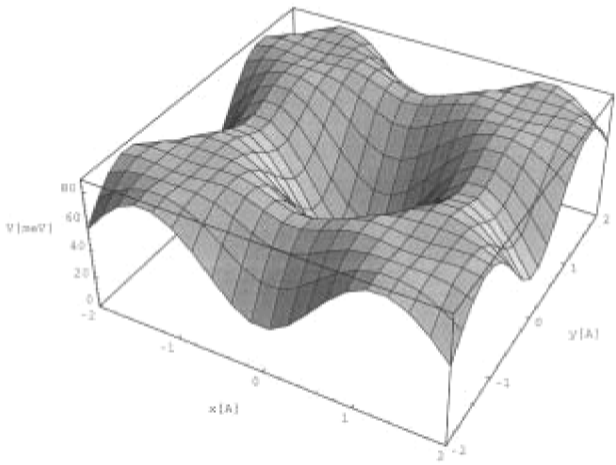


Figure 24. The adsorption potential energy surface $V_A(x, y)$ for sodium adatoms on Cu(001) surface determined from the quasi-elastic He scattering data. The copper atoms are located at $(x, y)$ positions $(\pm 1.28, \pm 1.28)$. The deep minimum in the potential at the centre corresponds to the hollow sites and the small dimples are directly above the copper atoms at the on-top sites. The barrier for motion along the [110] or [1$\bar{1}$0] azimuths is 75 meV and for motion along [100] or [010] azimuths 84 meV.

$B = 11.8$, $C = -0.2$, and $V_0 = 41.4$ meV. The best fit value of the friction was determined to be $\eta = 0.9$ THz.

As seen in figure 23, the theoretical results for the half width $\Delta E(\mathbf{q})$ from the solution of the Langevin equation with this choice of the adiabatic potential $V_A(\mathrm{u}r)$ and friction $\eta$ agree very well with the data. Furthermore, if we now look at the position and width of the T-mode as a function of temperature, there is also excellent agreement between the theory and experiment as shown in figure 25. Thus, we believe that while minor details of the PES may depend on the specific fitting procedures, the overall feature of the PES is very robust and completely determined by the He atom scattering data.

Finally, we note that from the theoretical analysis of the quasielastic peak in the long wavelength limit, the pure diffusive contribution of the Na adatom motion to the peak width can be extracted. It was found that there are sizable contributions from long jumps of two and three lattice sites. This is consistent with the pictures discussed in sections 2.1 and 3.3, since for this adsorption system the dimensionless friction $\eta/\omega_0$, where $\omega_0$ is the T-mode frequency, is about 0.1 and we are in the low friction regime, which favours long jumps.

### 4.2. *Diffusion of adatoms and clusters on strongly anisotropic surfaces*

The diffusion on strongly anisotropic surfaces has been a subject of considerable interest in recent times. Indeed, strongly anisotropic surfaces are the natural candidates for studying 1D (or better quasi 1D) diffusion processes, where mass transport takes place only along one direction. In this restricted geometry, the experimental determination of the microscopic diffusion mechanisms is expected to be easier, and issues such as the occurrence of long jumps should be more easily investigated, and compared to simple theoretical models (for example, 1D models). In the case of metals, the most studied anisotropic surfaces are W(211) [74], and the

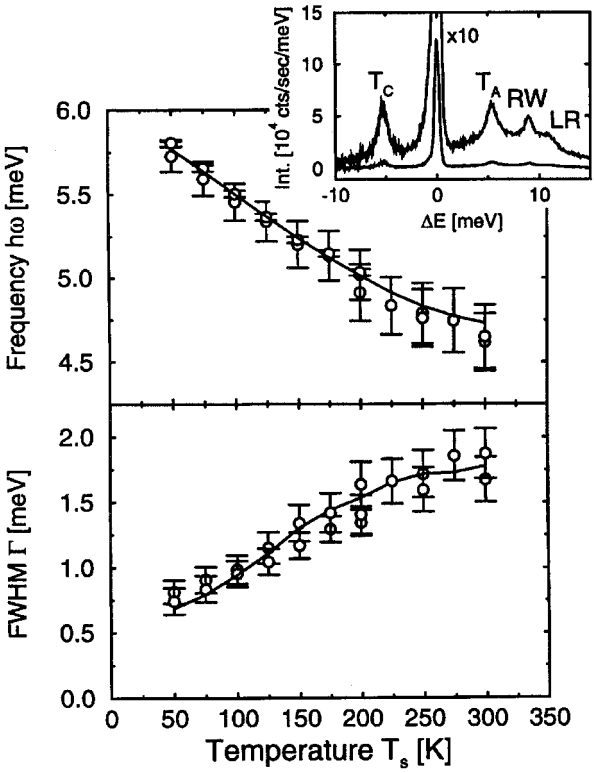


Figure 25. Temperature dependence of the frustrated translation vibration (T mode) peak position and FWHM for a sodium coverage $\theta = 0.028$. The solid line shows the T mode frequency and FWHM predicted by the theory.

(110) faces of fcc transition and noble metals. These latter (110) faces are characterized by channels along the easy $[1\bar{1}0]$ in-channel direction. However, in the unreconstructed $(1 \times 1)$ geometry, which is the most stable for Ag and Cu for example, these surfaces show also a significant diffusion along the cross-channel [001] direction, due to the occurrence of the exchange mechanism [87, 70, 58]. On the other hand, in the reconstructed $(1 \times 2)$ geometry (missing-row geometry), which is the most favourable for Au and Pt, the situation is better: the channels are much deeper, and cross-channel diffusion is very slow [272]. In the following we focus on diffusion of adatoms, dimers and chains ($n \geq 3$ atoms) on missing-row Au and Pt, and show that, unexpectedly, a rich phenomenology is found, which goes well beyond a simple 1D description of diffusion even on such strongly anisotropic surfaces.

4.2.1. *Adatom diffusion*

In the case of Pt(110)$(1 \times 2)$, isolated adatom diffusion has been studied by STM [7], and a considerable percentage of long jumps (of the order of at least 10%) have been found quite close to room temperature. The simplest diffusion mechanism on this surface is the jump along the channel bottom (the sequence $1a \rightleftarrows 1f \rightleftarrows 1e$ in figure 26). However, MD simulations [71] show that (essentially 1D) in-channel

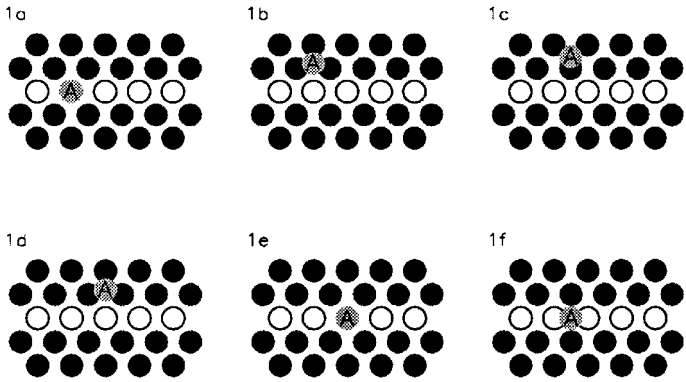


Figure 26. Schematic representation of the metastable-walk sequence (1a⇄1b⇄1c⇄1d⇄1e) and of the jump sequence (1a⇄1f⇄1e). Positions 1, 1c and 1d are metastable minima on the facet.

trajectories would justify a much lower percentage of long jumps than what is observed. But another mechanism is possible, and we shall refer to it as the metastable walk (MW) [273, 183] mechanism. In this new mechanism, the full 3D topology of the channel is explored by the diffusing adatom. In a MW, the adatom climbs up on one of the (111) facets of the channel, diffuses there passing through a network of metastable minima (see 1b, 1c and 1d in figure 26), and finally falls down again to the channel bottom. The barriers between the metastable minima are low, being very close to the barriers for diffusion on a (111) flat surface. From semi-empirical calculations it turns out that the MW mechanism has a larger barrier than the simple jump on Au (and on Pt too). On the other hand, *ab initio* calculations indicate that the MW trajectory could be the most favourable in Pt, even if these results are still somewhat under debate, since different density-functional schemes give qualitatively different results about the ordering of the barriers [183, 274]. However, for all available density-functional calculations incorporating some form of gradient correction, MW diffusion is at least as much favourable as jump diffusion. In any case, it is relatively easy to make effective long jumps by MW, because once the adatom is on the (111) facet, it can easily diffuse there for several lattice spacings before being retrapped at the channel bottom; at low $T$ the probability of an effective jump of $l$ lattice spacings decays as $\exp[-l\Delta E/(k_B T)]$, where $\Delta E$ is the difference between the barrier for going from 1b to 1c and the barrier from 1b to 1a in figure 26. $\Delta E$ can be rather small [273, 183]. This leads to a considerable percentage of effective long jumps, giving the most likely explanation of the experimental observations in reference [7] (STM cannot distinguish between a MW and a jump trajectory, but only record the adatom initial and final positions at the channel bottom).

4.2.2. *Dimer diffusion*

In the case of dimers, climbing on channel facets is even more important, and a new diffusion mechanism, the leapfrog, is likely to be the dominant one. In the dimer leapfrog, one of the atoms of the dimer is promoted on the (111) facet, where it finds two equivalent metastable minima, see 2b and 2d in figure 27, connected through a

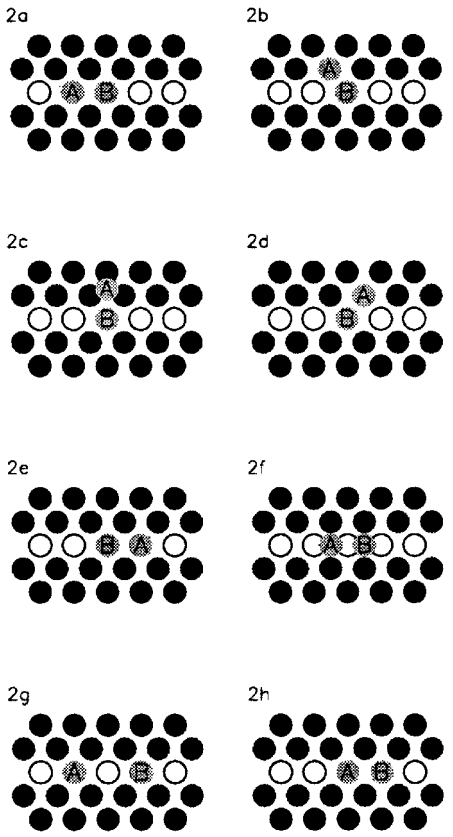


Figure 27. Schematic representation of the dimer leapfrog sequence (2a⇄2b⇄2c⇄2d⇄2e), of the concerted-jump sequence (2a⇄2f⇄2h), and of the dissociation-reassociation sequence (2a⇄2g⇄2h). In the leapfrog sequence, positions 2b and 2d are metastable minima, whereas 2c is a saddle point.

saddle point (2c). Again, the barrier between these metastable minima is low for pure Au/Au; the situation is different in the case of heterodimers, such as $Cu_2$ on Au or AuCu on Au [275]. On the other hand, for these heterodimers the leapfrog is not a favourable diffusion mechanism. Once the adatom is promoted, it jumps back and forth between the two minima for several times. At the end, the adatom has almost equal probability of coming back to the site of departure and of jumping down at the opposite side of the dimer, thus completing a diffusion move. The leapfrog mechanism resembles somewhat dimer rotation on fcc(111) surfaces, the latter being a quite important mechanism on such surfaces [276]. Calculations by semiempirical potentials [118] predict that leapfrog is the lowest-energy dimer-diffusion process for Au and Pt. Dimer-leapfrog has not yet been experimentally observed (and probably it would be extremely difficult to observe due to its very fast time scale [118]). Also *ab initio* results on Pt [274] indicate that leapfrog should be by far dominant. However, there are experimental results showing that Pt dimers easily dissociate, and thus diffuse by a dissociation-reassociation (DR) mechanism [277]. It has been suggested that the small dissociation barrier may be caused by CO contamination in the

experiments [274], but there is no evidence of such contamination from the usual spectroscopic methods [277]. In any case, whatever the cause of the low dissociation barrier is, DR can induce a considerable mobility of dimers. In the DR mechanism, the dimer breaks up, then the two adatoms diffuse independently and finally meet again in a position which can be quite far apart from the position of departure. If the diffusion of isolated adatoms is much faster than dissociation itself, only initial and final positions are observed, and the move looks as an effective long jump of the dimer. The length distribution of these effective long jumps falls off as $1/l^2$ [278].

4.2.3. *Chain diffusion*

When chains (with $N \geq 3$ atoms) are considered, the concerted jump (CJ) can be easily ruled out: its activation barrier is roughly proportional to $N$, because $N$ atoms have to be displaced together from their hollow position to close saddle points. Also the moves caused by DR have increasing effective barriers with $nN$. Let us consider for example a trimer, and try to move it by DR. In order to do that, two bonds must be broken, instead of the single bond of dimer DR. Analytical calculations [279] show that, at low $T$, the trimer effective-jump rate follows an Arrhenius law with barrier $E_{\text{eff}}(3)$:

$$E_{\text{eff}}(3) = E_{d3} + \frac{(E_{d2} - E_j)}{2}, \tag{119}$$

where $E_{d3}$ is the barrier for detaching a side atom from the trimer, $E_{d2}$ is the dimer dissociation barrier, and $E_j$ is the jump barrier of an isolated adatom. The contribution in parenthesis comes from the breaking of the second bond. For a tetramer, $E_{\text{eff}}(4)$ is even larger. Moreover, one should consider that the probability that dissociated adatoms, during their walk, to meet other adatoms or chains and stick to them increases with $N$, so that there is a considerable probability of observing a final chain with a different length from the initial chain. Therefore, chains should either change their length or to be practically immobile.

However, this is not the case for chains on missing-row surfaces, where, from the STM experiments performed by Linderoth *et al.* [117] (see the images of figure 28), there is evidence of chain diffusion. Therefore, chain diffusion must be caused by another mechanism, different from CJ and DR, and the mechanism is again the leapfrog (see figures 29 and 30). In fact, it is easily understood that the leapfrog diffusion barrier should depend weakly on the chain length $N$. Essentially, the rate-limiting step of the leapfrog sequence is the upward promotion (in figure 29, from the initial configuration 3a to the quite deep metastable minimum in 3c passing through 3b), whose barrier $E_{\text{up}}$ depends on the local environment of the promoted adatom, which is initially at the end of the chain. This local environment is practically independent on $n$, and thus $E_{\text{up}}$ is nearly the same for dimers, trimers and so on [279, 280]. However, a further point must be taken into account. Once one of the side adatoms is promoted above the chain, there is a probability $P_{LF}$ that it will jump down at the opposite end of the chain, thus completing the leapfrog sequence. Before jumping down, the adatom must diffuse above the chain (process 3c$\rightleftarrows$3d in figure 29) with a rate $r_{\text{above}}$ (this is indeed the rate for diffusion on a locally unreconstructed $(1 \times 1)$ surface) and, once it has reached the border, it can jump down with a rate $r_{\text{down}}$ (in figure 29, the sequence is 3d$\rightleftarrows$3e$\rightleftarrows$3f; usually the descent is by jump, the exchange barrier being much larger). The probability $P_{LF}$ depends on $N$ according

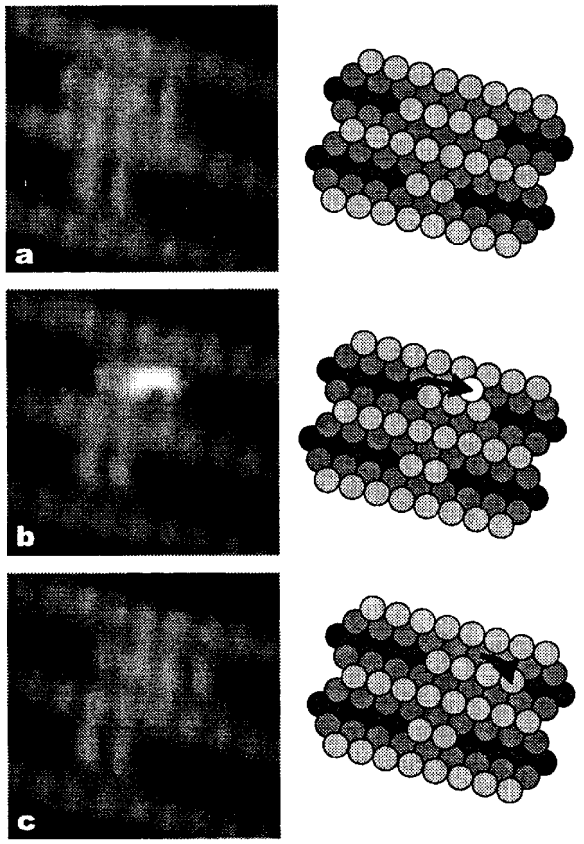


Figure 28. STM images of a leapfrog sequence for a Pt tetramer on missing-row Pt(110) (from reference [117]).

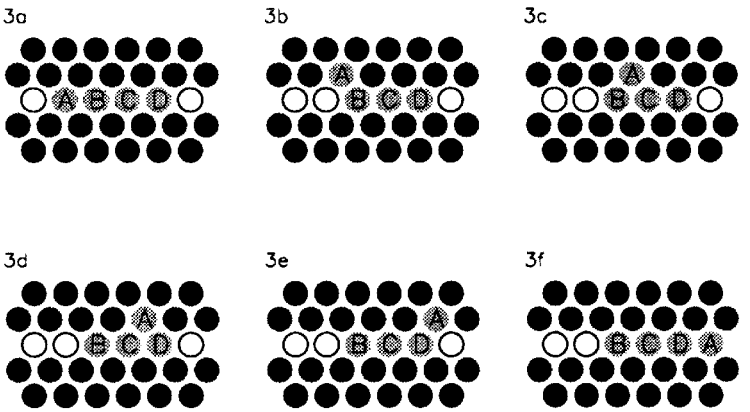


Figure 29. Schematic representation of the chain leapfrog process for a tetramer, the same process of the STM images in figure 28.

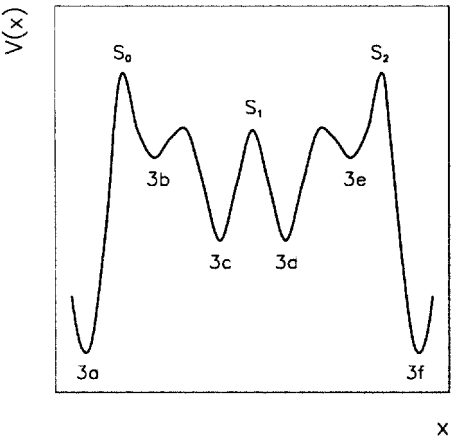


Figure 30. Potential energy profile along the path of the tetramer leapfrog sequence in figure 29. For a chain of $N$ atoms, $N-2$ deep metastable minima (as 3c and 3d) are found, plus two shallow minima (3b and 3e). The latter minima play little role in the kinetics of the sequence. The promotion energy $E_{up}$ is given by the energy difference between the saddle $S_0$ and 3a. The barrier for descending $E_{down}$ is the difference between $S_0$ and 3c. The barrier for diffusing above the chain $E_{above}$ is the difference between $S_1$ and 3c.

to the following expression [279]:

$$P_{LF} = \frac{b}{N-3-b(N-5)}, \tag{120}$$

where

$$b = \frac{r_{above}}{r_{above} + r_{down}}. \tag{121}$$

In Au and Pt [118], $r_{above} \gg r_{down}$ at the temperatures of experimental interest, so that $b \simeq 1$. This implies that $P_{LF}$ is constant for a wide range of $nN$. Asymptotically, $P_{LF} \propto N^{-1}$ for $N \rightleftarrows \infty$, but this limit is not physically important because multiple promotions become likely at large $N$. Multiple promotions stop the leapfrog mobility because they lead to the formation of new chains above the original chain. These new chains are in a local $(1 \times 1)$ geometry, so that they are practically immobile. Finally, it has been shown (by semiempirical calculations with EAM potentials [280]) that the presence of adatoms or chains in nearby channels, can cause some reduction of the energy barriers for leapfrogging; moreover, leapfrogging should be dominant also for chains on locally reconstructed Ag, Cu and Ni.

### 4.3. *Diffusion of adatoms along and across steps*

In the previous sections we have dealt with diffusion on perfectly flat surfaces, either isotropic or anisotropic. However, in most experimental situations, the presence of defects is unavoidable, and steps are probably the most common kind of defects. Indeed, terraces have always a finite extension (the maximum being of the order of some $10^3$ —even on the best quality crystals) and, even more important, steps are created continuously during crystal growth processes. In the latter processes, diffusion along and across steps is a key point for understanding the building

up of growth morphologies. For example, in the submonolayer regime, the shape of growing 2D islands is determined by the interplay between the flux of atoms coming from the surrounding terrace and the smoothing processes around the island edges [281–285, 1, 286, 287], the latter including diffusion along the lower edge of steps and corner crossing between adjacent steps as elementary constituents. When smoothing processes are active, the islands grow in compact shapes; otherwise instabilities develop, and fractal or dendritic islands grow. In the multilayer growth, on the other hand, also diffusion across steps becomes crucial. Indeed, smooth layer-by-layer growth can take place when interlayer downward mass transport is possible, and the latter implies that adatom can cross steps. In many cases, the crossing of steps is hindered by an additional barrier (the Ehrlich–Schwoebel barrier [4, 288]) because of the poor coordination of the adatom at the saddle-point configuration of the step-crossing process. If this happens, an upward adatom current can be built up during growth [289, 1]; this current causes instabilities such as mounding [290–296] and rippling [297, 298]. The same situation applies to the morphologies on individual step edges as well. For diffusion along the step edge, the kink Ehrlich–Schwoebel barrier controls the instability of the ledge [299, 300]. Finally, the presence of steps can affect the diffusion of adatoms not only just at the step edge, but also at larger distances. A well known consequence is the depletion of adatoms around 2D islands, which is caused by the lowering of diffusion barriers for the adatoms moving towards the island [301-303, 54, 41]. The literature on the subject of diffusion along and across steps, and on its consequences on growth is enormous. Here we intend to give only a general sketch of the elementary diffusion processes. In order to do that we focus on specific and widely studied systems, essentially on the low-index surfaces of Ag, comparing when possible Ag with other fcc metals, such as Pt and Al. These systems, which are rather simple indeed, shall display a very rich phenomenology, with strongly different behaviour taking place on different surfaces of the same element, showing that the presence of steps can deeply influence the diffusive properties of adatoms.

4.3.1. *Diffusion along steps and corner crossing*

Adatom diffusion along the upper edges of steps is usually not very different from terrace diffusion for metal-on-metal systems. Owing to the vicinity of the step, local relaxation may somewhat alter the diffusion barrier, but the coordination remains the same as in the middle of the terrace. On the other hand, at the lower edges of steps adatom coordination is usually increased with respect to the inner terrace. Therefore, the diffusive properties along lower step edges can be qualitatively different from those on the terrace. In the following, we consider diffusion along the lower edges of straight high-symmetry steps on the (001), (111) and (110) surfaces of an fcc crystal, mainly with reference to the case of Ag.

*(001) surfaces*—Let us consider first the (001) surface (see figure 31). Here two kinds of high-symmetry steps can be built up. A step of the first kind can be built up for example along the [110] direction. Atoms of this step are close-packed, being separated by a first-neighbour distance, and (111)-like microfacets are on the step riser. The second kind of step is built up for example along the [100] direction; it is not close-packed, since the atoms of the step are second neighbours and the microfacets on the riser are (110)-like. The diffusion of adatoms along the two steps has very different properties, being much faster along the [110] step than along the [100] step. For example (see table 2), in Ag, semiempirical and first-principle

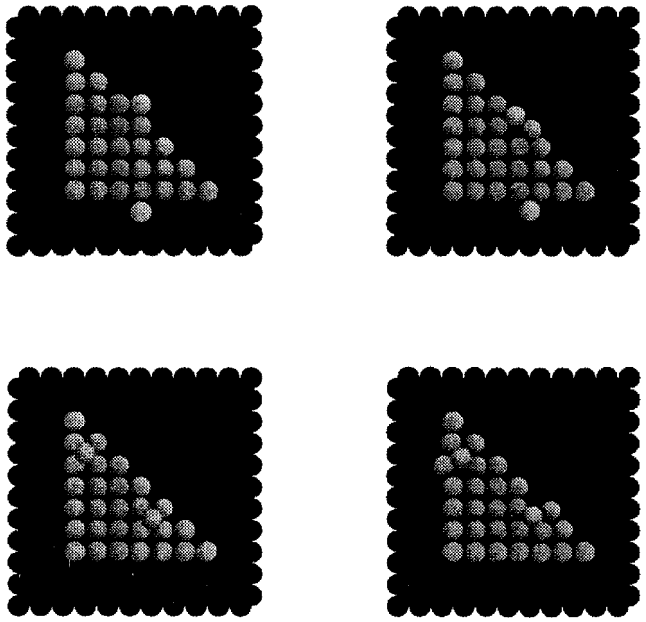

Figure 31. Diffusion along (top panels) and across (bottom panel) [110] close-packed steps and [100] steps. At left and right, starting and saddle-point positions, respectively, are shown. Diffusion along [110] steps is by jump, while diffusion along [100] steps and diffusion across both steps is preferentially by exchange. The crossing of the [001] steps is equivalent to the crossing of a kinked [110] step.

Table 2. Energy barriers (in eV) for diffusion on the flat Ag(001) surface, and along ($\parallel$) and across ($\perp$) steps. Diffusion across [100] steps is the same as diffusion across kinked [110] steps. Several theoretical results are reported: Tight Binding Second Moment Approximation (TBSMA, as developed by Rosato, Guillopé and Legrand (RGL) [194, 308]), from reference [58] and this work, Effective Medium Theory (EMT) from reference [101], Corrected Effective Medium (CEM) from reference [304], Embedded Atom in Voter–Chen parametrization (EAVC) from references [87, 41], Embedded Atom in Foiles–Daw–Baskes parametrization (EAFDB) from reference [41], Embedded Atom in Adams–Foiles–Wolfer parametrization (EAAFW) from reference [87], density functional theory in the Local Density Approximation (LDA) and with Generalized Gradient Corrections (GGA) from references [305, 97]. The experimental results are taken from references [306, 307].

| Diffusion Process | TBSMA | EMT | CEM | EAVC | EAFDB | EAAFW | LDA | GGA | Exp. |
|---|---|---|---|---|---|---|---|---|---|
| Flat surface, jump | 0.43 | 0.37 | 0.41 | 0.48 | 0.48 | 0.48 | 0.52 | 0.45 | $0.40 \pm 0.05$ |
| | | | | | | | | | 0.38 |
| Flat surface, exch. | 0.61 | 0.61 | 0.58 | 0.60 | 0.78 | 0.75 | 0.93 | 0.73 | |
| $\parallel$ [110] step, jump | 0.25 | 0.22 | | 0.26 | 0.26 | 0.26 | 0.30 | 0.27 | |
| $\parallel$ [100] step, jump | 0.71 | | | 0.78 | | 0.73 | | | |
| $\parallel$ [100] step, exch. | 0.69 | | | | | | | | |
| $\perp$ [110] step, jump | 0.59 | 0.48 | | 0.70 | | 0.59 | 0.70 | 0.55 | |
| $\perp$ [110] step, exch. | 0.55 | 0.52 | | 0.51 | | 0.64 | 0.52 | 0.45 | |
| $\perp$ [100] step, jump | 0.47 | | | 0.55 | | 0.51 | | | |
| $\perp$ [100] step, exch. | 0.38 | | | 0.31 | | 0.38 | | | |

calculations [58, 100, 101, 304, 87, 41, 305, 97] show that diffusion along the [110] step has a barrier of about 0.25 eV, which is even smaller than the barrier for adatom diffusion on the flat surface (the latter being of about 0.40 eV, as found both by experiments [306, 307] and calculations, see table 2). Diffusion along this step is therefore the fastest process on the (001) surface of silver. Similar results are found also for other metals such as Cu and Au (see reference [58]), indicating that this result has some general explanation. Indeed, the reason why the diffusion along this step is faster than the diffusion on the flat terrace can be understood by a simple bond-counting argument. In silver, adatoms on the flat surface diffuse preferentially by jumping among NN lattice sites [58, 100, 101, 304, 87, 41, 305, 97]. In the jump process, the adatom starts from a fourfold minimum to reach the saddle-point configuration, which is half way among the NN sites. In the saddle point configuration, only two bonds are retained, so that the jump process costs the breaking of two NN bonds. In the diffusion along [110] steps, the starting position has coordination five (see the left panel of figure 31): four NN in the layer below and one NN in the step. On the other hand, the saddle-point position has coordination four: two NN in the layer below and two in the step (see the right panel of figure 31). Therefore the process costs the breaking of a single NN bond, and this is the cause of the lower barrier. Indeed, the barrier for diffusion along [110] steps is not far from one half of the barrier for diffusion on the flat surface. Along the [100] step, the starting configuration has coordination six, while the saddle point for jumping has coordination three (with the NN bonds rather stretched), so that the barrier is much higher (about 0.71 eV in silver by semiempirical calculations in the Tight Binding Second Moment Approximation—TBSMA—as developed by Rosato, Guillopé and Legrand (RGL) [194, 308], see table 2). Indeed, the same type of calculation indicates that the exchange process (see the right panel of figure 31) is slightly better (0.69 eV) than the jump. Bond counting arguments can show that also in this exchange three NN bonds are lost at the saddle point.

These results show that here bond-counting arguments give useful predictions, provided that bond counting is done both at the minimum and at the saddle point; bond counting in the initial and in the final position would give clearly incorrect results in the above examples. Even more care has to be taken in the case of (111) surfaces (see below).

By the same line of reasoning as above, one could understand that corner crossing is much slower than diffusion along [110] steps; crossing from a [110] step to another step of the same symmetry costs two bonds (plus some stretching), so that semiempirical calculations give a barrier of 0.51 eV. In this case, at low temperatures the rate-limiting process in the smoothing of square islands limited by close-packed steps is thus corner crossing. However, this corner-crossing barrier is not far from the barrier for diffusion on the flat terrace. Therefore, when terrace diffusion is active so that adatom can diffuse, meet each other and form islands, also diffusion along steps and corner rounding are active, so that islands grow smooth, and it is practically impossible to grow fractal aggregates.

*(111) surfaces*—On fcc(111) surfaces there are two kinds of close-packed steps, usually referred to as A and B steps in the literature [309]. A steps have square (001)-like microfacets on the steps riser, while (111) steps present triangular microfacets (see figure 32). Semiempirical calculations for Ag [54] give that diffusion is by hopping mechanism and somewhat easier along step A than along step B. However, the important point is that diffusion along both steps is much slower than diffusion

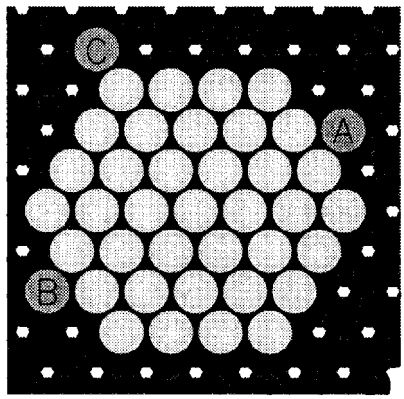


Figure 32. An fcc(111) surface with a hexagonal island on top of it. The island is limited by three A steps (square microfacets on the step riser) and by three B steps (triangular microfacets on the step riser). Adatoms A and B are along the A and B steps, respectively; adatom C is at a corner site.

on the flat terrace (see table 3). Another widely studied system in this geometry is Pt/Pt(111). On this system, a quite complete set of *ab initio* calculations is available [310]. These calculations are in good agreement with the experimental data [79]. According to reference [310] diffusion along both steps A and B occurs preferentially by hopping, as in Ag. This is different from what is found in Al, again by *ab initio* calculations: there, diffusion along B steps is by exchange with an atom of the step itself. In Pt, diffusion along A steps has a barrier which is lower by about 10% than

Table 3. Energy barriers (in eV) for diffusion on the flat Ag(111) surface, and along ($\parallel$) and across ($\perp$) steps. For diffusion processes across steps also the Ehrlich–Schwoebel barrier $E_S$ is given. The latter is determined experimentally by growth experiments where island may comprise kinked and unkinked steps of both A and B types. For the acronyms, see the caption of table 2. TBSMA results are taken from reference [315] and from this work, EMT, EAFDB and LDA results are taken from references [316], [317] and [318] respectively. The experimental result for terrace diffusion is taken from reference [316]; the experimental results on $E_S$ come from references [333], [334] and [335], from top to bottom.

| Diffusion Process | TBSMA | EMT | EAFDB | LDA | Exp. |
|---|---|---|---|---|---|
| flat surface | 0.067 | 0.067 | 0.055 | 0.082 | $0.097 \pm 0.010$ |
| ($\parallel$) A step, jump | 0.25 | | | | |
| ($\parallel$) B step, jump | 0.29 | | | | |
| $\perp$ A step, jump | 0.35, $E_S = 0.28$ | | | | |
| $\perp$ A step, exch. | 0.36, $E_S = 0.29$ | | | | |
| $\perp$ A step at kink, jump | 0.28, $E_S = 0.21$ | | | | |
| $\perp$ A step at kink, exch. | 0.24, $E_S = 0.17$ | | | | |
| $\perp$ B step, jump | 0.33, $E_S = 0.26$ | | | | |
| $\perp$ B step, exch. | 0.21, $E_S = 0.14$ | | | | |
| $\perp$ B step at kink, jump | 0.24, $E_S = 0.17$ | | | | |
| $\perp$ B step at kink, exch. | 0.31, $E_S = 0.24$ | | | | |
| average $E_S$ | | | | | $0.120 \pm 0.015$ |
| | | | | | $0.150 \pm 0.020$ |
| | | | | | 0.13 |

for diffusion along step B (0.71 against 0.77 eV [310]), again with the same qualitative behaviour as in Ag. On the other hand, in Al, the difference in the barriers is of the order of 30% [90, 91], and it would be even larger if the hopping mechanism along step B were considered. Also in Pt, terrace diffusion is much faster than diffusion at steps. The barrier for terrace diffusion is 0.29 eV [310] which compares well with the experimental result of $\simeq 0.26$ eV [311–313]. This means that diffusion along steps costs $0.4 - 0.5$ eV more than diffusion on the flat surface. NN bond counting (at the saddle point and at the minimum) gives that one bond is lost in *both* diffusion on the flat terrace *and* in diffusion along steps A and B. But at a closer inspection, the saddle points for diffusion along the steps are characterized by the net loss of a NN bond (from five bonds to four), plus considerable stretching or compression of the four remaining bonds [314]. This explains why diffusion along steps is much more difficult here than diffusion on the terrace (contrary to what happens on the (001) surface); this result is common to all calculations (first-principle and semiempirical) to our knowledge [314, 54, 315–319, 91, 320–322]. These results show that bond counting needs considerable care, since the relaxation (or compression) of bonds plays an important role.

Corner crossing on fcc(111) surfaces occurs through the intermediate (or corner) position C in figure 32. An adatom in C has a higher energy than at the step positions A and B in figure 32, but a lower energy than on the flat surface. The barriers for corner crossing are somewhat larger than those for diffusion along steps: for example, in Pt a sequence from the last site along an A step to C and then to the nearest site along the adjacent B step has to surmount an overall barrier of 0.84 eV [310], while the reverse costs 0.82 eV. On the other hand, according to *ab initio* calculations, atoms directly arriving at C find a lower barrier for going towards step B than towards step A. This is in some contradiction with the growth experiments in [285], where the resulting island-growth morphologies were explained by MC simulations assuming that the displacement from a corner site is easier towards an A step than towards a B step.

In any case, island-edge smoothing processes on fcc(111) surfaces are by far slower than terrace diffusion. In fact, on these surfaces, fractal or dendritic islands are easily grown [309, 285], contrary to what happens on the (001) surfaces.

*(110) surfaces*—Contrary to the previous cases, these surfaces are highly anisotropic (see figure 33). The energetics of these surfaces has been studied by semiempirical potentials in references [308, 323]. On Ag, a complete set of barriers has been calculated by semiempirical potentials [81]; these barriers have been successfully used in the interpretation of several experiments of submonolayer and multilayer growth, and of island dissolution [324–326, 298, 327], and they are reported in table 1. The RGL barriers for diffusion on the flat surface are in good agreement with the available experimental data, obtained by STM (from island counting) and by QHAS [327–329]. On these surfaces, we consider two kinds of steps of different symmetry. In figure 33 steps along the in-channel $[1\bar{1}0]$ direction and the cross-channel [001] direction are represented. Diffusion along the in-channel steps is not very different from in-channel diffusion on the flat surface, the only difference being the breaking of a second neighbour bond (the cross-channel bond with the closest adatom of the step), which costs a few hundredths of eV. On the other hand, diffusion along the [001] step is much more difficult. In fact, one has to add to the cross-channel diffusion barrier (which is already higher than the in-channel diffusion barrier) the breaking of a first-neighbour bond, which costs about 0.2 eV more.

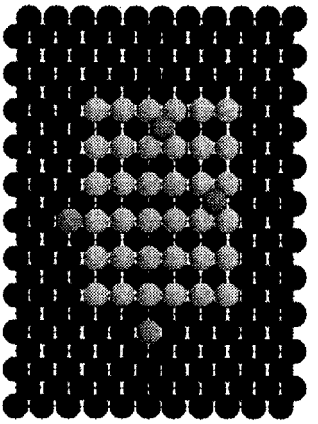

Figure 33. An fcc(110) with an island on top of it. The in-channel [1$\bar{1}$0] direction is horizontal, the cross-channel [001] direction is vertical. Adatoms are placed along the lower and upper edges of steps.

Because of that, [1$\bar{1}$0] steps are usually smooth, while [001] steps are rough, with a high density of kinks. Direct corner crossing from [001] to [1$\bar{1}$0] steps is very difficult, while the reverse costs more or less the same as cross-channel diffusion on the flat surface. Indeed, contrary to what happens on (001) and (111) surfaces, the barriers for diffusion along steps can be rationalized by a simple bond-breaking model, where bonds are counted at the initial position of the adatom [330].

Because of the above results, islands are smooth in the [1$\bar{1}$0] direction, and rough in the [001] direction. The interplay of terrace and step-edge diffusion leads to the growth of long chains of monoatomic width in a wide range of temperatures (130–200 K for Ag at the experimental fluxes [330]). These chains grow when diffusion along the [1$\bar{1}$0] direction is active both on the terrace and at step edges, but the strong first neighbour bonds are still stable. At higher temperatures, the breaking of first-neighbour bonds causes the transition to compact island shapes.

4.3.2. *Diffusion across steps: the Ehrlich–Schwoebel barrier*

There is strong evidence coming from both experimental results and from theoretical calculations, that the adiabatic potential felt by the adatom in the vicinity of a step is quite different from the adiabatic potential on a flat terrace. Schematically, for metal-on-metal diffusion, while the minimum at the upper side of the step can be slightly different than the minima on the flat terrace, the minimum at the lower side is much deeper (because of a gain in co-ordination) and the barrier in between the two can be significantly different than the barrier on the terrace. If the terrace barrier is $E_{\text{terrace}}$ and the barrier for crossing the step is $E_{\text{step}}$, the difference $E_S = E_{\text{step}} - E_{\text{terrace}}$ is known as the Ehrlich–Schwoebel barrier [4, 288]. $E_S$ is usually positive, because the saddle-point configuration at the step crossing has a poor co-ordination, as can be easily understood in the case of crossing by a hopping mechanism (see figure 34). However, step crossing may take place also by (simple or multiple [100, 101]) exchanges. These mechanisms are often characterized by a low $E_S$ [91], and in some cases (for example at kinks, see below) $E_S$ can be even negative [41]. Also the size of the terrace can influence the crossing of the steps: descent at

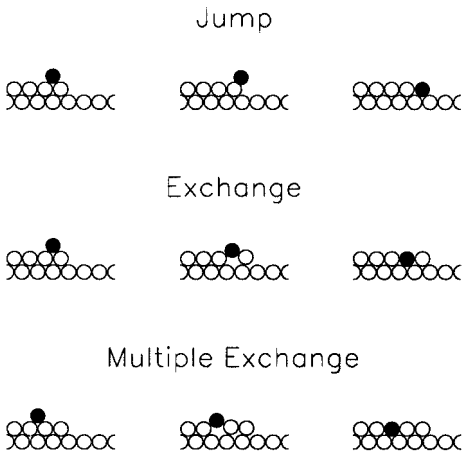


Figure 34. Descent at steps by jump, simple exchange and multiple exchange.

straight steps can be very different on small and large islands [302, 81]. Moreover, the effects of high-temperature relaxation of the step atoms may induce an effective reduction of $E_S$, in such a way that step crossing becomes more likely than reflection back to the inner terrace [70], even if the latter has a lower adiabatic barrier in the limit of $T \rightleftarrows 0$.

In the following, as we have done for diffusion along steps, we compare the crossing of monoatomic steps on the (001), (111) and (110) surfaces of Ag and other fcc metals, and then consider the crossing between different facets on fcc 3D clusters.

*(001) surfaces*—For Ag, several theoretical results are available (see table 2). At [110] steps, most calculations indicate that descent by exchange should be preferred, the jump having a somewhat higher barrier. In any case, if we compare the barrier for descent with the one for diffusion on the flat surface, we see that $E_S$ is rather low, of the order of 0.1 eV in maximum. On the other hand, descent at [100] steps (which is analogous to descent at kinked [110] steps) has a negative $E_S$ for the exchange process [41]. In fact, the exchanging atom of the step is well coordinated at the saddle point, in analogy to what happens to the case of adatom diffusion along [110] steps (see figure 31). These results indicate that interlayer mobility on Ag(001) should be very easy, and this is confirmed by the observation of layer-by-layer growth in a wide range of experimental conditions [331, 332]. At high temperatures, also multiple exchanges at [110] steps become likely. Indeed, multiple exchanges have been observed in MD simulations of Cu diffusion on vicinal (11$m$) surfaces (which have (001) terraces separated by close-packed steps of the [110] kind) [100, 101]; we expect that such processes should take place on Ag, too.

*(111) surfaces*—Contrary to what happens in the case of the (001) face, diffusion across steps on Ag(111) is always hindered by Ehrlich–Schwoebel barriers. Indeed, semiempirical calculations (see table 3) indicate that $E_S$ is always larger than 0.1 eV, for both A and B steps even at kinks. Therefore $E_S$ is in any case considerably larger than the barrier for terrace diffusion. With this respect, Ag(111) is very different from Ag(001), where $E_S$ is always a quite small fraction of the terrace-diffusion barrier, and in some cases is even negative. However, interlayer mobility is relatively easier across B steps, and at kinked A steps, where $E_S \approx 0.15$ eV. The latter value compares

well with the available experimental determinations [333–335], which give $E_S$ in the range of 0.11–0.17 eV, as reported in table 3. In the experiments, the symmetry of the steps where the crossing is taking place is not controlled, so that the measured barriers are very likely related to the dominant process, i.e. to the crossing at sites where $E_S$ is lower. With this in mind, the agreement between experiments and calculations is very good. In any case the important point is that Ag(111) grows three-dimensionally [336], and this in complete agreement with the above large Ehrlich–Schwoebel barriers.

In Pt and Al, the situation is different. Indeed, according to *ab initio* calculations [314], diffusion across steps in Pt is strongly anisotropic: crossing A steps is much easier than crossing B steps. $E_S$ is practically negligible at A steps. Since adatoms cross at A steps, Pt islands grown on Pt(111) should be bounded by B steps, and this is what is experimentally observed [337]. The situation is opposite in Al where *ab initio* calculations [90] give that crossing is easier at B steps, where $E_S$ is negligible. At A steps, $E_S$ is as large as the barrier for diffusion on the flat terrace.

*(110) surfaces*—Semiempirical calculations (see table 4) indicate that diffusion across steps on Ag(110) is much easier in the in-channel direction (i.e. across [001] steps) than in the cross-channel direction (i.e. across $[1\bar{1}0]$ steps). The former takes place by jumps, the latter by exchange, and in both case descent is easier at kinks. This is especially important for [001] steps, which have usually a high density of kinks. All intralayer and interlayer processes on this surface are thus leading to an easy in-channel mobility and to a slow cross-channel mobility. The anisotropy of interlayer diffusion plays a key role in the building up of peculiar surface instabilities, the ripples, both in sputtering [324] and growth experiments [297]. In growth experiments ripples rotate with increasing temperature: at low temperatures they are along the [001] direction, at intermediate temperatures they disappear, and at high temperatures they are placed along the $[1\bar{1}0]$ direction [297]. The formation and rotation of ripples is due to the interplay of the anisotropy of bonding and the anisotropy of diffusion [298].

*Interfacet diffusion on 3D nanoclusters*—Metal 3D nanoclusters, either supported or free, are often found as truncated octahedra (TO, in the case of free clusters) and square truncated pyramids (TP, in the case of supported clusters on square lattices) [338–340]. Both the TO and the TP expose (111) and (001) facets. For example, a TO has eight (111) and six (001) facets (see figure 35), while a TP (TP) has four (111) facets and a single (001) facet on the top. Therefore, interfacet diffusion processes are

Table 4. Energy barriers (in eV) for diffusion on the flat Ag(110) surface, and along (∥) and across (⊥) steps. TBSNA, EMT, EAVC and EAAFW results are taken from [81], [84], and [87].

| Diffusion Process | TBSMA | EMT | EAVC | EAAFW |
|---|---|---|---|---|
| flat surface along $[1\bar{1}0]$ | 0.28 | 0.29 | 0.25 | 0.32 |
| flat surface along [001], jump | 0.38 | 0.56 | 0.31 | 0.42 |
| ∥ $[1\bar{1}0]$ steps, jump | 0.30 | | | |
| ∥ [001] steps, exch. | 0.56 | | | |
| ⊥ $[1\bar{1}0]$ steps, exch. | 0.56 | | | |
| ⊥ [001] steps, jump at kinks | 0.35 | | | |

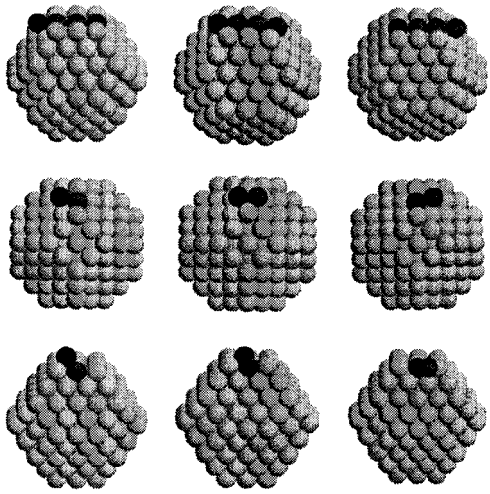

Figure 35. Step crossing on a truncated octahedron. Top row: exchange crossing by the chain mechanism which connects two (110) facets on opposite edges of a (001) facet. Middle row: exchange crossing between two adjacent (111) facets. Bottom row: exchange from a (001) facet to an adjacent (111) facet and (from right to left) *vice versa*.

important on such clusters: adatom crossing between two facets is analogous to adatom crossing at steps and the concept of an additional Ehrlich–Schwoebel barrier apply the same. On TO and TP structures, one expects that adatoms can cross between adjacent (111) facets, or from a (001) facet to an adjacent (111) and vice versa. This can indeed happen, as shown by TBSMA calculations [261], and the preferred mechanism is the exchange (see table 5). The $(111)\rightleftarrows(111)$ and the $(111)\rightleftarrows(001)$ crossings are indeed rather easy, with quite low barriers. To the opposite, the crossing $(001)\rightleftarrows(111)$ is much more difficult, because of the higher coordination of the adatom on a (001) facet. However, the most surprising result is that interfacet mobility is possible also between *non adjacent* (111) facets, and more precisely between two (111) facets on the opposing sites of the same (001) facet. This is possible through the chain process (see figure 35), which is a multiple-exchange

Table 5. Energy barriers (in eV) for interface diffusion on truncated octahedra and square truncated pyramids for Ag; the results are taken from reference [261].

| Diffusion Process | TBSNA |
|---|---|
| $(111)\rightleftarrows(111)$ jump | 0.34 |
| $(111)\rightleftarrows(111)$ exch. | 0.23 |
| $(111)\rightleftarrows(001)$ jump | 0.36 |
| $(111)\rightleftarrows(001)$ exch. | 0.32 |
| $(001)\rightleftarrows(111)$ jump | 0.64 |
| $(001)\rightleftarrows(111)$ exch. | 0.60 |
| chain through a $3\times3$ (001) facet | 0.19 |

process of a special kind. In fact, while multiple exchanges at steps and on vicinal surfaces [100, 70] are characterized by quite high barriers, and thus become important only at high temperatures, the chain process on TO and TP has such a low barrier that it is the dominant interfacet process, provided that the (001) intermediate facet is not too large (up to facet sizes of $5 \times 5$ on Ag). The chain process was found in simulations of diffusion on Al TO clusters [341]; the calculations in reference [261] confirm that it should be important also in Ag and Au. Jump, exchanges and chain processes are possible also on non-crystalline structures such as decahedra and icosahedra [342], and play a key role in the morphology transitions during cluster growth [343, 344].

## 4.4. *Collective diffusion on stepped surfaces*

### 4.4.1. *Langmuir model for stepped substrates*

The macroscopic collective diffusion coefficient $D_c$ is unavoidably affected by the existence of surface defects, especially in the form of impurities and surface steps [345, 346] even on a well-prepared sample substrate. There exist only limited efforts [347–351] in trying to understand how macroscopic collective diffusion depends on the microscopic jump rates near the steps. This is the question we address in this section. We will describe the theoretical results from a lattice gas model for the stepped substrates and compare the theory with a series of experimental studies of CO on Pt(111) surfaces with well characterized step densities.

Theoretically, this problem has been investigated [352, 353] within a Langmuir gas model, where the interaction between adsorbate particles is the exclusion of double occupancy of lattice sites. The model includes the effect of the Schwoebel barrier, extra binding at step edge, and enhanced diffusion along step edges as well as different prefactors at these sites. The corresponding (adiabatic) potential energy profile in direction perpendicular to step edges ($x$ direction) is shown in figure 36(a). An additional binding energy $E_B$ at the lower step edges can arise as a consequence of extra coordination for the adsorption sites there. Similarly, a Schwoebel barrier $E_S$ (see section 4.3.2) for jumps from the terrace to the lower step edges [288] can exist due to the reduced coordination at the saddle point as compared to the one for a jump on a terrace, for which the activation barrier is denoted by $E_0$. The barrier for jumps along lower step edges, $E_2$, is taken to be lower than $E_0$, leading to a higher jump rate along the lower step edges. The inert substrate surface is assumed to have a periodic array of straight steps separated by terraces of width of $L$ lattice sites.

The energy barriers lead to the following rates for nearest-neighbor jumps as shown in figure 36(b) and figure 36(c): $\Gamma_0$ on the terraces, $\Gamma_1$ from the lower edge to the same terrace, $\Gamma_1'$ from the terrace to lower edge, $\Gamma_u$ from the lower edge across the step up to the neighboring terrace, $\Gamma_d$ from the upper edge across the step down to the lower edge on the neighboring terrace, and $\Gamma_2$ along the lower step edge. These set of rates allow for modified prefactors $\nu_S$, $\nu_B$ and $\nu_2$, for jumps over step edge, detachment from (attachment to) step edge and jumps along the lower step edge, respectively [352]. They can be written as

$$\Gamma_0 = \nu_0 \exp\left[-E_0/(k_B T)\right] = \frac{\nu_0}{\nu_B}\,\xi\Gamma_1 = \frac{\nu_0}{\nu_B}\,\Gamma_1' = \frac{\nu_0}{\nu_S}\,\sigma\Gamma_d = \frac{\nu_0}{\nu_S}\,\xi\sigma\Gamma_u; \qquad (122)$$

$$\Gamma_2 = \nu_2 \exp\left[-E_2/(k_B T)\right], \qquad (123)$$

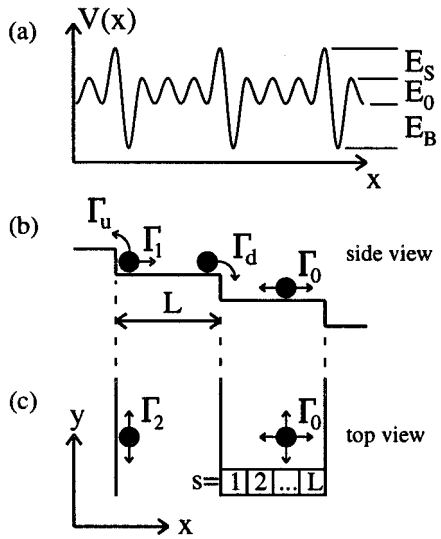


Figure 36. Geometry and jump rates of the lattice model for diffusion on a stepped substrate. (a) The potential profile in $x$ direction. (b) Side view of the model showing the various intrinsic hopping rates for jumps in the $x$ direction near step edges. The rate $\Gamma_1'$ (not shown) is for the process reverse to that with the rate $\Gamma_1$. (c) Top view of the model showing the size of one unit cell with the indices $s = 1, 2, \ldots, L$ of each lattice site within the cell.

where the parameters $\xi$ and $\sigma$ defined by $\xi = \exp[E_B/(k_BT)]$ and $\sigma = \exp[E_S/(k_BT)]$ describe the effective strengths of the binding at step edge and the Schwoebel barrier. Each adsorption site is labelled by the coordinate $(lLa, mb)$ of the unit cell together with a site index $s = 1, 2, \ldots, L$ within the unit cell (see figure 36(c)). Here $a$ and $b$ are the nearest neighbour distances along the $x$ and $y$ directions, respectively. For each site we then define a stochastic occupation variable $n_{l,m}^s(t)$, which due to the exclusion of double occupancy can take on only the values 0 and 1. In the present model, the adsorption potential is modified only for lattice sites at the lower step edge, and therefore one has only two distinct row coverages $\theta_e$ and $\theta_t$, for lower step edges and terraces, respectively, defined by

$$\left.\begin{aligned} \theta_e &= \langle n_{l,m}^1 \rangle; \\ \theta_t &= \langle n_{l,m}^2 \rangle = \langle n_{l,m}^3 \rangle = \cdots = \langle n_{l,m}^L \rangle. \end{aligned}\right\} \tag{124}$$

These occupation numbers are independent of the cell indices $(l, m)$ by symmetry, and they obey the detailed balance condition. To satisfy detailed balance corresponding to the potential profile of figure 36(a), the intrinsic prefactors were chosen to be symmetric with respect to reversal of each jump, i.e. the prefactors are identical for the rates $\Gamma_d$ and $\Gamma_u$, and also for the pair $\Gamma_1$ and $\Gamma_1'$. Also the Schwoebel barrier results in a symmetric temperature-dependent modification of rates $\Gamma_u$ and $\Gamma_d$ by the factor $\sigma$. Therefore, the prefactors $\nu_B$ and $\nu_S$ and the Schwoebel factor $\sigma$ do not affect static quantities like $\theta_e$ and $\theta_t$. Note that these symmetry properties guarantee that there is no diffusion bias although the potential profile of figure 36(a) is

asymmetric. The partial coverages are related by

$$\frac{\theta_e(1-\theta_t)}{\theta_t(1-\theta_e)} = \xi, \tag{125}$$

which allows us to express $\theta_e$ and $\theta_t$ as a function of the total coverage $\theta = \theta_t + (\theta_e - \theta_t)/L$ as

$$\left.\begin{aligned} \theta_e &= \theta_e(\xi, L, \theta) = \frac{1}{2(\xi-1)}\left(\beta_+ - \sqrt{\beta_-^2 + \alpha}\right); \\ \theta_t &= \theta_t(\xi, L, \theta) = \frac{1}{2(\xi-1)(L-1)}\left(\beta_- + \sqrt{\beta_-^2 + \alpha}\right), \end{aligned}\right\} \tag{126}$$

where $\beta_\pm = (\xi-1)(L\theta \pm 1) \pm L$ and $\alpha = 4(\xi-1)(L-1)L\theta$.

Under conditions typical to experiments on smooth surfaces, the value of the terrace width $L$ ranges from 50 to 500, and the extra binding at the step edges, characterized by $\xi = \exp[E_B/(k_BT)]$, satisfies the condition $\xi \gg 1$. Equation (126) then leads to the following observations. At very low coverages s.t. $\theta \leq 1/L$, the particles adsorb preferentially at the step edges because of the extra binding there so that $\theta_e \approx \theta L$ while terraces are practically empty with $\theta_t \approx 0$ [352]. This situation continues as the coverage is increased until one reaches the value $\theta = 1/L$. At this point, the step edges are fully occupied and the terraces remain empty with $\theta_e \approx 1$ and $\theta_t \approx 0$. Beyond that point, for $\theta > 1/L$, terraces start to be populated while the edge rows remain fully occupied, i.e. $\theta_e \approx 1$ with $\theta_t \approx \theta$. This can be seen more explicitly by expanding $\theta_e$ and $\theta_t$ in equation (126) to lowest order in the deviation $\theta - 1/L$. For $\xi \gg L$ one finds

$$\left.\begin{aligned} \theta_e &\approx 1 - \sqrt{\frac{L-1}{\xi}} + \frac{L}{2}\left(\theta - \frac{1}{L}\right) + O\left[\left(\theta - \frac{1}{L}\right)^2\right]; \\ \theta_t &\approx \sqrt{\frac{1}{(L-1)\xi}} + \frac{L}{2(L-1)}\left(\theta - \frac{1}{L}\right) + O\left[\left(\theta - \frac{1}{L}\right)^2\right]. \end{aligned}\right\} \tag{127}$$

This behaviour of $\theta_e$ and $\theta_t$ is the key to understand the variation of the diffusion coefficient with the coverage $\theta$. Since typically for large terraces the inverse width $1/L$ is less than a few percent, the experimental situation usually corresponds to the regime $\theta > 1/L$, and the influence of the steps on the measured values of diffusion rates differs substantially from the zero-coverage behaviour described in reference [354].

4.4.2. *Dynamical mean field solutions*

Two equivalent analytic approaches to study collective diffusion, the Mori projection operator formalism [126] and the Green's functions techniques [128–130] have been applied to solve for the collective diffusion coefficient $D_c$ for the model described above [352]. In both approaches, the diffusion coefficient is obtained by identifying the pole of the density correlation function in the DMF approximation as discussed in section 2.2. For small terrace widths ($2 \leq L \leq 8$), MC simulation studies were also performed [352] and the analytic theory agrees very well with the MC data, with no discernible systematic deviations. Thus the DMF provides a very accurate description of the present system. The computational effort in the MC simulations increases rapidly for increasing terrace width, and a full numerical study

of stepped surfaces with realistic terrace widths and system sizes is not feasible. The analytic DMF thus provides an accurate and powerful tool for studying problems such as the crossover from step-dominated to terrace-dominated diffusion as a function of temperature and terrace width. In the following, we shall discuss the analytic DMF result for the diffusion coefficient perpendicular to the steps ($D_{xx}$) and that parallel to the steps ($D_{yy}$) as given by the equations from reference [352]):

$$D_{xx} = \frac{\Gamma_0 L^2 a^2}{\left[L - 1 + \left(\frac{\theta_e}{\theta_t}\right)^2 \xi^{-1}\right]\left[L - 2 + \frac{\theta_t}{\theta_e}\left(\frac{\nu_0}{\nu_B} + \frac{\nu_0}{\nu_S}\sigma\right)\xi\right]}; \tag{128}$$

$$D_{yy} = \left[1 + \frac{\Gamma_2/\Gamma_0 - 1}{1 + (L-1)\left(\frac{\theta_t}{\theta_e}\right)^2 \xi}\right]\Gamma_0 b^2. \tag{129}$$

4.4.3. *Diffusion perpendicular to the steps*

In this section we examine the coverage and temperature dependence of the diffusion coefficient $D_{xx}$ perpendicular to the steps as given by equation (128). For $E_B = 0$ all row coverages are equal with $\theta_e \equiv \theta_t \equiv \theta$ so that all coverage dependence of $D_c$ cancels out, and even with large Schwoebel effect the properties of $D_c$ are relatively simple. Therefore, the main emphasis will be on cases where the extra binding at step edge is strong, i.e., $\xi = \exp[E_B/(k_B T)] \gg 1$. Based on the analysis below, behaviour of $D$ in other cases can be easily understood. Since step spacings of the order of few hundred lattice constants can be achieved for good sample surfaces, the regime $\theta \gg 1/L$ is the most relevant one for most experiments. In this limit, with $\exp[E_B/(k_B T)] \gg 1$ and $L \gg 1$, we have $\theta_e \approx 1$ and $\theta_t \approx \theta$, and the expression of $D_{xx}$ in equation (128) reduces to

$$D_{xx} \approx \frac{\Gamma_0 L a^2}{L + \theta\left[\frac{\nu_0}{\nu_B} + \frac{\nu_0}{\nu_S}\exp[E_S/(k_B T)]\right]\exp[E_B/(k_B T)]}. \tag{130}$$

With fixed values of intrinsic barriers and prefactors, this expression is an increasing function of $L$ and a decreasing function of $\theta$. The above equation has two regimes, one with $\nu_S/\nu_B \gg \exp[E_S/(k_B T)]$, which leads to the elimination of $E_S$ in the diffusion coefficient over steps so that $D_{xx} = \nu a^2 \exp\{-[(E_0 + E_B)/(k_B T)]\}$; the other with $\nu_S/\nu_B \ll \exp[E_S/(k_B T)]$. In both regimes $D_{xx}$ has a simple Arrhenius form to allow a straightforward fitting procedure. In the intermediate regime, $\nu_S/\nu_B \approx \exp[E_S/(k_B T)]$, however, the situation is more complicated.

In recent experimental studies, Xiao *et al.* [347, 355–357] have measured the diffusion coefficient of CO on Pt(111) as a function of temperature at coverages 0.3 ML and 0.5 ML for a number of substrates with controlled miscuts corresponding to different terrace widths $L$ described in the model here. They also distinguish between the different kind of steps labelled as A, B and AB types as shown in figure 37. Their results are shown in figure 38 for a CO coverage of 0.3 ML and in figure 39 for CO coverage of 0.5 ML. Assuming an Arrhenius behaviour for the diffusion coefficient $D_{xx}$ perpendicular to the steps, their data can be fitted by equation (130) quite well for all step densities ($L = 48, 24, 12$, for miscuts of 1, 2 and 4°, respectively) with $E_0 = 3.9 \pm 0.2$ kcal/mol [24, 358, 359] and

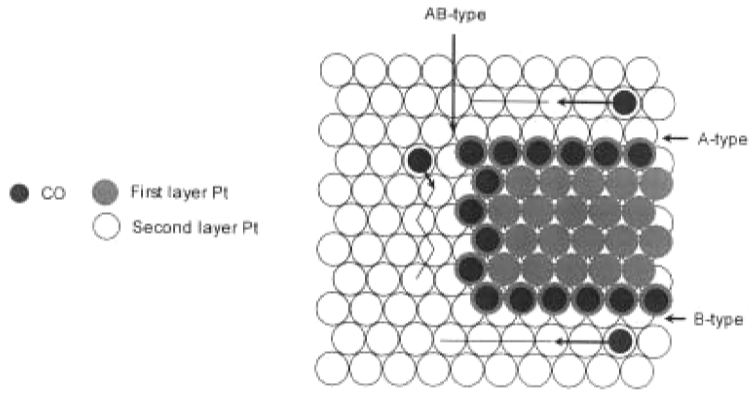


Figure 37. Different types of step orientations for CO on the Pt(111) surface.

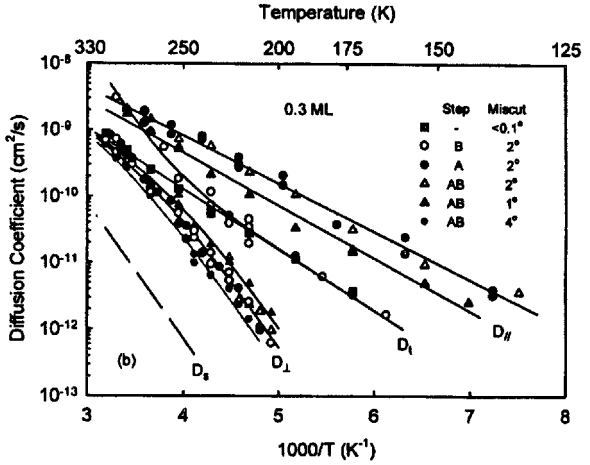


Figure 38. CO diffusion coefficient $D$ in the direction perpendicular or parallel to steps on vicinal to Pt(111) surfaces vs. reciprocal temperature in an Arrhenius plot for a number of step orientations and at 0.3 ML coverage. The data are from reference [357]. The solid lines represent fits to analytic results discussed in the text and in reference [357]. $D^t$ and $D^s$ represent limiting cases where terrace diffusion or step diffusion dominates.

$E_0 + (E_S) + E_B = 9.3 \pm 0.8$ kcal/mol, where $E_S$ in the parentheses appears only for the second regime. The corresponding prefactors from the fitting are $D_{t0} = 6 \times 10^{-7}$ cm$^2$/sec and $D_{xx0} = 6.4 \times 10^{-4}$ cm$^2$/sec ($D_{xx0} = \nu_B a^2$ in the first regime or $\nu_S a^2$ in the second regime of equation (130)). Judging from the quality of the fit, the measurement does not fall into the intermediate regime. The prefactor across the steps is about three orders of magnitude larger than over the terraces, similar to what has been reported for Ag/Ag(111) [335]. In the case of CO/Pt(111), the extra binding energy at the trapping site $E_B$ is found to be $E_B \simeq 71$ kcal/mol at low coverages. Now, with the terrace barrier $E_0$ independently measured, this leads to the value for the Schwoebel barrier of $E_S \simeq -1.6 - 1.3$ kcal/mol. Based on the above argument, it was concluded that the Schwoebel barrier for CO on Pt(111) is small if not negative

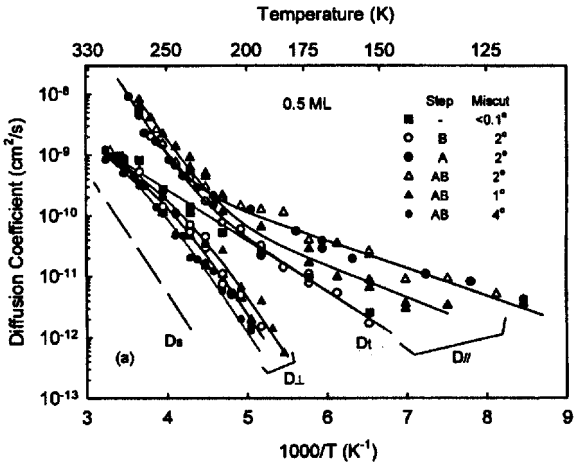


Figure 39. As for figure 38, but the CO coverage is 0.5 ML.

and diffusion perpendicular to steps is dominated only by the step edge trapping well. This is in contrast to the metal-on-metal systems studied by FIM and STM [360, 361, 333, 334] where the Schwoebel barrier was the only one of interest. In these experiments, the diffusion process after trapping at the step sites was not followed and diffusion out of the steps, i.e. dissociation of atoms from steps, was studied as an independent process [361]. For gas atom/molecule diffusion on stepped surfaces, this observation for CO/Pt(111) with the comparison with the theory is the first example illustrating that the additional trapping potential well at step edges could be the main factor that controls the diffusion perpendicular to steps.

4.4.4. *Diffusion parallel to step edges*

In general, diffusion in the direction parallel to the steps appears to have a relatively simple dependence on coverage and terrace width. The zero-coverage limit of $D_{yy}$ is particularly simple: in the absence of blocking we have $\theta_e/\theta_t \approx \exp[E_B/(k_BT)]$ so that equation (129) leads to

$$D_{yy}^{\theta_e \to 0} = \left[1 + \frac{\Gamma_2/\Gamma_0 - 1}{1 + (L-1)\exp[-E_B/(k_BT)]}\right]\Gamma_0 b^2, \tag{131}$$

which is the result obtained in reference [354]. Here the effects of the extra binding and the enhanced jump rate at step edges *both* increase $D_{yy}$.

For a fixed coverage $\theta \gg 1/L$ at low temperatures two effects compete with each other. First, for $E_2 < E_0$ the ratio $\Gamma_2/\Gamma_0 \propto \exp[(E_0 - E_2)/(k_BT)]$ and diffusion along the step edge row is increasingly faster than in the terrace region. At the same time, the occupation of the edge row increases as the factor $\xi = \exp[E_B/(k_BT)]$, which leads to an exponential increase in the blocking factor for diffusion along the step edge. These two effects determine the coverage and temperature dependence of diffusion in the direction parallel to the steps. In the low temperature limit with $L \gg 1$, we have $\theta_e \approx 1$ and $\theta_t \approx \theta$ so that equation (129) reduces to

$$D_{yy} \approx \left\{1 + \exp[(E_0 - E_2 - E_B)/(k_BT)]\frac{\nu_2}{L\nu_0\theta^2}\right\}\Gamma_0 b^2. \tag{132}$$

From this form we see that for $E_0 - E_2 > E_B$ the main contribution at low temperatures comes from diffusion along the lower step edge, i.e. from the second term on the right hand side. If, on the other hand, $E_0 - E_2 < E_B$, then at low temperatures the increase in the edge rate $\Gamma_2$ is not large enough to compensate the enhanced blocking, and the less-blocked terrace jumps with rate $\Gamma_0$ dominate. In other words, the behaviour of $D_{yy}$ depends on whether the larger proportion of mass transport occurs at step edges or on terraces.

This result can be readily compared with the experimental observations. As can be seen from figure 38 and figure 39, at temperatures above 225 K, data from all three samples (A, B, and AB type of steps) fall on a single line and can be interpreted as due to the same mechanism of diffusion via step edges. However, the diffusion data parallel to A and AB type of steps clearly follow another trend at low temperatures. It has been suggested that this is due to the opening of other easy channels of diffusion for these step orientations [357]. Here we concentrate on diffusion parallel to B type steps on the 2° miscut sample as shown in figure 38 and figure 39. Using $\nu_0 a^2 = 6 \times 10^{-7}$ cm$^2$/sec and $E_0 = 3.9$ kcal/mol to fit the data with equation (132) one obtains $E_2 + E_B = 10.3$ kcal/mol, and $\nu_2 a^2 \approx 5$ cm$^2$/sec, about $10^7$ times $\nu_0 a^2$. With the established value of $E_B$ of 7 kcal/mol [362, 358, 359, 363, 364], one then deduces the value $E_2 = 3.3$ kcal/mol. The fitting quality is excellent over the entire temperature range of the experiment, spanning close to four orders of magnitude of values of $D$, as shown by the solid line in figure 38 and figure 39.

However, the large value of $\nu_2$ is puzzling and does not seem to have simple physical origin. Recently, Xiao *et al.* [357, 365] have performed a MC simulation study using a normal prefactor at the step edges ($10^{-3}$ cm$^2$/sec). They were able to fit the data with the same quality as with (132) using the anomalously large prefactor for the step edge. The most likely explanation for this apparent paradox is that both the experimental studies and the MC simulation study are under highly *non-equilibrium* conditions and the initial mass transport cannot be described by the linear diffusion theory such as that given in (132). When the diffraction grating is created parallel to the step edges, the relaxation time for the step edge population to return to equilibrium value ($\theta_e \approx 1$) is anomalously long. During the transient period before the step edge population reaches its equilibrium value, there is a mechanism such that the adsorbed CO can hop from the high coverage terrace site to the step edge, diffuse along the step edge, and then hop back to the low coverage terrace site. This process appears in the actual mass transport with an effective large prefactor $\nu_2 a^2$. As the equilibrium situation is approached in the asymptotic long time limit, the net cross-channel mass transport between the terrace and the step edge is no longer effective and the diffusion should then be dominated by the terrace. Preliminary MC studies for longer times indeed confirm this slow approach to equilibrium for this geometry [366]. Thus, the accurate linear diffusion coefficient $D_{yy}$ must be extracted in the long time regime of the coverage grating decay, which imposes a significant experimental challenge. This example also indicates the care one must take in analysing the diffusion data with a linear analysis. In the presence of steps leading to new time scales and energy scales, nonlinear and non-equilibrium conditions such as those discussed in section 2.3 can often prevail.

### 4.5. *Diffusion coefficients near phase transition boundaries*

As discussed in the earlier chapters, there is no rigorous basis for the Arrhenius activated behaviour for the temperature dependence of the diffusion coefficients.

However, over the limited temperature range of the experiments, both the experimental and theoretical studies have shown that the diffusion coefficients obey an apparent Arrhenius form with an effective activation barrier. The most notable exception is when one is near a phase transition boundary. This could be due to either a phase transition for the substrate surface, as for example the surface reconstruction of W(100), or in the case of finite coverages, a phase transition between an ordered and disordered phases of the adsorbate layer or even between two ordered phases. Under these conditions, theoretical studies have shown that fluctuation effects near the phase boundary can lead to a strong non-Arrhenius temperature dependence as well as non-monotonic coverage dependence. Experimentally, these anomalous temperature and coverage dependencies have also been observed [8, 9]. This is the subject of the present section.

4.5.1. *Diffusion near a phase boundary for a substrate reconstruction*

First, we consider the case where the phase transition is that of the intrinsic substrate. In this case, we will show that the dominant effects of the phase transition on the adatom diffusion coefficient arise from its effect on the nonadiabatic frictional coupling rather than the adiabatic barrier. Consider the random frictional force acting on the adatom at the position $\mathbf{r}$ due to coupling with the vibrational excitations of the substrate. In the simple pair interaction model, this can be expressed in terms of the linear displacement $u_{\mathbf{q},\alpha}$ of each substrate atom from its equilibrium position as

$$f_\alpha(\mathbf{r}) = \sum_{\mathbf{q}} W(\mathbf{r}, \mathbf{q}) u_{\mathbf{q},\alpha}. \tag{133}$$

Here, $\mathbf{q}$ stands for the normal mode index of the phonon mode, $\alpha$ is the Cartesian component label and $W$ represents the coupling function. The frictional damping (in the Markovian limit) on the adatom is given by the self correlation function of this random force [126, 214] as

$$\eta = \sum_{\mathbf{q}} W^2(\mathbf{r}, \mathbf{q}) S(\mathbf{q}, \omega = 0), \tag{134}$$

where $S(\mathbf{q}, \omega = 0)$ is the (isotropic) dynamic structure factor of the substrate in the zero frequency limit defined as $\int_0^\infty \mathrm{d}t \langle u_{\mathbf{q},\alpha}(t)^* u_{\mathbf{q},\alpha}(0) \rangle$. According to general dynamical scaling arguments [367, 368], $S(\mathbf{q}, \omega)$ should take the scaling form near $T_c$ for a continuous phase transition as

$$N^d S(\mathbf{q}, \omega) = \xi_c^{z+\gamma/\nu} g_\pm(q\xi_c, \omega\xi_c^z), \tag{135}$$

where $g_\pm$ is a scaling function, $\xi_c \propto |T/T_c - 1|^{-\nu}$ is the divergent correlation length, $d$ is the system dimension, $\gamma$ the susceptibility exponent and $z$ is the dynamical critical exponent. Substitution of (135) back into (134) then leads to the conclusion that as one approaches $T_c$, the friction $\eta$ has a singular part that goes as $\eta \propto |T/T_c - 1|^{-x}$ with $x = \nu(z - d) + \gamma$. The dimension $d$ enters explicitly through the $q$ integration in (134) where we have assumed a typical short ranged coupling potential $W(q)$ that is regular at $q = 0$. Thus the friction $\eta$ can either diverge if $x > 0$ or be finite with a cusp only. For the surface reconstruction transition of the W(100) surface [369], the exponent $x$ has been explicitly evaluated for a model Hamiltonian and shown to have the value [369, 370] $x \approx 1.8$. Thus the diffusion coefficient of adatoms on this surface is predicted to vanish at the transition. One caveat here is

that the Markovian approximation tends to overestimate the critical effect. This is easy to understand because in the Markovian approximation, the magnitude of the single friction parameter $\eta$ is controlled by the memory function $\Sigma(\omega)$ evaluated at the characteristic adatom frequency $\omega_0$ which is set to zero. As one approaches $T_c$, the central peak in $S(\mathbf{q},\omega)$ responsible for the divergence of the friction gets narrower and narrower and eventually the Markovian approximation is going to break down when the width of the central peak becomes less than $\omega_0$. The critical effects can be maximized for an overdamped substrate in which the scale of the central peak in the dynamic structure factor is controlled by the intrinsic damping factor $\eta_s$ which could be much larger than $\omega_0$.

An analogous critical divergence of the frictional coupling occurs in type-II superconductors in the mixed phase when there is a partial penetration of an external magnetic field. The fields are concentrated in flux vortices which arrange themselves as a regular 'Abrikosov' lattice [371]. When a current $I$ is passed through, the flux line lattice (FLL) moves in response to the Lorentz force, leading to dissipation and an induced voltage $V$ which is proportional to the drift velocity of the lattice. Thus the conductance $C = I/V$ is just the inverse of the center of mass mobility $D_{CM}$ of the flux lattice. The conductance is expected to decrease monotonically towards the $H_{c2}$ phase boundary where the superconductor becomes normal because of the diminishing order parameter and hence a reduced pinning strength. However, experimentally, it was found that the conductance peaks sharply to a large value before dropping at the superconducting-normal transition [372, 373]. To date, however, there has been no satisfactory explanation for this peak effect. Recent experiments [374] have shown that the peak effect occurs at exactly the melting point of the flux lattice. This confirms the ideas that the mobility $D_{CM}$ for the flux lattice would vanish [375, 167] and hence the conductance would be anomalously large near a continuous or very weak first order melting transition due to the enhanced coupling of the pinning centers to the FLL through the critical fluctuations. Following the same argument leading to equation (134), we can find a similar expression for the random force acting on the pinning center due to the vibrational motion of the flux lattice. The force due to pinning centre on the flux lattice is exactly equal and opposite to this force. Thus, it can be easily seen that the friction on the flux lattice is proportional to the expression given in equation (134) and should diverge or become very large at a continuous or weakly first order transition of the flux lattice. This then lead naturally to the dip in the mobility of the flux lattice and the corresponding peak in the conductance which is the inverse of the mobility.

4.5.2. *Diffusion near the phase boundary of an adsorbate layer*

In this section, we first discuss the general theory of diffusion close to phase transition boundaries of a surface adsorbate system. The behaviour of the diffusion coefficients near second-order transition points can be analyzed using general scaling theory [376]. The collective diffusion coefficient is dominated by the scaling behaviour of the static structure factor, which leads to the following dependence:

$$\left.\begin{aligned} D_c(T) &\propto |1 - T/T_c|^{\gamma}, \theta = \theta_c; \\ D_c(\theta) &\propto |1 - \theta/\theta_c|^{\gamma/\beta}, T = T_c, \end{aligned}\right\} \tag{136}$$

where $T_c$ and $\theta_c$ denote the critical temperature and coverage, respectively, and $\gamma$ and $\beta$ are the usual susceptibility and order parameter critical exponents, respectively.

Thus, $D_c$ is expected to vanish close to second-order transition points. It is important to note that equations (136) apply only when the coverage (density) is the order parameter. When this is not the case, e.g., in the case of Model C discussed below [368], the critical behaviour is much weaker and may be virtually absent.

The case of tracer diffusion is more subtle due to the fact that within mean field theory, short range correlations do not play any role [376]. General scaling analysis reveals [376] that $D_t$ should have a non-singular part, and another part that has an energy-like singularity which along the critical coverage goes as $|1 - T/T_c|^{1-\alpha}$. This means that $D_t$ itself remains finite at $T_c$, but its slope has a singularity for $\alpha > 0$.

We now illustrate these general principles in the context of the lattice-gas model of O/W(110). The O/W(110) system is undoubtedly one of the most studied adsorption systems. Its phase diagram has been determined through experimental studies [377–380] using LEED spot profile analysis and STM. Its main features can be summarized as follows. At temperatures $T \geq 710\,\mathrm{K}$ [379], the system is in a disordered phase, while at lower temperatures there is a wide variety of ordered phases at different coverages, namely the $p(2 \times 1)$, $p(2 \times 2)$, and $(1 \times 1)$ phases corresponding to ideal coverages of 1/2, 3/4, and 1, respectively. At intermediate coverages, some coexistence regions also appear [380]. The substrate remains unreconstructed at all coverages [381–383], the oxygen atoms have well-defined adsorption sites on the surface, [380, 384, 385] and desorption of oxygen occurs only at temperatures as high as 1600 K or above [382, 383]. Therefore, this system is suitable for simulation studies using a lattice-gas description over a wide temperature range.

We summarize here the results from MC simulation studies [386, 387] based on a lattice-gas model including the three-particle interactions [388]. The phase diagram in the $T - \theta$ plane is shown in figure 40. The dynamic algorithm used is the TDA discussed in section 3.5. earlier. We will come back and discuss the significance and difference of choosing different dynamic algorithms later. In figures 41 and 42, the behaviour of the diffusion coefficients is shown. First, we note that the DMF (see section 3.5) gives quite a good approximation of $D_c$, while it is much less satisfactory for $D_t$, which is clearly overestimated at low temperatures. On the other hand, the

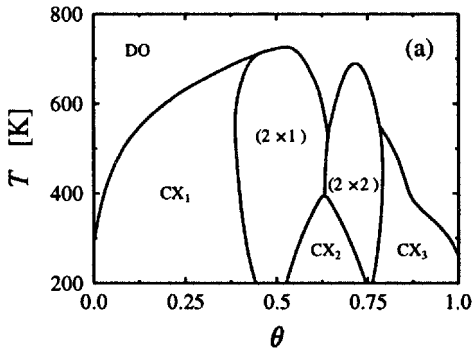


Figure 40. Schematic phase diagram of the O/W(110) system in the $T - \theta$ plane [338]. The energy parameters of the model have been scaled so that the critical temperature of the order-disorder phase transition at $\theta = 0.45$ is $T_c = 710\,\mathrm{K}$. DO denotes the disordered region, while $(2 \times 1)$ and $(2 \times 2)$ denote the ordered phases. The $\mathrm{CX}_i$, $i = 1, 2, 3$, are the coexistence phases.

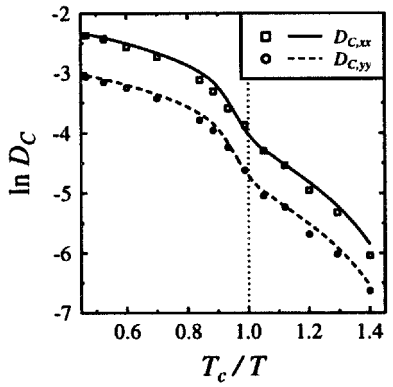


Figure 41. Results for $D_c$ in an Arrhenius plot at $\theta = 0.45$. The results along the two principal axes $(x, y)$ are based on the density fluctuation method and are given by squares and circles, respectively. The error bars are of the size of the symbols. The lines are approximate results neglecting memory effects. The critical temperature $T_c$ of the order-disorder phase transition is denoted by a dotted line.

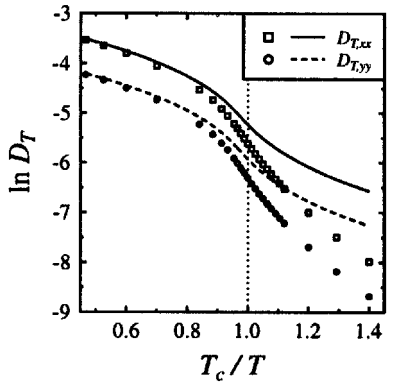


Figure 42. Results for $D_t$ in an Arrhenius plot at $\theta = 0.45$. The results along the two principal axes $(x, y)$ are given by squares and circles, respectively. The error bars are much smaller than the size of the symbols. The lines are approximate results neglecting memory effects. Again, the critical temperature $T_c$ is denoted by a dotted line.

use of the Darken equation for $D_c$ would lead to an evident underestimation of $D_c$ at low temperatures. More importantly, it is evident that the behaviour displayed by the diffusion coefficients in figures 41 and 42 cannot be reasonably described by a constant effective activation barrier over the whole temperature regime. Further, for this kind of a *non-Arrhenius temperature dependence*, there is no unique way of defining a temperature dependent barrier. One way is to use the local slope while another possibility is to choose a constant effective prefactor and leave all the temperature dependence in the effective barrier. These two procedures would lead to very different values for the barrier. We now follow the practice commonly used in analysis of experiments and define an effective diffusion barrier $E_A^D$ as the local slope

of an Arrhenius plot, namely

$$E_A^D \equiv -\frac{\partial}{\partial(1/k_B T)} \ln D. \tag{137}$$

In figures 41 and 42, the local slope is approximately constant at low and high temperatures away from $T_c$. This implies that the diffusion coefficients obey simple Arrhenius behaviour in these limits. Overall, however, the Arrhenius form with a single activation barrier cannot successfully describe their temperature dependence since near $T_c$ the diffusion coefficients show strong temperature variation.

Since the definition of $D_c$ contains the inverse compressibility [8] it is often assumed that this is the main origin of the anomalous temperature dependence near phase transitions [389, 390], as discussed above. However, for the O/W(110) system which is in the symmetry class of a 2D $xy$ model with a cubic anisotropy field, the critical effects in $D_c$ are controlled by the specific heat exponent $\alpha$ which is nonuniversal and *negative* [391]. It is thus expected that near $T_c$ there is just a rounded cusp for the compressibility $\chi_T$ whose size dependence is very weak, and thus the non-Arrhenius behaviour of *both* $D_t$ *and* $D_c$ is predominantly determined by the average local jump rate $\Gamma$ of single particles. Indeed, the temperature dependence of $\Gamma$ shown by circles in figure 43 is very similar to that of $D_c$ as well as $D_t$, with a turning point and sharp temperature variations near $T_c$. It is evident that $\xi$ only slightly steepens the slope of $D_c$ vs. $1/T$ around $T_c$.

The effective diffusion barrier $E_A^D$ as extracted from (137) for $D_t$ is shown in figure 44. It has a very pronounced peak centered at $T_c$, accompanied by a strong increase in the value of the corresponding prefactor $D_0$ shown in the inset of figure 44. This is yet another example of the well-known compensation effect [8, 392]. Here the compensation simply results from the fact that when the temperature dependence is non-Arrhenius, there is no unique way of separating the prefactor and the barrier contributions. Since the temperature dependence of the diffusion coefficient itself

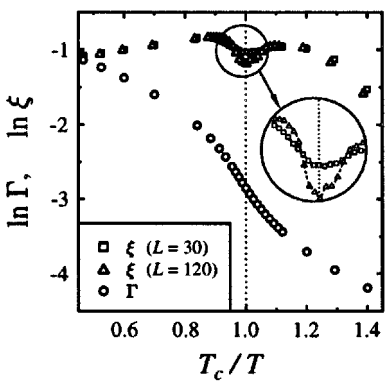


Figure 43. Results for the (dimensionless) thermodynamic factor $\xi$ (squares for $L_B = 30$ and triangles for $L_B = 120$) and the average transition rate $\Gamma$ (circles) in an Arrhenius plot. For $\xi$, results with two system sizes $L_B$ are given to demonstrate the cusp-like behaviour; the critical regime is further illustrated in the inset. The $L_B$ dependence (not shown) of $\Gamma$ is extremely weak. The error bars are smaller than the sizes of the symbols. The thermodynamic factor has been shifted for clarity's sake. The critical temperature of the order-disorder phase transition is denoted by $T_c$ and a dotted line.

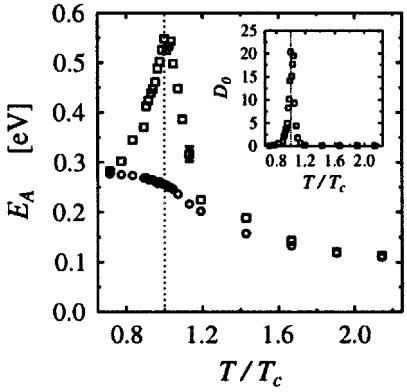


Figure 44. Results for the effective activation barriers $E_A$. The squares denote results based on the Arrhenius form, while open circles represent the data based on the tail of the waiting-time distribution. For the former, a typical error bar is shown, while for the latter the errors are smaller than the size of the symbols. Behaviour of the prefactor $D_0$ is illustrated in the inset. The critical temperature is denoted by a dotted line.

near $T_c$ is smooth and nonsingular, any dramatic change in the temperature dependence of the effective barrier $E_A^D$ *must* be followed by a corresponding change in the effective prefactor $D_0$.

To understand the observed strong temperature variation of $E_A^D$ near $T_c$, we need to consider the energetics of the microscopic jump processes which determine the average jump rate $\Gamma$. At finite coverages, there is a very complex distribution $P(E_A)$ for the instantaneous activation barriers $E_A$ which an adatom needs to overcome in a jump attempt from one configuration to another. For the particular model under study, the range of values is illustrated in figure 45. At high temperatures, $P(E_A)$ is

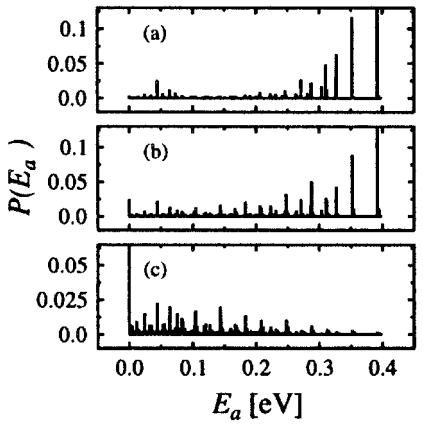


Figure 45. Normalized probability distributions $P(E_A)$ of the instantaneous activation barriers $E_A$ at three different temperatures: (a) $T = 0.714T_c$, (b) $T = 1.012T_c$, and (c) $T = 2.143T_c$. The barrier which correspond to a jump from a fully ordered row in the perfect $p(2 \times 1)$ phase to an empty channel nearby, thus forming a vacancy behind is 0.392 eV. In all the three figures, one of the peaks extends beyond the vertical scale: In (a) $P(0.392\,\text{eV}) = 0.496$, in (b) $P(0.392\,\text{eV}) = 0.171$, and in (c) $P(0.0\,\text{eV}) = 0.120$. For these histograms, more than $10^7$ samples were taken.

strongly peaked at small values of $E_A$, while at low temperatures the situation is completely the opposite. The change in the distribution takes place around $T_c$, thus characterizing the ordering of the adlayer as the temperature is decreased below $T_c$. This change in turn results in a strong temperature dependence of the average transition rate $\Gamma$ around $T_c$, as shown in figure 43. The peak in $E_A^D$ does not refer to any microscopic rate-limiting jump process. Instead, it arises from an entropic contribution to $\Gamma$ which has a strong temperature dependence in the vicinity of $T_c$. We note that these conclusions apply to both tracer and collective diffusion since the qualitative behaviour of $D_t$ and $D_c$ around $T_c$ is similar.

Uebing and Zhdanov (UZ) [393] have also studied the critical effects on diffusion coefficients for the same system (using a different model Hamiltonian) and observe a near-Arrhenius behaviour for $\Gamma$ as reflected in their results for $D_t$. This is in sharp contrast to the results of Vattulainen *et al.* [386, 147, 387, 394] shown above. In the study of UZ, the dynamic algorithm chosen is a variation of the initial value (IV) dynamics algorithm. As emphasized before in section 3.5, a dynamical quantity such as $\Gamma$, unlike the equilibrium properties, does not depend only on the lattice-gas Hamiltonian but also on the details of the stochastic dynamics chosen in the MC studies. It was found through comparison of simulation studies [395] using different dynamic algorithms, that other dynamics such as Metropolis and Kawasaki are consistent with TDA results and show a prominent non-Arrhenius behaviour for the rate $\Gamma$ near $T_c$. A comprehensive study of the validity of various MC dynamic algorithms was made through comparison with MD simulations which does not have the unrealistic dynamics of MC [395, 251]. It was found that the initial value dynamics of the type used by UZ does not describe the activation barrier qualitatively correctly in all cases.

The importance of how the *adatom–adatom* interaction part is treated becomes evident, when transition algorithms are analyzed using the cumulant expansion [396]. For IV dynamics this gives [251] $\langle w_{i,f} \rangle \sim \langle \exp [\beta E(\mathbf{n})] \rangle = \exp [\beta \langle E(\mathbf{n}) \rangle + \beta^2 (\langle E(\mathbf{n})^2 \rangle - \langle E(\mathbf{n}) \rangle^2)/2 + \cdots]$, while for, e.g., Kawasaki dynamics $\langle w_{i,f} \rangle \sim \exp[\beta \langle E(\mathbf{n}) - E(\mathbf{n}') \rangle]$. Thus, in IV dynamics $w_{i,f}$ depends only on the single particle initial energy $E(\mathbf{n})$ and its fluctuations, while in other transition algorithms $w_{i,f}$ involves the energy *difference* $E(\mathbf{n}') - E(\mathbf{n})$. This seemingly minor fact leads to a major difference as regards the critical behaviour of $D_t$. We conclude that the choice of the transition algorithm close to a critical point is nontrivial. This highlights the fact that one should not use results for simple model kinetics to draw general conclusions on critical behaviour of dynamic quantities as done in a recent study of the critical exponents for the diffusion coefficients [397].

### 4.6. *Memory effects in surface diffusion*

As can be seen from the definitions of $D_t$ and $D_c$ presented in section 2.2, the single-particle velocity correlation function $\phi(t) \equiv \langle \mathbf{v}(t) \cdot \mathbf{v}(0) \rangle$ and the flux–flux correlation function $\psi(t) \equiv \langle \mathbf{J}_T(t) \cdot \mathbf{J}_T(0) \rangle$ are the fundamental quantities from which the diffusion coefficients arise. In surface diffusion, an exponential decay (or an exponentially damped oscillation) of $\phi(t)$ is observed, if adparticle diffusion is considered to be the Brownian motion of independent particles in a periodic potential, with uncorrelated collisions with the substrate excitations [398, 20, 219, 45, 34, 53, 218]. This result is an immediate consequence of the assumption of a constant friction in the Langevin equation of equation (63). However, in real systems the temporal behaviour of the correlation functions is influenced by the presence of

substrate-particle and particle-particle interactions. It is instructive to examine these two sources of memory effects separately.

4.6.1. *Memory effects due to surface phonons*

As already discussed in the context of the GLE in section 3.3, the friction is in general related to the time-dependent memory function $\Sigma(t, t')$ which contains both substrate and adparticle degrees of freedom. Thus, even in the case of a single adparticle diffusing on an active substrate, memory effects can be present if the substrate has no time to relax during the adparticle motion. The importance of such memory effects can be estimated by considering the ratio between the time scale of the surface excitations (phonons) and that of the adparticle motion (electronic excitations are usually too fast to contribute to the memory effects, cf. section 3.3.2). The magnitude of these two time scales can be approximated by the Debye frequency $\omega_D$ for the substrate (or the maximum phonon frequency), and by the vibrational frequency of the adparticle in the potential minima $\omega_0$. Then, the Markovian limit of no memory effects is given by the condition $\omega_D/\omega_0 \gg 1$, i.e. when the particle motion is much slower than the substrate vibrations. In this limit, the memory function can be approximated by a delta function in time, leading to the so-called initial value approximation (IVA) for the time-dependent microscopic friction coefficient [211–214, 33, 20]. For adatom diffusion on metal surfaces, typical magnitude of the vibrational frequency is $\omega_D = \mathcal{O}(10^{13})$ Hz while $\omega_0 = \mathcal{O}(10^{12})$ Hz. Thus, at least in these systems the Markovian approximation should be reasonable.

For the case of single adparticles, the memory effects have been examined for various model systems [211–213, 25, 34, 45, 218, 58]. In particular, Cucchetti and Ying (CY) [218] carried out a systematic study of the influence of memory effects to adparticle diffusion and its vibrational motion. They used a simple adiabatic model potential, with the adparticle coupled to a set of phonon modes described by a collection on harmonic oscillators. By using such effective phonons, the phonon density of states can be tuned to correspond to a realistic situation. CY studied the simple Debye model of phonons using MD techniques in three different cases corresponding to $\omega_D = 10\omega_0$, $\omega_D = \omega_0$, and $\omega_D = 0.1\omega_0$. In the first case, the IVA describes $D_t$ very accurately corresponding to a constant friction in the GLE. Also, at low temperatures the diffusion barrier is given by its adiabatic value. However, for the two other cases where memory effects are important, both the magnitude of $D_t$ and the effective Arrhenius barrier differ from the Markovian limit. Owing to the lack of relaxation of the substrate during the adparticle motion, the effective barrier has a *higher* value than its adiabatic value. The increase in the barrier is proportional to the relaxation energy of the substrate atoms, and can be a significant fraction of the original barrier.

4.6.2. *Memory effects in many-particle systems*

In the case of interacting many-particle systems, the memory effects are even more subtle. Memory effects can be studied in terms of the behaviour of the time-dependence of the correlation functions $\phi(t)$ and $\psi(t)$ and the associated memory functions [398, 399], through the MEM as discussed in section 2.2. For many-particle diffusion, a distinction has to be made between the corresponding tracer and collective diffusion coefficients.

*Tracer diffusion in a lattice gas model of O/W(110):*—Recently, the role of memory effects in diffusion of oxygen adatoms on a W(110) surface was considered

in a lattice-gas model with TDA using MC simulations [125, 147, 387, 394, 387, 120, 122, 400]. The model is described in section 4.5.2, and the phase diagram is given in figure 40. In the case of O/W(110), the exact separation of dynamical correlations (cf. section 2.1, equation (36)) was used to study the contribution of memory effects to diffusion. A detailed comparison between the diffusion coefficients and their DMF counterparts at $T = 590\,\mathrm{K}$ and 465 K revealed [122] that directional correlations between successive jumps of the adatoms are indeed responsible for the memory effects. Such memory effects are strongest at low temperatures and close to the ideal coverages corresponding to ordered phases, i.e., around $\theta = 1/2$ and $\theta = 3/4$ in the model of O/W(110). These effects can be studied by introducing the generalized velocity autocorrelation function $\phi_g(t)$ in the lattice gas. $\phi_g(t)$ is defined by

$$\phi_g(t) = \frac{1}{N\tau_0^2} C_t(p\tau_0), \tag{138}$$

with $t = p\tau_0$ and $C_t$ defined in equation (33) in section 2.2. In all finite-coverage cases studied, it was found that the velocity autocorrelation function $\phi_g(t)$ can be well fitted to the form [400, 401]

$$\phi_g(t) = \frac{\phi_g(0)}{1 + At^x}, \tag{139}$$

which leads to an *algebraic decay* $\phi_g(t) \sim t^{-x}$ for $At^x \gg 1$. The same is true for $\psi_g(t)$ as well. Figure 46 shows typical correlation functions for different coverages showing the algebraic decay, and figure 47 shows the effective exponent $x$ as a function of temperature [400]. At high temperatures where interaction effects become less important, $x$ approaches the value of two in accordance with the Langmuir gas limit [402]. Within the ordered phases, however, the value of $x$ was found to depend on the details of ordering in a nontrivial way. Within the disordered phase, ordering plays no significant role and then the nature of interactions seems to be a sufficient criterion to determine the value of $x$: for repulsive interactions $x \simeq 2$ (or larger), while attractive interactions lead to $x < 2$. In ordered phases, however, the same idea is not sufficient for a proper description of $x$. Namely, if one considers the case at

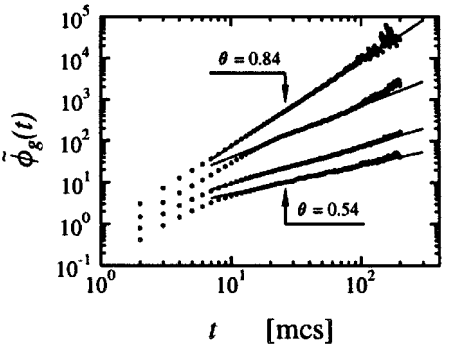


Figure 46. Typical results for $\tilde{\phi}_g(t) \equiv [\phi_g(t)/\phi_g(0)]^{-1} - 1$ at $T = 465\,\mathrm{K}$ in the O/W(110) model system [400]. At later times the decay of $\phi_g(t)$ starts to cross over to an exponential form. Results are shown for four coverages from top to bottom: $\theta = 0.84$, 0.74, 0.59 and 0.54, respectively. Full lines are fits to the data. Some curves have been shifted for clarity.

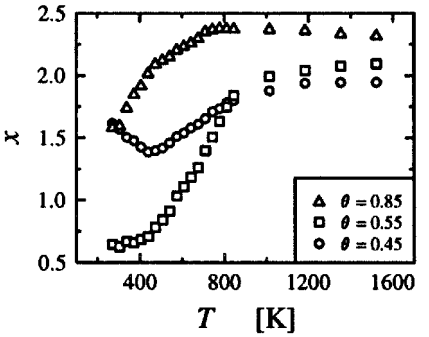


Figure 47. Results for the temperature dependence of the fitted decay exponent $x$ at various coverages $\theta$ in the O/W(110) model system. Error bars are smaller than the size of the symbols.

high coverages and at low temperatures, then the system is dominated by repulsive interactions, but nevertheless $x < 2$ within the ordered phases and in the vicinity of phase boundaries. Therefore, within the ordered phases, the behaviour of $x$ is governed by ordering effects that determine the local structure in which adatoms diffuse, while the nature of interactions is less important.

*Tracer diffusion in a model polymer system*—Another model where the memory effects were studied is that for flexible, chainlike molecules on flat surfaces. The chains were modelled by the 2D fluctuating-bond model with MC dynamics [403, 404], in which each segment excludes four nearest and next-nearest neighbour sites on a square lattice. The exclusion induces a strong entropic repulsion between the molecules even if there are no direct interactions present. The repulsion strongly influences diffusion in this system, and has been studied in detail in references [405–407]. For this study the model was augmented with an additional direct Lennard–Jones type of attraction between the segments of different chains. This model allows a systematic tuning of the interplay between repulsive and attractive interactions. Details on the model and parameters can be found in reference [120]. The results are in complete qualitative agreement with the results for the O/W(110) system. In all cases studied, it was again found that there is a power-law decay regime $\phi_g(t) \propto t^{-x}$ at intermediate times, with an exponent $x$ whose value depends on the interaction strength. At a fixed coverage $\theta = 0.25$, $x = 2.0 \pm 0.1$ in the athermal limit, $x = 1.7 \pm 0.2$ for a weak attractive interaction between the segments of different chains, and $x = 1.5 \pm 0.2$ for strongly attractive chains. In this case there are no ordered phases and the effective value of $x$ *decreases* when attractive interactions become stronger. The dependence on the coverage $\theta$ was also studied, and in the case of exclusion interactions only it was found that $x = 2.0 \pm 0.1$, $2.6 \pm 0.2$ and $2.6 \pm 0.4$ for $\theta = 0.25$, 0.5, and 0.75 in respective order. These results indicate that the effective $x$ may be larger than two with increasing repulsion.

*Tracer diffusion in hard circles on surfaces*—The third model studied recently is for 2D Brownian hard spheres (circles) on surfaces [259, 108]. The surface was taken to be completely smooth with no periodic potential. The results for the velocity autocorrelation and memory functions indicate that these functions display an intermediate power law decay; however, the memory effects are relatively weak and $x \approx 1.2$. In reference [108], the memory function for the case of tracer diffusion was also calculated using the mode-mode coupling approximation.

*Collective diffusion results in the model system O/W(110)*—The decay of velocity correlations in collective diffusion was also considered in the O/W(110) model system by calculating $\psi_g(t)$ numerically at $\theta = 0.55$ [251]. The memory effects in collective diffusion are expected to be much weaker than in the tracer case. The correlation function $\psi_g(t)$ was found to have a positive leading term, $\psi_g(0)$, and a negative tail at times $t > 0$. After a very small crossover time, an effective power-law form, $\psi_g(t) \propto t^{-y}$ was found at intermediate times, with $y = 1.23 \pm 0.05$ at $T = 676$ K and $y = 1.02 \pm 0.10$ at $T = 270$ K. Therefore, the results for $\psi_g(t)$ are in qualitative agreement with previous results for $\phi_g(t)$ and suggest that the exponent $y$ is non-universal, and thus subject to interaction effects.

*Collective diffusion in the model polymer system*—The FB model polymer system was also studied, and an approximate power-law decay $\psi_g(t) \sim t^{-y}$ found at relatively short times [251]. Exponents were found to be $y = 1.8 \pm 0.1$ at $\theta = 0.40$ and $y = 2.0 \pm 0.1$ at $\theta = 0.65$. With strong interchain attractions, $y = 1.5 \pm 0.1$ at $\theta = 0.40$ was found. These results are in qualitative agreement with the tracer diffusion case.

### 4.7. *Nonequilibrium diffusion in the lattice-gas model of O/W(110)*

#### 4.7.1. *Diffusion during domain growth*

We now illustrate the approaches on diffusion under nonequilibrium conditions presented in section 2.3, in the context of the lattice-gas model of O/W(110). The diffusion of oxygen adatoms in the model was studied during domain growth with MC simulations combined with the TDA ($\Delta = 0.0437$ eV) by Vattulainen *et al.* [165]. The system was prepared at a fully disordered state at $\theta = 0.45$ corresponding to infinite temperature, and then instantaneously quenched to several temperatures (465–635 K) below the order-disorder transition temperature of the $p(2 \times 1)$ phase. The concept of equivalent times scales presented in section 2.3 was used to calculate the correlation functions of equation (45) and equation (46) for the effective (non-equilibrium) tracer and collective diffusion coefficients, and the corresponding average single-particle transition rates $\Gamma(T, t)$ [408].

Figure 48 shows the results for the effective Arrhenius barriers as extracted in different time intervals. The effective Arrhenius barriers at very early times are close

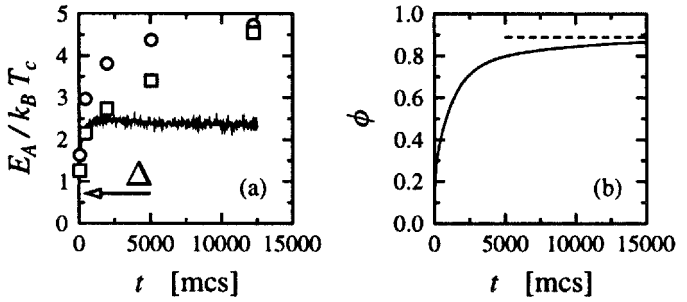


Figure 48. (a) Results for the effective Arrhenius barriers as extracted from the generalized correlation functions following a quench into the $p(2 \times 1)$ phase. Circles are data for tracer diffusion ($E_A^T$), squares for collective diffusion ($E_A^C$), and the full line for the jump rate ($E_A^\Gamma$). Equilibrium limits for tracer and collective diffusion are about $4.8 k_B$ T. The bare TDA barrier is denoted by an arrow. (b) Temporal behaviour of the order parameter for the $p(2 \times 1)$ phase after a quench to $T = 465$ K. The dashed line shows the equilibrium limit.

to the bare TDA barrier $\Delta$, after which they rapidly increase towards their equilibrium values. In the present case the attractive interactions dominate within the $p(2 \times 1)$ phase leading to larger barriers than within the disordered phase. The results are in good agreement with the experimental data of Tringides *et al.* [409, 377].

More recently, Vattulainen [408] has also studied the origin of the nonequilibrium barriers using the decomposition of equations (36) for tracer and collective diffusion under nonequilibrium conditions. He has concluded that the contribution from the (nonequilibrium) jump rate $\Gamma(T, t)$ to the barriers is relatively small, and for tracer diffusion the deviation from equilibrium comes mostly from dynamical correlation effects, while for collective diffusion it is due to the thermodynamic factor.

4.7.2. *Nonequilibrium diffusion during profile spreading*

The lattice-gas model of O/W(110) has also been used to study the temporal evolution of density profiles, and the collective diffusion coefficient as extracted from the Boltzmann–Matano (BM) analysis of section 2.3. [152, 153]. The studies were carried out again using MC dynamics with the TDA algorithm. The initial state of the system was prepared to mimic typical BM experiments. The spreading coverage profile $\theta(x, t)$ is defined for a semi-infinite system which ranges from $-\infty$ to $+\infty$ in the $x$ direction, and whose width is $L_y = 30 - 1000$ in the $y$ direction with periodic boundary conditions. The initial profile at $t = 0$ is a step function at $x = 0$, and the profile then evolves in the $x$ direction. The temperature was chosen to be $T = 590$ K.

First, Nikunen *et al.* [152] studied the evolution of coverage profiles throughout the whole range of coverages starting from $\theta(x, t = 0) = 1$ for $x < 0$. A series of scaled density profiles $\theta(x/\sqrt{t})$ are shown in figure 49. As can be further seen in figure 50, the effective $D_c$ as extracted using the BM analysis shows marked time dependence and has not reached the equilibrium linear response regime even in the

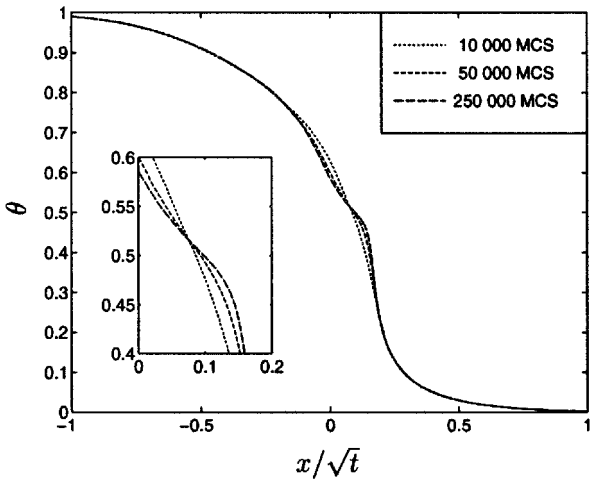


Figure 49. Scaled coverage profiles at three different times during the profile evolution process. In the data, several profiles from the time regimes 10000–12000 MCS, 50000–60000 MCS, and 250000–300000 MCS have been collapse to obtain the scaled profiles. The inset shows the details of the profiles within the $p(2 \times 1)$ phase.

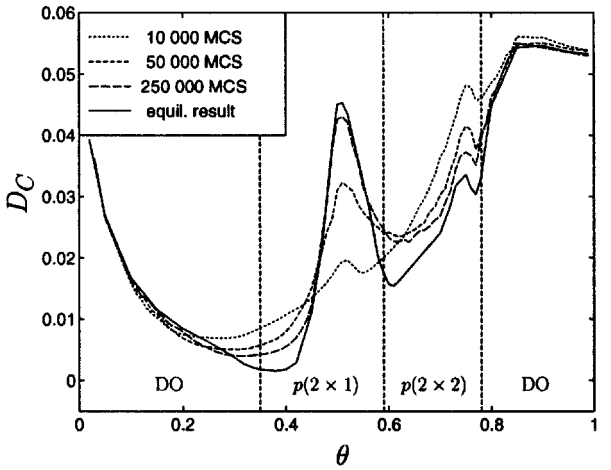


Figure 50. Coverage dependence of the effective $D_c$'s as extracted from BM analysis corresponding to the profiles shown in figure 49. The true equilibrium result is also shown for comparison. The dashed lines indicate the locations of the phase boundaries in the model of O/W(110).

longest times studied. There are particularly large deviations near phase boundaries and within the ordered phases. Nikunen *et al.* used the decomposition of equations (36) for $D_c$ to deduce that the deviations from equilibrium are mainly due to the non-equilibrium effects in the particle number fluctuations, in accordance with the domain growth case discussed in the previous section.

Most recently, Nikunen *et al.* [153] also studied the influence of the initial conditions on the nonequilibrium effects during profile spreading. They considered the so-called partial spreading case where the initial coverage $\theta(x, t = 0) = 1/2$ for $x < 0$ instead of unity. As expected, the nonequilibrium effects in both the scaled density profiles and $D_c$'s extracted from them are considerably weaker than those from the full spreading case. They also found that these effects did not depend much on the initial degree of order within the overlayer at $x < 0$. However, there was a difference in the degree of nonequilibrium effects when spreading was considered either along or perpendicular to the atomic rows, starting from a perfectly ordered $p(2 \times 1)$ phase. The difference between the full and partial spreading cases can also be illustrated by considering the response function

$$\Psi(T, \theta, t) \equiv \left| \frac{\partial \phi_c(T, \theta, t)}{\partial \theta} \right|_T, \tag{140}$$

where $\phi_c(T, \theta, t)$ is the (non-equilibrium) local order parameter. The maxima of $\Psi(\theta)$ can be used to characterize the location of the phase boundaries in the system. In figure 51 we show typical results for $\Psi$ for the case of full and partial spreading. The phase boundaries as approximated by maxima in $\Psi$ are much closer to the equilibrium limit for the case of partial spreading, as expected from the BM results.

### 4.8. *Quantum diffusion*

We have been focusing in this review mainly on the thermally activated diffusive behaviour of adatoms on surfaces. However, for light adatoms such as Hydrogen

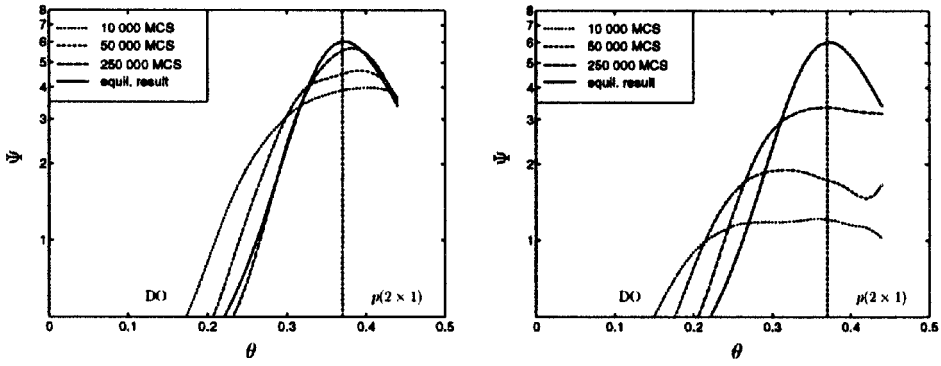


Figure 51. Results for the response function $\Psi$ for $0 \leq \theta \leq 1/2$ at $T = 590\,\mathrm{K}$ corresponding to (a) partial spreading from $\theta(x, t = 0) = 1/2$ $(x < 0)$, and (b) full spreading. Dashed lines show the phase boundary as determined from the maximum of $\Psi$ in equilibrium.

and its isotopes, the dominant mechanism for transport to neighboring sites at low temperatures is through tunnelling rather than thermal activation over the barrier. The crossover point can be estimated by equating the tunnelling probability to the thermal activation factor $\exp(-E_A/k_BT)$. For a simple 1D cosine potential with a barrier of 160 meV, this yields a crossover temperature of 60 K from a simple WKB estimate of the tunnelling probability. This transition from a classical to quantum mechanical dynamics is therefore easily within the experimentally observable range with most of the standard techniques outlined in section 1.2.

Experimentally, the first measurements of diffusion of hydrogen atoms on metal surfaces were made by field emission microscopy (FEM) [410, 411]. Clear transitions from activated diffusion to approximately temperature independent diffusion were observed for Ni and W surfaces and attributed to the onset of quantum tunnelling at low temperatures. Other experimental techniques were subsequently applied to study the diffusion of hydrogen adatoms, including QHAS, STM and various optical techniques [412–415]. However, at present there does not seem to be a universal pattern for the details of crossover from the classical activated diffusion behaviour to the quantum tunnelling regime. In the FEM study for Ni and W substrate surfaces [410, 411, 416] and in the latest STM study for H/Cu(001) [413], a sharp crossover from classical diffusion to very weak temperature dependence was observed at a crossover temperature in the range of 60–100 K. The data for H/Cu(001) from [413] are shown in figure 52. However, the QHAS study for H/Pt(111) [412] yields no crossover down to $T \sim 100$ K as shown in figure 53. For the system H/Ni(111), recent optical studies [414] showed a crossover behaviour from the classical regime to a second activated regime with a much lower activation energy below $T \approx 100$ K as shown in figure 54. This is in direct contradiction with the FEM data on the same system [411] (see figure 55) which showed a crossover to a temperature independent diffusion at low temperatures. Thus, it is fair to say that while there are strong indications that quantum tunnelling is active at low temperatures, the detailed mechanism of quantum diffusion for hydrogen adatoms is not yet understood.

Theoretically, there have been a number of studies addressing this problem [417–420, 35, 421–423]. One popular approach is through the quantum transition state theory (QTST) [417, 418]. This is a generalization of the classical TST by replacing

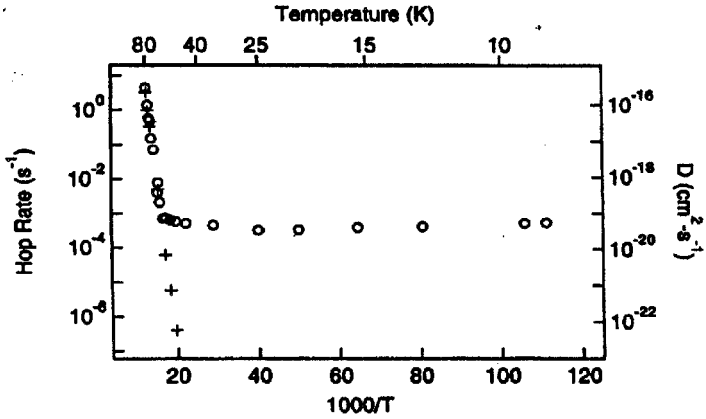


Figure 52. Arrhenius plot of the hopping rate of H (circles) and D (+) from [413]. The right axis gives the equivalent diffusion coefficient D related to the hopping rate $\Gamma$ by $D = \frac{1}{4}a^2\Gamma$, where $a$ is the lattice constant.

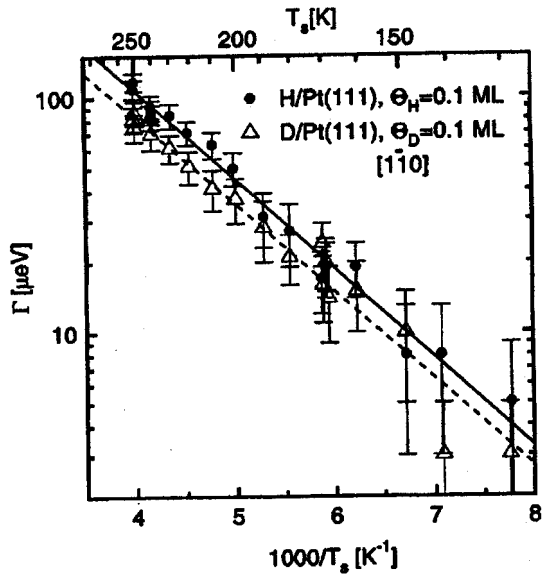


Figure 53. Arrhenius plot of the temperature dependence of the quasielastic peak width $\Delta\omega$ at $\Delta\mathbf{K} = -0.44\,\bar{1}$ near the zone centre. From Graham *et al.* [412].

the probability density in the classical theory with the probability distribution of the centroid:

$$P(x) = Q^{-1} \int \mathcal{D}[x(\tau)]\delta(x - \bar{x}) \exp\left\{-\frac{1}{\hbar} S[x(\tau)]\right\}, \tag{141}$$

with the centroid $\bar{x}$ defined as

$$\bar{x} = \frac{1}{\beta\hbar} \int_0^{\beta\hbar} x(\tau)\, \mathrm{d}\tau. \tag{142}$$

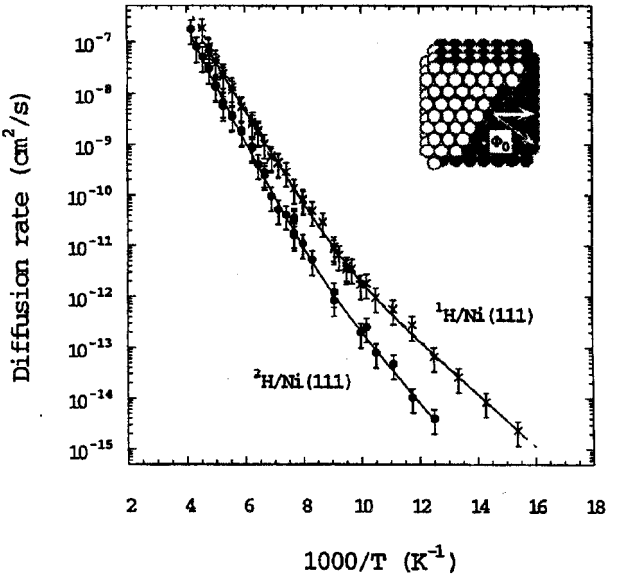


Figure 54. Arrhenius plot of the diffusion rate for hydrogen (crosses) and deuterium (solid circles) at coverage $\theta = 0.3$ from Cao *et al.* [414]). The solid lines represent the fit using the sum of two activated Arrhenius terms. The inset shows the orientation of the sample and the arrow points along the direction that the diffusion rates are measured.

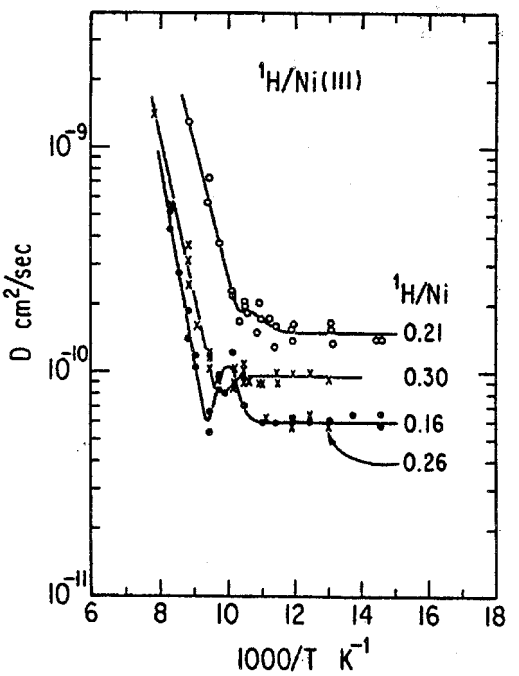


Figure 55. Log $D_c$ versus $\frac{1}{T}$ for H on Ni(111) for a number of coverages from the FEM study of Lin and Gomer [411].

The thermal transition rate is then given by

$$k = \tfrac{1}{2}\bar{\nu}P(x^*), \tag{143}$$

where $x^*$ is the co-ordinate of the transition state and $\bar{\nu}$ is a (weakly) temperature dependent factor. At high temperatures, the cyclic paths $x(\tau)$ contract to points and the centroid coincides with the position of the classical co-ordinate. At low temperatures, the dominant contribution to $P(x)$ comes from paths which are located at two stable minima simultaneously, so-called instantons. When applied to H/Ni(100), the QTST study yielded a sharp crossover from classical activation behaviour to a weakly temperature independent regime in qualitative agreement with the experimental observations [421, 422]. However, the theoretical value of the crossover temperature of 60 K is low compared to the experimental value of 100 K. Moreover, the theoretical value for the diffusion coefficient at low temperatures is about three orders of magnitude smaller than the observed value. Also, the tunnelling rate for deuterium is a further five orders of magnitude down from hydrogen, in strong disagreement with the observed anomalous isotope effect that the diffusion coefficient for hydrogen and deuterium at low temperatures is of the same order of magnitude [411]. Part of this discrepancy could be due to the fact that the QTST essentially yields the WKB expression for the tunnelling probability at low temperatures, which could be quantitatively inaccurate for the parameters of the H/Ni(100) in which the zero point energy is a large fraction of the total barrier.

We should point out that, typically in the theoretical studies, only the phonon frictional coupling is included. In addition to the non-adiabatic friction contribution, the coupling to phonons could lead to an activated behaviour even in the tunnelling regime, with an activation energy equal to the so-called small polaron activation energy. Physically, this is due to the fact that the lattice relaxes and lower its energy when the hydrogen adatom is at a minimum site. Thus, for tunnelling to occur, the system must first go into an excited states where only the symmetric phonons contributing to the relaxation are present whereas the asymmetric modes are absent. This implies that the small polaron activation energy is a fraction of the relaxation energy which is typically a few meV for H on metal surfaces [421, 422, 413]. For adsorption on metal surfaces, the electronic friction is also present and it could lead to a weak temperature dependence at low temperatures that behaves as $T^{2K-1}$, where $K$ is a constant [424]. These effects are actually observed in a recent STM study of the H/Cu(001) system [413]. In this system, the data indicate a crossover from a classical thermal activated regime to a quantum tunnelling regime with a small activation energy of $\approx 3$ meV that was attributed to be the small polaron activation behaviour. For temperatures below 25 K, the observed weak temperature dependence was attributed to the electronic friction which obeys the $T^{2K-1}$ power law with $K = 0.25 \pm 0.05$.

The quantum diffusion problem has also been studied with the Mori PO formalism [126]. Just like the classical case as described in section 3.3., a matrix continued fraction expansion can be developed for the velocity self-correlation function. The only difference is that in the quantum case the equilibrium correlation functions occurring in the expansion have to be evaluated fully quantum mechanically, taking into account the non-commutability of the position and momentum variables. This was accomplished by a path integral formalism. In a study applying this formalism to H/Ni(100) [35], it was found that there is a sharp crossover from the classical thermal activated behaviour to a temperature independent low

temperature tunnelling regime at $T \approx 100\,\mathrm{K}$, in good agreement with the experimental data. The difference of this study from the QTST approach is that in the implicit evaluation of the tunnelling probability, the WKB approximation is avoided and also the broadening of the levels due to frictional coupling with the substrate is included. However, this study was performed in the high friction limit with a friction parameter $\eta$ as an adjustable parameter. While the high friction limit may not properly correspond to the real H/Ni(001) system, it is expected to give the right order of magnitude for $D_t$, and correct qualitative behaviour. Indeed, when the polaron mass of the hydrogen atom is taken into account, the value of the dimensionless friction parameter $\eta/\omega$ needed to fit the experimental value of $D_t \approx 10^{-12}\ \mathrm{cm}^2/sec$ is of order of unity which is reasonable.

Recently, yet another approach known as the Monte Carlo Wave Function (MCWF) method [425, 426] has been applied to the problem of quantum diffusion. In the MCWF approach, the evolution of a quantum state $|\Psi(t)\rangle$ is described by a stochastic wave equation, in which the adiabatic Hamiltonian $\mathcal{H}_S$ is only a part of the evolution operator:

$$|\Psi(t+\delta t)\rangle = \frac{f_0}{\sqrt{1-\delta p}} \exp\left(\frac{-i\mathcal{H}\delta t}{\hbar}\right)|\Psi(t)\rangle + \sum_{\mu} \frac{f_\mu}{\sqrt{\delta p_\mu/\delta t}} C_\mu |\Psi(t)\rangle. \tag{144}$$

Here the effect of each operator $C_\mu$ acting on the quantum system represents a collision with the reservoir degrees of freedom that takes the system from one quantum state to another. The new Hamiltonian $\mathcal{H}$ is non-Hermitian, built from the original adiabatic Hamiltonian $\mathcal{H}_S$ with an imaginary part added to account for dissipation:

$$\mathcal{H} = \mathcal{H}_S - \frac{i\hbar}{2} \sum_{\mu} C_\mu^+ C_\mu. \tag{145}$$

The stochastic nature of quantum evolution here is described by the quantities $f_0$ and $f_\mu$. They are random numbers such that the mean value of $f_\mu$ is related to the scattering probabilities

$$\delta p_\mu = \delta t \langle \Psi(t)|C_\mu^\dagger C_\mu|\Psi(t)\rangle, \tag{146}$$

with $\langle f_\mu \rangle = \delta p_\mu$, and $\langle f_0 \rangle = 1 - \delta p$, with $\delta p = \sum p_\mu$ giving the probability for coherent propagation under $\mathcal{H}$. With this choice of dynamics, it can be shown [425, 426] that the quantity $\bar{\sigma}(t)$ obtained by averaging $\sigma(t) = |\Psi(t)\rangle\langle\Psi(t)|$ over all possible outcomes at time $t$ of the MCWF evolution equation, coincides with the density matrix $\rho_S(t)$ obtained from the solution of the so-called Linblad form of the master equation [427] at *all* times $t$, provided that they coincide at $t = 0$. The particular form of the collision operators chosen in equation (144) is the most general one that preserves the normalization and positive definiteness of the corresponding $\rho_S(t)$. The MCWF method allows direct analysis of trajectories in real space and time. It also allows to examine the effect of individual scattering events to the dynamics of the wave packet. In this sense the difference between the MCWF and density matrix approaches is similar to that between the Langevin and

Fokker–Planck equation descriptions of stochastic classical motion (see the discussions in section 3.3).

Badescu *et al.* [36] have recently applied the MCWF formalism to study quantum diffusion for the system H/Ni(111). An empirical potential was adjusted to yield the correct classical activation barrier of $\approx 200$ meV and the observed parallel vibrational mode of $\approx 96$ meV. The result for the diffusion coefficient in the low temperature regime ($T \leq 120$ K) is shown in figure 56. There is clear activated behaviour $D_t \propto \exp[-E_A/(k_B T)]$, with an activation energy $E_A = 98.1 \pm 0.5$ meV. This is in excellent agreement with the experimental data of Cao *et al.* [414] shown in figure 56 as well. The absolute value depends on the parameter $\tilde{\eta}$ which is the collision rate of the H atom with the background normalized by the bandwidth of the first excited vibrational band. Previously, this low temperature activated regime has been attributed to small polaron activated behaviour as opposed to the classical thermal activation of $\approx 200$ meV in the high temperature regime. However, this explanation is rather implausible since all theoretical calculations for the relaxation energy (an upper bound for the polaron activation energy) for hydrogen on metal surfaces have yielded a value of only a few meV [421, 422], which is also confirmed by experimental observations for H/Cu(001) [413]. Instead, the MCWF study has shown that the more plausible mechanism for this low temperature activation barrier comes from the fact that the lowest lying vibrational ground states are extremely localized and correspond to bands of negligible bandwidth ($\approx 10^{-6}$ meV). The actual diffusion mechanism occurs through thermal excitation to the first vibrational excited states which are more delocalized and then tunnelling to the neighbouring sites. This is why the activation energy for the diffusion coefficient at low temperatures tracks almost exactly the vibrational excitation energy. In this regard, we also note that recent vibrational spectroscopy measurements [428, 429] for this system show evidence of delocalization of the hydrogen atoms through the doublet splitting of the higher vibrational states, in agreement with the observation with the diffusion study.

As mentioned above, one major advantage of the MCWF formalism is the ability to visualize the trajectories directly in real space. A typical trajectory from reference

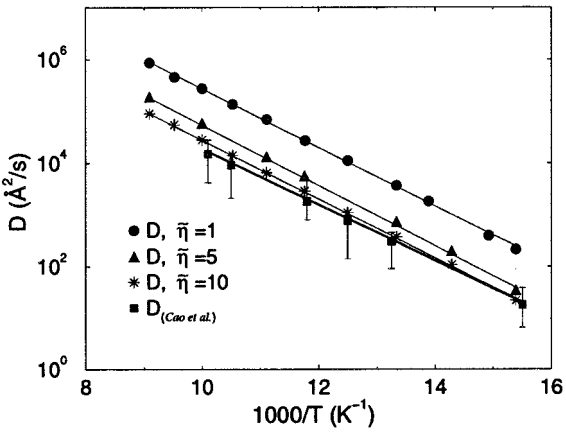


Figure 56. Temperature dependence of $D_t$ between 80 K and 140 K, for values of normalized collision rate $\tilde{\eta} = 1$, 5, 10 from Badescu *et al.* [36]. The Arrhenius dependence is evident. The experimental data of Cao *et al.* [414] are shown for comparison.

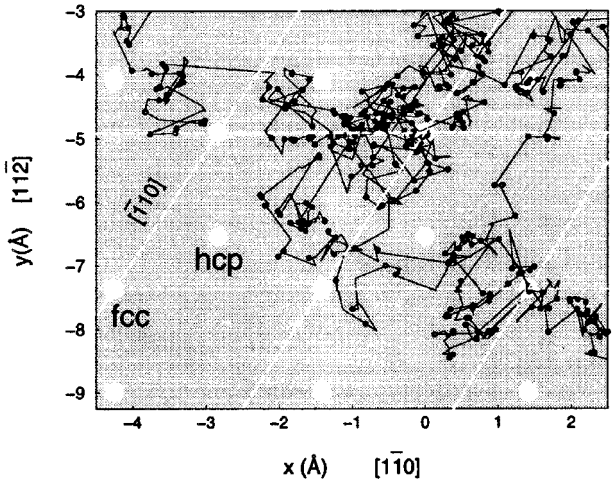


Figure 57. Portion of a trajectory for the quantum stochastic motion of hydrogen adatom on Pt(111) at $T = 70\,\mathrm{K}$, for $\tilde{\eta} = 1$ from reference [36]. The black filled circles are points of interband transitions. During an excitation and a subsequent deexcitation, a particle suffers several intraband collisions, represented by the broken lines between the black circles. The large white circles are the fcc and hcp adsorption sites.

[36] is shown in figure 57. The other point to note is that there are sections of the trajectory where the wave packet tunnels coherently through several sites before its motion becomes randomized through de-excitation to the lower band. This can be quantified by studying the tunnelling length distribution $P_\ell$ which is displayed in figure 58 for the values $\tilde{\eta} = 0.1, 0.4, 1$ and 4. We define the tunnelling length $\ell$ as the distance travelled by a wave packet in the upper band before it suffers a collision. As can be seen in figure 58, $P_\ell$ decreases exponentially with $\ell$. At small collision rates,

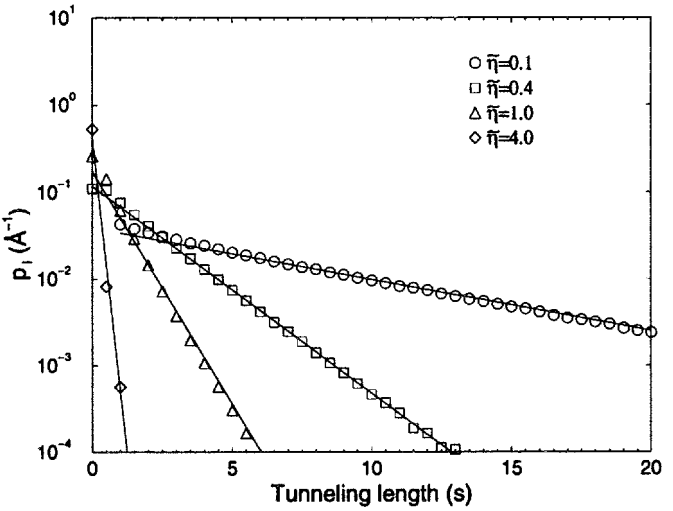


Figure 58. Histograms of tunnelling lengths $\ell$ for different values of $\tilde{\eta} \in \{0.1, 0.4, 1, 4\}$ from reference [36]. $T = 90\,\mathrm{K}$, and the unit of length is the nearest neighbour distance $s$. Points on the plot at $\ell = ns$ represent the fraction of jumps with lengths between $\ell = (n \pm \frac{1}{2})s$.

long coherent tunnelling processes are much more likely. This is analogous to the long jumps in the small friction limit as discussed in sections 2.1 and 3.3.

All the theoretical results point to the fact that the details of the crossover from the classical activation regime to the quantum diffusion regime depend sensitively on the shape of the potential and not just on gross features such as the barrier height for tunnelling. Thus, it is probably not too surprising that very different temperature dependence and crossover behaviour have been observed for different systems. Future progress in this area would require good first principle or semi-empirical adsorption potentials as the input for any theoretical analysis of quantum diffusion.

### 4.9. *Island diffusion on metal surfaces*

The modern methods for manufacturing thin films and surface nanostructures have in recent years acquired such precision that atomic-level control of the surface structures is beginning to come within reach. Surface growth is a process where many microscopic processes operate at a same time affecting the properties of the growing film [3, 11]. In the present review, we have already discussed extensively many issues associated with the diffusion of simple adparticles (adatoms and molecules). As already seen in section 4.2 in the case of chains on missing-row fcc(110) surfaces, the motion of single adatoms also leads to the movement of 2D clusters on the surface, known as island diffusion [430–432]. This process affects the surface growth process, and its role in determining the island size distribution already in the early stages of submonolayer growth has been demonstrated [433–436, 3, 437–439]. Even 3D clusters can diffuse fast on surfaces, as it has been experimentally observed for gold and antimony clusters on graphite [440], and explained in terms of the mismatch between the adatoms on the cluster bottom and the graphite substrate [441, 442]. We will in the following concentrate on 2D adatom island diffusion on metal surfaces.

#### 4.9.1. *Diffusion of large islands*

In the limit of large island sizes with the number of atoms in the island $N \gg 1$, the theoretical arguments of Khare *et al.* [114, 115] explain island diffusion in terms of the shape fluctuations of the outer boundary. This makes it possible to relate the macroscopic motion of islands to the atomistic processes occurring on the boundary. The three basic mechanisms considered are periphery diffusion (PD), terrace diffusion (TD) where a particle can detach from and attach to the edge, and evaporation-condensatio n (EC) events. These processes lead to a general dependence of the (tracer) diffusion coefficient of the centre of mass of the island on its size as

$$D \propto e^{-\beta E_s} N^{-\alpha}, \tag{147}$$

where $E_s$ is an effective Arrhenius barrier, and $\alpha$ is a scaling exponent. The island diffusion coefficient $D$ is related to $D_{CM}$, as defined in section 2.2, by $D = D_{CM}/N$. For 2D islands, a general expression for $\alpha$ is given by

$$2\alpha = 2 + \frac{1}{1 + (R/R_{st})(R_{su}/R_{st})} - \frac{2 + (R/R_{st})(R_{su}/R_{st})}{1 + (R/R_{st})(R_{su}/R_{st}) + (R/R_{st})^2}, \tag{148}$$

where $R = \sqrt{s/\pi}$. The parameters $R_{st}$ and $R_{su}$ are related to periphery and terrace diffusion coefficients, respectively. Allowing only one of the mass transport mechanisms EC, TD or PD at a time for large enough islands, the exponents 1/2, 1, 3/2 are obtained, respectively (see figure 3 in reference [115]). We note that the case of 1D islands such as the chains on missing row fcc(110) surfaces (see section 4.2) is quite different. There, the leapfrog mechanism [118] (which can be thought as a peculiar kind of periphery diffusion) induces a $N$-independent mobility for a wide range of chain lengths (up to $N \simeq 20$ in typical experimental conditions [279]); asymptotically, the exponent $\alpha$ is equal to 1, provided that multiple promotions above the chain are negligible [279]. On the other hand, TD is completely inefficient in displacing 1D chains already for tetramers [279].

When both the TD and the PD mechanisms are present, clear dependence of $\alpha$ on $N$ should be observed, and finally one should always find $\alpha = 1$ for $N \rightleftarrows \infty$. Simulation studies tailored to correspond exactly to one of the possible processes and based on idealized energetics have indeed yielded one of the exponents $\alpha = 1/2, 1$ and $3/2$ depending on the process included [430–432, 115].

The existence of a scaling law of the type in equation (147) was predicted already prior to the treatment of Khare *et al.* After the first computer simulations [430–432], several studies have been conducted on models of fcc(111) [443–446] and fcc(100) [112, 119, 447–449] metal surfaces. Experiments on island diffusion have been carried out on (111) [450, 451] and (100) [113, 116] metal surfaces. A scaling law for the diffusion coefficient with a scaling exponent $\alpha$ in accordance with equation (147) has been reported in several simulation studies [443, 445, 446, 448, 452, 119, 449]. However, there has been controversy regarding the value of $\alpha$ and its relation to the microscopic diffusion mechanisms. In particular, the STM experiments of Pai *et al.* [116] showed that the diffusion of Cu islands on Cu(100) and Ag islands on Ag(100) surfaces is characterized by exponents $\alpha \approx 1.25$ and $\alpha \approx 1.14$, respectively, at room temperature. The range of island sizes in their experiments varied from about 80 to 800. They attributed these results to the interplay between atoms and kinks at the island periphery. Heinonen *et al.* [119] have shown using MC simulations and energetics based on EMT that for fcc(001) metals (Ag, Cu, Ni) the scaling exponent for large islands in the size region $N > 10^2$ is different from that for smaller islands (see figure 59). They found a crossover from the PD to the TD mechanism in the limit of large islands, with the effective $\alpha$ changing towards the TD value of unity. In their model, the TD mechanism was due to the rapid diffusion of *vacancies* within the island. The value of $\alpha$ at room temperature was very close to the experimental results of Pai *et al.* [116] for the same island sizes.

Some other simulations of island diffusion on metallic fcc surfaces have given values $1.75 < \alpha < 2.1$ in the size range $N \approx 100$ [112, 444, 445]. On the other hand, in simulations where attachment/detachment is dominant, scaling exponent attains values close to $\alpha = 1/2$, as expected for the EC process [448]. The deviations of the simulation results from the predictions of the idealized theories have been explained in terms of the dimensional arguments very similar already used in the earliest studies. The density of kinks and the number of adatoms on the boundary have been used in many phenomenological models devised to explain the simulation results [443, 445–447]. Also more exotic boundary processes have been suggested to influence the value of $\alpha$ [448]. However, at least for fcc(001) metals, at least some of the results reported in the simulations can be more naturally explained by the crossover effect suggested by Heinonen *et al.* [119].

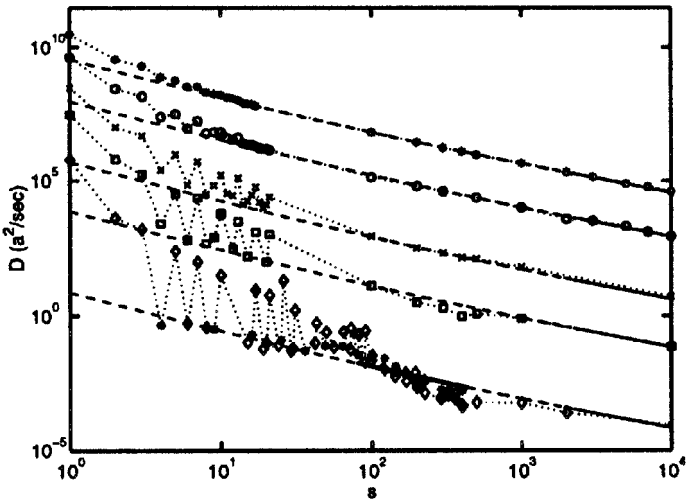


Figure 59. Monte Carlo results for the adatom island diffusion coefficient $D$ for island sizes $s \equiv N$ in the range $1 - 10^4$, at $T = 1000$, 700, 400 and 300 K (from top to bottom). The figure is taken from reference [119]. For $T = 300$ K, the island with size $s = n^2$, with $n$ integer, are indicated by stars. The dotted lines are just guides to the eye. The dashed lines indicate fits to equation (36) of reference [115]. Error bars are of the size of the symbols or less except for the case of 300 K for $s \gtrsim 300$, where the scatter in the data indicates the errors. The thick line at 300 K shows the experimental results of reference [116] for Cu. At large sizes, the asymptotic exponent $\alpha = 1$ is reached ($D$ scales as $s^{-1}$), while at intermediate sizes effective exponents in the range $1 \leq \alpha \leq 3/2$ are obtained.

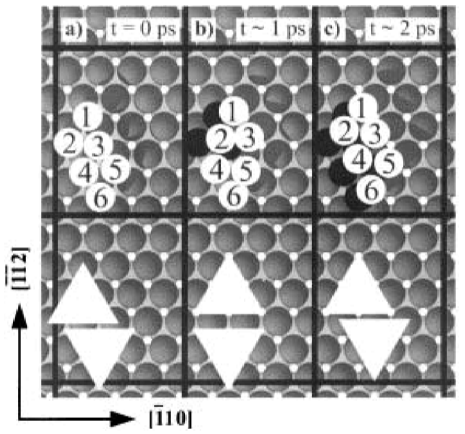


Figure 60. Sequence of frames from a Molecular Dynamics simulation showing diffusion via reptation of 2D platinum hexamers on Pt(111). The figure is reprinted from reference [455], with permission from Elsevier Science. Top panels: locations of $Pt_6$ atoms (white) on the substrate at the times shown. Initial adatom positions are in black. Lower panels: schematic illustration (triangles) of subcluster units (trimers) undergoing reptational glide motion. (a) $t = 0$, homogeneous fcc hexamer in a minimum-energy configuration, oriented along [01]. (b) $t \simeq 1$ ps, the hexamer becomes a mixed fcc/hcp cluster due to the gliding of the top trimer (triangle) into adjacent hcp sites. (c) $T \simeq 2$ ps, the double-shear diffusion event is completed via the gliding of the lower trimer (triangle) into hcp sites.

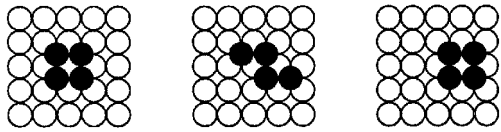

Figure 61. Schematic representation of the dimer shearing diffusion mechanism for a tetramer on a fcc(001) surface [464]. At first, half of the tetramer is displaced into the intermediate metastable configuration of the middle panel, and then the second half follows.

4.9.2. *Diffusion of small islands*

As discussed in section 4.2, single adatom motion leads naturally to the diffusion of smaller islands. On fcc(111) surfaces, additional *collective* diffusion mechanisms have been proposed, such as gliding [463, 454], and dislocation motion [454]. Also, snake-like 'reptation' of small islands has been suggested based on MD simulations [455]. However, experimental evidence for such processes is mostly lacking at present [456]. What is clearly seen in experiments is the nonmonotonic size-dependence of adatom cluster diffusion [457, 458]. For fcc(111) surfaces, it has been shown by EAM calculations [459, 460] and first-principles energetics [461] that this is due to concerted atomic diffusion mechanisms. For the fcc(001) case, such oscillations persist to relatively large island sizes at low temperatures [119, 462, 463]. Qualitatively, the oscillations can be explained by single-atom energetics, but recently it has been discovered that concerted many-body mechanisms play an important role for island sizes up to about $N = 20$ [174, 464]. Such mechanisms include *dimer shearing* [464] and *trimer shearing* within and on the periphery of the islands which constitute the rate-limiting steps for diffusion of many small islands.

## 5. Conclusions and outlook

In this article, we have presented a discussion of the various aspects of single particle and collective diffusion processes on solid surfaces. In view of the existing recent review articles focusing on the experimental situation of this subject, we have decided to concentrate on the theoretical issues. However, the nature of this field is such that theoretical advances go hand in hand with the experimental measurements. Thus, it is not productive to discuss the theoretical concepts without making direct contact with the experimental data and using real systems to illustrate the relevance of the theoretical approaches and concepts. Thus, theoretical discussions in this article are invariably accompanied by presentations of the relevant experimental data.

While we have witnessed an explosion of measurements of surface diffusion coefficients for a large number of systems, some of the central concepts such as memory effects and dependence of the prefactor on microscopic parameters have not received sufficient attention, and are sometimes even misunderstood or misinterpreted in the literature. It is for this purpose that we have here started the discussion of specific issues with chapters introducing the basic concepts, before discussing the more involved theoretical approaches to study surface diffusion. Particular care has been devoted to distinguish the jump rates, which deal with motion on microscopic length and time scales, from the diffusion coefficients which are only properly defined in the 'hydrodynamic' limit of long length and time scales. It is also pointed out here

that care must be taken to ensure that one is in the linear response regime to be able to characterize the mobility of the surface adatoms by the collective or the tracer diffusion coefficients. These aspects are particularly relevant for STM measurements where most of the attention has been focused on the microscopic jump rates. Recent advances in STM techniques have showed that real time and real space snapshots are also possible [465], and in this case a detailed experimental study of the relation between microscopic and macroscopic motion would be extremely interesting.

For what concerns the theoretical approaches, we have avoided going into technical details, but have tried to give an overview of the most commonly used modern approaches. With the advances in first principles computation techniques, they have been increasingly applied to the study of surface diffusion. Within the harmonic TST theory, both the adiabatic barrier and the prefactor have been determined for a number of systems [12]. It seems that for systems such as metal on metal substrates, this is an excellent approximation. However, the TST probably does not work as well at a quantitative level for other systems. From the theoretical point of view, the most interesting aspect of the physics that determines the diffusion coefficients lies in the nonadiabatic coupling of the adatoms with the substrate excitations, as well as with each other at finite coverages. This nonadiabatic coupling gives rise to fluctuation and damping which ultimately determines the value of the prefactor. In fact, in the case where the time scales of the motion of the adatom and the substrate are comparable, it has been demonstrated that the damping depends on the history of the adatom motion, i.e., memory effects are important. In this case, not only is the prefactor dependent on the nonadiabatic coupling, but even the diffusion barrier differs from the adiabatic value [218]. For the collective diffusion case, the situation is even more complicated as one has to average over all the system configurations even just for the diffusion barrier. At present, the main theoretical approaches beyond the TST rely on using numerical simulation methods either through the MD or MC approaches. Finally, some of the qualitative issues such as long jumps and validity of TST can be understood through the Langevin equation approach, which separates the coupling of the adatom with the substrate naturally into an adiabatic potential and nonadiabatic fluctuation and damping terms.

The final section in this article deals with the specific applications of the various theoretical approaches to different systems and comparison with experimental data when available. Our aim has not been to present an exhaustive study of the different systems, but rather to understand many of the issues that are common to the study of surface diffusion in various systems. Example of these are the effects of steps and impurities in the measurement of surface diffusion coefficients, memory effects and how they manifest themselves in measured quantities, dominant mechanisms in cluster diffusion and quantum diffusion etc. Obviously, we cannot hope to have covered all the topics and systems that are actively under investigation. Our choice of the subjects here has been biased by our own view as to the importance of the issues and by the limitations of our expertise. Many interesting topics such as electromigration [466–470], diffusion of adatoms and dimers on semiconductor surfaces [471–474, 176, 475, 202], diffusion of 3D clusters on solid and liquid surfaces [440–442, 476, 477], diffusion of adatoms on heterogeneous surfaces [478, 347, 479], stochastic resonance [60, 61, 63], and diffusion of polymers and colloids [405–407, 259, 108] have been left out because of space limitations. None the less, we hope that the issues covered here are of sufficient interest and illustrate how rich the field is and how much progress has been made in this field over the past few years. We feel that

at this stage, the challenges of the accurate determination of the diffusion coefficients for different systems both conceptually and experimentally have largely been met, although many systems remain to be investigated. The challenge of better understanding the underlying physics and the microscopic factors controlling the diffusion rates still remains. The continued refinement of the experimental techniques such as optical diffraction and QHAS methods in **k** space, and the STM method in real space is certain to yield more and more diffusion measurements with increasing accuracy for different adsorption systems. Together with the advance in the theoretical approaches, this means that the field should remain active and exciting for many years to come.

**Acknowledgements**

The authors wish to thank F. Baletto, F. Besenbacher, L. Y. Chen, Z. Chvoj, A.-P. Hynninen, E. Kuusela, I. T. Koponen, J. M. Lahtinen, T. Linderoth, J. Merikoski, F. Montalenti, P. Nikunen, T. S. Rahman, O. Trushin, I. Vattulainen, A. F. Voter, and X. Xiao, for their help in the realization of this review. This work has been in part supported by the Academy of Finland through its Centre of Excellence programme.

**References**

[1] Pimpinelli, A., and Villain, J., 1998, *Physics of Crystal Growth* (Cambridge University Press: Cambridge).
[2] Barabàsi, A.-L. and Stanley, H. E., 1995, *Fractal Concepts in Surface Growth* (Cambridge University Press: Cambridge).
[3] Jensen, P., 1999, *Rev. Mod. Phys.,* **71,** 1695.
[4] Ehrlich, G., and Hudda, F. G., 1966, *J. Chem. Phys.,* **44,** 1039.
[5] Kellogg, G. L., 1994, *Surf. Sci. Rep.,* **21,** 1.
[6] Ehrlich, G., 1991, *Surf. Sci.,* **246,** 1.
[7] Linderoth, T. R., Horch, S., Lægsgaard, E., Stensgaard, I., and Besenbacher, F., 1997, *Phys. Rev. Lett.,* **78,** 4978.
[8] Gomer, R., 1990, *Rep. Prog. Phys.,* **53,** 917.
[9] Naumovets, A. G., and Vedula, Yu. S., 1985, *Surf. Sci. Rep.,* **4,** 365.
[10] Seebauer, E. G., and Allen, C. E., 1995, *Prog. Surf. Sci.,* **49,** 265.
[11] Brune, H., 1998, *Surf. Sci. Rep.,* **31,** 121.
[12] Barth, J. V., 2000, *Surf. Sci. Rep.,* **40,** 75.
[13] Tsong, T. T., 2000, *Prog. Surf. Sci.*, **64,** 199.
[14] Giesen, M., 2001, *Prog. Surf. Sci.,* **68,** 1.
[15] Naumovets, A. G., and Zhang, Z., 2002, *Surf. Sci.,* **500,** to be published.
[16] H'anggi, P., Talkner P., and Borkovec, M., 1990, *Rev. Mod. Phys.,* **62,** 251.
[17] Tringides, M. C., and Gomer, R., 1992, *Surf. Sci.,* **265,** 283.
[18] Risken, H., 1989, *The Fokker–Planck Equation* (Berlin: Springer).
[19] Van Kampen, N. G., 1981, *Stochastic Processes in Physics and Chemistry* (Amsterdam: North-Holland).
[20] Ala-Nissila, T., and Ying, S. C., 1992, *Prog. Surf. Sci.,* **39,** 227.
[21] Allen, M. P., and Tildesley, D. J., 1987, *Computer Simulation of Liquids* (Oxford: Clarendon).
[22] Danani, A., Ferrando, R., Scalas, E., and Torri, M., 1997, *Int. J. Mod. Phys.* B, **11,** 2217.
[23] Conrad, E. H., Kiriukhin, A. and Tringides, M. C., 1998, *Phys. Rev. Lett.,* **81,** 3175.
[24] Ma, J., Xiao, X., Dinardo, N. J., and Loy, M. M. T., 1998, *Phys. Rev.* B, **538,** 4977.
[25] Chen, L. Y., and Ying, S. C., 1993, *Phys. Rev. Lett.,* **71,** 4361.

[26] Graham, A. P., Hofmann, F., Toennies, J. P., Chen, L. Y., and Ying, S. C., 1997, *Phys. Rev. Lett.,* **78,** 3900.
[27] Graham, A. P., Hofmann, F., Toennies, J. P., Chen, L. Y., and Ying, S. C., 1997, *Phys. Rev.* B, **56,** 10567.
[28] Barth, J. V., Brune, H., Fischer, B., Weckesser, J., and Kern, K., 2000, *Phys. Rev. Lett.,* **84,** 1732.
[29] Fichthorn, K. A., and Scheffler, M., 2000, *Phys. Rev. Lett.,* **84,** 5371.
[30] Bogicevic, A., Ovesson, S., Hyldgaard, P., Lundqvist, B. I., Brune H., and Jennison, D. R., 2000, *Phys. Rev. Lett.,* **85,** 1910.
[31] Arrhenius, S., 1889, *Z. Phys. Chem. (Leipzig),* **4,** 226.
[32] Van't Hoff, J. H., 1884, in *Etudes de Dynamiques Chimiques* (Amsterdam: F. Muller & Co.).
[33] Ala-Nissila, T., and Ying, S. C., 1990, *Phys. Rev. Lett.,* **65,** 879.
[34] Chen, L. Y., and Ying, S. C., 1994, *Phys. Rev.* B, **49,** 13838.
[35] Chen, L. Y., and Ying, S. C., 1994, *Phys. Rev. Lett.,* **73,** 700.
[36] Badescu, S. C., Ala-Nissila, T., and Ying, S. C., 2001, *Phys. Rev. Lett.,* **86,** 5092.
[37] Sanders, D. E., and Depristo, A. E., 1992, *Surf. Sci.,* **264,** L169.
[38] Cohen, J. M., 1994, *Surf. Sci.,* **306,** L545.
[39] Ferrando, R., and Tréglia, G., 1996, *Phys. Rev. Lett.,* **76,** 2109.
[40] Kallinteris, G. C., Evangelakis, G. A., and Papanicolaou, N. I., 1996, *Surf. Sci.,* **369,** 185.
[41] Kürpick, U., and Rahman, T. S., 1998, *Phys. Rev.* B, **57,** 2482.
[42] Chudley, C. T., and Elliott, R. J., 1961, *Proc. Phys. Soc. (London),* **77,** 353.
[43] Hughes, D., 1995, *Random Walks and Random Environments*, Vol. I (Oxford: University Press).
[44] Weiss, G. H., 1994, *Aspects and Applications of the Random Walk* (Amsterdam: North-Holland).
[45] Ferrando, R., Spadacini, R., Tommei, G. E., and Caratti, G., 1994, *Surf. Sci.,* **311,** 411.
[46] Mel'nikov, V. I., 1991, *Phys. Rep.,* **209,** 1.
[47] Ferrando, R., Spadacini, R., and Tommei, G. E., 1992, *Surf. Sci.,* **265,** 273.
[48] Ferrando, R., Spadacini, R., and Tommei, G. E., 1993, *Phys. Rev.* E, **48,** 2437.
[49] Georgievskii, Yu., and Pollak, E., 1994, *Phys. Rev.* E, **49,** 5098.
[50] Ferrando, R., Spadacini, R., and Tommei, G. E., 1995, *Phys. Rev.* E, **51,** 126.
[51] Beenakker, J. J. M., and Krylov, S. Yu., 1998, *Surf. Sci.,* **411,** L816.
[52] Ferrando, R., Montalenti, F., Spadacini, R., and Tommei, G. E., 2000, *Phys. Rev.* E, **61,** 6344.
[53] Chen, L. Y., Baldan, M. R., and Ying, S. C., 1996, *Phys. Rev.* B, **54,** 8856.
[54] Ferrando, R., and Tréglia, G., 1994, *Phys. Rev.* B, **50,** 12104.
[55] Caratti, G., Ferrando, R., Spadacini, R., and Tommei, G. E., 1996, *Phys. Rev.* E, **54,** 4708.
[56] Caratti, G., Ferrando, R., Spadacini, R., and Tommei, G. E., 1997, *Phys. Rev.* E, **55,** 4810.
[57] Caratti, G., Ferrando, R., Spadacini, R., and Tommei, G. E., 1998, *Chem. Phys.,* **234,** 157.
[58] Montalenti, F., and Ferrando, R., 1999, *Phys. Rev.* B, **59,** 5881.
[59] Hershkovitz, E., Talkner, P., Pollak, E., and Georgievskii, Yu., 1999, *Surf. Sci.,* **421,** 73.
[60] Kallunki, J., Dubé, M., and Ala-Nissila, T., 1999, *J. Phys. Cond. Mat.,* **11,** 9841.
[61] Kallunki, J., Dubé, M., and Ala-Nissila, T., 2000, *Surf. Sci.,* **460,** 39.
[62] Talkner, P., Hershkovitz, E., Pollak, and E., Hänggi, P., 1999, *Surf. Sci.,* **437,** 198.
[63] Borromeo, M., and Marchesoni, F., 2000, *Surf. Sci.,* **465,** L771.
[64] Voter, A. F., Doll, J. D., and Cohen, J. M., 1989, *J. Chem. Phys.,* **91,** 2045.
[65] Cohen, J. M., and Voter, A. F., 1989, *J. Chem. Phys.,* **91,** 5082.
[66] Dobbs, K. D., and Doren, D. J., 1992, *J. Chem. Phys.,* **97,** 3722.
[67] Ellis, J., and Toennies, J. P., 1993, *Surf. Sci.,* **317,** 99.
[68] Boisvert, G., and Lewis, L. J., 1996, *Phys. Rev.* B, **54,** 2880.

[69] Evangelakis, G. A., and Papanicolaou, N. I., 1996, *Surf. Sci.,* **347,** 376.
[70] Ferrando, R., 1996, *Phys. Rev. Lett.,* **82,** 4195.
[71] Jacobsen, J., Jacobsen, K. W., and Sethna, J. P., 1997, *Phys. Rev. Lett.,* **79,** 2843.
[72] Prévot, G., Cohen, C., Schmaus, D., and Pontikis, V., 2000, *Surf. Sci.,* **459,** 57.
[73] Lovisa, M., and Ehrlich, G., 1989, *J. Phys. (Paris) Colloq.,* **50,** C8-279.
[74] Senft, D. C., and Ehrlich, G., 1995, *Phys. Rev. Lett.,* **74,** 294.
[75] Ellis, J., and Toennies, J. P., 1993, *Phys. Rev. Lett.,* **70,** 2118.
[76] Frenken, J. W. M., Hinch, B. J., Toennies, J. P., and WOLL, CH., 1990, *Phys. Rev.* B, **41,** 938.
[77] Ferrando, R., Spadacini, R., and Tommei G. E., 1992, *Phys. Rev.* B, **45,** 444.
[78] Van Gastel, R., Somfai, E., Van Albada, S. B., Van Saarloos, W., and Frenken, J. W. M., 2001, *Phys. Rev. Lett.,* **86,** 1562.
[79] Bassett, D. W., and Webber, P. R., 1978, *Surf. Sci.,* **70,** 520.
[80] Halicioglu, T., and Pound, G. M., 1979, *Thin Solid Films,* **57,** 241.
[81] Hontinfinde, F., Ferrando, R., and Levi, A. C., 1996, *Surf. Sci.,* **366,** 306.
[82] Kellogg, G. L., 1991, *Phys. Rev. Lett.,* **67,** 216.
[83] Chen, C., and Tsong, T. T., 1991, *Phys. Rev. Lett.,* **66,** 1610.
[84] Stoltze, P., 1994, *J. Phys. Cond. Mat.,* **6,** 9495.
[85] Hansen, L., Stoltze, P., Jacobsen, K. W., and Nørskov, J. K., 1991, *Phys. Rev.* B, **44,** 6523.
[86] Perkins, L. S., and Depristo, A. E., 1994, *Surf. Sci.,* **317,** L1152.
[87] Liu, C. L., Cohen, J. M., Adams, J. B., and Voter, A. F., 1991, *Surf. Sci.,* **253,** 334.
[88] Roelofs, L. D., Martin, J. I., and Sheth, R., 1991, *Surf. Sci.,* **250,** 17.
[89] Evangelakis, G. A., Kallinteris, G. C., and Papanicolaou, N. I., 1997, *Surf. Sci.,* **394,** 185.
[90] Stumpf, R., and Scheffler, M., 1993, *Phys. Rev. Lett.,* **72,** 254.
[91] Stumpf, R., and Scheffler, M., 1996, *Phys. Rev.* B, **53,** 4958.
[92] Delorenzi, G., and Jacucci, G., 1985, *Surf. Sci.,* **164,** 526.
[93] Feibelman, P. J., 1990, *Phys. Rev. Lett.,* **65,** 729.
[94] Kellogg, G. L., and Feibelman, P. J., 1990, *Phys. Rev. Lett.,* **64,** 3143.
[95] Chen, C. L., and Tsong, T. T., 1990, *Phys. Rev. Lett.,* **64,** 3147.
[96] Feibelman, P. J., 1999, *Surf. Sci.,* **423,** 169.
[97] Yu, B. D., and Scheffler, M., 1997, *Phys. Rev.* B, **56,** 15569.
[98] Feibelman, P. J., and Stumpf, R., 1999, *Phys. Rev.* B, **59,** 5892.
[99] Black, J. E., and Tian, Z. J., 1993, *Phys. Rev. Lett.,* **71,** 2445.
[100] Merikoski, J., and Ala-Nissila, T., 1995, *Phys. Rev.* B, **52,** R8715.
[101] Merikoski, J., Vattulainen, I., Heinonen, J., and Ala-Nissila, T., 1997, *Surf. Sci.,* **387,** 167.
[102] Braun, O. M., Dauxois, P., and Peyrard, M., 1996, *Phys. Rev.* B, **54,** 313.
[103] Evangelakis, G. A., Papageorgiou, D. G., Kallinteris, G. C., Lekka, Ch. E., and Papanicolaou, N. I., 1998, *Vacuum,* **50,** 165.
[104] Papageorgiou, D. G., and Evangelakis, G. A., 2000, *Surf. Sci.,* **461,** L543.
[105] Hansen, J. P., and McDonald, I. R., 1976, *Theory of Simple Liquids* (New York: Academic Press).
[106] Forster, D., 1990, *Hydrodynamic Fluctuations, Broken Symmetry, and Correlation Functions* (Reading, MA: Addison-Wesley).
[107] Lovesey, S. W., 1986, *Theory of Neutron Scattering from Condensed Matter*, Vols I and II (Oxford: Oxford Science).
[108] Lahtinen, J. M., Hjelt, T., Ala-Nissila, T., and Chvoj, Z., 2001, *Phys. Rev.* E, **64,** 021204.
[109] Doi, M., and Edwards, S. F., 1986, *The Theory of Polymer Dynamics* (Oxford: Oxford University Press).
[110] Mazenko, G. F., 1983, in *Surface Mobilities on Solid Materials*, edited by V. T. Bihn (New York: Plenum).
[111] Zhdanov, V. P., 1991, *Elementary Physico-Chemical Processes on Solid Surfaces* (New York: Plenum).
[112] Voter, A. F., 1986, *Phys. Rev.* B, **34,** 6819.

[113] Wen, J.-M., Chang, S.-L., Burnett, J. W., Evans, J. W., and Thiel, P. A., 1994, *Phys. Rev. Lett.,* **73,** 2591.
[114] Khare, S. V., Bartelt, N. C., and Einstein, T. L., 1995, *Phys. Rev. Lett.,* **75,** 2148.
[115] Khare, S. V., and Einstein, T. L., 1996, *Phys. Rev.* B, **54,** 11752.
[116] Pai, W. W., Swan, A. K., Zhang, Z., and Wendelken, J. F., 1997, *Phys. Rev. Lett.,* **79,** 3210.
[117] Linderoth, T. R., Horch, S., Petersen, S., Helveg, S., Lægsgaard, E., Stensgaard, I., and Besenbacher, F., 1999, *Phys. Rev. Lett.,* **82,** 1494.
[118] Montalenti, F., and Ferrando R., 1999, *Phys. Rev. Lett.,* **82,** 1498.
[119] Heinonen, J., Koponen, I., Merikoski, J., and Ala-Nissila, T., 1999, *Phys. Rev. Lett.,* **82,** 2733.
[120] Ying, S. C., Vattulainen, I., Merikoski, J., Hjelt, T., and Ala-Nissila, T., 1998, *Phys. Rev.* B, **58,** 2170.
[121] Vattulainen, I., 1997, Studies of surface diffusion under equilibrium and non-equilibrium conditions. PhD thesis, Helsinki Institute of Physics, University of Helsinki, Helsinki, Finland.
[122] Vattulainen, I., Ying, S. C., Ala-Nissila, T., and Merikoski, J., 1999, *Phys. Rev.* B, **59,** 7697.
[123] Reed, D. A., and Ehrlich, G., 1981, *Surf. Sci.,* **102,** 588
[124] Ferrando, R., Scalas, E., and Torri, M., 1994, *Phys. Lett.* A, **186,** 415.
[125] Hjelt, T., Vattulainen, I., Merikoski, J., Ala-Nissila, T., and Ying, S. C., 1997, *Surf. Sci.,* **380,** L501.
[126] Mori, H., 1965, *Prog. Theor. Phys.,* **33,** 423.
[127] Fick, E., and Sauermann, G., 1990, *The Quantum Statistics of Dynamic Processes* (Berlin: Springer).
[128] Tahir-Kheli, R. A., and Elliott, R. J., 1983, *Phys. Rev.* B, **27,** 844.
[129] Tahir-Kheli, R. A., 1983, *Phys. Rev.* B, **27,** 6072.
[130] Ala-Nissila, T., Kjoll, J., Ying, S. C., and Tahir-Kheli, R. A., 1991, *Phys. Rev.* B, **44,** 2122.
[131] Bunde, A., and Dieterich, W., 1985, *Phys. Rev.* B, **31,** 6012.
[132] Torri, M., Ferrando, R., Scalas, E., and Brivio, G. P., 1994, *Surf. Sci.,* **307–309,** 565.
[133] Danani, A., Ferrando, R., Scalas, E., Torri, M., and Brivio, G. P., 1995, *Chem. Phys. Lett.,* **236,** 533.
[134] Chumak, A. A., and Tarasenko, A. A., 1996, *Surf. Sci.,* **364,** 424.
[135] Danani, A., Ferrando, R., Scalas, E., and Torri, M., 1998, *Surf. Sci.,* **409,** 117.
[136] Danani, A., Ferrando, R., Scalas, E., and Torri, M., 1998, *Surf. Sci.,* **402–404,** 281.
[137] Myshlyavtsev, A. V., and Zhdanov, V. P., 1993, *Surf. Sci.,* **291,** 145.
[138] Chvoj, Z., Chab, V., and Conrad, H., 1999, *Surf. Sci.,* **426,** 8.
[139] Chvoj, Z., Conrad, H., and Chab, V., 1999, *Surf. Sci.,* **442,** 455.
[140] Masin, M., Chvoj, Z., and Conrad, H., 2000, *Surf. Sci.,* **457,** 185.
[141] Masin, M., and Chvoj, Z., 2000, *Surf. Sci.,* **454–456,** 552.
[142] Masin, M., and Chvoj, Z., 2000, *Surf. Rev. Lett.,* **7,** 219.
[143] Tarasenko, A. A., Jastrabik, L., and Uebing, C., 1998, *Phys. Rev.* B, **57,** 10166.
[144] Tarasenko, A. A., Jastrabik, L., and Uebing, C., 1999, *Langmuir,* **15,** 5883.
[145] Tarasenko, A. A., Jastrabik, L., Nieto, F., and Uebing, C., 1999, *Phys. Rev.* B, **59,** 8252.
[146] Uebing, C., and Gomer, R., 1997, *Surf. Sci.,* **381,** 33.
[147] Vattulainen, I., 1998, *Surf. Sci.,* **412–413,** L911.
[148] Ferrando, R., and Scalas, E., 1993, *Surf. Sci.,* **281,** 178.
[149] Spohn, H., 1991, *Large Scale Dynamics of Interacting Particles* (Berlin: Springer).
[150] Vlachos, D. G., and Katsoulakis, M. A., 2000, *Phys. Rev. Lett.,* **85,** 3898.
[151] Chvoj, Z., 2000, *J. Phys. Cond. Mat.,* **12,** 2135.
[152] Nikunen, P., Vattulainen, I., and ALA-Nissila, T., 2000, *Surf. Sci.,* **447,** L162.
[153] Nikunen, P., Vattulainen, I., and Ala-Nissila, T., 2001, *J. Chem. Phys.,* **114,** 6335.
[154] Chvoj, Z., 2001, Proceedings of the NATO Workshop on Collective Diffusion on Surfaces: Collective Behavior and the Role of Adatom Interactions, edited by M. C. Tringides and Z. Chvoj (Dordrecht: Kluwer), pp. 143–155.

[155] KAWASAKI, K., 2000, *J. Phys. Cond. Mat.,* **12,** 6343.
[156] GOUYET, J. F., 1995, *Phys. Rev.* E, **51,** 1695.
[157] NASSIF, R., BOUGHALEB, Y., HEKKOURI, A., GOUYET, J. F., and KOLB, M., 1998, *Eur. Phys. J.* B, **1,** 453.
[158] BURGERS, J. M., 1974, *The Nonlinear Diffusion Equation: Asymptotic Solutions and Statistical Problem* (Dordrecht: Kluwer).
[159] DOU, D., CASAS-VAZQUEZ, J., and LEBON, G., 1998, *Extended Irreversible Thermodynamics* (Berlin: Springer).
[160] MATANO, C., 1933, *Japanese Journal of Physics,* **8,** 109.
[161] CRANK, J., 1995, *The Mathematics of Diffusion* (Oxford: Oxford University Press).
[162] CAZABAT, A. M., FRAYSSE, N., HESLOT, F., LEVINSON, P., MARSH, J., TIBERG, F., and VALIGNAT, M. P., 1994, *Adv. in Colloid & Interface Sci.*, **48,** 1.
[163] NAUMOVETS, A. G., PALIY, M. V., VEDULA, YU, S., LOBURETS, A. T., and SENENKO, N. B., 1995, *Prog. Surf. Sci.*, **48,** 59.
[164] LOBURETS, A. T., NAUMOVETS, A. G., and VEDULA, YU. S., 1998, *Surf. Sci.*, **399,** 297.
[165] VATTULAINEN, I., MERIKOSKI, J., ALA-NISSILA, T., and YING, S. C., 1996, *Surf. Sci.*, **366,** L697.
[166] PERSSON, B. N. J., 1998, *Sliding Friction—Physical Principles and Applications* (Berlin: Springer).
[167] GRANATO, E., ALA-NISSILA, T., and YING, S. C., 2000, *Phys. Rev.* B, **62,** 11834.
[168] BARKEMA, G. T., and MOUSSEAU, N., 1996, *Phys. Rev. Lett.,* **77,** 4358.
[169] JÓNSSON, H., MILLS, G., and JACOBSEN, K. W., 1998, in *Classical and Quantum Dynamics in Condensed Phase Simulations,* edited by B. J. Berne, G. Ciccotti and D. F. Coker (Singapore: World Scientific).
[170] DELLAGO, C., BOLHUIS, P. G., and CHANDLER, D., 1998, *J. Chem. Phys.,* **108,** 9236.
[171] MUNRO, L. J., and WALES, D. J., 1999, *Phys. Rev.* B, **59,** 3969.
[172] HENKELMAN, G., and JÓNSSON, H., 1999, *J. Chem. Phys.,* **111,** 7010.
[173] CHEN, L. Y., and YING, S. C., 1999, *Phys. Rev. B,* **60,** 16965.
[174] TRUSHIN, O. S., SALO, P., and ALA-NISSILA, T., 2000, *Phys. Rev.* B, **62,** 1611.
[175] KLEY, A., RUGGERONE, P., and SCHEFFLER, M., 1997, *Phys. Rev. Lett.*, **79,** 5278.
[176] GORINGE, C. M., and BOWLER, D. R., 1997, *Phys. Rev.* B, **56,** R7073.
[177] LEPAGE, J. G., ALOUANI, M., DORSEY, D. L., WILKINS, J. W., and BLÖCHL, P. E., 1998, *Phys. Rev.* B, **58,** 1499.
[178] PENEV, E., KRATZER, P., and SCHEFFLER, M., 2001, *Phys. Rev.* B, **64,** 085401.
[179] KRESSE G., and HAFNER, J., 1993, *Phys. Rev.* B, **47,** 558.
[180] KRESSE G., and FURTHMÜLLER, J., 1996, *Comput. Mater. Sci.,* **6,** 15.
[181] KRESSE G., and FURTHMÜLLER, J., 1996, *Phys. Rev.* B, **54,** 11609.
[182] BOISVERT, G., and LEWIS, L. J., 1997, *Phys. Rev.* B, **56,** 7643.
[183] LORENSEN, H. T., NØRSKOV, J. K., and JACOBSEN, K. W., 1999, *Phys. Rev.* B, **60,** R5149.
[184] CAR, R., and PARRINELLO, M., 1985, *Phys. Rev. Lett.,* **55,** 2741.
[185] MUSOLINO, V., SELLONI, A., and CAR, R., 1999, *Phys. Rev. Lett.,* **83,** 3242.
[186] MARZARI, N., VANDERBILT, D., DE VITA, A., and PAYNE, M. C., 1999, *Phys. Rev. Lett.,* **82,** 3296.
[187] JACOBSEN, K. W., NØRSKOV, J. K., and PUSKA, M. J., 1987, *Phys. Rev.* B, **35,** 7423.
[188] DAW, M. S., and BASKES, M. I., 1984, *Phys. Rev.* B, **29,** 6443.
[189] FOILES, S. M., BASKES, M. I., and DAW, M. S., 1986, *Phys. Rev.* B, **33,** 7983.
[190] FRIEDEL, J., 1969, in *The Physics of Metals,* edited by J. M. Ziman (Cambridge: Cambridge University Press), p. 340.
[191] PETTIFOR, D. G., 1970, *J. Phys.* C, **3,** 367.
[192] DUCASTELLE, F., 1970, *J. Phys. (Paris),* **31,** 1055.
[193] GUPTA, R. P., 1981, *Phys. Rev.* B, **23,** 6265.
[194] ROSATO, V., GUILLOPÉ, M., and LEGRAND, B., 1989, *Phil. Mag.* A, **59,** 321.
[195] FINNIS, M. W., and SINCLAIR, J. E., 1984, *Phil. Mag.* A, **50,** 45.
[196] ERCOLESSI, F., TOSATTI, E., and PARRINELLO, 1986, *Phys. Rev. Lett.,* **57,** 719.
[197] ERCOLESSI, F., TOSATTI, E., and PARRINELLO, 1986, *Phil. Mag.* A, **58,** 213.
[198] VOTER, A. F., 1997, *Phys. Rev. Lett.,* **78,** 3908.
[199] SØRENSEN, M. R., and VOTER, A. F., 2000, *J. Chem. Phys.*, **112,** 9599.

[200] Wang, C. Z., Pan, B. C., and Ho, K. M., 1999, *J. Phys. Cond. Mat.,* **11,** 2043.
[201] Fu, C.-C., Weissmann, M., and Saul, A., 2001, *Appl. Surf. Sci.,* **175–176,** 36.
[202] Fu, C.-C., Weissmann, M., and Saul, A., 2001, *Surf. Sci.,* **481,** 97.
[203] Eyring, H., 1935, *J. Chem. Phys.,* **3,** 107.
[204] Chandler D., 1978, *J. Chem. Phys.,* **68,** 2959.
[205] Mel'nikov, V. I., and Meshkov, S. V., 1986, *J. Chem. Phys.,* **85,** 1018.
[206] Kramers, H. A., 1940, *Physica,* **7,** 284.
[207] Pollak, E., 1986, *J. Chem. Phys.,* **85,** 865.
[208] Voter, A. F., and Doll, J. D., 1985, *J. Chem. Phys.,* **82,** 80.
[209] Cohen, J. M., and Voter, A. F., 1989, *J. Chem. Phys.,* **91,** 5082.
[210] Kürpick, U., Kara, A., and Rahman, T. S., 1997, *Phys. Rev. Lett.,* **78,** 1086.
[211] Wahnström, G., 1985, *Surf. Sci.,* **159,** 311.
[212] Wahnström, G., 1986, *Phys. Rev.* B, **33,** 1020.
[213] Wahnström, G., 1986, *J. Chem. Phys.,* **84,** 5931.
[214] Ying, S. C., 1990, *Phys. Rev.* B, **41,** 7068.
[215] Kubo, R., 1966, *Rep. Prog. Phys.,* **29,** 255.
[216] Igarashi, A., Munakata, T., 1988, *J. Phys. Soc. Jpn.,* **57,** 2439.
[217] Caratti, G., Ferrando, R., Spadacini, R., Tommei G. E., and Zelenskaya, I., 1998, *Chem. Phys. Lett.,* **290,** 509.
[218] Cucchetti, A., and Ying, S. C., 1996, *Phys. Rev.* B, **54,** 3300.
[219] Ferrando, R., Spadacini, R., Tommei G. E., and Caratti, G., 1993, *Physica* A, **195,** 506.
[220] Braun, O. M., 2001, *Phys. Rev.* E, **63,** 11102.
[221] Haydock, R., 2001, *Phys. Rev.* B, **63,** 125413.
[222] Festa, R., and Galleani, R., 1978, *Physica* A, **90,** 229.
[223] Banavar, J. R., Cohen, M. H., and Gomer, R., 1981, *Surf. Sci.,* **107,** 113.
[224] Mazroui, M., Hairibi, M., and Boughaleb, Y., 1999, *Phys. Lett.* A, **253,** 227.
[225] Cucchetti, A., and Ying, S. C., 1999, *Phys. Rev.* B, **60,** 11110.
[226] Mazroui, M., Asakilil A., and Boughaleb, Y., 1998, *Surf. Sci.,* **409,** 528.
[227] Mazroui, M., and Boughaleb Y., 2001, *Int. J. Mod. Phys.* B, **15,** 2193.
[228] Bhatnagar, P. L., Gross, E. P., and Krook, M., 1954, *Phys. Rev.,* **94,** 511.
[229] Berezhkovskii, A. M., Bicout, D. J., and Szabo, A., 1999, *J. Chem. Phys.,* **111,** 11050.
[230] Krylov, S. Yu., Prosyanov, A. S., and Beenakker, J. J. M., 1997, *J. Chem. Phys.,* **107,** 6970.
[231] Ferrando, R., Montalenti, F., Spadacini, R., and Tommei, G. E., 1999, *Chem. Phys. Lett.,* **315,** 153.
[232] Ferrando, R., Montalenti, F., Spadacini, R., and Tommei, G. E., 1999, *Phys. Rev.* E, **61,** 6344.
[233] Persson, B. N. J., 1991, *Phys. Rev.* B, **44,** 3277
[234] Persson, B. N. J., and Rydberg, R., 1985, *Phys. Rev.* B, **32,** 3586.
[235] Pollak, E., Gershinski, G., Georgievskii, Y., and Betz, G., 1996, *Surf. Sci.,* **365,** 159.
[236] Roelofs, L. D., Greenblatt, B. J., and Boothe, N., 1995, *Surf. Sci.,* **334,** 248.
[237] Hynninen, A.-P., and Ala-Nissila, T., unpublished ms.
[238] Feynman, R. P., and Hibbs, A. R., 1965, *Quantum Mechanics and Path Integrals* (New York: McGraw-Hill).
[239] Schmid, A., 1982, *J. Low Temp. Phys.,* **49,** 609.
[240] Brandbyge, M, Hedegard, P., Heinz, T. F., Misewich, J. A., and Newns, M., 1995, *Phys. Rev.* B, **52,** 6042.
[241] Dellago, C., Bolhuis, P. G., Csajka, F. S., and Chandler, D., 1998, *J. Chem. Phys.,* **108,** 1964.
[242] Chen, L. Y., unpublished manuscript.
[243] Anderson, J. B., 1995, *Adv. Chem. Phys.*, **71,** 381.
[244] Braun, O. M., and Kivshar, Yu. S., 1994, *Phys. Rev.* B, **50,** 13388.
[245] Braun, O. M., Zelenskaya, I. I., and Kivshar, YU. S., 1994, *Int. J. Mod. Phys.* B, **8,** 2353.
[246] Braun, O. M., Dauxois, P., Palyi, M. V., and Peyrard, M., 1996, *Phys. Rev.* B, **54,** 321.

[247] METROPOLIS, M., ROSENBLUTH, A. W., ROSENBLUTH, M. N., TELLER, A. N., KELLER, E., 1953, *J. Chem. Phys.,* **6,** 1087.
[248] KAWASAKI, K., 1966, *Phys. Rev.* B, **145,** 224.
[249] TRINGIDES, M. C., and GOMER, R., 1984, *Surf. Sci.,* **145,** 121.
[250] UEBING C., and GOMER, R., 1991, *J. Chem. Phys.,* **95,** 7626.
[251] VATTULAINEN, I., MERIKOSKI, J., YING, S. C., and ALA-NISSILA, T., 2000, *Europhys. Lett.,* **51,** 361.
[252] NIETO, F., TARASENKO, A. A., and UEBING, C., 2000, *Europhys. Lett.,* **51,** 363.
[253] KOTRLA, M., 1996, *Comput. Phys. Commun.,* **96,** 82.
[254] BORTZ, A. B., KALOS, M. H., and LEBOWITZ, J. L., 1975, *J. Comput. Phys.,* **17,** 10.
[255] BULNES, F., PEREYRA, V. D., and RICCARDO, J. L., 1998, *J. Chem. Phys.,* **58,** 86.
[256] MOTTET, C., FERRANDO, R., HONTINFINDE, F., and LEVI, A. C., 1999, *Eur. Phys. J.* D, **9,** 561.
[257] SERRA, A., and FERRANDO, R., unpublished manuscript.
[258] ZALUSKA-KOTUR, M. A., KRUKOWSKI, S., and TURSKI, L. A., 1999, *Surf. Sci.,* **441,** 320.
[259] LAHTINEN, J. M., HJELT, T., and ALA-NISSILA, T., 2000, *Surf. Sci.,* **454–456,** 598.
[260] ZALUSKA-KOTUR, M. A., KRUKOWSKI, S., ROMANOWSKI, Z., and TURSKI, L. A., 2000, *Surf. Sci.,* **457,** 357.
[261] BALETTO, F., MOTTET, C., and FERRANDO, R., 2000, *Surf. Sci.,* **446,** 31.
[262] KÜRPICK, U., RAHMAN, T. S., and KÜRPICK, P., 1997, *Surf. Sci.,* **383,** 113.
[263] EVANGELAKIS, G. A., VAMVAKOPOULOS E., PANTELIOS, D. and PAPANICOLAOU, N. I., 1999, *Surf. Sci.,* **425,** L393.
[264] VOTER, A. F., 1997, *J. Chem. Phys.,* **106,** 4665.
[265] MONTALENTI, F., SÖRENSEN, M. R., and VOTER, A. F., 2001, *Phys. Rev. Lett.*, **87,** 126101.
[266] LAUBEREAU, A., and KAISER, W., 1977, in *Chemical and Biological Applications of Lasers,* edited by C. B. Moore, Vol. 2 (New York: Academic Press).
[267] MARKS, S., CORNELIUS, P. A., and HARRIS, C. B., 1980, *J. Chem. Phys.,* **73,** 3069.
[268] VINEYARD, G. H., 1958, *Phys. Rev.,* **110,** 999.
[269] GADZUK, J. W., and LUNTZ, A. C., 1984, *Surf. Sci.,* **144,** 429.
[270] LEVI, A. C., SPADACINI, R., and TOMMEI, G. E., 1982, *Surf. Sci.,* **121,** 504.
[271] NEUGEBAUER, J., and SCHEFFLER, M., 1993, *Phys. Rev. Lett.,* **71,** 577.
[272] MONTALENTI, F., and FERRANDO, R., 1999, *Surf. Sci.,* **433-435,** 445.
[273] MONTALENTI, F., and FERRANDO, R., 1998, *Phys. Rev.* B, **58,** 3617.
[274] FEIBELMAN, P. J., 2000, *Phys. Rev.* B, **61,** R2452.
[275] MONTALENTI, F., and FERRANDO, R., 1999, *Surf. Sci.,* **432,** 27.
[276] BOISVERT, G., and LEWIS, L. J., 1999, *Phys. Rev.* B, **59,** 9846.
[277] LINDEROTH, T. R., HORCH, S., PETERSEN, S., HELVEG, S., SCHÖNNING, M., LAEGSGAARD, E., STENSGAARD, I., and BESENBACHER, F., 2000, *Phys. Rev.* B, **61,** 2448.
[278] MONTALENTI, F., and FERRANDO, R., 1999, *Phys. Rev.* B, **60,** 11102.
[279] MONTALENTI, F., and FERRANDO, R., 2000, *J. Chem. Phys.,* **113,** 349.
[280] KÜRPICK, U., 2001, *Phys. Rev.* B, **63,** 45409.
[281] PIMPINELLI, A., VILLAIN, G., and WOLF, D. E., 1993, *J. Phys.* I, **3,** 447.
[282] BARTELT, M. C., and EVANS, J. W., 1994, *Surf. Sci.,* **314,** L829.
[283] ZHANG, Z., CHEN, X., and LAGALLY, M., 1994, *Phys. Rev. Lett.,* **73,** 1829.
[284] BALES, G. S., and CHRZAN, D. C., 1995, *Phys. Rev. Lett.,* **74,** 4879.
[285] HOHAGE, M., BOTT, M., MORGENSTERN, M., ZHANG, Z., MICHELY, T., and COMSA, G., 1996, *Phys. Rev. Lett.,* **73,** 2366.
[286] PIMPINELLI, A., and FERRANDO, R., 1999, *Phys. Rev.* B, **60,** 17016.
[287] ZHONG, J., WANG, E., NIU, Q., and ZHANG, Z., 2000, *Phys. Rev. Lett.,* **84,** 3895.
[288] SCHWOEBEL, R. L., 1968, *J. Appl. Phys.,* **40,** 614.
[289] VILLAIN, J., 1991, *J. Phys.* I, **1,** 19.
[290] STROSCIO, J. A., PIERCE, D. T., STILES, M. D., and ZANGWILL, A., 1995, *Phys. Rev. Lett.,* **75,** 4246.
[291] ZUO, J. K., and WENDELKEN, J. F., 1997, *Phys. Rev. Lett.,* **78,** 2791.

[292] Thurmer, K., Koch, R., Weber, M., and Rieder, K. H., 1995, *Phys. Rev. Lett.,* **75,** 1767.
[293] Bott, M., Michely, T., and Comsa, G., 1992, *Surf. Sci.,* **272,** 161.
[294] Amar, J. G., and Family, F., 1996, *Phys. Rev. Lett.,* **77,** 4584.
[295] Ramana Murty, M. V., and Cooper, B. H., 1999, *Phys. Rev. Lett.,* **83,** 352.
[296] Das Sarma, S., Punyindu, S., and Toroczkai, Z., 2000, *Surf. Sci.,* **457,** L369.
[297] Buatier De Mongeot, F., Costantini, G., Boragno, C., and Valbusa, U., 2000, *Phys. Rev. Lett.,* **84,** 2445.
[298] Hontinfinde, F., and Ferrando, R., 2001, *Phys. Rev.* B, **63,** 121403(R).
[299] Pierre-Louis, O., D'Orsogna, M. R., and Einstein, T. L., 1999, *Phys. Rev. Lett.,* **82,** 3661.
[300] Rusanen, M., Koponen, I. T., Heinonen, J., and Ala-Nissila, T., 2001, *Phys. Rev. Lett.,* **86,** 5317.
[301] Wang, S. C., and Ehrlich, G., 1993, *Phys. Rev. Lett.,* **70,** 41.
[302] Villarba, M., and Jonsson, H., 1994, *Surf. Sci.,* **317,** 15.
[303] Wang, R., and Fichthorn, K., 1993, *Mol. Simulation,* **11,** 105.
[304] Perkins, L. S., and Depristo, A. E., 1993, *Surf. Sci.,* **294,** 67.
[305] Yu, B. D., and Scheffler, M., 1996, *Phys. Rev. Lett.,* **77,** 1095.
[306] Langelaar, M. H., Breeman, M., and Boerma, D. O., 1996, *Surf. Sci.,* **352–354,** 597.
[307] Bardotti, L., Bartelt, M. C., Jenks, C. J., Stoldt, C. R., Wen, J.-M., Zhang, C.-M., Thiel, P. A., and Evans, J. W., 1998, *Langmuir,* **14,** 1487.
[308] Guillopé, M., and Legrand, B., 1989, *Surf. Sci.,* **215,** 577.
[309] Michely, T., Hohage, M., Bott, M., and Comsa, G., 1993, *Phys. Rev. Lett.,* **71,** 1659.
[310] Feibelman, P. J., 1999, *Phys. Rev. B,* **60,** 4972.
[311] Feibelman, P. J., Nelson, J., and Kellogg, G. L., 1994, *Phys. Rev.* B, **49,** 10548.
[312] Kyuno, K., and Ehrlich, G., 1998, *Surf. Sci.,* **397,** 191.
[313] Bott, M., Hohage, M., Morgenstern, M., Michely, T., and Comsa, G., 1996, *Phys. Rev. Lett.,* **76,** 1304.
[314] Feibelman, P. J., 1998, *Phys. Rev. Lett.,* **81,** 168.
[315] Ferrando, R., and Tréglia, G., 1995, *Surf. Sci.,* **331–333,** 920.
[316] Brune, H., Bromann, K., Röder, H., Kern, K., Jacobsen, J., Stolze, P., Jacobsen, K., and Nørskov, J., 1995, *Phys. Rev.* B, **52,** R14380.
[317] Boisvert, G., Lewis, L. J., and Yelon, A., 1995, *Phys. Rev. Lett.,* **75,** 469.
[318] Ratsch, C., and Scheffler, M., 1998, *Phys. Rev.* B, **58,** 13163.
[319] Jacobsen, J., Jacobsen, K. W., Stolze, P., and Nørskov, J. K., 1995, *Phys. Rev. Lett.,* **74,** 2295.
[320] Trushin, O. S., Kotrla, M., and Maca, F., 1997, *Surf. Sci.,* **389,** 55.
[321] Maca, F., Kotrla, M., and Trushin, O. S., 1999, *Vacuum* **54,** 113
[322] Maca, F., Kotrla, M., and Trushin, O. S., 2000, *Surf. Sci.,* **454–456,** 579.
[323] Merikoski, J., Häkkinen, H., Manninen, M., Timonen, J., and Kaski, K., 1994, *Int. J. Mod. Phys.* B, **8,** 3175.
[324] Rusponi, S., Boragno, C., and Valbusa, U., 1997, *Phys. Rev. Lett.,* **78,** 2795.
[325] Morgenstern, K., Lægsgaard, E., Stensgaard, I., and Besenbacher, F., 1999, *Phys. Rev. Lett.,* **83,** 1613.
[326] Rusponi, S., Boragno, C., Ferrando, R., Hontinfinde, F., and Valbusa, U., 1999, *Surf. Sci.,* **440,** 451.
[327] De Giorgi, C., Boragno, C., Ferrando, R., and Valbusa, U., 2001, *Surf. Sci.,* **487,** 49.
[328] Pedemonte, L., Tatarek, R., and Bracco, G., 2001, *Surf. Sci.,* to be published.
[329] Pedemonte, L., Tatarek, R., Vladiskovic, M., and Bracco, G., to be published.
[330] Mottet, C., Ferrando, R., Hontinfinde, F., and Levi, A. C., 1998, *Surf. Sci.,* **417,** 220.
[331] Elliott, W. C., Miceli, P. F., Tse, T., and Stephens, P. W., 1996, *Phys. Rev.* B, **54,** 17938.
[332] Suzuki, Y., Kikuchi, H., and Koshizuka, N., 1988, *Jpn. J. Appl. Phys.,* **27,** L1175.
[333] Bromann, K., Brune, H., Röder, H., and Kern, K., 1995, *Phys. Rev. Lett.,* **75,** 677.

[334] Meyer, J. A., Vrijmoeth, J., Van der Vegt, H. A., Vlieg, E., and Behm, R. J., 1995, *Phys. Rev.* B, **51,** 14790.
[335] Roos, K. R., and Tringides, M. C., 2000, *Phys. Rev. Lett.,* **85,** 1480.
[336] Van Der Vegt, H. A., Van Pinxteren, H. M., Lohmeier, M., Vlieg, E., and Thornton, J. M. C., 1992, *Phys. Rev. Lett.,* **68,** 3335.
[337] Kalff, M., Comsa, G., and Michely, T., 1998, *Phys. Rev. Lett.,* **81,** 1255.
[338] Martin, T. P., 1996, *Phys. Rep.,* **273,** 199.
[339] Henry, C. R., 1998, *Surf. Sci. Rep.,* **31,** 231.
[340] Reinhard, D., Hall, B. D., Ugarte, D., and Monot, R., 1997, *Phys. Rev.* B, **55,** 7868.
[341] Valkealahti, S., and Manninen, M., 1998, *Phys. Rev. B,* **57,** 15533.
[342] Baletto, F., and Ferrando, R., 2001, *Surf. Sci.*, **490,** 361.
[343] Baletto, F., Mottet, C., and Ferrando, R., 2000, *Phys. Rev. Lett.*, **84,** 5544.
[344] Baletto, F., Mottet, C., and Ferrando, R., 2001, *Phys. Rev.* B, **63,** 155 408.
[345] Wagner, H., 1979, in *Solid Surface Physics,* edited by G. Höhler (Berlin: Springer).
[346] Krug, J., and Spohn, H., 1991, in *Solids far From Equilibrium,* edited by G. Godreche (Cambridge: Cambridge University Press).
[347] Xiao, X. D., Xie, Y., Jacobsen, C., Galloway, H., Salmeron, M., and Shen, Y. R., 1995, *Phys. Rev. Lett.,* **74,** 3860.
[348] Uebing, C., and Gomer, R., 1994, *Surf. Sci.,* **306,** 419.
[349] Uebing, C., and Gomer, R., 1994, *Surf. Sci.,* **306,** 427.
[350] Uebing, C., and Gomer, R., 1994, *Surf. Sci.,* **317,** 165.
[351] Uebing, C., 1994, *Phys. Rev.* B, **49,** 13913.
[352] Merikoski, J. and Ying, S. C., 1997, *Phys. Rev.* B, **56,** 2166.
[353] Merikoski, J. and Ying, S. C., 1997, *Surf. Sci.,* **381,** L623.
[354] Natori, A., and Godby, R. W., 1993, *Phys. Rev.* B, **47,** 15816.
[355] Ma, J., Cai, L., Xiao, X., and Loy, M. M. T., 1999, *Surf. Sci.,* **425,** 131.
[356] Ma, J., Xiao, X., and Loy, M. M. T., 1999, *Surf. Sci.* **436,** L661.
[357] Xiao, X., 2001, in *Proceedings of the NATO Workshop on Collective Diffusion on Surfaces: Collective Behavior and the Role of Adatom Interactions*, edited by M. C. Tringides and Z. Chvoj (Dordrecht: Kluwer), pp. 117–127.
[358] Reutt-Robey, J. E., Dobven, D. J., Chabal, Y. J., and Christian, S. B, 1988, *Phys. Rev. Lett.,* **61,** 2778.
[359] Reutt-Robey, J. E., Dobven, D. J., Chabal, Y. J., and Christian, S. B, 1990, *J. Chem. Phys.,* **93,** 9113.
[360] Wang, S.-C , and Tsong, T. T., 1982, *Surf. Sci.,* **121,** 85.
[361] Fu, T.-Y., Wu, H.-T., and Tsong, T. T., 1998, *Phys. Rev.* B, **58,** 2340.
[362] Siddiqui, H. R., Guo, X., Chorkendoff, I., and Yates JR., J. T., 1987, *Surf. Sci.,* **191,** L813.
[363] Collins, D. M., and Spicer, W. E., 1977, *Surf. Sci.,* **69,** 85.
[364] Luo, J. S., Tobin, R. G., Lambert, D. K., Fisher, G. B. and Dimaggio, C. L., 1992, *Surf. Sci.,* **274,** 53.
[365] Wang, X. R., Xiao, X., and Zhang, Z., unpublished manuscript.
[366] Merikoski, J. and Ying, S. C., unpublished manuscript.
[367] Halperin B. I., and Hohenberg, P. C., 1969, *Phys. Rev.,* **177,** 952.
[368] Hohenberg, P. C., and Halperin, B. I., 1977, *Rev. Mod. Phys.,* **49,** 435.
[369] Ala-Nissila, T., Han, W. K., and Ying, S. C., 1992, *Phys. Rev. Lett.,* **68,** 1866.
[370] Baldan, M. R., Granato E., and Ying, S. C., 2000, *Phys. Rev.* B, **62,** 11834.
[371] Abrikosov, A. A., 1957, *Soviet Phys. JETP,* **5,** 1174.
[372] Shi, J., Ling, X. S., Liang, R., Bonn D. A., and Hardy, W. N., 1999, *Phys. Rev.* B, **60,** R12593.
[373] Ling, X. S., Berger , J. E., and Prober, D. E., 1998, *Phys. Rev.* B, **57,** R3249.
[374] Ling, X. S., Park, S. R., McClain, B. A., Choi, S. M., Dender D. C., and Lynn, J. W., 2001, *Phys. Rev. Lett.,* **86,** 712.
[375] Ala-Nissila, T., Granato, E., and Ying, S. C., 1990, *J. Phys.: Cond. Matt.,* **2,** 8537.
[376] Kutner, R., Binder K., and Kehr, K. W., 1982, *Phys. Rev.* B, **26,** 2967.
[377] Wu, P. K., Tringides, M. C., and Lagally, M. G., 1989, *Phys. Rev.* B, **39,** 7595.

[378] Ching, W. Y., Huber, D. L., Lagally, M. G., and Wang, G.-C., 1978, *Surf. Sci.,* **77,** 550.
[379] Wang, G.-C., Lu, T.-M., and Lagally, M. G., 1978, *J. Chem. Phys.,* **69,** 479.
[380] Johnson, K. E., Wilson, R. J., and Chiang, S., 1993, *Phys. Rev. Lett.,* **71,** 1055.
[381] Brundle, C. R., and Broughton, J. Q., 1990, in *The Chemical Physics of Solid Surfaces and Heterogeneous Catalysis: Chemisorption Systems,* edited by D. A. King and D. P. Woodruff, Vol. 3A (Amsterdam: Elsevier), Chap. 3.
[382] Engel, T., Niehus, H., and Bauer, E., 1975, *Surf. Sci.,* **52,** 237.
[383] Bauer, E., and Engel, T., 1978, *Surf. Sci.,* **71,** 695.
[384] Van Hove, M. A., and Tong, S. Y., 1975, *Phys. Rev. Lett.,* **35,** 1092.
[385] Elbe, A., Meister, G., and Goldmann, A., 1997, *Surf. Sci.,* **371,** 438.
[386] Vattulainen, I, Merikoski, J., Ala-Nissila, T., and Ying, S. C., 1997, *Phys. Rev. Lett.,* **79,** 257.
[387] Vattulainen, I, Merikoski, J., Ala-Nissila, T., and Ying, S.C., 1998, *Phys. Rev. Lett.,* **80,** 5456.
[388] Sahu, D., Ying, S. C., and Kosterlitz, J. M., 1988, in *The Structure of Surfaces II,* edited by J. F. Van Der Veen and M. A. Van Hove (Berlin: Springer), p. 470.
[389] Uebing, C., and Zhdanov, V. P., 1999, *J. Chem. Phys.,* **111,** 11234.
[390] Uebing, C., and Zhdanov, V. P., 1998, *Phys. Rev. Lett.,* **80,** 5455.
[391] Kosterlitz, J. M., 1998, private communication.
[392] Meyer, Von W., and Neldel, H., 1937, *Z. Tech. Phys.,* **12,** 588.
[393] Uebing, C., and Zhadanov, V. P., 1998, *J. Chem. Phys.,* **109,** 3197.
[394] Vattulainen, I., Merikoski, J., Ala-Nissila, T. and Ying, S. C., 1998, *Phys. Rev.* B, **57,** 1896.
[395] Vattulainen, I., Merikoski, J., Ala-Nissila, T., and Ying, S. C., 1999, *J. Chem. Phys.,* **111,** 11232.
[396] Goldenfeld, N., 1993, *Lectures on Phase Transitions and the Renormalization Group* (Reading: Addison-Wesley).
[397] Nieto, F., Tarasenko, A. A. and Uebing, C., 1998, *Europhys. Lett.,* **43** 558.
[398] Boon, J. P., and Yip, S., 1980, *Molecular Hydrodynamics* (New York: Dover).
[399] March, N. H., and Tosi, M. P., 1976, *Atomic Dynamics in Liquids* (New York: Dover).
[400] Vattulainen, I., Hjelt, T., Ala-Nissila, T., and Ying, S. C., 2000, *J. Chem. Phys.,* **113,** 10284.
[401] Kuusela, E., and Ala-Nissila, T., 2001, *Phys. Rev.* E, **63,** 061505.
[402] Hjelt, T., Vattulainen, I., Ala-Nissila, T., and Ying, S. C., 2000, *Surf. Sci.,* **449,** L255.
[403] Carmesin, I., and Kremer, K., 1988, *Macromolecules,* **21,** 2819.
[404] Carmesin, I., and Kremer, K., 1995, *Monte Carlo and Molecular Dynamics Simulations in Polymer Science,* edited by K. Binder (Oxford: Oxford University Press).
[405] Ala-Nissila, T., Herminghaus, S., Hjelt, T., and Leiderer, P., 1996, *Phys. Rev. Lett.,* **76,** 4003.
[406] Hjelt, T., Vattulainen, I., Merikoski, J., Ala-Nissila, T., and Ying, S. C., 1998, *Surf. Sci.,* **402/404,** 253.
[407] Hjelt, T., and Vattulainen, I., 2000, *J. Chem. Phys.,* **112,** 4731.
[408] Vattulainen, I., 2001, in *Proceedings of the NATO Workshop on Collective Diffusion on Surfaces: Collective Behavior and the Role of Adatom Interactions*, edited by M. C. Tringides and Z. Chvoj (Dordrecht: Kluwer), pp. 169–178.
[409] Tringides, M. C., Wu, P. K., and Lagally, M. G., 1987, *Phys. Rev. Lett.,* **59,** 315.
[410] Difoggio, R., and Gomer, R., 1982, *Phys. Rev.* B, **25** 3490.
[411] Lin, T. S., and Gomer, R., 1991, *Surf. Sci.,* **225,** 41.
[412] Graham, A. P., Menzel, A., and Toennies, J. P., 1999, *J. Chem. Phys.,* **111,** 1676.
[413] Lauhon, L. J., and Ho, W., 2000, *Phys. Rev. Lett.,* **85,** 4566.
[414] Cao, G. X., Nabighian, E., and Zhu, X. D., 1997, *Phys. Rev. Lett.,* **79,** 3696.
[415] Wong, A., Lee, A., and Zhu, X. D., 1995, *Phys. Rev.* B, **51,** 4418.
[416] Daniels, E. A., and Gomer, R., 1995, *Surf. Sci.,* **336,** 245.
[417] Gillian, M. J., 1987, *Phys. Rev. Lett.,* **58,** 563.

[418] Gillian, M. J., 1987, *J. Phys.* C, **20,** 3621.
[419] Haug, K., Wahnström, G., and Metiu, H., 1988, *J. Chem. Phys.,* **90,** 540.
[420] Sun, Y. C., and Voth, G. A., 1993, *J. Chem. Phys.,* **98,** 7451.
[421] Mattson, T. R., and Wahnström, G., 1997, *Phys. Rev.* B, **56,** 14944.
[422] Mattson, T. R., Wahnström, G., and Bengtsson, L., 1997, *Phys. Rev.* B, **56,** 2258.
[423] Pouthier, V., and Light, J. C., 2000, *J. Chem. Phys.,* **113,** 1204.
[424] Kondo, J., 1984, *Physica,* **125B,** 279.
[425] Castin, Y., and Molmer, K., 1996, *Phys. Rev.* A, **54,** 5275.
[426] Molmer, K., Castin, Y., and Dalibard, J., 1993, *J. Opt. Soc. Am.* B, **10,** 524.
[427] Linblad, G., 1976, *Commun. Math. Phys.,* **48,** 119.
[428] Okuyama, H., Ueda, T., Aruga, T., and Nishijima, M., 2001, *Phys. Rev.* B, **63,** 233403.
[429] Okuyama, H., Ueda, T., Aruga, T., and Nishijima, M., 2001, *Phys. Rev.* B, **63,** 233404.
[430] Binder, K., and Stauffer, D., 1974, *Phys. Rev. Lett.,* **33,** 1006.
[431] Binder, K., Stauffer, D., and Müller-Krumbhaar, 1975, *Phys. Rev.* B, **12,** 5261.
[432] Rao, M., Kalos, M. H., Lebowitz, J. L., and Marro, J., 1976, *Phys. Rev.* B, **13,** 4328.
[433] Kuipers, L., and Palmer, R. E., 1996, *Phys. Rev.* B, **53,** R7646.
[434] Furman, I., and Biham, O., 1997, *Phys. Rev.* B, **55,** 7917.
[435] Stoldt, C. R., Jenkins, C. J., Thiel, P. A., Cadilhe, A. M., and Evans, J. W., 1999, *J. Chem. Phys.,* **111,** 5157.
[436] Krapivsky, P. L., Mendes, J. F. F., and Redner, S., 1999, *Phys. Rev.* B, **59,** 15950.
[437] Furman, I., and Biham, O., 2000, *Phys. Rev.* B, **62,** R10649.
[438] Lee S. B., and Gupta, B. G., 2000, *Phys. Rev.* B, **62,** 7545.
[439] Kyuno, K., and Ehrlich, G., 2000, *Phys. Rev. Lett.,* **84,** 2658.
[440] Bardotti, L., Jensen, P., Hoareau, A., Treilleux, M., and Cabaud, B., 1995, *Phys. Rev. Lett.,* **74,** 4694.
[441] Deltour. P., Barrat, J.-L., and Jensen, P., 1997, *Phys. Rev. Lett.,* **78,** 4597.
[442] Luedtke, W. D., and Landman, U., 1999, *Phys. Rev. Lett.,* **82,** 3835.
[443] Kang, H. C., Thiel, P. A., and Evans, J. W., 1990, *J. Chem. Phys.,* **93,** 9018.
[444] Bitar, L., Serena, P. A., García-Mochales, P., García, N., and Bihn, V. T., 1995, *Surf. Sci.,* **339,** 221.
[445] Sholl, D. S., and Skodje, R. T., 1995, *Phys. Rev. Lett.,* **75,** 3158.
[446] Bogicevic, A., Liu, S., Jacobsen, J., Lundqvist, B., and Metiu, H., 1998, *Phys Rev.* B, **57,** R9459.
[447] Lo, A., and Skodje, R. T., 1999, *J. Chem. Phys.,* **111,** 2726.
[448] Pal, S., and Fichthorn, K. A., 1999, *Phys. Rev.* B, **60,** 7804.
[449] Müller, T., and Selke, W., 1999, *Eur. Phys. J.* B, **10,** 549.
[450] Morgenstern, K., Rosenfeld, G., Poelsema, B., and Comsa, G., 1995, *Phys. Rev. Lett.,* **74,** 2058.
[451] Morgenstern, K., Rosenfeld, G., and Comsa, G., 1996, *Phys. Rev. Lett.,* **76,** 2113.
[452] Mills, G., Mattsson, T. R., Møllnitz, L., and Metiu, H., 1999, *J. Chem. Phys.,* **111,** 8639.
[453] Reiss, H., 1968, *J. Appl. Phys.,* **39,** 5045.
[454] Hamilton, J. C., Daw, M. S., and Foiles, S. M., 1995, *Phys. Rev. Lett.,* **74,** 2760.
[455] Chirita, V., Munger, E. P., Greene, J. E., and Sundgren, J.-E., 1999, *Surf. Sci.,* **436,** L641.
[456] Wang, S. C., and Ehrlich, G., 1997, *Phys. Rev. Lett.,* **79,** 4234.
[457] Wang, S. C., and Ehrlich, G., 1990, *Surf. Sci.,* **239,** 301.
[458] Kellogg, G. L., 1994, *Phys. Rev. Lett.,* **73,** 1833.
[459] Liu, C. L., and Adams, J. B., 1992, *Surf. Sci.,* **268,** 73.
[460] Chang, C. M., Wei, C. M., and Chen, S. P., 1996, *Phys. Rev.* B, **54,** 17083.
[461] Chang, C. M., Wei, C. M., and Chen, S. P., 2000, *Phys. Rev. Lett.* **85,** 1044.
[462] Sanchez, J. R., and Evans, J. W., 1999, *Phys. Rev.* B, **59,** 3224.
[463] Salo, P., Hirvonen, J., Koponen, I. T., Trushin, O., Heinonen, J., and Ala-Nissila, T., 2001 *Phys. Rev.* B, **64,** 161405.

[464] Shi, Z.-P., Zhang, Z., Swan, A. K., and Wendelken J. F., 1996, *Phys. Rev. Lett.,* **76,** 4927.
[465] Renisch, S., Schuster, R., Wintterlin J., and Ertl, G., 1999, *Phys. Rev. Lett.,* **82,** 3839.
[466] Latyshev, A. V., Aseev, A. L., Krasilnikov, A. B., and Stenin, S. I., 1989, *Surf. Sci.,* **213,** 157.
[467] Stoyanov, S., 1998, *Surf. Sci.,* **416,** 200.
[468] Metois, J. J., Heyraud, J. C., Pimpinelli, A., 1999, *Surf. Sci.,* **420,** 250.
[469] Metois, J. J., and Stoyanov, S., 1999, *Surf. Sci.,* **440,** 407.
[470] Pierre-Louis, O., and Einstein, T. L., 2000, *Phys. Rev.* B, **62,** 13697.
[471] Borovsky, B., Krueger, M., and Ganz, E., 1997, *Phys. Rev. Lett.,* **78,** 4229.
[472] Borovsky, B., Krueger, M., and Ganz, E., 1999, *Phys. Rev.* B, **59,** 1598.
[473] Tromp, R. M., and Mankos, M., 1998, *Phys. Rev. Lett.,* **81,** 1050.
[474] Brocks, G., and Kelly, P. J., 1996, *Phys. Rev. Lett.,* **76,** 2362.
[475] Salmi, M., Alatalo, M., Ala-Nissila, T., and Nieminen, R. M., 1999, *Surf. Sci.,* **425,** 31.
[476] Michely, Th., Ye, G. X., Weidenhof, V., and Wuttig, M., 1999, *Surf. Sci.,* **432,** 228.
[477] Ye, G. X., Xia, A.-G., Gao, G.-L., Lao, Y.-F., and Tao, X.-M., 2001, *Phys. Rev.* B, **63,** 125405.
[478] Ramirez-Pastor, A. J., Bulnes, F., and Nieto, F., 2001, *Surf. Sci.,* **476,** 161.
[479] Mayagoitia, V., Rojas, F., Riccardo, J. L., Pereyra, V., and Zgrablich, G., 1990, *Phys. Rev.* B, **41,** 7150.